ENCLOSURE 9

GEH Technical Report

WG3-U63-ERD-S-0001 Revision 3

Firewater Service Complex Seismic Analysis Report

REVISION STATUS SHEET

Document Title: Firewater Service Complex Seismic Analysis Report

Revision #: 3 **Type:** Engineering Report – Design

Safety Related Classification Code: N/A **MPL No.:** A25-5020, U63-5030

"|" Vertical Sidebar Denotes Change

Rev #	DOORS BL	Change Number	MM/DD/YYYY	Preparing Organization	Issue / Release Status	Verification Status
0	N/A	ECO-0015266	06/22/2015	GEH	Issued for Use-Design	Verified
1	N/A	ECO-0018894	09/25/2015	GEH	Issued for Use-Design	Verified
2	N/A	ECO-0020376	11/12/2015	GEH	Issued for Use-Design	Verified
3	N/A	ECO-0023195	03/10/2016	GEH	Issued for Use-Design	Verified

MADE BY	APPROVALS	AUTH. DATE
Luben Todorovski GEH	Tanya B. Kirby GEH	06/22/2015

REVISION CHART (CONT)

Rev #	DOORS BL	Change Number	MM/DD/YYYY	Preparing Organization	Issue / Release Status	Verification Status

RECORD OF REVISION

Rev #	Description
0	Initial issue
1	Incorporate comments on Rev.0
2	Incorporate comments on Rev. 1
3	Incorporate comments on Rev. 2

TABLE OF CONTENTS

LIST OF TABLES

LIST OF FIGURES

LIST OF ACRONYMS

ARS	Acceleration Response Spectra
BE	Best Estimate
CB	Control Building
CPSD	Cumulative Power Spectral Density
CSDRS	Certified Seismic Design Response Spectra
DCD	Design Control Document
DM	Direct Method
ESBWR	Economic Simplified Boiling Water Reactor
EW	East-West
FFT	Fast Fourier Transformation
FIRS	Foundation Input Response Spectra
FPE	Fire Pump Enclosure
FSAR	Final Safety Analysis Report
FWS	Firewater Storage Tank
FWSC	Firewater Service Complex
GMM	Ground Motion Model
ISG	Interim Staff Guidance
ISRS	In-Structure Response Spectra
LB	Lower Bound
LMSM	Lumped Mass-Stick Model
MSM	Modified Subtraction Method
NA3	North Anna Unit 3
NEI	Nuclear Energy Institute
NS	North-South
OBE	Operating Basis Earthquake
PSD	Power Spectral Density
SDOF	Single Degree of Freedom
SRP	Standard Review Plan
SRSS	Square Root of the Sum of the Squares
SSE	Safe Shutdown Earthquake
SSI	Soil-Structure Interaction
SSSI	Structure-Soil-Structure Interaction
UB	Upper Bound

1. INTRODUCTION AND PURPOSE

This report presents the North Anna Unit 3 (NA3) site-specific Soil-Structure Interaction (SSI) analyses performed for the the Economic Simplified Boiling Water Reactor (ESBWR) Firewater Service Complex (FWSC).

The NA3 site-specific SSI analysis follows the methodology presented in the standard ESBWR Design Control Document (DCD) FWSC seismic analysis report (Reference 2-j) using the Modified Subtraction Method (MSM) and the SASSI2010 computer program. The SASSI structural (HOUSE) models are developed from the standard design SASSI model described in Section 4.3 coupled with site-specific strain-compatible dynamic subsurface properties. The SASSI structural (HOUSE) model also includes near-field solid elements that represent the concrete fill layer placed on the surface of the Zone III-IV rock, up to the bottom of the FWSC basemat.

The FWSC site-specific design basis is developed based on the envelope of the results obtained from two sets of site-specific FWSC SSI analyses performed with the input control motion applied:

a. as a surface input motion compatible to the spectra defining the site-specific design motion at the bottom of the FWSC foundation at El. 282 ft NAVD 88 (standard design El. 2.15 m) and

b. as an in-column motion compatible to the spectra defining the site-specific design motion at the bottom of the concrete fill at nominal El. 220 ft NAVD 88 (standard design El. -16.8 m)

The consideration of two different control motion elevations captures the effects of seismic wave propagation through concrete fill, and thus addresses potential deamplification of the high frequency input motion as the seismic waves propagate through the in-situ saprolite. The FWSC site-specific design basis that is developed based on the envelope of results obtained from the analyses that use these two sets of input control motions meets the intent of ISG-017 (Reference 2-m), which requires the spectra defining the design motion at the surface to be enveloped by deterministic SSI analysis at the top of the considered soil columns.

In accordance with SRP 3.7.2, three subsurface profiles are considered for each input control motion, namely, a Best Estimate (BE) profile, a Lower Bound (LB) profile, and an Upper Bound (UB) profile to account for the effects of the potential variability in the properties of the soils and rock at the FWSC location of the NA3 site. LB, BE and UB properties are also assigned to the near-field elements modeling the concrete fill below the FWSC basemat to account for the variation of concrete properties.

The FWSC structural models used for the SSI analysis represent stiffness properties of uncracked reinforced concrete structures to provide conservative seismic responses for the NA3 rock site with high frequency design ground motion. The results of the analyses of the FWSC model with full (uncracked concrete) stiffness and Operating Basis Earthquake

(OBE) damping are used for the development of site-specific In-Structure Response Spectra (ISRS). The results obtained from the analyses of the FWSC model, with full (uncracked concrete) stiffness and Safe Shutdown Earthquake (SSE) damping, are used for the calculation of the site-specific seismic load demands on the FWSC reinforced concrete structures. The results of the site-specific sensitivity analyses presented in Appendix B ensure that the site-specific design basis, which is based on the analyses of FWSC models with full (uncracked concrete) stiffness properties, adequately addresses the effects of structural stiffness variations due to concrete cracking.

The results of the site-specific SSI analyses of the standalone FWSC model presented in this report are enveloped with the results of the structure-soil-structure interaction (SSSI) analyses of the FWSC-CB model documented in Reference 2-r. This is to develop the FWSC site-specific seismic design basis that includes the amplifications due to the SSSI effects of the CB on the seismic response of the FWSC. These enveloping site-specific seismic demands are compared with the seismic design envelopes documented in the standard design FWSC seismic analysis report (Reference 2-j) to determine any exceedances of the NA3 site-specific seismic demands relative to the standard design. The enveloping site-specific ISRS presented in this report are also used as input for the site-specific seismic design and qualification of the FWSC equipment and components.

The enveloping site-specific demands presented in this report are obtained from the FWSC SSI analyses and the FWSC-CB SSSI analyses of models representing fully bonded conditions between the concrete fill supporting the FWSC foundation and the surrounding soil. Reference 2-dd presents an evaluation of the effects of possible separation between the concrete fill and surrounding soil on the seismic response of the FWSC structures at the NA3 site. This soil separation evaluation is based on results of SSI and SSSI sensitivity analyses performed on FWSC standalone and FWSC-CB combined models simulating conditions of maximum separation between the concrete fill and the surrounding soil.

1.1 Limitations on Use

This report is issued without limitation.

2. REFERENCES

a. TODI WG3-3-A25-TDI-0004, "North Anna 3 Maximum Ground Water Level", Revision 0
b. TODI WG3-3-A25-TDI-0005, "North Anna 3 Power Block Excavation/Backfill Drawings, Concrete Backfill Properties & Plot Plan", Revision 5
c. TODI WG3-3-A25-TDI-0006, "North Anna 3 Best Estimate Elevation of Top of Zone III Rock and Top of Zone III-IV Rock for RB/FB, CB and FWSC Structures", Revision 0
d. TODI WG3-A25-TDI-S-0004, "North Anna 3 RB/FB, CB & FWSC SSI Analyses EPRI 2013 GMPE Based Inputs", Revision 0
e. TODI WG3-A25-TDI-S-0005, "North Anna 3 RB/FB, CB & FWSC Distances from Adjacent Structures & Sheet Piling", Revision 0

f. TODI WG3-A25-TDI-S-0006, "North Anna 3 RB/FB, CB & FWSC Outcrop SSI Design Motion Time-Histories", Revision 0
g. 105E4483, "ESBWR Firewater Service Complex General Arrangement Drawing", Revision 1
h. 26A6642AL, "ESBWR Design Control Document Tier 2 Chapter 3 Appendices 3A – 3F", Revision 10
i. 26A6642AN, "ESBWR Design Control Document Tier 2 Chapter 3 Appendices 3G – 3L", Revision 10
j. 26A7419, "ESBWR Seismic Analysis of Firewater Service Complex", Revision 1
k. 26A7420, "ESBWR Firewater Service Complex Structural Design Report", Revision 2
l. 26A7421, "ESBWR Stability Analysis of Firewater Service Complex", Revision 1
m. USNRC, "Interim Staff Guidance on Ensuring Hazard-Consistent Seismic Input for Site Response and Soil-Structure Interaction Analyses", DC/COL-ISG-017 (NRC ADAMS Accession Number ML092230543)
n. SER-DMN-032, "North Anna 3 Seismic Soil-Structure Interaction Analyses Results for CB and FWSC Structural Evaluation", Revision 3
o. USNRC, NUREG-0800, "Standard Review Plan for the Review of Safety Analysis Reports for Nuclear Power Plants - LWR Edition", Section 3.7.1, "Seismic Design Parameters", Revision 3, March 2007
p. USNRC, NUREG-0800, "Standard Review Plan for the Review of Safety Analysis Reports for Nuclear Power Plants - LWR Edition", Section 3.7.2, "Seismic System Analysis", Revision 4, September 2013
q. USNRC, Regulatory Guide 1.60: "Design Response Spectra for Seismic Design of Nuclear Power Plants", Revision 1, December 1973
r. WG3-U73-ERD-S-0002, "North Anna 3 Control Building and Firewater Service Complex Seismic Structure-Soil-Structure Interaction Analysis Report", Revision 6
s. WG3-U63-ERD-S-0002, "North Anna 3 Firewater Service Complex Stability Analysis Report", Revision 1
t. WG3-U73-ERD-S-0001, "North Anna 3 Control Building Seismic Analysis Report", Revision 2
u. SER-DMN-011, "Benchmarking of SASSI2010 MSM Results from NA3 Site-Specific SSI Analysis", Revision 1
v. USNRC, "Interim Staff Guidance on Seismic Issues Associated with High Frequency Ground Motion in Design Certification and Combined License Applications", DC/COL-ISG-01 (NRC ADAMS Accession Number ML081400293)
w. USNRC, Regulatory Guide 1.61: "Damping Values for Seismic Design of Nuclear Power Plants", Revision 1, March 2007
x. ASCE 43-05: "Seismic Design Criteria for Structures, Systems, and Components in Nuclear Facilities"
y. S/VTR-SAS, "Validation Test Report for SASSI2010 Version 1", Revision I
z. Ostadan, F. and Deng, N., "SASSI2010 Version 1.0 User's Manual", May 2012
aa. SER-DMN-014, "Additional Oscillators for Fully Cracked Model for RAI 3.7.2-14(f) Response", Revision 1

bb. DBR-0009791, "Soil-Structure Interaction Absolute Acceleration Transfer Functions With Respect to Outcrop Motion and Design Motion Power Spectral Densities For RB/FB SSI, CB SSI, FWSC SSI, CB-FWSC SSSI, and CB-RB/FB SSSI Analyses", Revision 5

cc. WG3-U71-ERD-S-0001, "North Anna 3 Reactor/Fuel Building Complex Seismic Analysis Report", Revision 4

dd. SER-DMN-034, "Evaluation of FWSC Concrete Fill and Effects of Separation between Concrete Fill and Surrounding Soil", Revision 2

ee. SER-DMN-033, "Evaluation of the Adequacy of the Frequencies Used for Seismic Response Analyses", Revision 1

3. SITE-SPECIFIC INPUT

3.1 Site-Specific Subsurface Properties

The SSI analyses of the FWSC at the NA3 site consider BE, LB, and UB dynamic properties of the in-situ subgrade materials at the FWSC location that are compatible with the strains generated by the site-specific design ground motion. The site-specific strain-compatible dynamic properties of the in-situ rock and saprolite subgrade materials are assigned to the far-field SASSI SITE models and the excavated volume elements of the SASSI structural (HOUSE) models. Reference 2-d provides the site-specific strain-compatible dynamic subsurface properties used as input for the FWSC SSI analysis. These strain-compatible properties are listed in Tables 3.1-1 through 3.1-3.

The P-wave velocity of the saprolite located below the groundwater level is set no less than that of the water to capture the effect of groundwater on P-wave velocity of saturated soil unless the Poisson's ratio value that relates the S- and P-wave velocities becomes too high. A maximum value of 0.48 is used for the Poisson's ratio of subgrade materials in order to ensure the numerical stability of the SASSI2010 analysis results.

The FWSC SSI analyses also consider BE, LB, and UB dynamic properties for the concrete fill placed below the FWSC basemat. The dynamic properties used for the concrete fill are independent of strain, reflecting the linear elastic behavior of the concrete under the small earthquake-induced strains. These dynamic properties are assigned to the near-field solid elements in the SASSI structural (HOUSE) models representing the block of concrete fill below the FWSC foundation. Reference 2-d provides the BE, LB, and UB dynamic properties of the structural and concrete fill materials that are listed in Tables 3.1-4 through 3.1-6.

The site-specific SSI analyses of the FWSC neglect the effects of the structural fill placed around the FWSC basemat and the concrete fill because the strain-compatible dynamic properties of the structural fill provided in Tables 3.1-4 through 3.1-6 are similar to those of the surrounding in-situ saprolite. The comparisons presented in Figure 3.1-1 show that the structural fill and the in-situ saprolite have similar shear wave velocities, compression wave velocities and damping. The comparisons presented in Table 3.1-7 also show that the values of the average strain-compatible shear wave velocities ($V_{s\text{-}ave}$) and shear column frequencies

(f_{sc}) of the structural fill are very close to those of the in-situ saprolite. The FWSC-CB combined model used for the FWSC-CB SSSI analyses presented in Reference 2-r includes the structural fill placed in the gap between the CB and FWSC and around the concrete fill below the FWSC foundation. The inclusion of the structural fill in the combined model addresses the effects of the structural fill on the FWSC seismic response.

The analyses presented in this report are performed on models representing fully bonded conditions between the concrete fill supporting the FWSC foundation and the surrounding soil. Reference 2-dd presents the sensitivity analyses performed on models simulating conditions of maximum separation between the concrete fill under the FWSC foundation and the surrounding soil. The effects of separation between the concrete fill and surrounding soil on the seismic response of the FWSC structures and NA3 site-specific design basis are addressed based on results of these sensitivity analyses as described in Section 7 of Reference 2-dd.

3.2 Site-Specific Input Motion

Reference 2-d provides four sets of statistically independent ground motion time histories used as input control motion in the three orthogonal directions for the SSI analyses of the FWSC. One set of surface input motion acceleration time histories serves as the input control motion at the bottom of the FWSC basemat El. 282 ft NAVD88. These surface ground motion time histories that represent the outcrop free-field motion at the FWSC foundation bottom elevation are compatible with the envelope of the FWSC FIRS and the broadband spectra specified in RG 1.60 (Reference 2-q), anchored at 0.1 g. The analyses performed with surface input motion ensure that the site-specific SSI analysis of the FWSC meets the intent of ISG-017 (Reference 2-m), which requires the spectra defining the design motion at the surface to be enveloped by deterministic SSI analysis at the top of the considered soil columns.

Three sets of in-column ground motion acceleration time histories are used for the analysis of the FWSC for the BE, LB, and UB profiles with the deep input control motion at the bottom of the concrete fill. These three ground motion time histories are compatible with the SSE design spectra defining the free-field outcrop design ground motion at the bottom of the concrete fill El. 220 ft NAVD88.

Figures 3.2-1 through 3.2-3 present the 5% damped Acceleration Response Spectra (ARS), the Power Spectral Density (PSD), and the Cumulative Power Spectral Density (CPSD) of the FWSC surface (at El. 282 ft) and in-column (at El. 220 ft) input acceleration time histories illustrating the energy content of the input motion at different frequencies. The presented PSDs are computed based on the strong motion portion of the time record for which duration is defined by the time interval, required for Arias intensities, to increase from 5% to 75%. Plus/minus 20% frequency averaging intervals are applied in compliance with SRP 3.7.1 (Reference 2-o).

4. SOIL-STRUCTURE INTERACTION ANALYSIS

4.1 Analysis Method

The NA3 site-specific SSI analyses of the FWSC follow the methodology presented in DCD Section 3A.5.2 (Reference 2-h) and utilizes the SASSI2010 computer program. However, unlike the SSI analysis performed for the standard design that considers the FWSC basemat resting on the surface of the supporting subgrade with infinite horizontal layering, the site-specific SSI analysis uses the SASSI structural (HOUSE) model that explicitly includes the concrete fill below the FWSC foundation as a block embedded in the in-situ soil and rock. For the NA3 site-specific SSI analysis, a refined mesh is used for the excavated volume portion of the model to ensure it can pass high frequency waves. This results in a total number of interaction nodes that can exceed the program limitation for impedance calculations if the Direct (flexible volume) Method (DM) is used. Therefore, the simplified Modified Subtraction Method (MSM) is employed instead where only selected nodes of the excavated volume are specified as interaction nodes, as described in Section 4.3. Specifically, interaction nodes are defined at the five exterior sides of the excavated volume, and two additional horizontal planes within the excavated volume (El. -1.60 m and El. -5.91 m). Reference 2-u provides the benchmarking evaluations of the accuracy of MSM solutions relative to the corresponding solutions by the DM.

The SASSI2010 program uses finite elements with complex moduli for modeling the dynamic properties of the structure, foundation, near-field concrete fill, and the excavated volume. The model details are described in Reference 2-j and Section 4.3. Structural responses in terms of accelerations, ISRS, relative displacements, element forces, and moments are computed directly from the SASSI2010 results.

The two orthogonal horizontal components of the input motion are applied as vertically propagating shear waves. The vertical component of the input motion is applied as vertically propagating compression waves. The SSI analyses are performed separately for each one of the three directional components of input ground motion. The maximum co-directional seismic response forces, moments, accelerations and displacements for each of the three ground motion input time history components are combined using the Square Root of the Sum of the Squares (SRSS) method. The co-directional base reactions are combined using the algebraic sum method in the time domain for sliding and soil bearing evaluations.

The co-directional ISRS are combined using the SRSS method. The ISRS are developed for responses at the edges of the Firewater Storage Tanks (FWS) tank and the Fire Pump Enclosure (FPE) building by taking into account coupling effects between vertical and rocking and between lateral and torsional motions. Section 5.3 presents the procedure used for the development of ISRS.

4.2 Soil-Structure Interaction Analysis Cases

Table 4.2-1 summarizes all SSI cases analyzed for the NA3 FWSC as follows:

- Cases 1 through 6 are analyzed utilizing the FWSC $\mathbf{UC_{OBE}}$ structural model with UB stiffness properties and OBE damping to develop the NA3 site-specific seismic design basis ISRS and to calculate maximum displacements of the FWSC structures relative to free-field ground motion. Cases 1 through 3 are performed using the surface control motion input at the bottom of the FWSC basemat El. 282 ft NAVD 88. Cases 4 through 6 are performed using the in-column control motions input at the bottom of the concrete fill El. 220 ft NAVD 88.
- Cases 7 through 9 are analyzed utilizing the FWSC $\mathbf{UC_{SSE}}$ structural model with upper bound stiffness properties and SSE damping and in-column control motions input at the bottom of the concrete fill El. 220 ft NAVD 88 to develop the NA3 site-specific seismic design basis load demands on the FWSC structures and to calculate base reactions for the FWSC stability and bearing pressure evaluations.
- Cases S1 through S6 are analyzed utilizing the FWSC $\mathbf{CR_{SSE}}$ structural model with reduced (cracked) stiffness properties and SSE damping supported on the LB, UB, and BE subgrade profiles to provide responses to the concrete cracking sensitivity evaluation described in Appendix B. Cases S1 through S6 are performed using in-column control motion inputs at the bottom of the FWSC basemat and at the bottom of the concrete fill.

The frequency step and Fast Fourier Transformation (FFT) numbers used for all of the analysis cases are 0.0244 Hz and 8192, respectively. Table 4.2-2 provides a list of frequencies of analysis used for the SASSI2010 runs for the FWSC model with full (uncracked) stiffness properties. The frequencies used for the sensitivity analyses of the FWSC model with reduced (cracked) stiffness are presented in Appendix B. As described in Section 5.1, acceleration transfer function results obtained from each analysis case are inspected to ensure that selected frequencies of analyses provide numerically accurate results.

Values (of cut-off frequencies of analyses) are used that are equal to or lower than the passing frequency of the SSI model (the highest frequency of seismic waves that can be transmitted through the SSI model). The selected values of cut-off frequencies of analyses ensure that the SSI analysis provides FWSC site-specific design ISRS that, per requirements of ISG-01 (Reference 2-v), is adequate for the design and qualification of components and equipment for frequencies up to 50 Hz. As shown in Table 4.2-1, the cut-off frequencies of analyses are equal to or higher than 50 Hz for all analysis cases with the exception of the analysis of the LB subgrade profile (analysis Cases 1, 4 and 7 in Table 4.2-1) for which a cut-off frequency of 36 Hz is used.

Results of the SSI analyses presented in Section 5 (Figures 5.3-1 through 5.3-3) show that the analyses of the UB subgrade profile govern the FWSC responses at high frequencies. The cut-off frequencies used for the analyses of the UB subgrade profiles capture virtually all ($\approx$ 99%) of the input motion energy. The analyses of the BE and LB subgrade profiles use cut-off frequencies that enable the capture of at least 95% and 81% of the input motion energy, respectively. The comparisons in Section 5 of the results obtained from the set of six

analyses of the FWSC $\mathbf{UC_{OBE}}$ model with full stiffness properties and OBE damping for the different subgrade profiles show that the analyses of the UB and BE profiles provide results for maximum accelerations, member forces, and base reactions that bound the results obtained from the analyses of the LB subgrade profile (Figures 5.2-1 through 5.2-4). The UB and BE profiles also provide bounding ISRS results for frequencies higher than 25 Hz, which is at least 10 Hz lower than the lowest value of 36 Hz used as the cut-off frequency for the FWSC site-specific SSI analyses of the LB subgrade profile.

4.3 Analysis Models

The model used for the site-specific SSI analysis of the FWSC shown in Figure 4.3-1 is a half model based on the three-dimensional Lumped Mass-Stick Model (LMSM) that was used for the standard design seismic response in the DCD, which considers shear, bending, torsion, and axial deformations. This model is designated in DCD Table 3A.6-1 as the base model. The stiffness of the structural elements of the FWSC is represented by a single set of stick elements that consider the vertical and horizontal eccentricity.

The site-specific SSI model differs from the standard design base model in that:

- A block of near-field solid elements embedded in the in-situ soil and rock is used to model the concrete fill placed below the FWSC basemat
- The lower 4% OBE damping value is assigned to the reinforced concrete structure for the purpose of calculating the FWSC site-specific design ISRS per requirements of SRP 3.7.2 (Reference 2-p) and RG 1.61 (Reference 2-w)
- The rigid massless outriggers are installed at each floor elevation to facilitate calculation of ISRS and displacements at floor edges

The FWSC SSI analyses use the FWSC $\mathbf{UC_{OBE}}$ model with full (uncracked concrete) stiffness properties and OBE damping values for the reinforced concrete structures. Additional cases are performed using full (uncracked) concrete stiffness properties, 7% SSE damping values similar to DCD Section 3.A.4.2 (Reference 2-h), and input motion applied at the bottom of the concrete fill ($\mathbf{UC_{SSE}}$ model). The responses obtained from the analyses of the FWSC model with SSE damping values are used for the development of site-specific load demands on the FWSC structures and the base reaction time histories for the foundation uplift and stability evaluations.

The foundation basemat is modeled using plate elements in the same manner as the DCD SASSI analysis model. In accordance with the SASSI2010 requirement in Reference 2-z, the size of the plate element does not exceed 20% of the length of the shear wave passing through the soil material in order to capture sufficient input motion energy.

Full (uncracked concrete) stiffness properties are assigned to the LMSM elements and the basemat plate elements in the SASSI structural (HOUSE) model to ensure that the SSI analysis yields conservative results for the NA3 rock site and high frequency design motion. In accordance with the RG 1.61 (Reference 2-w) and SRP 3.7.2 (Reference 2-p) requirements, the dynamic $\mathbf{UC_{OBE}}$ model used for the development of the FWSC site-

specific ISRS is assigned OBE structural damping. The use of lower OBE structural damping values ensures that the ISRS peaks envelop the condition when the stresses and dissipation of energy in the structures are low (Section C.1.2 of Reference 2-w).

The development of site-specific seismic structural load demands, foundation uplift, and stability evaluations are based on responses obtained from the FWSC $\mathbf{UC_{SSE}}$ model with UB (uncracked concrete) stiffness properties in conjunction with SSE structural damping. Per Section C.1.2 of Reference 2-w, the use of SSE damping for the development of structural loads is adequate because the stresses obtained from models with SSE damping will remain lower than the stress limits considered by the applicable structural design codes. The use of SSE damping for the foundation uplift and stability evaluations is adequate because these analyses generate foundation reaction forces and moments at the bottom of basemat that are consistent with the seismic structural load demands generated from the FWSC $\mathbf{UC_{SSE}}$ model.

Appendix B presents the evaluation of the effects of concrete cracking on the SSI response of NA3 FWSC that is based on the results of the sensitivity analyses of the FWSC $\mathbf{CR_{SSE}}$ dynamic model with reduced structural stiffness properties representing fully cracked concrete condition, i.e., conditions where all of the concrete structural members are cracked. In this model, the effects of concrete cracking on the shear, flexural, and axial stiffness of the reinforced concrete walls are captured by reducing the section properties for the shear areas, torsional moment of inertia, and flexural moments of inertia of the stick elements by 50%. In order to simulate the full 100% axial stiffness of the cracked walls as recommended by ASCE 43-05 (Reference 2-x), the axial areas of the stick members are the same as the areas of the stick members in the licensing basis models with full (uncracked concrete) stiffness properties. SSE damping values are assigned to these models in conjunction with the reduced (cracked concrete) stiffness properties to represent the higher dissipation of energy in the structures when subjected to high stresses corresponding to the fully cracked concrete condition. The $\mathbf{CR_{SSE}}$ model used for the sensitivity study on the concrete cracking effects also has Single Degree of Freedom (SDOF) oscillators that represent the local out-of-plane vibrations of the FWS roof under cracked concrete conditions.

The standard design basis LMSM used as the basis for development of the FWSC SASSI2010 model is shown in Figure 4.3-1. Figures 4.3-2 through 4.3-4 present the SASSI2010 model used for site-specific SSI analyses. The model axes in the X-direction and Y-direction represent the north-south (NS) direction and the east-west (EW) direction of the NA3 site, respectively. These directions are referenced to plant north. Plant north for NA3 is oriented 23.54 degrees east of true north (Reference 2-b). The Z-axis represents the vertical direction.

The SASSI structural (HOUSE) model also includes the concrete fill block resting on top of the Zone III-IV rock that supports the FWSC foundation. The concrete fill that is embedded in the in-situ saprolite and Zone III rock is modeled using brick solid elements. As shown in Figures 4.3-2 through 4.3-4, the concrete fill block, as well as the excavated volume, are modeled from the top of the Zone III-IV rock at El. -16.84 m (El. 220.0 ft NAVD 88) to the bottom of the basemat foundation at El. 2.15 m (El. 282.3 ft NAVD 88). The size of the elements in all directions for the excavated volume is determined, in accordance with

SASSI2010 requirements, not to exceed 20% of the length of the shear wave passing through the soil material in order to capture sufficient input motion energy. The passing and cut-off frequencies of analysis are shown in Table 4.2-1. The passing frequencies are calculated on the basis of both the maximum horizontal and vertical dimensions of the excavated volume and backfill mesh. The table shows that the model maximum passing frequencies for all subsurface profiles are no smaller than the cut-off frequency of analysis.

The excavated volume in the FWSC NA3 site-specific SSI model has a uniform mesh. The maximum aspect ratio of the 3-D thin shell elements for the basemat is 1:1.4. The maximum aspect ratio of the 3-D solid brick elements is 1:2.9. As described in Reference 2-y, the accuracy of the SASSI2010 program has been verified and validated for models with a maximum aspect ratio of 1:4 for both the 3-D thin shell and 3-D solid brick finite elements.

The structural fill placed around the concrete fill is regarded as part of in-situ soil since the properties of in-situ soil and structural fill are similar as shown in Figure 3.1-1. Table 3.1-7 also shows that the values of the average strain-compatible shear wave velocities ($V_{s\text{-}ave}$) and shear column frequencies (f_{sc}) of the structural fill are very close to those of the in-situ saprolite. The FWSC-CB combined model used for the FWSC-CB SSSI analyses presented in Reference 2-r includes the structural fill placed in the gap between the CB and FWSC and around the concrete fill below the FWSC foundation. The inclusion of the structural fill in the combined model and the fact that the site-specific design basis for FWSC is the envelope of the FWSC SSI and FWSC-CB SSSI analysis results addresses the effects of the structural fill on the FWSC seismic response.

The soil properties used for the site-specific SSI analysis are shown in Tables 4.3-1 through 4.3-3. They consist of 50 layers on top of the half-space. The maximum value of soil Poisson's ratio considered in the site models is 0.48. It is within the range of accuracy that the SASSI2010 program has been verified and validated (Reference 2-y). The shear and compression wave velocities, unit weights, and damping ratios are not adjusted from the original strain iterated soil profiles that are listed in Tables 3.1-1 through 3.1-3. Instead, the layering of the profiles of strain-compatible properties that were developed from the results of the site response analysis is used and some layers are either combined or divided so that the site models used for site-specific SSI analyses can meet the passing frequency requirements. A graphical comparison between the adjusted soil profiles used in the SSI analyses and the corresponding strain iterated soil profiles from the site response analyses are provided in Figure 4.3-5 for shear and compression wave velocities and damping ratios. As shown, there are no differences between the SSI analyses soil profiles and the site response soil profiles.

The top of the half-space in the FWSC models is established at the DCD elevation -120.8 m (El. 126 ft., NAVD 88). Consistent with SASSI manual recommendations, the half-space simulation consists of an additional ten layers with viscous dashpots added at the base of the site finite element model to account for the dissipation of energy at the model lower boundary. The half-space model has a thickness of 1.5 V_s/f, where V_s is the shear wave velocity of the half-space and f is the frequency of the analysis. The total depth of the site model used for SSI analyses of FWSC is more than 123 m, which exceeds two times the

maximum footprint dimension of the FWSC basemat of 52 m. Results of the sensitivity study presented in Appendix H of Reference 2-cc demonstrate that the depth of the lower boundary of the site model used for the site-specific SSI analyses does not affect the results of the analysis.

As indicated in Figure 4.3-4, the FWSC stick models are connected to the basemat at El. 2.15 m (El. 282.3 ft NAVD 88) by a set of rigid beams without mass along the footprint of walls of the FWS and the FPE.

Three-dimensional (3-D) spring elements are established at the interface between the concrete fill solid elements and the FWSC basemat shell elements as well as the interface between the concrete fill elements and the surrounding in-situ soil. These spring elements are assigned global stiffness properties high enough to ensure that they do not affect the dynamic properties of the analyzed SSI system. The spring elements at the FWSC basemat and concrete fill interface provide spring force results that serve as input for the calculation of base contact pressures and foundation bearing pressure demands. The spring force results also serve as input for the calculation of seismic driving forces for the site-specific stability evaluations.

5. ANALYSIS RESULTS

This section presents the following results of the FWSC site-specific SSI analysis:

a. Acceleration transfer functions for responses at key locations from analyses of FWSC models with full stiffness properties (analysis Cases 1 through 9 in Table 4.2-1).

b. Acceleration transfer functions relative to outcrop input motion at El. 220 ft for responses at the top of the FWS and FPE LMSMs from the analyses of the FWSC model with full stiffness properties and OBE damping using deep input control motion (analysis Cases 4 through 6 in Table 4.2-1).

c. Maximum acceleration of floor lumped masses and SDOF oscillator masses from analyses of FWSC model with full stiffness properties and OBE damping (analysis Cases 1 through 6 in Table 4.2-1).

d. Maximum forces and moments of stick beam elements from the analyses of the FWSC model with full stiffness properties and OBE damping (analysis Cases 1 through 6 in Table 4.2-1).

e. Maximum displacements relative to free-field motion calculated from the results of the SSI analyses of the FWSC model with full stiffness properties and OBE damping (analysis Cases 1 through 6 in Table 4.2-1).

f. ISRS with 5% damping for responses at key locations from the analyses of FWSC model with full stiffness properties and OBE damping (analysis Cases 1 through 6 in Table 4.2-1).

g. Base contact pressures obtained from the analyses of FWSC model with full stiffness properties and SSE damping (analysis Cases 7 through 9 in Table 4.2-1).

Acceleration transfer function results for responses at FWSC key locations demonstrate sufficient accuracy of the interpolated results. The responses obtained from analyses of different soil profiles are compared to evaluate the effects of variation of soil properties and elevations of control motion on the FWSC seismic response.

The comparisons in Section 5.2 of the results of the maximum accelerations and member forces from analyses of the FWSC model with OBE damping for all subgrade profiles and the two different elevations of the input control motion show that the analyses performed using input control motion at the bottom of the concrete fill El. 220 ft NAVD 88 provide bounding results for the maximum responses of the FWSC structures. The analysis of the UB profile using deep input control motion at the bottom of the concrete fill provides bounding site-specific seismic demands on the FWSC structures. The only exception is the torsional moment demand on the FWS tank structure that is governed by the results of the analysis of the BE profile with deep input control motion at the bottom of the concrete fill. The comparisons of the 5% damped ISRS in Section 5.3 show that analyses performed using deep input control motion at the bottom of the concrete fill also provide bounding results for the FWSC ISRS at frequencies higher than 18 Hz.

The conclusions made in Section 5.2 that are based on the results from the model with OBE damping are also applicable for the model with SSE damping because, as shown by the acceleration transfer function results in Section 5.1, the structural damping has negligible effect on the frequencies of the structural peak responses and only affects the peak response amplitudes. Therefore, the development of the site-specific seismic load demands on the FWSC structures in Section 6.1 are based on the envelope of the maximum force and acceleration results obtained from the SSI analyses of the model with full (uncracked concrete) properties and SSE damping using the in-column control motion that is input at the bottom of the concrete fill El. 220 ft NAVD 88 (analysis Cases 7 through 9 in Table 4.2-1). The envelope of the results from the set of six analyses performed on the FWSC model with full (uncracked concrete) stiffness properties and OBE damping (analysis Cases 1 through 6 in Table 4.2-1) are used for development of the FWSC site-specific ISRS as described in Section 6.2.

5.1 Transfer Function

Figures 5.1-1(a through d) through 5.1-9(a through d) present plots of the amplitudes of the acceleration transfer functions obtained from the SASSI2010 analyses of the FWSC $\mathbf{UC_{SSE}}$ and $\mathbf{UC_{OBE}}$ models (analysis Cases 1 through 9 in Table 4.2-1) for the responses at the following key locations within the FWSC:

Location	Node Number	SASSI Model Node Number
FWS Wall Top	9	209
FWS Base	1	201
FPE Top	405	405
FPE Base	404	404

Figures 5.1-1 through 5.1-6 present plots of the amplitudes of the acceleration transfer functions from the analyses of the FWSC $\mathbf{UC_{OBE}}$ model with full structural stiffness properties and OBE damping for the BE, LB, and UB profiles, respectively. Figures 5.1-1 through 5.1-3 present the results from the analyses of the $\mathbf{UC_{OBE}}$ model with surface input motion at the bottom of FWSC basemat El. 282ft NAVD 88 (analysis Cases 1 through 3 in Table 4.2-1). Figures 5.1-4 through 5.1-6 present plots of the amplitudes of the acceleration transfer functions from analyses of the $\mathbf{UC_{OBE}}$ model with surface input motion applied at the bottom of the concrete fill at El. 220 ft NAVD 88 (analysis Cases 4 through 6 in Table 4.2-1). The acceleration transfer function results from the analyses of the $\mathbf{UC_{SSE}}$ model with full (uncracked concrete) stiffness properties and SSE damping for the BE, LB, and UB profiles are presented in Figures 5.1-7 through 5.1-9, respectively. Each figure contains four sets of plots (a through d) presenting responses of the four key locations listed above. Each set includes three plots presenting the FWSC response in the three orthogonal directions due to the three earthquake components.

The computed values of the transfer function in Figures 5.1-1 through 5.1-6 are depicted with dots. The interpolated values of the transfer functions are depicted by solid lines. The plots show that the interpolated transfer functions generally have no numerical anomalies (e.g., sharp narrow spikes) that can potentially impact the accuracy of the frequency domain SSI analyses results. By including additional frequencies of analysis, it was determined in Reference 2-ee that the isolated anomalies in the transfer function interpolation do not affect the accuracy of the calculated responses.

The transfer function plots indicate that the co-directional responses (the responses in the direction of the applied earthquake) govern the seismic response of the FWSC at the NA3 rock site. Figures 5.1-1 (b and d) through 5.1-3 (b and d) present the transfer function results from the analyses of the BE, LB, and UB profiles for the response of the FWSC basemat. The most pronounced cross-directional responses of the FWSC basemat can be observed in the transfer function results in Figures 5.1-1(b) through 5.1-3(b) for the vertical response due to the NS (X) component of the earthquake and the NS response due to the vertical component of the earthquake that represent the rocking of the FWS foundation in the NS direction. This is expected behavior since the two FWSs are located separately in the NS direction. The analysis of the LB profile yields the largest amplitudes of the cross-directional transfer functions presented in Figure 5.1-2(b) representing the FWS basemat response in the NS direction due to the vertical earthquake and FWS basemat response in vertical direction due to the NS component of the input motion. This indicates that the softer subgrade amplifies the rocking response of the FWSC basemat in the NS direction. The transfer functions in Figures 5.1-1 through 5.1-3 for the response of the FWSC structures in the NS direction due to the EW earthquake component and the response in the EW direction due to the NS earthquake component show that the torsional response of the FWS and FPE structures are negligibly small.

The only difference that can be observed between the transfer function results obtained from the analyses of the $\mathbf{UC_{OBE}}$ model presented in Figures 5.1-4 through 5.1-6 and those obtained from the $\mathbf{UC_{SSE}}$ model presented in Figures 5.1-7 through 5.1-9 is in the amplitudes

of the transfer functions peaks. This indicates that the different damping values assigned to the FWSC structures affect only the amplitude of the peak responses and have no effect on the frequencies where the peaks of the transfer function occur.

As expected, the horizontal transfer functions in Figures 5.1-4 through 5.1-9 obtained from the analyses of the FWSC $\mathbf{UC_{OBE}}$ and $\mathbf{UC_{SSE}}$ models with deep input control motion at El. 220 ft NAVD 88 are characterized with peaks at the frequencies that are close to the shear column frequencies of the in-situ subgrade materials around the concrete fill block listed in Table 3.1-7. These frequencies are close to the frequencies where dips occur in the response spectra of the input in-layer acceleration time histories presented in Figures 3.2-1 to 3.2-3. Therefore, these large peaks in the acceleration transfer functions that represent the response amplifications relative to in-column input motion are not reflected in the ARS results presented in Section 5.3.

The large peaks at soil column frequencies are not present in the transfer functions that represent the structural responses relative to the input outcrop motion, which makes them better indicators of structural responses obtained from the FWSC analyses with deep input control motion. These outcrop transfer functions are calculated in the following three steps:

1. FFTs are performed on the time histories of in-layer and outcrop ground motions at the bottom of the concrete fill El. 220 ft NAVD 88.
2. The ratio between the outcrop motions and in-layer Fourier spectra yields transfer functions representing the transformation of the FWSC deep in-layer motion into an outcrop motion.
3. The product of the complex in-layer/outcrop transfer functions and the SASSI2010 calculated complex transfer functions of the structural response relative to in-column motion provide the outcrop motion transfer functions.

Reference 2-bb documents the calculations of the transfer functions relative to the outcrop motion.

Figure 5.1-10 presents the transfer functions representing the transformation of the horizontal and vertical in-layer motion acceleration time histories used as input for the SSI analysis of the LB, BE, and UB profiles with deep input control motion at El. 220 ft NAVD 88 (analysis Cases 4 through 9 in Table 4.2-1) into outcrop motion time histories. The first valleys in the horizontal motion in-layer/outcrop transfer functions occur at frequencies close to the embedment shear column frequencies listed in Table 3.1-7.

Figures 5.1-11 and 5.1-12 present, with dashed lines, the outcrop transfer functions amplitude for the co-directional responses at the top of NS (X), EW (Y), and vertical (Z) directions obtained from the SSI analysis of the FWSC $\mathbf{UC_{OBE}}$ model with deep input motion at El. 220 ft NAVD 88 for the LB, BE and UB subgrade profiles (analysis Cases 4 through 6 in Table 4.2-1). The plots compare these outcrop transfer function results with the transfer function results obtained from the analyses of the $\mathbf{UC_{OBE}}$ model with surface input motion for the LB, BE, and UB subgrade profiles (analysis Cases 1 through 3 in Table 4.2-1). These transfer functions that are presented with solid lines in Figures 5.1-11 and 5.1-12

are obtained directly from the SASSI2010 MOTION module. The plots also show, with solid and dashed lines, the spectra of the outcrop design motion at El. 282 ft and El. 220 ft NAVD 88, respectively.

The comparisons in Figure 5.1-11 show that:

- The variation of subgrade properties affects the response of the FWSC by shifting the peak responses to higher frequencies as the stiffness of the subgrade increases.
- The outcrop transfer functions obtained from the analyses with deep control motion at El. 220 ft NAVD88 are with higher peak amplitudes than those calculated from the analyses with surface input motion reflecting the amplification of the response as the seismic waves propagate through the block of concrete fill.
- The peak horizontal SSI responses of the FWSC structures occur at frequencies between 8 and 14 Hz. The peak vertical SSI responses occur at frequencies higher than 20 Hz.
- The largest peak amplitudes in the transfer functions at frequencies close to the peaks of the input motion spectra are obtained from the analysis of the UB subgrade profile with the deep control motion at El. 220 ft NAVD 88 thus indicating that this analysis yields bounding responses for the FWSC structures.

5.2 Maximum Accelerations and Member Forces

Appendix A provides tables with the results for the FWS and FPE maximum accelerations and member forces that are obtained from the SSI analysis of the FWSC models with full stiffness properties (analysis Cases 1 through 9 in Table 4.2-1). Plots of maximum accelerations and maximum stick member shear forces and torsional moments obtained from the analyses of the FWSC $\mathbf{UC_{OBE}}$ model with full stiffness properties and OBE damping (analysis Cases 1 to 6 in Table 4.2-1) are presented herein to illustrate the effect of different subgrade conditions and input motion control point elevations on the FWSC maximum responses.

Figures 5.2-1 (a and b) and 5.2-2 (a and b) present comparisons of the results of the analyses of LB, BE, and UB subgrade profiles for maximum absolute accelerations at FWS and FPE lumped mass locations, respectively. Figures 5.2-1(a) and 5.2-2(a) compare the results obtained from the analyses with surface input motion at El. 282 ft NAVD 88 (analysis Cases 1 through 3 in Table 4.2-1). Figures 5.2-1(b) and 5.2-2(b) compare the results obtained from the analyses with deep input motion at El. 220 ft NAVD 88 (analysis Cases 4 through 6 in Table 4.2-1). Table 5.2-1 compares the maximum accelerations results for the FWSC SDOF oscillators representing the out-of-plane response of the FWS roof and the horizontal responses of the sloshing and impulsive hydrodynamic modes of vibration of the water contained in the FWS tank.

Figures 5.2-3 (a and b) and 5.2-4 (a and b) present comparisons of the maximum shear forces and torsional moments on the FWS and FPE structures obtained from the analyses of FWSC $\mathbf{UC_{OBE}}$ model for LB, BE, and UB subgrade profiles. Figures 5.2-3(a) and 5.2-4(a) compare the results obtained from the analyses with surface input motion at El. 282 ft NAVD 88

(analysis Cases 1 through 3 in Table 4.2-1). Figures 5.2-3(b) and 5.2-4(b) compare the results obtained from the analyses with deep input motion at El. 220 ft NAVD 88 (analysis Cases 4 through 6 in Table 4.2-1).

The comparisons in Figures 5.2-1 through 5.2-4 show that the analysis of UB subgrade profile with deep input control motion (analysis Case 6 in Table 4.2-1) governs the maximum responses of the FWSC structures with the exception of torsional moment demand on the FWS that are governed by the analysis of the BE profile with deep input motion at El. 220 ft NAVD 88 (analysis Case 5 in Table 4.2-1). The comparisons in Table 5.2-1 show that the analysis Case 6 also governs the maximum responses of the FWSC SDOF oscillators.

Figures 5.2-5 (a and b) and 5.2-6 (a and b) compare the envelope of the results obtained from the analysis with surface and deep input motions to illustrate how different elevations of the input motion affect the FWS and FPE maximum accelerations and member forces. The comparisons show that the high frequency content of the input motion transmitted through the concrete fill block resulted in significantly higher results for the FWS and FPE maximum accelerations and forces.

The observations made from the comparisons of maximum acceleration and member force responses are consistent with the outcrop transfer function results in Section 5.1. The conclusions made in these subsections that are based on the results from the $\mathbf{UC_{OBE}}$ model with full stiffness properties and OBE damping are also applicable for the $\mathbf{UC_{SSE}}$ model with full stiffness properties and SSE damping because, as discussed in Section 5.1, the structural damping has negligible effect on the frequencies of the structural peak responses.

5.3 Acceleration Response Spectra

This section presents comparisons of the 5% damped ARS results for the responses at the same selected locations within the FWSC as the ones listed in Section 5.1 for the transfer functions and some selected slab oscillators. These spectra are obtained from the analyses of the $\mathbf{UC_{OBE}}$ model for the LB, BE, and UB subgrade profiles using surface and deep input control motions at El. 282 ft and El. 220 ft NAVD 88, respectively.

The following is the procedure used for the development of the floor ISRS:

1. For each of the four outrigger locations (ne, nw, se, sw) at particular floor elevations, three components (X, Y, and Z) of the ARS, due to input motion in three directions (X, Y, and Z), are calculated by the SASSI MOTION module to obtain a total of 36 ARS results:

$$\text{Outrigger}^{(ne)} \rightarrow (f_{XX}^{(ne)}, f_{XY}^{(ne)}, f_{XZ}^{(ne)}, f_{YX}^{(ne)}, f_{YY}^{(ne)}, f_{YZ}^{(ne)}, f_{ZX}^{(ne)}, f_{ZY}^{(ne)}, f_{ZZ}^{(ne)})$$

$$\text{Outrigger}^{(nw)} \rightarrow (f_{XX}^{(nw)}, f_{XY}^{(nw)}, f_{XZ}^{(nw)}, f_{YX}^{(nw)}, f_{YY}^{(nw)}, f_{YZ}^{(nw)}, f_{ZX}^{(nw)}, f_{ZY}^{(nw)}, f_{ZZ}^{(nw)})$$

$$\text{Outrigger}^{(se)} \rightarrow (f_{XX}^{(se)}, f_{XY}^{(se)}, f_{XZ}^{(se)}, f_{YX}^{(se)}, f_{YY}^{(se)}, f_{YZ}^{(se)}, f_{ZX}^{(se)}, f_{ZY}^{(se)}, f_{ZZ}^{(se)})$$

$$\text{Outrigger}^{(sw)} \rightarrow (f_{XX}^{(sw)}, f_{XY}^{(sw)}, f_{XZ}^{(sw)}, f_{YX}^{(sw)}, f_{YY}^{(sw)}, f_{YZ}^{(sw)}, f_{ZX}^{(sw)}, f_{ZY}^{(sw)}, f_{ZZ}^{(sw)})$$

where f_{ij} represent ARS in j-direction due to earthquake in i-direction.

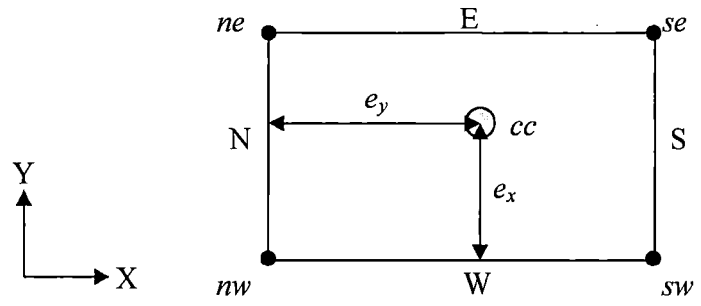

2. The spectra for the nodal responses, due to the three input motion components in the X, Y, and Z directions, are combined using the SRSS method to obtain a total of 12 ARS of the response of each of the four outrigger nodes (ne, nw, se, sw) in three orthogonal directions (X, Y, and Z):

$$f_X^{(ne)} = \sqrt{f_{XX}^{(ne)2} + f_{YX}^{(ne)2} + f_{ZX}^{(ne)2}} \quad , \quad f_Y^{(ne)} = \sqrt{f_{XY}^{(ne)2} + f_{YY}^{(ne)2} + f_{ZY}^{(ne)2}}$$

$$f_Z^{(ne)} = \sqrt{f_{XZ}^{(ne)2} + f_{YZ}^{(ne)2} + f_{ZZ}^{(ne)2}}$$

$$f_X^{(nw)} = \sqrt{f_{XX}^{(nw)2} + f_{YX}^{(nw)2} + f_{ZX}^{(nw)2}} \quad , \quad f_Y^{(nw)} = \sqrt{f_{XY}^{(nw)2} + f_{YY}^{(nw)2} + f_{ZY}^{(nw)2}}$$

$$f_Z^{(nw)} = \sqrt{f_{XZ}^{(nw)2} + f_{YZ}^{(nw)2} + f_{ZZ}^{(nw)2}}$$

$$f_X^{(se)} = \sqrt{f_{XX}^{(se)2} + f_{YX}^{(se)2} + f_{ZX}^{(se)2}} \quad , \quad f_Y^{(se)} = \sqrt{f_{XY}^{(se)2} + f_{YY}^{(se)2} + f_{ZY}^{(se)2}}$$

$$f_Z^{(se)} = \sqrt{f_{XZ}^{(se)2} + f_{YZ}^{(se)2} + f_{ZZ}^{(se)2}}$$

$$f_X^{(sw)} = \sqrt{f_{XX}^{(sw)2} + f_{YX}^{(sw)2} + f_{ZX}^{(sw)2}} \quad , \quad f_Y^{(sw)} = \sqrt{f_{XY}^{(sw)2} + f_{YY}^{(sw)2} + f_{ZY}^{(sw)2}}$$

$$f_Z^{(sw)} = \sqrt{f_{XZ}^{(sw)2} + f_{YZ}^{(sw)2} + f_{ZZ}^{(sw)2}}$$

3. The ARS calculated for each outrigger location are enveloped to obtain the three ARS for the floor response in three orthogonal directions (X, Y, and Z):

$$F_X = max(f_X^{(ne)}, f_X^{(nw)}, f_X^{(se)}, f_X^{(sw)})$$

$$F_Y = max(f_Y^{(ne)}, f_Y^{(nw)}, f_Y^{(se)}, f_Y^{(sw)})$$

$$F_Z = max(f_Z^{(ne)}, f_Z^{(nw)}, f_Z^{(se)}, f_Z^{(sw)})$$

4. The calculations in steps 1 to 3 are performed for each of the six SSI analysis cases considered. The final site-specific design ISRS is calculated by broadening the envelope of the ARS results of the six FWSC SSI analysis cases and the six FWSC-CB SSSI analysis cases as presented in Section 6.3.

5. The calculations in steps 1 to 4 are performed for each ISRS damping value.

The following is the procedure for the development of ISRS for the out-of-plane response of FWS roof:

1. For each SDOF oscillator, the ARS of the SDOF response, due to the input motion in three directions (X, Y, and Z), are calculated by the SASSI MOTION module to obtain a total of three ARS results:

   SDOF $\rightarrow (f_{XZ}, f_{YZ}, f_{ZZ})$

2. The spectra for the SDOF responses due to the three input motion components in the X, Y, and Z directions are combined using the SRSS method to obtain:

   SDOF $\rightarrow \quad f_Z^{(SDOF)} = \sqrt{f_{XZ}^{\ 2} + f_{YZ}^{\ 2} + f_{ZZ}^{\ 2}}$

3. The calculations in steps 1 and 2 are performed for each of the six SSI analysis Cases 1 through 6 in Table 4.2-1. The final site-specific design SDOF ISRS is calculated by broadening the envelope of the ARS results of the six FWSC SSI analysis cases and the six FWSC-CB SSSI analysis cases as presented in Section 6.3.

Figures 5.3-1 (a through d), Figures 5.3-2 (a through d), and Figures 5.3-3 (a through d), respectively, present the 5% damped ISRS for the response in NS(X), EW(Y), and vertical (Z) directions at the four key locations within the FWSC. Appendix F presents the 5% damped ISRS for the responses of SDOF mass representing the out-of-plane response of the FWS roof. The figures present the ISRS obtained from the analyses with surface input motion at El. 282 ft NAVD 88 (analysis Cases 1 to 3 in Table 4.2-1) with solid lines. The ISRS obtained from the analyses with deep input motion at El. 220 ft NAVD88 (analysis Cases 4 to 6 in Table 4.2-1) is presented with dashed lines. The site-specific ISRS are compared with the corresponding standard design ISRS that is presented with solid black lines.

The comparison of the ISRS results obtained from the different site-specific SSI analyses shows that the responses obtained from the analyses with deep input motion at El. 220 ft NAVD 88 govern the horizontal and vertical ISRS for frequencies higher than 10 Hz and 18 Hz, respectively. The analyses with surface input motion at El. 282 ft NAVD88 (analysis Case 1 in Table 4.2-1) govern the ISRS at frequencies lower than 9 Hz.

The comparisons in Figure 5.3-1, Figure 5.3-2, and Figure 5.3-3 indicate that the FWSC site-specific ISRS can exceed the corresponding standard design spectra. Large exceedances can be observed in the site-specific ISRS for the EW response of the FWSC basemat and the FPE at frequencies between 5 and 15 Hz. The exceedance in the FWS roof SDOF oscillator ISRS presented in Appendix F occurs at frequencies corresponding to the frequencies of the oscillator.

The ISRS exceedances are due to the higher energy content of the NA3 site-specific design motion than to the standard design Certified Seismic Design Response Spectra (CSDRS) at mid-range frequencies and due to the lower OBE structural damping values used for the site-specific SSI analyses versus the SSE damping values used for the standard design SSI

analyses. Such exceedances will be considered in the site-specific design for NA3 as will be further described in Section 6.

5.4 Maximum Relative Displacements

The following is the procedure used for development of the maximum floor displacements relative to the free-field motion:

1. For each of the four outrigger locations (ne, nw, se, sw) at particular floor elevations, three components (X, Y, and Z) of maximum relative displacements due to the input motion in three directions (X, Y, and Z) are calculated by the SASSI MOTION module to obtain a total of 36 maximum relative displacement values:

   $\text{Outrigger}^{(ne)} \rightarrow (d_{XX}^{(ne)}, d_{XY}^{(ne)}, d_{XZ}^{(ne)}, d_{YX}^{(ne)}, d_{YY}^{(ne)}, d_{YZ}^{(ne)}, d_{ZX}^{(ne)}, d_{ZY}^{(ne)}, d_{ZZ}^{(ne)})$

   $\text{Outrigger}^{(nw)} \rightarrow (d_{XX}^{(nw)}, d_{XY}^{(nw)}, d_{XZ}^{(nw)}, d_{YX}^{(nw)}, d_{YY}^{(nw)}, d_{YZ}^{(nw)}, d_{ZX}^{(nw)}, d_{ZY}^{(nw)}, d_{ZZ}^{(nw)})$

   $\text{Outrigger}^{(se)} \rightarrow (d_{XX}^{(se)}, d_{XY}^{(se)}, d_{XZ}^{(se)}, d_{YX}^{(se)}, d_{YY}^{(se)}, d_{YZ}^{(se)}, d_{ZX}^{(se)}, d_{ZY}^{(se)}, d_{ZZ}^{(se)})$

   $\text{Outrigger}^{(sw)} \rightarrow (d_{XX}^{(sw)}, d_{XY}^{(sw)}, d_{XZ}^{(sw)}, d_{YX}^{(sw)}, d_{YY}^{(sw)}, d_{YZ}^{(sw)}, d_{ZX}^{(sw)}, d_{ZY}^{(sw)}, d_{ZZ}^{(sw)})$

   where d_{ij} represents displacement in j-direction due to earthquake in i-direction.

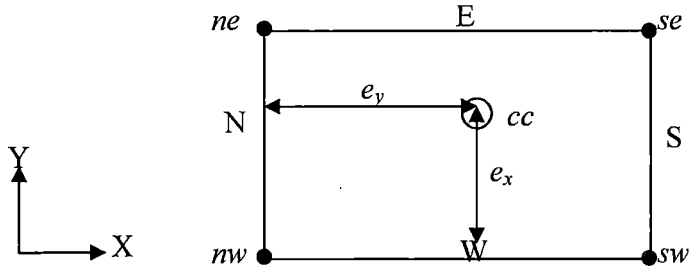

2. The nodal displacements due to the three input motion components in the X, Y, and Z directions are combined using the SRSS method to obtain a total of twelve values of the maximum displacements of each of the four outrigger nodes (ne, nw, se, sw) in three orthogonal directions (X, Y, and Z):

$$d_X^{(ne)} = \sqrt{d_{XX}^{(ne)2} + d_{YX}^{(ne)2} + d_{ZX}^{(ne)2}}, \quad d_Y^{(ne)} = \sqrt{d_{XY}^{(ne)2} + d_{YY}^{(ne)2} + d_{ZY}^{(ne)2}}$$

$$d_Z^{(ne)} = \sqrt{d_{XZ}^{(ne)2} + d_{YZ}^{(ne)2} + d_{ZZ}^{(ne)2}}$$

$$d_X^{(nw)} = \sqrt{d_{XX}^{(nw)2} + d_{YX}^{(nw)2} + d_{ZX}^{(nw)2}}, \quad d_Y^{(nw)} = \sqrt{d_{XY}^{(nw)2} + d_{YY}^{(nw)2} + d_{ZY}^{(nw)2}}$$

$$d_Z^{(nw)} = \sqrt{d_{XZ}^{(nw)2} + d_{YZ}^{(nw)2} + d_{ZZ}^{(nw)2}}$$

$$d_X^{(se)} = \sqrt{d_{XX}^{(se)2} + d_{YX}^{(se)2} + d_{ZX}^{(se)2}}, \quad d_Y^{(se)} = \sqrt{d_{XY}^{(se)2} + d_{YY}^{(se)2} + d_{ZY}^{(se)2}}$$

$$d_Z^{(se)} = \sqrt{d_{XZ}^{(se)2} + d_{YZ}^{(se)2} + d_{ZZ}^{(se)2}}$$

$$d_X^{(sw)} = \sqrt{d_{XX}^{(sw)2} + d_{YX}^{(sw)2} + d_{ZX}^{(sw)2}} \quad , \quad d_Y^{(sw)} = \sqrt{d_{XY}^{(sw)2} + d_{YY}^{(sw)2} + d_{ZY}^{(sw)2}}$$

$$d_Z^{(sw)} = \sqrt{d_{XZ}^{(sw)2} + d_{YZ}^{(sw)2} + d_{ZZ}^{(sw)2}}$$

3. The maximum displacements calculated for each outrigger location are enveloped to obtain the maximum displacements of the floor in the X, Y, and Z directions:

   $D_X = max(d_X^{(ne)}, d_X^{(nw)}, d_X^{(se)}, d_X^{(sw)})$

   $D_Y = max(d_Y^{(ne)}, d_Y^{(nw)}, d_Y^{(se)}, d_Y^{(sw)})$

   $D_Z = max(d_Z^{(ne)}, d_Z^{(nw)}, d_Z^{(se)}, d_Z^{(sw)})$

4. The calculations in steps 1 to 3 are performed for each of the six SSI analysis cases considered. The final site-specific values of the design maximum displacements of the floor relative to the free-field motion are obtained as the envelope of results of the six FWSC SSI analysis cases and the six FWSC-CB analysis cases, as described in Section 6.2.

Appendix A presents the results of the site-specific SSI analyses of the FWSC $\mathbf{UC_{OBE}}$ model with full (uncracked concrete) stiffness properties and OBE damping values (Cases 1 through 6 in Table 4.2-1) for the maximum displacements of FWSC structures relative to the free-field motion. Table 5.4-1 presents the maximum displacements of the FWSC SDOF oscillators relative to the free-field motion obtained from the analyses Cases 1 through 6 in Table 4.2-1.

5.5 Base Reactions and Contact Pressures

The results of the FWSC site-specific SSI analyses for contact spring forces are also used to calculate the time histories of the seismic driving forces used as input for the sliding stability evaluations and dynamic bearing pressure calculations documented in Reference 2-s. The time histories of the horizontal and vertical driving seismic forces in the three orthogonal directions are calculated as the algebraic sum of the spring forces in the three directions at each time step from all contact spring elements located at the interfaces between the FWSC basemat and the supporting concrete fill. The sum of the contact forces results from the springs located at the bottom surface and four vertical surfaces of the concrete fill block and provides the input used for the evaluation of the sliding stability at the other critical sliding plane located at the concrete fill / Zone III-IV rock interface at nominal El. 220 ft NAVD 88.

The contact spring elements located at the bottom of the FWSC basemat provide the input needed for the calculation of the dynamic bearing pressures in Reference 2-s. The calculations of the dynamic bearing pressures are based on the time histories of:

- The overturning base moments that are calculated for the two horizontal directions by summing the moments generated by each contact spring reaction at the FWSC basemat bottom

- The vertical driving seismic forces that are calculated as the algebraic sum of the vertical spring forces at each time step from all contact spring elements located at the interface between the FWSC basemat bottom and the supporting concrete fill.

The time histories of the vertical spring forces obtained from the contact springs located at the bottom of the FWSC basemat are also used to develop the base contact pressure plots that are used to calculate the minimum base contact area. The FWSC foundation uplift calculations are performed using the results of the three SSI analyses of the FWSC model with full (uncracked concrete) stiffness properties and SSE damping for the LB, BE, and UB subgrade profiles using input motion applied at the bottom of concrete fill El. 220 ft (analysis Cases 7 to 9 in Table 4.2-1). These are the analyses cases that provide the site-specific enveloping seismic load demands on FWSC structures as discussed in Section 5.2. The calculations are performed for each of the three critical soil cases in the following steps:

1. Extract the FWSC basemat bottom contact spring vertical forces $P^i_{jZ}(t)$ at each time step from the SASSI runs, where j (=*X, Y* and *Z*) is the input excitation direction and *i* is the contact spring element number. The total vertical seismic base reaction is calculated as:

$$S_Z(t) = \sum_{i=1}^{N} (P^i_{XZ}(t) + P^i_{YZ}(t) + P^i_{ZZ}(t))$$

where, *N* is the total number of the contact spring elements located at the FWSC basemat bottom.

2. Calculate the total vertical base reaction as:

$$R_V(t) = D - B - S_Z(t)$$

where, *D* is the FWSC seismic weight and *B* is the groundwater buoyancy force.

3. Calculate the overturning moments toward the NS and EW direction induced by the vertical seismic base reaction as follows:

$$M_{NS}(t) = \sum_{i=1}^{N} \left(P^i_{XZ}(t) + P^i_{YZ}(t) + P^i_{ZZ}(t)\right) * X_i$$

$$M_{EW}(t) = \sum_{i=1}^{N} \left(P^i_{XZ}(t) + P^i_{YZ}(t) + P^i_{ZZ}(t)\right) * Y_i$$

where, *Xi* and *Yi* are the NS and EW directional coordinates of the contact spring location in the coordinate system with origin at the geometrical center of the basemat, respectively.

4. Calculate the time histories of base reaction eccentricity as:

$$Ecc(t) = \frac{1}{R_V(t)} \sqrt{M_{NS}(t)^2 + M_{EW}(t)^2}$$

5. The critical time step when the maximum uplift of the FWSC basemat occurs is determined as the time instance when the value of the base reaction eccentricity *Ecc(t)* is the largest.

6. The plot of the base contact area is developed using the base spring force results at the critical time step that yields the maximum value for base eccentricity.

7. The base contact pressures on the tributary area of the spring element i are calculated by dividing the base spring forces by its tributary area and then subtracting the uniform static pressure due to the effective weight of the building (the FWSC seismic weight minus the ground water buoyancy) as follows:

$$\sigma_{iz} = \frac{P_{XZ}^{i}(t_c) + P_{YZ}^{i}(t_c) + P_{ZZ}^{i}(t_c)}{A_i} - \frac{D-B}{A}$$

where A is the footprint area of the basemat and A_i is the tributary area of the spring element *i*. The positive value of σ_{iz} indicates that the tributary area is in tension, or uplifted.

8. The contact area of the foundation is determined as the area where the value of the contact pressure σ_{iz} is negative.

The configuration of the FWSC structures and model are nearly symmetrical with respect to both the NS (X) and EW(Y) direction vertical planes, so the effect of different phasing of the X and Y input motions in the calculation of the contact area is insignificant. Therefore, the contact ratio calculations are performed considering the following two combinations of input motion directions:

a) $R_D+R_B+Ex+Ey+Ez$

b) $R_D+R_B-Ex-Ey-Ez$

Figures 5.5-1 and 5.5-2 present the time histories of the eccentricities of vertical base reactions obtained from the SSI analyses of the FWSC $\mathbf{UC}_{\mathbf{SSE}}$ model with full stiffness properties and SSE damping for the LB, BE, and UB profiles (analysis Cases 7 to 9 in Table 4.2-1) for the two combinations of input motion directions being considered. The critical instances of time when the eccentricity of the vertical base reaction has maximum value are identified with red lines. Table 5.5-1 summarizes, for each critical analysis case, the calculations of maximum base reaction eccentricities and minimum contact area. It shows that the analysis of the BE profile (analysis Case 8 in Table 4.2-1) yields the minimum value for the foundation contact area for the +Ex+Ey+Ez combination of input motion directions.

Figure 5.5-3 presents a contour plot of the SASSI2010 base contact pressure results for the analysis of the most critical BE profile at the critical instance of time t = 1.155 sec when the uplift of FWSC basemat is the largest. The positive values of the contact pressures in the

figures represent tension of the base contact springs. The negative values represent compression of the base contact springs and are used to determine the portion of the basemat that is in contact with the underlying subgrade. The plots in Figure 5.5-3 show that the contact area between the FWSC basemat and the underlying concrete fill remains larger than 85%. Therefore, the minimum base contact area is larger than 80% which, per guidance of SRP 3.7.2 (Reference 2-p), ensures that the possible uplift of the FWSC basemat has negligible effect on the FWSC seismic response and results of site-specific FWSC SSI analyses documented in this report and performed on linear elastic models.

As shown in Figure 4.3-4, rigid beams connect the nodes of the FWSC basemat located around the base of the FWS and FPE structures. These rigid beams ensure that the FWSC dynamic model adequately represents the in-plane stiffness contribution of the FWS and FPE walls on the overall stiffness of the basemat. Therefore, the SASSI2010 results presented in Figure 5.5-3 provide an adequate distribution of the base contact pressures used for calculations of the uplift area.

6. ENVELOPING SEISMIC RESPONSES

The envelopes of results from the site-specific SSI analyses of the FWSC models with full stiffness properties and OBE damping values (Cases 1 through 6 in Table 4.2-1) and SSE damping values (Cases 7 through 9 in Table 4.2-1) are compared with the corresponding standard design envelopes documented in Reference 2-j in order to determine any exceedances of the NA3 site-specific seismic demands relative to the corresponding standard design seismic demands.

The site-specific enveloping seismic responses presented in this section form the basis for seismic design and evaluation of the FWSC at the NA3 site. The site-specific SSSI evaluation documented in Reference 2-r shows that the responses obtained from the SSI analysis of the standalone FWSC models presented in this report do not envelop the SSSI effects of the CB on the FWSC seismic response. Therefore, the results of the site-specific SSI analyses of the FWSC standalone models presented in Section 5 are used together with the corresponding results of the site-specific SSSI analyses of the FWSC-CB combined model presented in Section 6.0 of Reference 2-r to develop the bases for the site-specific design and evaluation of the NA3 FWSC.

6.1 Enveloping Structural Load Demands

The site-specific seismic structural loads representative of the seismic demands on the FWSC structures are developed following the methodology used to develop the standard design enveloping maximum structural loads presented in Reference 2-j. The horizontal load demands on the FWSC structures are developed from the diagrams of the maximum enveloping shear forces and maximum enveloping torsional moments. The vertical site-specific seismic load demands on the FWSC structures are developed from the diagrams of the maximum enveloping vertical floor mass accelerations. The maximum enveloping bending moments are also used for the structural evaluation of the FWSC to account for the effects of floor rocking on the wall axial forces. The maximum enveloping vertical

acceleration of the SDOF oscillator mass at the top of the FWS LMSM is used to develop the local out-of-plane load demands on the FWS roof.

The site-specific enveloping seismic load demands on the FWSC structures are developed as an envelope of the results for maximum member forces and vertical accelerations obtained from the SSI and SSSI analyses of the FWSC standalone and the FWSC-CB combined models with full (uncracked concrete) stiffness properties and SSE damping using deep input control motion applied at the bottom of the concrete fill at El. 220 ft NAVD 88. The comparisons presented in Section 5.2 of the maximum responses obtained from the site–specific SSI analyses of the FWSC model with full stiffness properties and OBE damping showed that the analyses with deep input motions yield maximum response results that envelope the results of the analyses with surface input motion at El. 282 ft NAVD 88. The same conclusion was derived in Section 6.2 of Reference 2-r based on the comparisons of the maximum responses obtained from the site-specific SSSI analyses of the FWSC-CB combined model with full stiffness properties and OBE damping.

Table 6.1-1 presents the envelope of results for maximum member forces and moments obtained from the site-specific FWSC SSI analyses of the FWSC model with full (uncracked concrete) stiffness properties and SSE damping (analysis Cases 7 to 9 in Table 4.2-1). These results are enveloped with the corresponding results of the SSSI analysis of the FWSC-CB combined model with full stiffness properties and SSE damping (analysis Cases FC7 to FC9 in Table 4.2-2 of Reference 2-r) to obtain the enveloping maximum forces and moments that represent the site-specific seismic load demands on the FWSC structures at the NA3 site. The torsional moments in these tables and similar tables in the appendices are the calculated results from the SSI analyses. They need to be combined with the accidental torsion in the structural evaluation. In Table 6.1-2, the amplitudes of the site-specific enveloping maximum member forces and moments are compared with the corresponding standard design values presented in Reference 2-j.

Table 6.1-3 presents the envelope of results for maximum accelerations at the FWSC lumped mass locations obtained from the site-specific FWSC SSI analyses of the FWSC model with full stiffness properties and SSE damping (analysis Cases 7 to 9 in Table 4.2-1). These results are enveloped with the corresponding results of the site-specific SSSI analysis of the FWSC-CB combined model with full stiffness properties and SSE damping (analysis Cases FC7 to FC9 in Table 4.2-2 of Reference 2-r) to obtain the site-specific enveloping maximum accelerations at the FWSC lumped mass locations. Table 6.1-4 presents the comparison of these site-specific enveloping maximum accelerations with the corresponding standard design enveloping accelerations.

Table 6.1-5 presents the envelope of results for maximum accelerations of the FWSC SDOF oscillators obtained from the site-specific FWSC SSI analyses of the FWSC model with full stiffness properties and SSE damping (analysis Cases 7 to 9 in Table 4.2-1). These results are enveloped with the corresponding results from the FWSC-CB SSSI analysis (Cases FC7 through FC9 in Reference 2-r) to obtain enveloping maximum accelerations used for the calculation of the site-specific out-of-plane seismic loads on the FWS roof and the site-specific hydrodynamic seismic loads from the water contained in the FWS tank. Table 6.1-5

also presents a comparison of the site-specific enveloping maximum accelerations of the FWSC SDOF oscillators with the corresponding standard design values.

Table 6.1-6 presents the calculations of the equivalent average acceleration representing the out-of-plane seismic load demand on the FWS roof. The site-specific out-of-plane seismic load on FWSC roof is calculated based on the results of the FWSC SSI analyses and the FWSC-CB SSSI analysis of models with full stiffness properties and SSE damping for enveloping maximum vertical accelerations of:

- the SDOF oscillator in Table 6.1-5 that represent the out-of-plane response of the FWS roof in flexible models of vibrations with frequencies < 50 Hz and
- the FWS LMSM lumped mass at the roof El. 19.70 m in Table 6.1-3 that represent the rigid mode out-of-plane response of the FWS roof

Appendix D of Reference 2-t describes the methodology used for the calculation of the site-specific out-of-plane loads on the CB flexible slabs that is identical to the methodology used in Reference 2-k to develop the FWS roof out-of-plane seismic load for the standard design of the FWSC structures.

In Table 6.1-6, the site-specific out-of-plane seismic load demands on the FWS roof are compared with the corresponding loads used for the standard design of the FWSC structures in Reference 2-j.

Figures 6.1-1 and 6.1-2 present diagrams of the site-specific horizontal load demands on the FWS and FPE structures, respectively. The diagrams of the vertical load demands on these two FWSC structures are presented in Figures 6.1-3 and 6.1-4. The green solid lines in these figures represent the envelope of results from the site-specific FWSC SSI analyses of the FWSC model with full stiffness properties and SSE damping (analysis Cases 7 to 9 in Table 4.2-1). The envelope of the results from the site-specific SSSI analysis of the FWSC-CB combined model with full stiffness properties and SSE damping (analysis Cases FC7 to FC9 in Table 4.2-2 of Reference 2-r) are presented with red dashed lines. Figures 6.1-1 through 6.1-4 compare the site-specific load demands with the corresponding loads used for the standard design of the FWSC structures in Reference 2-j that are presented with blue dashed lines.

The comparisons presented in Figures 6.1-1 through 6.1-4 and Tables 6.1-1 through 6.1-6 show that in general, the standard design envelop the site-specific load demands on the FWSC structures at the NA3 site with a few small exceedances that have a local effect. The largest exceedance can be observed in the torsional load demands on the FWS structure that are approximately 2.5 times the torsion considered in the standard design. As shown in Table 6.1-6, the out-of-plane load on the FWS roof can exceed the corresponding standard design load by 32%. The comparisons presented in Figure 6.1-1 and Table 6.1-2 indicate small (< 10%) exceedances in the site-specific shear load demands on the FWS structure.

Site-specific evaluations of the FWSC structures are performed to address these exceedances in the site-specific load demands and to calculate the available margins at the NA3 site.

These site-specific evaluations use site-specific seismic loads that are developed based on the enveloping site-specific load diagrams presented in this report.

6.2 Enveloping Maximum Displacements

Table 6.2-1 presents the envelope of results from the site-specific FWSC SSI analyses of the FWSC model with full (uncracked concrete) stiffness properties and OBE damping (analysis Cases 1 to 6 in Table 4.2-1) for the FWSC maximum displacement relative to the free-field motion. These results are enveloped with the corresponding results of the SSSI analysis of the FWSC-CB combined model with full stiffness properties and OBE damping (analysis Cases FC1 to FC6 in Table 4.2-2 of Reference 2-r) to obtain the enveloping maximum displacements of the FWSC structures relative to the free-field motion. In Table 6.2-2, the site-specific enveloping maximum displacements are compared with the corresponding standard design displacements presented in Reference 2-j. Except for a few exceedances, denoted by the shaded values in Table 6.2-2, these comparisons show that the NA3 high frequency design motion results in displacements that are enveloped by the standard design. The only significant (>2%) exceedances are those of the FWSC basemat. These exceedances in FWSC basemat displacements only affect the design of external utilities attached to the FWSC and will be addressed by NA3 site-specific design.

6.3 Site-Specific Design ISRS

Appendix E presents figures of site-specific enveloping ISRS for critical damping ratios 2, 3, 4, 5, 7, 10, and 20% at all locations in the FWSC that are peak broadened by $\pm$15% and valley filled. These ISRS represent the envelope of ISRS results from:

- The site-specific SSI analyses of the FWSC standalone model with full (uncracked concrete) stiffness properties and OBE damping (Cases 1 to 6 in Table 4.2-1).
- The site-specific SSSI analyses of the FWSC-CB combined model with full stiffness properties and OBE damping (Cases FC1 to FC6 in Table 4.2-2 of Reference 2-r).

The site-specific design ISRS are enhanced, as discussed in Section 7, so that they can be used for site-specific design and qualification of FWSC equipment and components.

7. CONCLUSIONS

The following are the conclusions from the results of the NA3 site-specific SSI analyses of the FWSC structures:

- Site-specific seismic demands slightly exceed the seismic demands used for the standard design of the FWSC structures.
- The site-specific evaluation of the FWSC structures uses input seismic loads that are based on the site-specific enveloping loads presented in Section 6.1 that include the site-specific SSSI effects of the CB on the FWSC seismic response. The evaluation presented in Reference 2-dd shows that the separation between the concrete fill under FWSC foundation and surrounding soil can amplify the site-specific seismic demands

on FWSC structures. In order to address these amplifications, the enveloping loads presented in Section 6.1 are also enveloped with the seismic load demands obtained from the sensitivity analyses of models representing maximum separation between the concrete fill and the soil that are presented in Reference 2-dd. These loads, enhanced to bound effects of soil separation, are further amplified as described in Section B.5 of Appendix B to also bound the effects of concrete cracking. Reference 2-n provides a summary of criteria and approach used for enhancing the FWSC seismic load demands and presents these enhanced bounding seismic structural loads used as input for the site-specific evaluation of the FWSC structures.

- Site-specific enveloping ISRS presented in Appendix E are developed for all damping values and locations within the FWSC based on the envelope of the results of the SSI and SSSI analyses of the FWSC standalone and FWSC combined models with full uncracked concrete stiffness properties and OBE damping. These ISRS envelop the site-specific SSSI effects of the CB on the FWSC seismic response. The site-specific ISRS shall be enhanced twice. First, the ISRS are enhanced as described in Section 7 of Reference 2-dd to address the effects of separation between the concrete fill and surrounding soil. These ISRS are then enhanced again as described in Appendix B of this report to address the effects of concrete cracking. Reference 2-n provides a summary of criteria and approach used for enhancing the FWSC design ISRS and presents the bounding design ISRS for responses of FWSC at the key locations listed in Section 5.1. Bounding design ISRS shall be developed for other FWSC locations following the same criteria and approach.

Table 3.1-1: BE Site-Specific In-Situ Strain-Compatible Dynamic Subsurface Properties

Layer #	Thickness (m)	Top-Depth (m)	Unit Weight (t/m^3)	V_s (m/s)	V_p (m/s)	Damping (%)
1	0.91	0.00	2.00	226	1153	4.18
2	0.91	0.91	2.00	226	1153	4.18
3	0.91	1.83	2.00	226	1153	4.18
4	0.91	2.74	2.00	226	1153	4.18
5	0.91	3.66	2.00	298	1463	5.00
6	0.91	4.57	2.00	298	1463	5.00
7	0.91	5.49	2.00	298	1463	5.00
8	1.22	6.40	2.00	298	1463	5.00
9	1.22	7.62	2.00	298	1463	5.00
10	1.22	8.84	2.08	432	1814	3.97
11	0.91	10.06	2.08	596	1821	2.89
12	0.61	10.97	2.08	596	1821	2.89
13	1.22	11.58	2.32	763	2331	0.64
14	1.22	12.80	2.32	763	2331	0.64
15	1.22	14.02	2.32	763	2331	0.64
16	1.22	15.24	2.32	763	2331	0.64
17	1.22	16.46	2.32	821	2508	0.53
18	1.22	17.68	2.32	821	2508	0.53
19	0.91	18.90	2.61	1976	4225	1.00
20	0.91	19.81	2.61	1976	4225	1.00
21	0.91	20.73	2.61	2128	4273	1.00
22	1.22	21.64	2.61	2128	4273	1.00
23	1.22	22.86	2.61	2128	4273	1.00
24	0.91	24.08	2.63	2421	4613	1.00
25	1.22	24.99	2.63	2421	4613	1.00
26	1.22	26.21	2.63	2421	4613	1.00
27	0.91	27.43	2.63	2638	4772	1.00
28	1.22	28.35	2.63	2638	4772	1.00
29	1.22	29.57	2.63	2638	4772	1.00
30	0.91	30.78	2.63	2512	4787	1.00
31	1.22	31.70	2.63	2512	4787	1.00
32	1.22	32.92	2.63	2512	4787	1.00
33	0.91	34.14	2.63	2639	4937	1.00
34	1.22	35.05	2.63	2639	4937	1.00
35	1.22	36.27	2.63	2639	4937	1.00
36	0.91	37.49	2.63	2689	4722	1.00
37	1.22	38.40	2.63	2689	4722	1.00
38	1.22	39.62	2.63	2689	4722	1.00
39	0.91	40.84	2.63	2847	5150	1.00
40	1.22	41.76	2.63	2847	5150	1.00
41	1.22	42.98	2.63	2847	5150	1.00
42	0.91	44.20	2.63	2804	5245	1.00
43	1.22	45.11	2.63	2804	5245	1.00
44	1.22	46.33	2.63	2804	5245	1.00
45		47.55	2.63	2804	4794	1.00

Note: The elevation with respect to which the depths are referenced is 2.15 m (El. 282.3 ft NAVD 88), which is the bottom of the FWSC basemat.

Table 3.1-2: LB Site-Specific In-Situ Strain-Compatible Dynamic Subsurface Properties

Layer #	Thickness (m)	Top-Depth (m)	Unit Weight (t/m^3)	V_s (m/s)	V_p (m/s)	Damping (%)
1	0.91	0.00	2.00	147	750	6.63
2	0.91	0.91	2.00	147	750	6.63
3	0.91	1.83	2.00	147	750	6.63
4	0.91	2.74	2.00	147	750	6.63
5	0.91	3.66	2.00	184	940	8.25
6	0.91	4.57	2.00	184	940	8.25
7	0.91	5.49	2.00	184	940	8.25
8	1.22	6.40	2.00	184	940	8.25
9	1.22	7.62	2.00	184	940	8.25
10	1.22	8.84	2.08	310	1463	6.08
11	0.91	10.06	2.08	436	1463	4.37
12	0.61	10.97	2.08	436	1463	4.37
13	1.22	11.58	2.32	581	1775	1.14
14	1.22	12.80	2.32	581	1775	1.14
15	1.22	14.02	2.32	581	1775	1.14
16	1.22	15.24	2.32	581	1775	1.14
17	1.22	16.46	2.32	655	2002	0.94
18	1.22	17.68	2.32	655	2002	0.94
19	0.91	18.90	2.61	1464	3130	1.82
20	0.91	19.81	2.61	1464	3130	1.82
21	0.91	20.73	2.61	1738	3488	1.82
22	1.22	21.64	2.61	1738	3488	1.82
23	1.22	22.86	2.61	1738	3488	1.82
24	0.91	24.08	2.63	1977	3767	1.82
25	1.22	24.99	2.63	1977	3767	1.82
26	1.22	26.21	2.63	1977	3767	1.82
27	0.91	27.43	2.63	2154	3897	1.82
28	1.22	28.35	2.63	2154	3897	1.82
29	1.22	29.57	2.63	2154	3897	1.82
30	0.91	30.78	2.63	2051	3909	1.82
31	1.22	31.70	2.63	2051	3909	1.82
32	1.22	32.92	2.63	2051	3909	1.82
33	0.91	34.14	2.63	2155	4031	1.82
34	1.22	35.05	2.63	2155	4031	1.82
35	1.22	36.27	2.63	2155	4031	1.82
36	0.91	37.49	2.63	2195	3855	1.82
37	1.22	38.40	2.63	2195	3855	1.82
38	1.22	39.62	2.63	2195	3855	1.82
39	0.91	40.84	2.63	2324	4205	1.82
40	1.22	41.76	2.63	2324	4205	1.82
41	1.22	42.98	2.63	2324	4205	1.82
42	0.91	44.20	2.63	2289	4282	1.82
43	1.22	45.11	2.63	2289	4282	1.82
44	1.22	46.33	2.63	2289	4282	1.82
45		47.55	2.63	2290	3915	1.82

Note: The elevation with respect to which the depths are referenced is 2.15 m (El. 282.3 ft NAVD 88), which is the bottom of the FWSC basemat.

Table 3.1-3: UB Site-Specific In-Situ Strain-Compatible Dynamic Subsurface Properties

Layer #	Thickness (m)	Top-Depth (m)	Unit Weight (t/m^3)	V_s (m/s)	V_p (m/s)	Damping (%)
1	0.91	0.00	2.00	348	1463	2.64
2	0.91	0.91	2.00	348	1463	2.64
3	0.91	1.83	2.00	348	1463	2.64
4	0.91	2.74	2.00	348	1463	2.64
5	0.91	3.66	2.00	483	2030	3.03
6	0.91	4.57	2.00	483	2030	3.03
7	0.91	5.49	2.00	483	2030	3.03
8	1.22	6.40	2.00	483	2030	3.03
9	1.22	7.62	2.00	483	2030	3.03
10	1.22	8.84	2.08	600	2524	2.60
11	0.91	10.06	2.08	814	2488	1.92
12	0.61	10.97	2.08	814	2488	1.92
13	1.22	11.58	2.32	1002	3060	0.36
14	1.22	12.80	2.32	1002	3060	0.36
15	1.22	14.02	2.32	1002	3060	0.36
16	1.22	15.24	2.32	1002	3060	0.36
17	1.22	16.46	2.32	1028	3141	0.30
18	1.22	17.68	2.32	1028	3141	0.30
19	0.91	18.90	2.61	2667	5703	0.55
20	0.91	19.81	2.61	2667	5703	0.55
21	0.91	20.73	2.61	2607	5233	0.55
22	1.22	21.64	2.61	2607	5233	0.55
23	1.22	22.86	2.61	2607	5233	0.55
24	0.91	24.08	2.63	2965	5650	0.55
25	1.22	24.99	2.63	2965	5650	0.55
26	1.22	26.21	2.63	2965	5650	0.55
27	0.91	27.43	2.63	3231	5845	0.55
28	1.22	28.35	2.63	3231	5845	0.55
29	1.22	29.57	2.63	3231	5845	0.55
30	0.91	30.78	2.63	3077	5863	0.55
31	1.22	31.70	2.63	3077	5863	0.55
32	1.22	32.92	2.63	3077	5863	0.55
33	0.91	34.14	2.63	3232	6047	0.55
34	1.22	35.05	2.63	3232	6047	0.55
35	1.22	36.27	2.63	3232	6047	0.55
36	0.91	37.49	2.63	3293	5783	0.55
37	1.22	38.40	2.63	3293	5783	0.55
38	1.22	39.62	2.63	3293	5783	0.55
39	0.91	40.84	2.63	3487	6308	0.55
40	1.22	41.76	2.63	3487	6308	0.55
41	1.22	42.98	2.63	3487	6308	0.55
42	0.91	44.20	2.63	3434	6424	0.55
43	1.22	45.11	2.63	3434	6424	0.55
44	1.22	46.33	2.63	3434	6424	0.55
45		47.55	2.63	3434	5872	0.55

Note: The elevation with respect to which the depths are referenced is 2.15 m (El. 282.3 ft NAVD 88), which is the bottom of the FWSC basemat.

Table 3.1-4: BE Dynamic Properties of Structural and Concrete Fill Materials

Layer #	Thickness (m)	Top-Depth (m)	Unit Weight (t/m^3)	V_s (m/s)	V_p (m/s)	Damping (%)
1	0.91	0.00	2.08	227	1158	4.74
2	0.91	0.91	2.08	231	1180	4.83
3	0.91	1.83	2.08	239	1219	4.97
4	0.91	2.74	2.08	239	1216	5.33
5	0.91	3.66	2.08	258	1314	5.17
6	0.91	4.57	2.08	253	1291	5.47
7	0.91	5.49	2.08	253	1291	5.65
8	1.22	6.40	2.08	260	1325	5.67
9	1.22	7.62	2.08	258	1318	5.96
10	1.22	8.84	2.08	272	1389	5.75
11	0.91	10.06	2.08	271	1383	5.95
12	0.61	10.97	2.08	271	1383	5.95
Lean Concrete			2.32	2134	3325	1.00

Note: The elevation with respect to which the depths are referenced is 2.15 m (El. 282.3 ft NAVD 88), which is the bottom of the FWSC basemat.

Table 3.1-5: LB Dynamic Properties of Structural and Concrete Fill Materials

Layer #	Thickness (m)	Top-Depth (m)	Unit Weight (t/m^3)	V_s (m/s)	V_p (m/s)	Damping (%)
1	0.91	0.00	2.08	146	744	7.33
2	0.91	0.91	2.08	150	763	7.50
3	0.91	1.83	2.08	153	782	7.85
4	0.91	2.74	2.08	155	788	8.29
5	0.91	3.66	2.08	160	818	8.02
6	0.91	4.57	2.08	155	790	8.50
7	0.91	5.49	2.08	158	805	8.54
8	1.22	6.40	2.08	158	809	8.87
9	1.22	7.62	2.08	157	799	9.19
10	1.22	8.84	2.08	168	856	8.74
11	0.91	10.06	2.08	162	825	9.35
12	0.61	10.97	2.08	162	825	9.35
Lean Concrete			2.32	1829	2850	1.82

Note: The elevation with respect to which the depths are referenced is 2.15 m (El. 282.3 ft NAVD 88), which is the bottom of the FWSC basemat.

Table 3.1-6: UB Dynamic Properties of Structural and Concrete Fill Materials

Layer #	Thickness (m)	Top-Depth (m)	Unit Weight (t/m^3)	V_s (m/s)	V_p (m/s)	Damping (%)
1	0.91	0.00	2.08	354	1463	3.06
2	0.91	0.91	2.08	358	1463	3.11
3	0.91	1.83	2.08	373	1463	3.15
4	0.91	2.74	2.08	368	1463	3.42
5	0.91	3.66	2.08	414	1463	3.33
6	0.91	4.57	2.08	413	1463	3.52
7	0.91	5.49	2.08	406	1463	3.74
8	1.22	6.40	2.08	426	1463	3.63
9	1.22	7.62	2.08	427	1463	3.87
10	1.22	8.84	2.08	442	1463	3.78
11	0.91	10.06	2.08	455	1463	3.79
12	0.61	10.97	2.08	455	1463	3.79
Lean Concrete			2.32	2438	3800	0.55

Note: The elevation with respect to which the depths are referenced is 2.15 m (El. 282.3 ft NAVD 88), which is the bottom of the FWSC basemat.

Table 3.1-7: Comparisons of the Average Strain-Compatible Shear Wave Velocities and Shear Column Frequencies of In-Situ Materials

Soil Case	Zone III Rock			Structural Fill/Saprolite					Full Column				
					Backfill		In-Situ			Backfill		In-Situ	
	Depth (m)	$V_{s\text{-}ave}$ (m/s)	f_{sc} (Hz)	Depth (m)	$V_{s\text{-}ave}$ (m/s)	f_{sc} (Hz)	$V_{s\text{-}ave}$ (m/s)	f_{sc} (Hz)	Depth (m)	$V_{s\text{-}ave}$ (m/s)	f_{sc} (Hz)	$V_{s\text{-}ave}$ (m/s)	f_{sc} (Hz)
LB	7.3	604	20.6	11.7	157	3.4	192	4.1	19.0	243	3.2	261	3.5
BE		781	26.7		252	5.4	298	6.4		383	5.1	391	5.2
UB		1010	34.5		405	8.7	461	9.9		598	7.9	584	7.7

Table 4.2-1: FWSC Site-Specific SSI Analysis Cases, Passing and Cut-off Frequencies

Case No.	Structural Model Properties*)	Subgrade Profile	Method	Control Motion El.	Frequency (Hz)		Captured Motion Energy		
					Passing	Cut-off	X	Y	Z
1	UC_{OBE}	LB	MSM	282 ft	36	36	89%	87%	83%
2		BE			55	55	97%	97%	95%
3		UB			84	70	100%	100%	99%
4		LB	MSM	220 ft	36	36	87%	81%	84%
5		BE			55	55	98%	96%	95%
6		UB			84	70	100%	99%	99%
7	UC_{SSE}	LB	MSM	220 ft	36	36	87%	81%	84%
8		BE			55	55	98%	96%	95%
9		UB			84	70	100%	99%	99%
Sensitivity Analyses for Evaluations of Concrete Cracking Effects (Appendix B)									
S1	CR_{SSE}	LB	MSM	282 ft	36	36	89%	87%	83%
S2		LB	MSM	220 ft	36	36	87%	81%	84%
S3		UB	MSM	282 ft	84	70	100%	100%	99%
S4		UB	MSM	220 ft	84	70	100%	99%	99%
S5		BE	MSM	282 ft	55	55	97%	97%	95%
S6		BE	MSM	220 ft	55	55	98%	96%	95%

*) Structural Properties:

UC_{OBE} – Uncracked reinforced concrete and OBE damping values

UC_{SSE} – Uncracked reinforced concrete and SSE damping values

CR_{SSE} – Cracked reinforced concrete with 50% reduced shear and bending stiffness and SSE damping values

Table 4.2-2: List of Frequencies of Analysis

Frequency No.	Frequency (Hz)		
	FWSC SSI Analysis		
	LB	BE	UB
1	0.0244	0.0244	0.0244
41	1.0010	1.0010	1.0010
82	2.0020	2.0020	2.0020
123	3.0029	3.0029	3.0029
164	4.0039	4.0039	4.0039
205	5.0049	5.0049	5.0049
246	6.0059	6.0059	6.0059
287	7.0068	7.0068	7.0068
328	8.0078	8.0078	8.0078
369	9.0088	9.0088	9.0088
410	10.0098	10.0098	10.0098
451	11.0107	11.0107	11.0107
492	12.0117	12.0117	12.0117
532	12.9883	12.9883	12.9883
573	13.9893	13.9893	13.9893
614	14.9902	14.9902	14.9902
655	15.9912	15.9912	15.9912
696	16.9922	16.9922	16.9922
737	17.9932	17.9932	17.9932
778	18.9941	18.9941	18.9941
819	19.9951	19.9951	19.9951
860	20.9961	20.9961	20.9961
901	21.9971	21.9971	21.9971
942	22.9980	22.9980	22.9980
983	23.9990	23.9990	23.9990
1024	25.0000	25.0000	25.0000
1065	26.0010	26.0010	26.0010
1106	27.0020	27.0020	27.0020
1147	28.0029	28.0029	28.0029
1188	29.0039	29.0039	29.0039
1229	30.0049	30.0049	30.0049
1270	31.0059	31.0059	31.0059
1311	32.0068	32.0068	32.0068
1352	33.0078	33.0078	33.0078
1393	34.0088	34.0088	34.0088
1434	35.0098	35.0098	35.0098
1475	36.0107	36.0107	36.0107
1516		37.0117	37.0117
1557		38.0127	38.0127
1598		39.0137	39.0137
1639		40.0146	40.0146
1680		41.0156	41.0156
1721		42.0166	42.0166
1762		43.0176	43.0176
1803		44.0186	44.0186
1844		45.0195	45.0195
1885		46.0205	46.0205
1926		47.0215	47.0215

Table 4.2-2: List of Frequencies of Analysis (Continued)

Frequency No.	Frequency (Hz) FWSC SSI Analysis		
	LB	BE	UB
1966		47.9980	47.9980
2007		48.9990	48.9990
2048		50.0000	50.0000
2089		51.0010	51.0010
2130		52.0020	52.0020
2171		53.0029	53.0029
2212		54.0039	54.0039
2253		55.0049	55.0049
2294			56.0059
2335			57.0068
2376			58.0078
2417			59.0088
2458			60.0098
2499			61.0107
2540			62.0117
2581			63.0127
2622			64.0137
2663			65.0146
2703			65.9912
2744			66.9922
2785			67.9932
2826			68.9941
2867			69.9951

Note: SSI analysis of LB profile performed for frequencies up to 36 Hz (Frequency number 1475).

Table 4.3-1: Site Model Properties for SSI Analysis of BE Profile

EL [m]	Soil						Backfill					
	Unit Weight [t/m^3]	V_s [m/sec]	V_p [m/sec]	Damping [%]	Highest Frequency [Hz]	Poisson's ratio	Unit Weight [t/m^3]	V_s [m/sec]	V_p [m/sec]	Damping [%]	Highest Frequency [Hz]	Poisson's ratio
2.15	2.00	226	1153	4.18	54.7	0.480	2.32	2134	3325	1.00	517.3	0.150
1.40												
1.40	2.00	226	1153	4.18	54.7	0.480	2.32	2134	3325	1.00	517.3	0.150
0.65												
0.65	2.00	226	1153	4.18	54.7	0.480	2.32	2134	3325	1.00	517.3	0.150
-0.10												
-0.10	2.00	226	1153	4.18	54.7	0.480	2.32	2134	3325	1.00	517.3	0.150
-0.85												
-0.85	2.00	226	1153	4.18	54.7	0.480	2.32	2134	3325	1.00	517.3	0.150
-1.60												
-1.60	2.00	298	1463	5.00	69.3	0.478	2.32	2134	3325	1.00	496.2	0.150
-2.46												
-2.46	2.00	298	1463	5.00	69.3	0.478	2.32	2134	3325	1.00	496.2	0.150
-3.32												
-3.32	2.00	298	1463	5.00	69.3	0.478	2.32	2134	3325	1.00	496.2	0.150
-4.18												
-4.18	2.00	298	1463	5.00	69.3	0.478	2.32	2134	3325	1.00	496.2	0.150
-5.04												
-5.04	2.00	298	1463	5.00	68.5	0.478	2.32	2134	3325	1.00	490.5	0.150
-5.91												
-5.91	2.00	298	1463	5.00	68.5	0.478	2.32	2134	3325	1.00	490.5	0.150
-6.78												
-6.78	2.08	432	1814	3.97	70.8	0.470	2.32	2134	3325	1.00	349.8	0.150
-8.000												
-8.000	2.08	596	1821	2.89	78.4	0.440	2.32	2134	3325	1.00	280.7	0.150
-9.520												
-9.520	2.32	763	2331	0.64	94.1	0.440	2.32	2134	3325	1.00	263.4	0.150
-11.140												
-11.140	2.32	763	2331	0.64	93.6	0.440	2.32	2134	3325	1.00	261.8	0.150
-12.770												
-12.770	2.32	763	2331	0.64	93.6	0.440	2.32	2134	3325	1.00	261.8	0.150
-14.400												
-14.400	2.32	821	2508	0.53	134.5	0.440	2.32	2134	3325	1.00	349.8	0.150
-15.620												
-15.620	2.32	821	2508	0.53	134.5	0.440	2.32	2134	3325	1.00	349.8	0.150
-16.840												
-16.840	2.61	1976	4225	1.00	215.9	0.360						
-18.670												
-18.670	2.61	2128	4273	1.00	127.0	0.335						
-22.020												
-22.020	2.63	2421	4613	1.00	144.5	0.310						
-25.37												
-25.37	2.63	2638	4772	1.00	157.4	0.280						
-28.72												
-28.72	2.63	2512	4787	1.00	149.5	0.310						
-32.08												
-32.08	2.63	2639	4937	1.00	157.5	0.300						
-35.43												
-35.43	2.63	2689	4722	1.00	160.5	0.260						
-38.78												
-38.78	2.63	2847	5150	1.00	169.4	0.280						
-42.14												
-42.14	2.63	2804	5245	1.00	167.4	0.300						
-45.49												
-45.49	2.63	2804	4794	1.00	-	0.240						
-												

Table 4.3-2: Site Model Properties for SSI Analysis of LB Profile

EL [m]	Soil						Backfill					
	Unit Weight [t/m³]	V_s [m/sec]	V_p [m/sec]	Damping [%]	Highest Frequency [Hz]	Poisson's ratio	Unit Weight [t/m³]	V_s [m/sec]	V_p [m/sec]	Damping [%]	Highest Frequency [Hz]	Poisson's ratio
2.15	2.00	147	750	6.63	35.6	0.480	2.32	1829	2850	1.82	443.3	0.150
1.40												
1.40	2.00	147	750	6.63	35.6	0.480	2.32	1829	2850	1.82	443.3	0.150
0.65												
0.65	2.00	147	750	6.63	35.6	0.480	2.32	1829	2850	1.82	443.3	0.150
-0.10												
-0.10	2.00	147	750	6.63	35.6	0.480	2.32	1829	2850	1.82	443.3	0.150
-0.85												
-0.85	2.00	147	750	6.63	35.6	0.480	2.32	1829	2850	1.82	443.3	0.150
-1.60												
-1.60	2.00	184	940	8.25	42.7	0.480	2.32	1829	2850	1.82	425.3	0.150
-2.46												
-2.46	2.00	184	940	8.25	42.7	0.480	2.32	1829	2850	1.82	425.3	0.150
-3.32												
-3.32	2.00	184	940	8.25	42.7	0.480	2.32	1829	2850	1.82	425.3	0.150
-4.18												
-4.18	2.00	184	940	8.25	42.7	0.480	2.32	1829	2850	1.82	425.3	0.150
-5.04												
-5.04	2.00	184	940	8.25	42.2	0.480	2.32	1829	2850	1.82	420.4	0.150
-5.91												
-5.91	2.00	184	940	8.25	42.2	0.480	2.32	1829	2850	1.82	420.4	0.150
-6.78												
-6.78	2.08	310	1463	6.08	50.8	0.476	2.32	1829	2850	1.82	299.8	0.150
-8.000												
-8.000	2.08	436	1463	4.37	57.3	0.451	2.32	1829	2850	1.82	240.6	0.150
-9.520												
-9.520	2.32	581	1775	1.14	71.7	0.440	2.32	1829	2850	1.82	225.8	0.150
-11.140												
-11.140	2.32	581	1775	1.14	71.2	0.440	2.32	1829	2850	1.82	224.4	0.150
-12.770												
-12.770	2.32	581	1775	1.14	71.2	0.440	2.32	1829	2850	1.82	224.4	0.150
-14.400												
-14.400	2.32	655	2002	0.94	107.3	0.440	2.32	1829	2850	1.82	299.8	0.150
-15.620												
-15.620	2.32	655	2002	0.94	107.3	0.440	2.32	1829	2850	1.82	299.8	0.150
-16.840												
-16.840	2.61	1464	3130	1.82	160.0	0.360						
-18.670												
-18.670	2.61	1738	3488	1.82	103.7	0.335						
-22.020												
-22.020	2.63	1977	3767	1.82	118.0	0.310						
-25.37												
-25.37	2.63	2154	3897	1.82	128.5	0.280						
-28.72												
-28.72	2.63	2051	3909	1.82	122.0	0.310						
-32.08												
-32.08	2.63	2155	4031	1.82	128.6	0.300						
-35.43												
-35.43	2.63	2195	3855	1.82	131.0	0.260						
-38.78												
-38.78	2.63	2324	4205	1.82	138.3	0.280						
-42.14												
-42.14	2.63	2289	4282	1.82	136.6	0.300						
-45.49												
-45.49	2.63	2290	3915	1.82	-	0.240						
-												

Table 4.3-3: Site Model Properties for SSI Analysis of UB Profile

EL [m]	Soil						Backfill					
	Unit Weight [t/m^3]	V_s [m/sec]	V_p [m/sec]	Damping [%]	Highest Frequency [Hz]	Poisson's ratio	Unit Weight [t/m^3]	V_s [m/sec]	V_p [m/sec]	Damping [%]	Highest Frequency [Hz]	Poisson's ratio
2.15	2.00	348	1463	2.64	84.3	0.470	2.32	2438	3800	0.55	591.0	0.150
1.40												
1.40	2.00	348	1463	2.64	84.3	0.470	2.32	2438	3800	0.55	591.0	0.150
0.65												
0.65	2.00	348	1463	2.64	84.3	0.470	2.32	2438	3800	0.55	591.0	0.150
-0.10												
-0.10	2.00	348	1463	2.64	84.3	0.470	2.32	2438	3800	0.55	591.0	0.150
-0.85												
-0.85	2.00	348	1463	2.64	84.3	0.470	2.32	2438	3800	0.55	591.0	0.150
-1.60												
-1.60	2.00	483	2030	3.03	112.3	0.470	2.32	2438	3800	0.55	566.9	0.150
-2.46												
-2.46	2.00	483	2030	3.03	112.3	0.470	2.32	2438	3800	0.55	566.9	0.150
-3.32												
-3.32	2.00	483	2030	3.03	112.3	0.470	2.32	2438	3800	0.55	566.9	0.150
-4.18												
-4.18	2.00	483	2030	3.03	112.3	0.470	2.32	2438	3800	0.55	566.9	0.150
-5.04												
-5.04	2.00	483	2030	3.03	111.0	0.470	2.32	2438	3800	0.55	560.4	0.150
-5.91												
-5.91	2.00	483	2030	3.03	111.0	0.470	2.32	2438	3800	0.55	560.4	0.150
-6.78												
-6.78	2.08	600	2524	2.60	98.3	0.470	2.32	2438	3800	0.55	399.6	0.150
-8.000												
-8.000	2.08	814	2488	1.92	107.1	0.440	2.32	2438	3800	0.55	320.7	0.150
-9.520												
-9.520	2.32	1002	3060	0.36	123.7	0.440	2.32	2438	3800	0.55	300.9	0.150
-11.140												
-11.140	2.32	1002	3060	0.36	122.9	0.440	2.32	2438	3800	0.55	299.1	0.150
-12.770												
-12.770	2.32	1002	3060	0.36	122.9	0.440	2.32	2438	3800	0.55	299.1	0.150
-14.400												
-14.400	2.32	1028	3141	0.30	168.5	0.440	2.32	2438	3800	0.55	399.6	0.150
-15.620												
-15.620	2.32	1028	3141	0.30	168.5	0.440	2.32	2438	3800	0.55	399.6	0.150
-16.840												
-16.840	2.61	2667	5703	0.55	291.4	0.360						
-18.670												
-18.670	2.61	2607	5233	0.55	155.6	0.335						
-22.020												
-22.020	2.63	2965	5650	0.55	177.0	0.310						
-25.37												
-25.37	2.63	3231	5845	0.55	192.8	0.280						
-28.72												
-28.72	2.63	3077	5863	0.55	183.1	0.310						
-32.08												
-32.08	2.63	3232	6047	0.55	192.9	0.300						
-35.43												
-35.43	2.63	3293	5783	0.55	196.5	0.260						
-38.78												
-38.78	2.63	3487	6308	0.55	207.5	0.280						
-42.14												
-42.14	2.63	3434	6424	0.55	205.0	0.300						
-45.49												
-45.49	2.63	3434	5872	0.55	-	0.240						
-												

Table 5.2-1: Maximum Accelerations of SDOF Oscillators

SDOF Oscillator				Acceleration (g)						
Elev. (m)	Node No.	Description	Direction	Motion El. 282 ft			Motion El. 220 ft			Envelope
				LB	BE	UB	LB	BE	UB	
19.70	11	FWS Roof	Vert. (Z)	1.34	1.62	1.58	2.10	3.26	4.22	4.22
12.10	60	FWS Water Sloshing Mode	NS (X)	0.10	0.10	0.10	0.10	0.10	0.10	0.10
			EW (Y)	0.07	0.07	0.07	0.09	0.09	0.09	0.09
8.81	30	FWS Water Impulsive Mode	NS (X)	0.77	0.85	0.72	0.80	0.85	1.02	1.02
			EW (Y)	0.68	0.73	0.64	0.74	0.81	1.08	1.08

Note: The shaded values are the governing case(s).

Table 5.4-1: Maximum Displacements of SDOF Oscillators Relative to Free-Field

SDOF Oscillator				Displacement (cm)						
Elev. (m)	Node No.	Description	Direction	Motion El. 282 ft			Motion El. 220 ft			Envelope
				LB	BE	UB	LB	BE	UB	
19.70	11	FWS Roof	Vert. (Z)	0.04	0.04	0.04	0.08	0.08	0.09	0.09
12.10	60	FWS Water Sloshing Mode	NS (X)	43.76	44.01	44.05	42.79	43.19	43.19	44.05
			EW (Y)	28.68	28.72	28.74	37.35	37.65	37.66	37.66
8.81	30	FWS Water Impulsive Mode	NS (X)	0.53	0.33	0.13	0.18	0.15	0.12	0.53
			EW (Y)	0.53	0.26	0.07	0.26	0.20	0.19	0.53

Note: The shaded values are the governing case(s).

Table 5.5-1: Summary of Maximum Base Reaction Eccentricity Results

Combination	Analysis	UC_{SSE} Model Deep Input Motion at El. 220 ft NAVD 88		
		BE	UB	LB
+Ex+Ey+Ez	Max. Eccentricity (m)	19.7	12.0	8.8
	at Time (s)	1.155	1.485	1.160
	Minimum Contact Ratio (%)	85.8	91.7	97.4
-Ex-Ey-Ez	Max. Eccentricity (m)	9.2	12.9	7.2
	at Time (s)	1.140	1.140	3.095
	Minimum Contact Ratio (%)	89.7	86.3	95.9

Note: The shaded values are the governing case.

Table 6.1-1: FWSC Site-Specific Enveloping Maximum Member Forces and Moments

Structure	Element			SSI Analyses Envelope					SSSI Analyses Envelope*)					NA3 Enveloping				
	Elev. (m)	No.	Node No.	Shear (MN)		Bending (MN-m)		Torsion (MN-m)	Shear (MN)		Bending (MN-m)		Torsion (MN-m)	Shear (MN)		Bending (MN-m)		Torsion (MN-m)
				NS	EW	NS	EW		NS	EW	NS	EW		NS	EW	NS	EW	
FWS	19.70	9	10	4.3	4.7	4	3	1.2	4.7	5.2	5	3	2.4	4.7	5.2	5	3	2.4
			9			14	14				16	15				16	15	
	17.25	8	9	10.5	11.5	23	21	3.6	11.4	12.8	25	21	7.4	11.4	12.8	25	21	7.4
			8			40	39				44	43				44	43	
	15.53	7	8	14.6	16.0	48	46	6.0	15.8	17.8	54	48	12.2	15.8	17.8	54	48	12.2
			7			71	72				80	80				80	80	
	13.81	6	7	18.3	20.0	79	77	8.2	19.7	22.1	88	85	16.7	19.7	22.1	88	85	16.7
			6			107	112				120	123				120	123	
	12.10	5	6	20.8	22.7	113	115	9.9	22.4	25.1	126	127	20.0	22.4	25.1	126	127	20.0
			5			133	141				149	155				149	155	
	11.00	4	5	22.6	24.5	137	143	11.1	24.3	27.2	153	158	22.3	24.3	27.2	153	158	22.3
			4			159	170				178	188				178	188	
	9.90	3	4	24.2	26.1	163	173	12.2	25.8	29.0	182	191	24.4	25.8	29.0	182	191	24.4
			3			187	199				207	222				207	222	
	8.81	2	3	38.1	40.0	190	206	13.6	40.5	44.5	212	226	27.1	40.5	44.5	212	226	27.1
			2			269	287				290	318				290	318	
	6.73	1	2	39.3	41.9	272	290	15.0	41.6	46.1	294	321	29.6	41.6	46.1	294	321	29.6
	4.65		8002			354	376				379	417				379	417	
FPE	8.25	402	405	4.1	6.8	2	6	5.8	3.9	7.1	2	7	6.2	4.1	7.1	2	7	6.2
	4.65	401	404			14	26				12	27				14	27	

Note: The shaded values are the governing case(s).

*) Obtained from the FWSC-CB SSSI Analyses in Reference 2-r

Table 6.1-2: Comparison of Site-Specific and Standard Design Enveloping Maximum Member Forces and Moments

Structure	Element			Standard Design					NA3 Enveloping					Difference				
	Elev. (m)	No.	Node No.	Shear (MN)		Bending (MN-m)		Torsion (MN-m)	Shear (MN)		Bending (MN-m)		Torsion (MN-m)	Shear		Bending		Torsion
				NS	EW	NS	EW		NS	EW	NS	EW		NS	EW	NS	EW	
FWS	19.70	9	10	4.6	5.1	4	7	0.7	4.7	5.2	5	3	2.4	3%	1%	8%	-51%	237%
			9			14	19				16	15				13%	-20%	
	17.25	8	9	11.1	12.1	22	27	2.2	11.4	12.8	25	21	7.4	2%	6%	14%	-20%	237%
			8			39	47				44	43				14%	-8%	
	15.53	7	8	15.5	16.5	45	57	3.6	15.8	17.8	54	48	12.2	2%	8%	18%	-17%	239%
			7			71	84				80	80				13%	-5%	
	13.81	6	7	19.3	20.1	76	92	4.9	19.7	22.1	88	85	16.7	2%	10%	16%	-8%	243%
			6			107	124				120	123				12%	-1%	
	12.10	5	6	22.8	23.8	111	128	5.8	22.4	25.1	126	127	20.0	-2%	6%	13%	-1%	247%
			5			134	153				149	155				11%	1%	
	11.00	4	5	24.6	25.3	136	157	6.4	24.3	27.2	153	158	22.3	-1%	7%	13%	1%	250%
			4			163	184				178	188				9%	2%	
	9.90	3	4	26.1	26.6	166	187	6.9	25.8	29.0	182	191	24.4	-1%	9%	10%	2%	255%
			3			194	216				207	222				6%	3%	
	8.81	2	3	43.3	45.5	197	221	7.5	40.5	44.5	212	226	27.1	-6%	-2%	8%	2%	262%
			2			279	295				290	318				4%	8%	
	6.73	1	2	45.3	48.0	281	299	8.1	41.6	46.1	294	321	29.6	-8%	-4%	5%	8%	264%
	4.65		8002			366	375				379	417				3%	11%	
FPE	8.25	402	405	8.1	7.4	2	10	15.1	4.1	7.1	2	7	6.2	-50%	-4%	-24%	-32%	-59%
	4.65	401	404			28	27				14	27				-51%	0%	

Note: The shaded values are exceedances of site-specific loads with respect to standard design.

Table 6.1-3: Site-Specific Enveloping Maximum Accelerations at FWSC Lumped Mass Locations

Elev. (m)	Node No.	Location	SSI Analyses Envelope			SSSI Analyses Envelope*)			NA3 Enveloping		
			NS (g)	EW (g)	Vert. (g)	NS (g)	EW (g)	Vert. (g)	NS (g)	EW (g)	Vert. (g)
19.70	10	FWS	2.00	2.18	1.43	2.21	2.42	1.40	2.21	2.42	1.43
17.25	9	FWS	1.85	2.02	1.43	2.00	2.26	1.40	2.00	2.26	1.43
15.53	8	FWS	1.68	1.83	1.40	1.80	2.04	1.38	1.80	2.04	1.40
13.81	7	FWS	1.49	1.60	1.35	1.58	1.78	1.33	1.58	1.78	1.35
12.10	6	FWS	1.28	1.35	1.27	1.35	1.50	1.26	1.35	1.50	1.27
11.00	5	FWS	1.14	1.21	1.21	1.20	1.32	1.20	1.20	1.32	1.21
9.90	4	FWS	1.00	1.11	1.15	1.05	1.13	1.13	1.05	1.13	1.15
8.81	3	FWS	0.87	1.01	1.07	0.94	1.00	1.06	0.94	1.01	1.07
6.73	2	FWS	0.66	0.76	0.91	0.70	0.81	0.92	0.70	0.81	0.92
4.65	8002	Basemat Top	0.62	0.65	0.72	0.63	0.66	0.75	0.63	0.66	0.75
2.15	8001	Basemat Bottom	0.63	0.57	0.88	0.66	0.58	0.90	0.66	0.58	0.90
8.25	405	FPE	0.81	1.42	0.72	0.77	1.46	0.77	0.81	1.46	0.77
6.45	402	FPE	0.72	1.04	0.68	0.70	1.10	0.72	0.72	1.10	0.72

Note: The shaded values are the governing case(s).

*) Obtained from the FWSC-CB SSSI Analyses in Reference 2-r

Table 6.1-4: Comparison of Site-Specific and Standard Design Enveloping Maximum Accelerations

Elev. (m)	Node No.	Location	Standard Design			NA3 Enveloping			Difference		
			NS (g)	EW (g)	Vert. (g)	NS (g)	EW (g)	Vert. (g)	NS	EW	Vert.
19.70	10	FWS	2.16	2.40	1.69	2.21	2.42	1.43	2%	1%	-15%
17.25	9	FWS	1.99	2.09	1.64	2.00	2.26	1.43	0%	8%	-13%
15.53	8	FWS	1.80	1.81	1.58	1.80	2.04	1.40	0%	12%	-11%
13.81	7	FWS	1.60	1.63	1.58	1.58	1.78	1.35	-1%	9%	-15%
12.10	6	FWS	1.43	1.59	1.43	1.35	1.50	1.27	-5%	-5%	-11%
11.00	5	FWS	1.33	1.52	1.23	1.20	1.32	1.21	-10%	-13%	-1%
9.90	4	FWS	1.24	1.44	1.13	1.05	1.13	1.15	-15%	-22%	2%
8.81	3	FWS	1.15	1.37	1.05	0.94	1.01	1.07	-18%	-26%	2%
6.73	2	FWS	0.77	0.88	1.00	0.70	0.81	0.92	-9%	-8%	-9%
4.65	8002	Basemat Top	0.71	0.77	0.78	0.63	0.66	0.75	-12%	-14%	-4%
2.15	8001	Basemat Bottom	0.70	0.76	0.78	0.66	0.58	0.90	-6%	-23%	15%
8.25	405	FPE	1.72	1.60	1.12	0.81	1.46	0.77	-53%	-8%	-31%
6.45	402	FPE	1.19	1.19	1.09	0.72	1.10	0.72	-40%	-8%	-34%

Note: The shaded values are exceedances of site-specific loads with respect to standard design.

Table 6.1-5: Site-Specific Enveloping Maximum Accelerations of FWSC SDOF Oscillators

SDOF Oscillator				Acceleration (g)				Difference
Elev. (m)	Node No.	Description	Direction	SSI Analyses Envelope	SSSI Analyses Envelope*)	NA3 Enveloping	Standard Design	
19.70	11	FWS Roof	Vert. (Z)	3.36	3.98	3.98	3.26	22%
12.10	60	FWS Water Sloshing Mode	NS (X)	0.10	0.10	0.10	0.30	-66%
			EW (Y)	0.09	0.09	0.09	0.40	-78%
8.81	30	FWS Water Impulsive Mode	NS (X)	0.87	0.94	0.94	1.10	-15%
			EW (Y)	1.01	1.00	1.01	1.40	-28%

Note: The shaded values are exceedances of site-specific loads with respect to standard design.

*) Obtained from the FWSC-CB SSSI Analyses in Reference 2-r

Table 6.1-6: Site-Specific Out-of-Plane Load on FWS Roof

Slab		Flexible Mode (SDOF Oscillator)				Rigid Mode (LMSM)				Eq. Ave. Acc. (g)			Difference
Elev. (m)	Location	Weight (kN)	Mass Node	Acceleration (g)		Weight (kN)	Mass Node	Acceleration (g)		NA3 Site-Specific		Stand. Design	
				SSSI Envelope*)	SSI Envelope			SSSI Envelope*)	SSI Envelope	SSSI Envelope	SSI Envelope		
19.70	FWS Roof	1339	11	3.98	3.36	2480	10	1.40	1.43	2.30	2.11	1.74	32%

Note: The shaded values are the governing case.

*) Obtained from the FWSC-CB SSSI Analyses in Reference 2-r

Table 6.2-1: FWSC Site-Specific Enveloping Maximum Displacements Relative to Free-Field Motion

Elev. (m)	Node No.	Location	SSI Analyses Envelope			SSSI Analyses Envelope*)			NA3 Enveloping		
			NS (cm)	EW (cm)	Vert. (cm)	NS (cm)	EW (cm)	Vert. (cm)	NS (cm)	EW (cm)	Vert. (cm)
19.70	10	FWS	0.59	0.59	0.05	0.25	0.36	0.04	0.59	0.59	0.05
17.25	9	FWS	0.57	0.59	0.10	0.24	0.34	0.09	0.57	0.59	0.10
15.53	8	FWS	0.56	0.58	0.10	0.22	0.32	0.09	0.56	0.58	0.10
13.81	7	FWS	0.55	0.57	0.10	0.21	0.30	0.09	0.55	0.57	0.10
12.10	6	FWS	0.54	0.55	0.10	0.19	0.28	0.09	0.54	0.55	0.10
11.00	5	FWS	0.54	0.55	0.10	0.18	0.26	0.09	0.54	0.55	0.10
9.90	4	FWS	0.54	0.54	0.09	0.17	0.25	0.09	0.54	0.54	0.09
8.81	3	FWS	0.53	0.53	0.09	0.16	0.23	0.08	0.53	0.53	0.09
6.73	2	FWS	0.52	0.51	0.09	0.13	0.20	0.08	0.52	0.51	0.09
4.65	8002	Basemat Top	0.52	0.50	0.08	0.09	0.14	0.09	0.52	0.50	0.09
2.15	8001	Basemat Bottom	0.51	0.48	0.10	0.10	0.16	0.07	0.51	0.48	0.10
8.25	405	FPE	0.52	0.51	0.06	0.09	0.18	0.05	0.52	0.51	0.06
6.45	402	FPE	0.52	0.50	0.03	0.09	0.17	0.03	0.52	0.50	0.03

Note: The shaded values are the governing case.

*) Obtained from the FWSC-CB SSSI Analyses in Reference 2-r

Table 6.2-2: Comparison of Site-Specific and Standard Design Enveloping Maximum Displacements

Elev. (m)	Node No.	Location	Standard Design			NA3 Enveloping			Difference		
			NS (cm)	EW (cm)	Vert. (cm)	NS (cm)	EW (cm)	Vert. (cm)	NS	EW	Vert.
19.70	10	FWS	0.71	0.80	0.28	0.59	0.59	0.05	-17%	-26%	-83%
17.25	9	FWS	0.68	0.75	0.28	0.57	0.59	0.10	-16%	-22%	-64%
15.53	8	FWS	0.66	0.71	0.28	0.56	0.58	0.10	-15%	-19%	-64%
13.81	7	FWS	0.64	0.67	0.28	0.55	0.57	0.10	-14%	-16%	-65%
12.10	6	FWS	0.62	0.63	0.28	0.54	0.55	0.10	-12%	-12%	-65%
11.00	5	FWS	0.61	0.60	0.28	0.54	0.55	0.10	-12%	-9%	-66%
9.90	4	FWS	0.60	0.58	0.28	0.54	0.54	0.09	-11%	-7%	-66%
8.81	3	FWS	0.58	0.55	0.28	0.53	0.53	0.09	-8%	-3%	-67%
6.73	2	FWS	0.55	0.51	0.28	0.52	0.51	0.09	-5%	1%	-69%
4.65	8002	Basemat Top	0.51	0.46	0.28	0.52	0.50	0.09	1%	8%	-68%
2.15	8001	Basemat Bottom	0.50	0.42	0.28	0.51	0.48	0.10	3%	13%	-63%
8.25	405	FPE	0.53	0.52	0.28	0.52	0.51	0.06	-2%	-2%	-80%
6.45	402	FPE	0.52	0.49	0.28	0.52	0.50	0.03	-1%	2%	-90%

Note: The shaded values are exceedances of site-specific loads with respect to standard design.

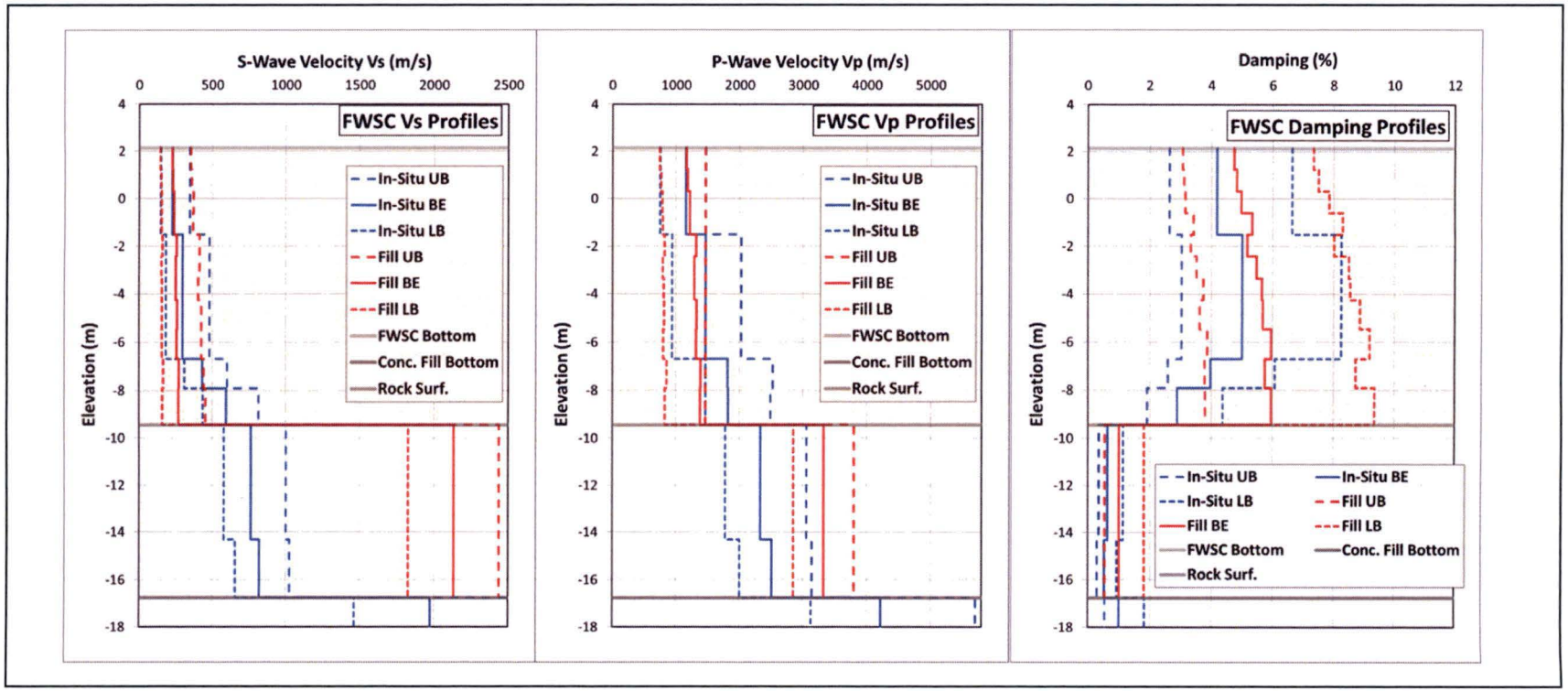

Note: The beige shaded area represents the structural fill replacing the in-situ saprolite layer.

Figure 3.1-1: Comparisons Between Shear and Compression Wave Velocity and Damping Ratio of Structural Fill and In-Situ Saprolite

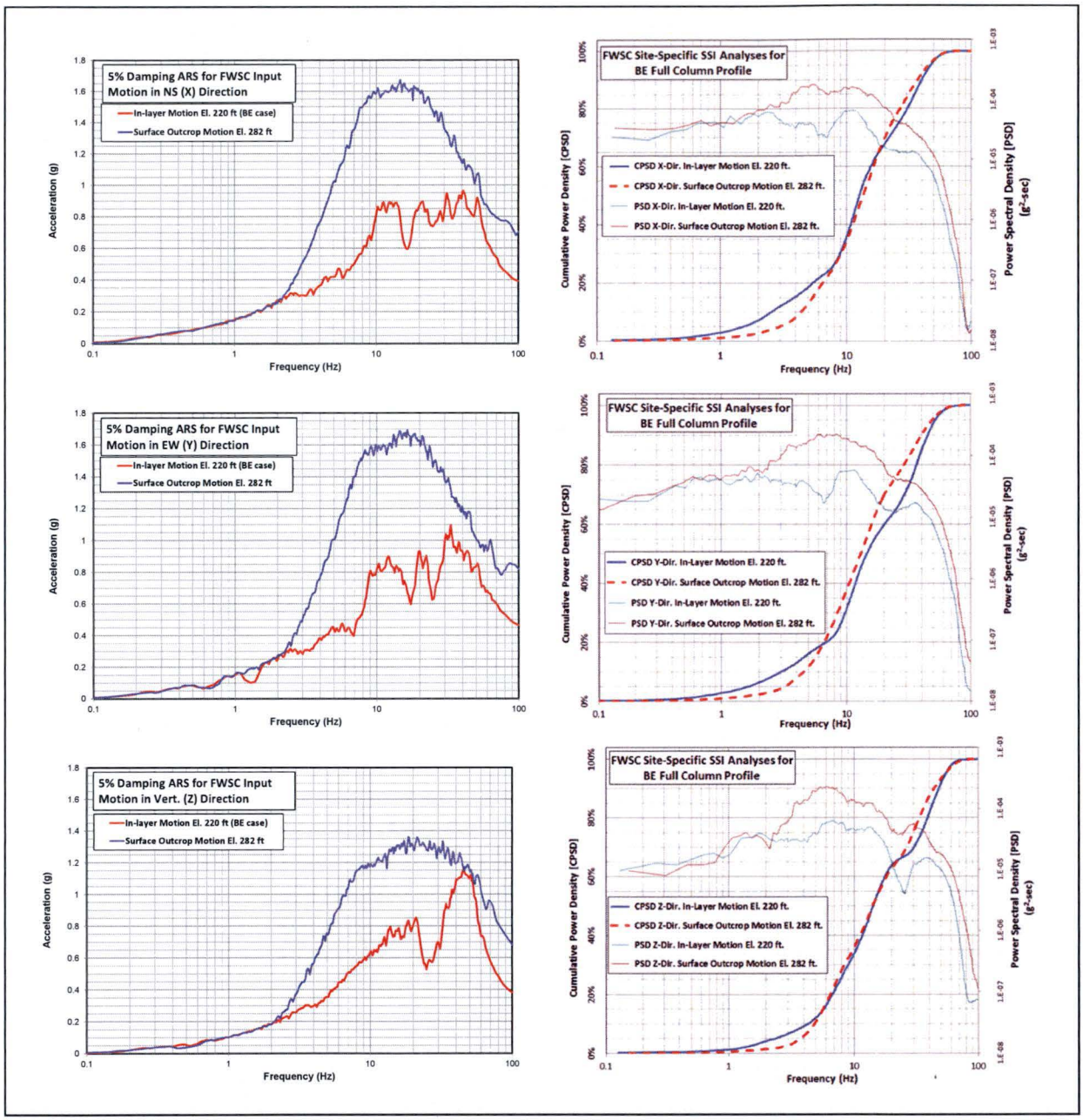

Figure 3.2-1: 5% Damped ARS, PSD, and CPSD of Input Acceleration Time Histories for FWSC Analysis of BE Subgrade Profile

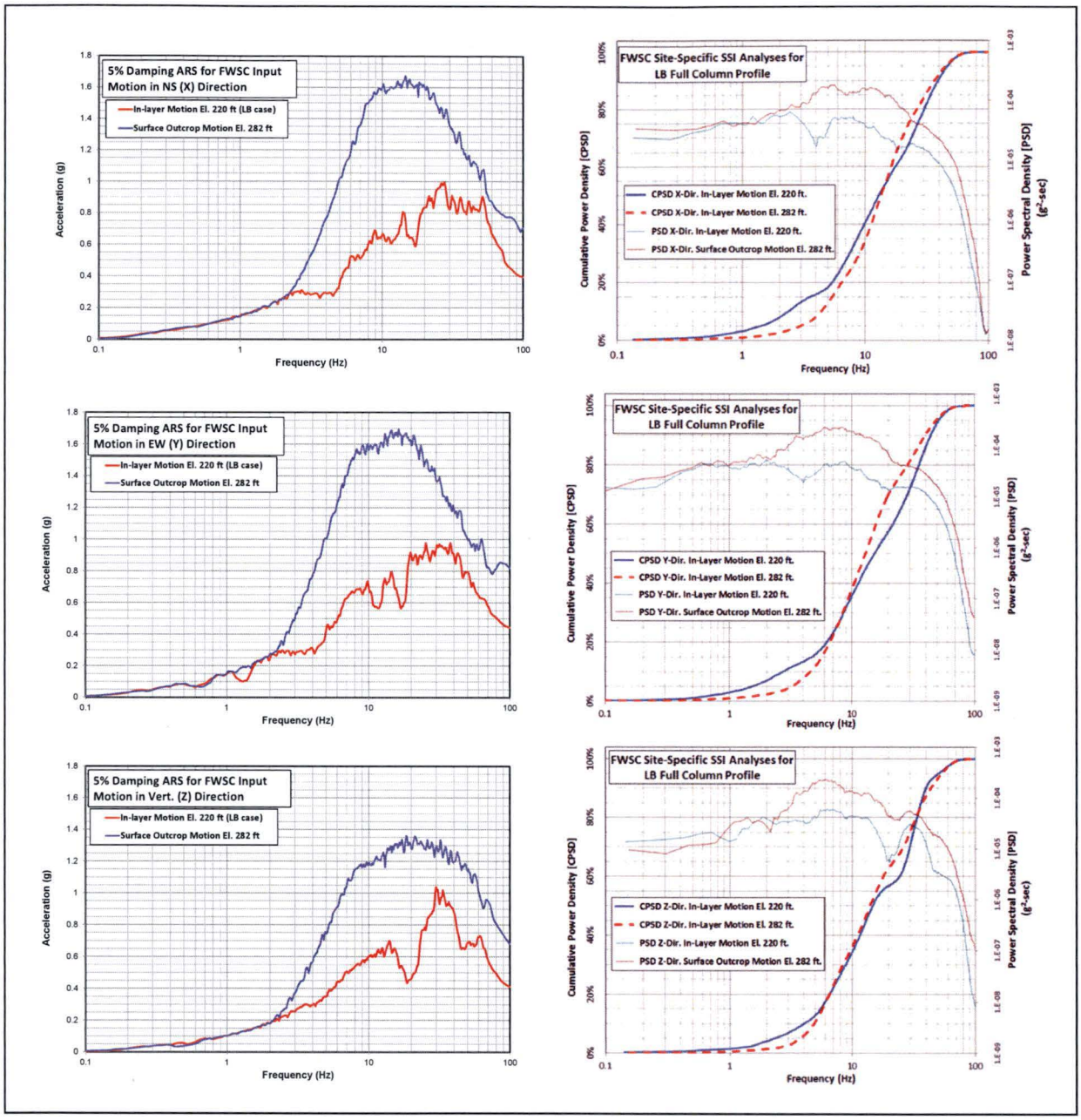

Figure 3.2-2: 5% Damped ARS, PSD, and CPSD of Input Acceleration Time Histories for FWSC Analysis of LB Subgrade Profile

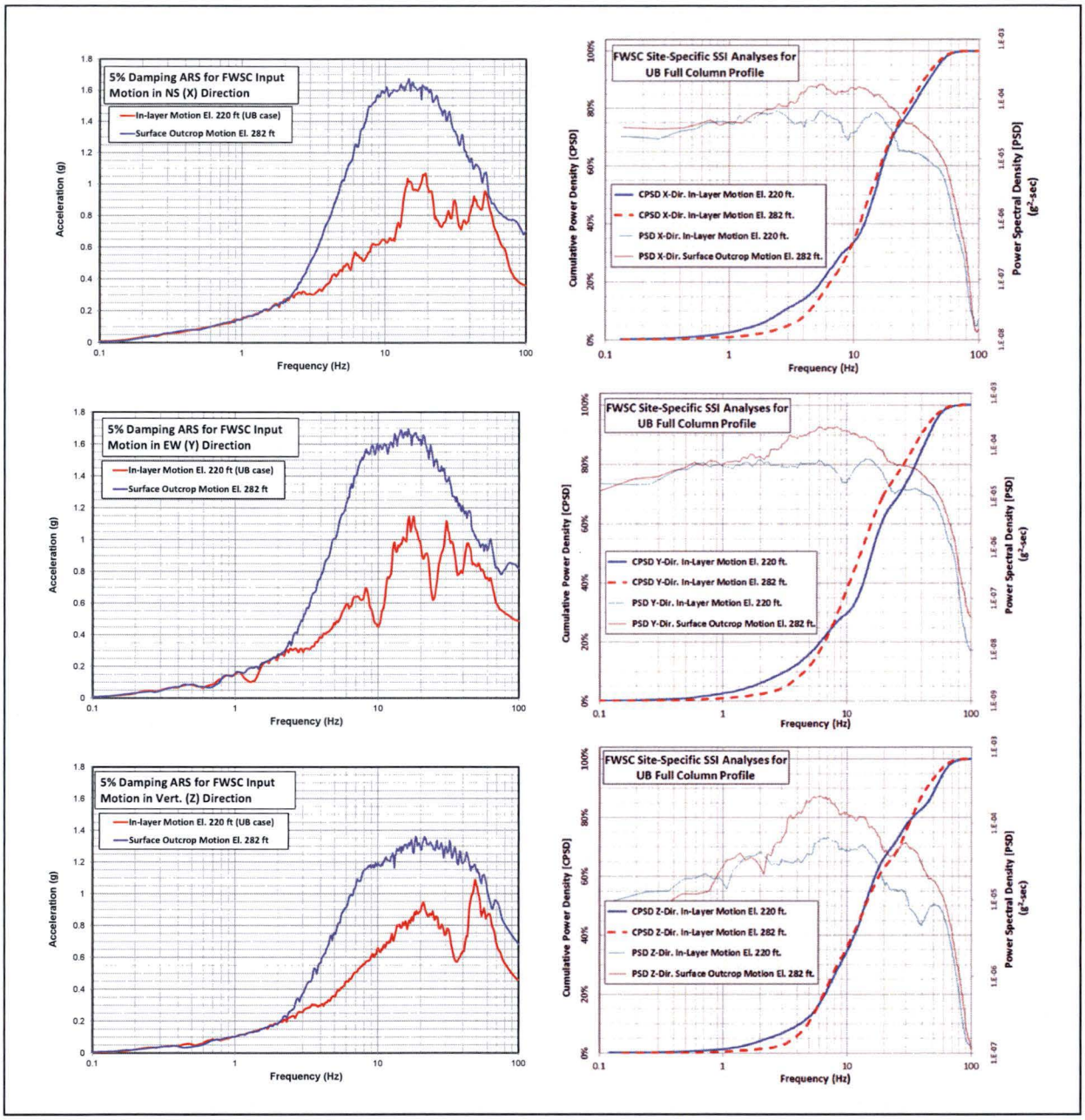

Figure 3.2-3: 5% Damped ARS, PSD, and CPSD of Input Acceleration Time Histories for FWSC Analysis of UB Subgrade Profile

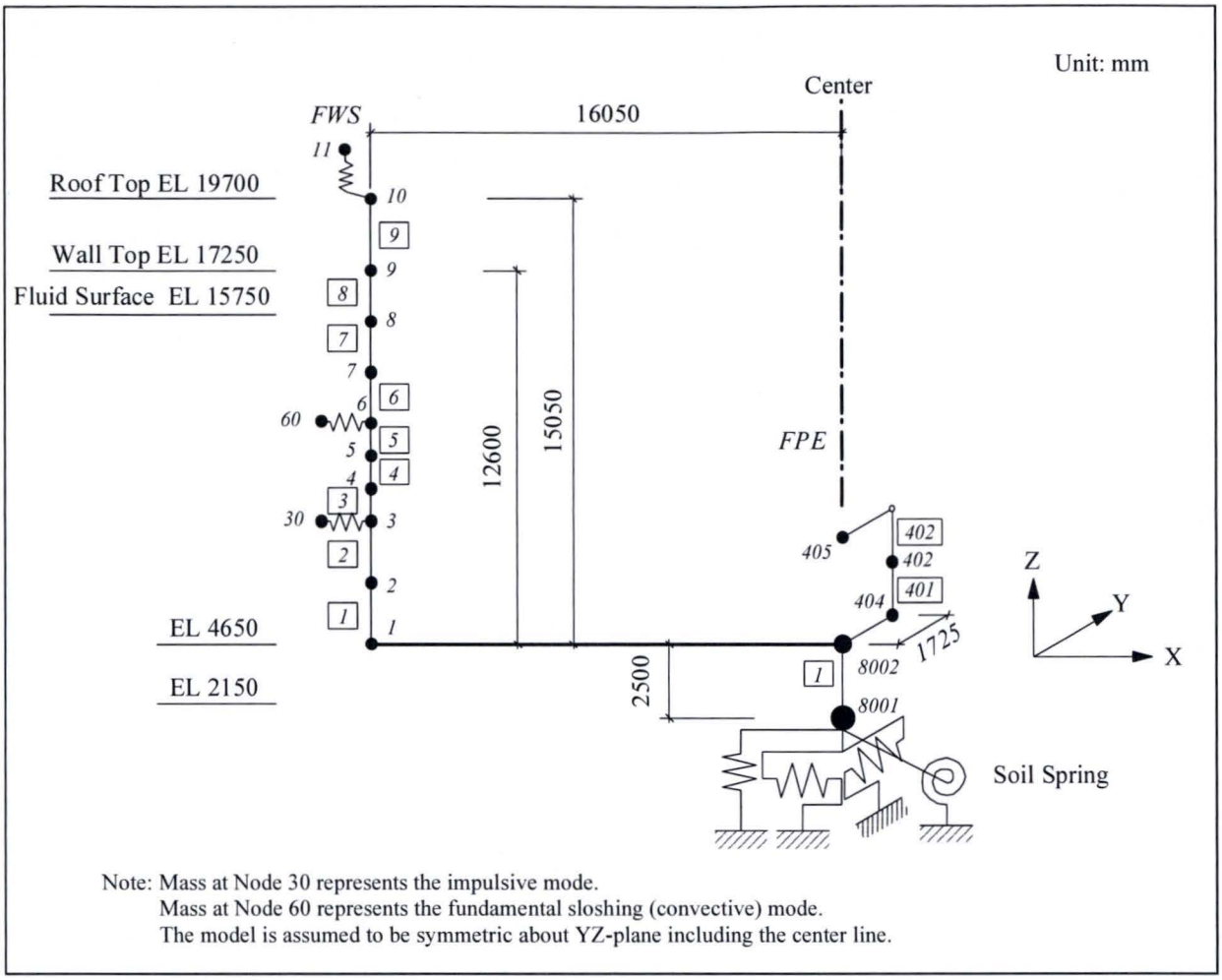

Note: Mass at Node 30 represents the impulsive mode.
Mass at Node 60 represents the fundamental sloshing (convective) mode.
The model is assumed to be symmetric about YZ-plane including the center line.

Figure 4.3-1: FWSC Seismic Analysis Stick Model

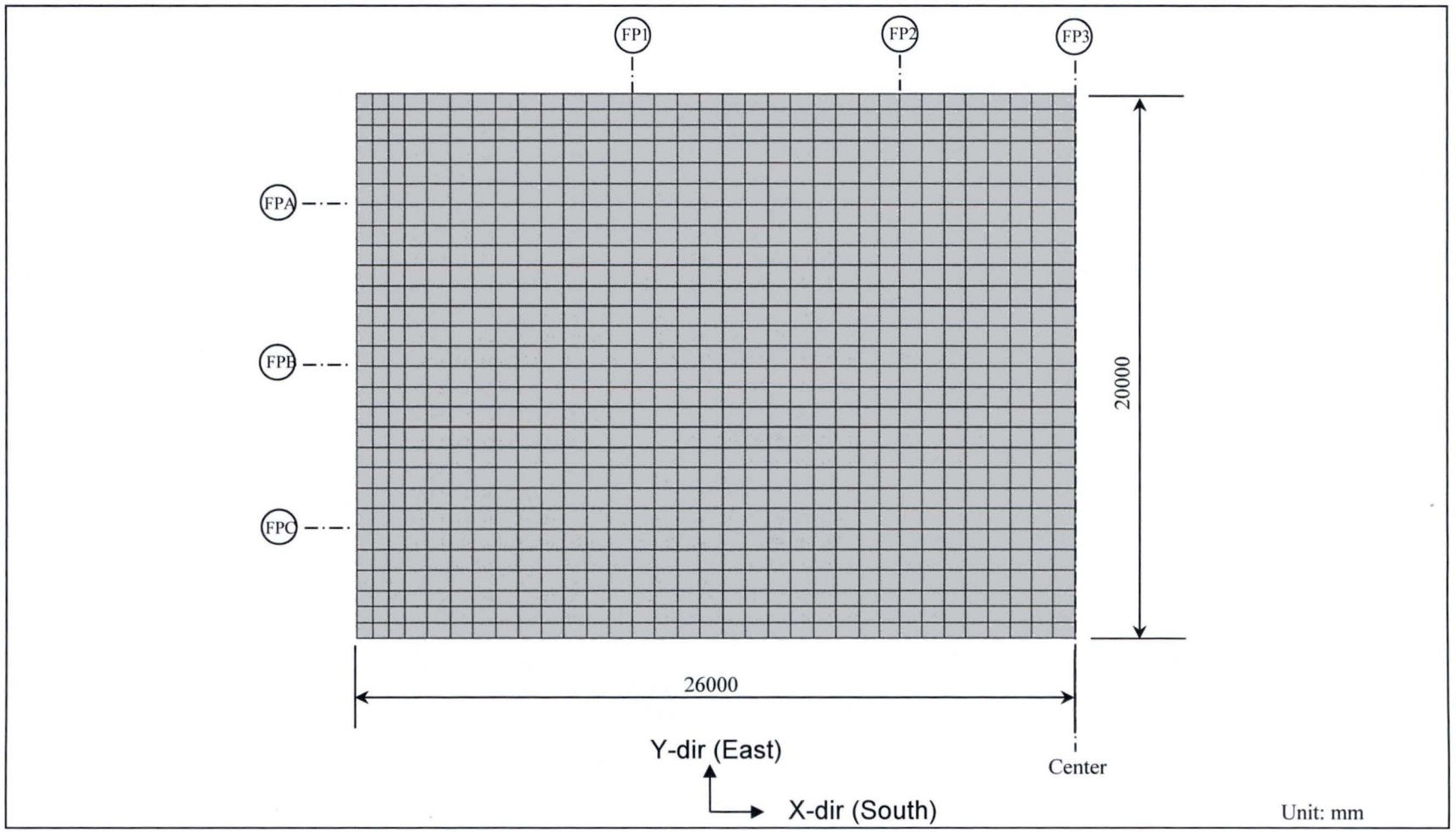

Figure 4.3-2: SASSI2010 Plate Elements for FWSC Basemat

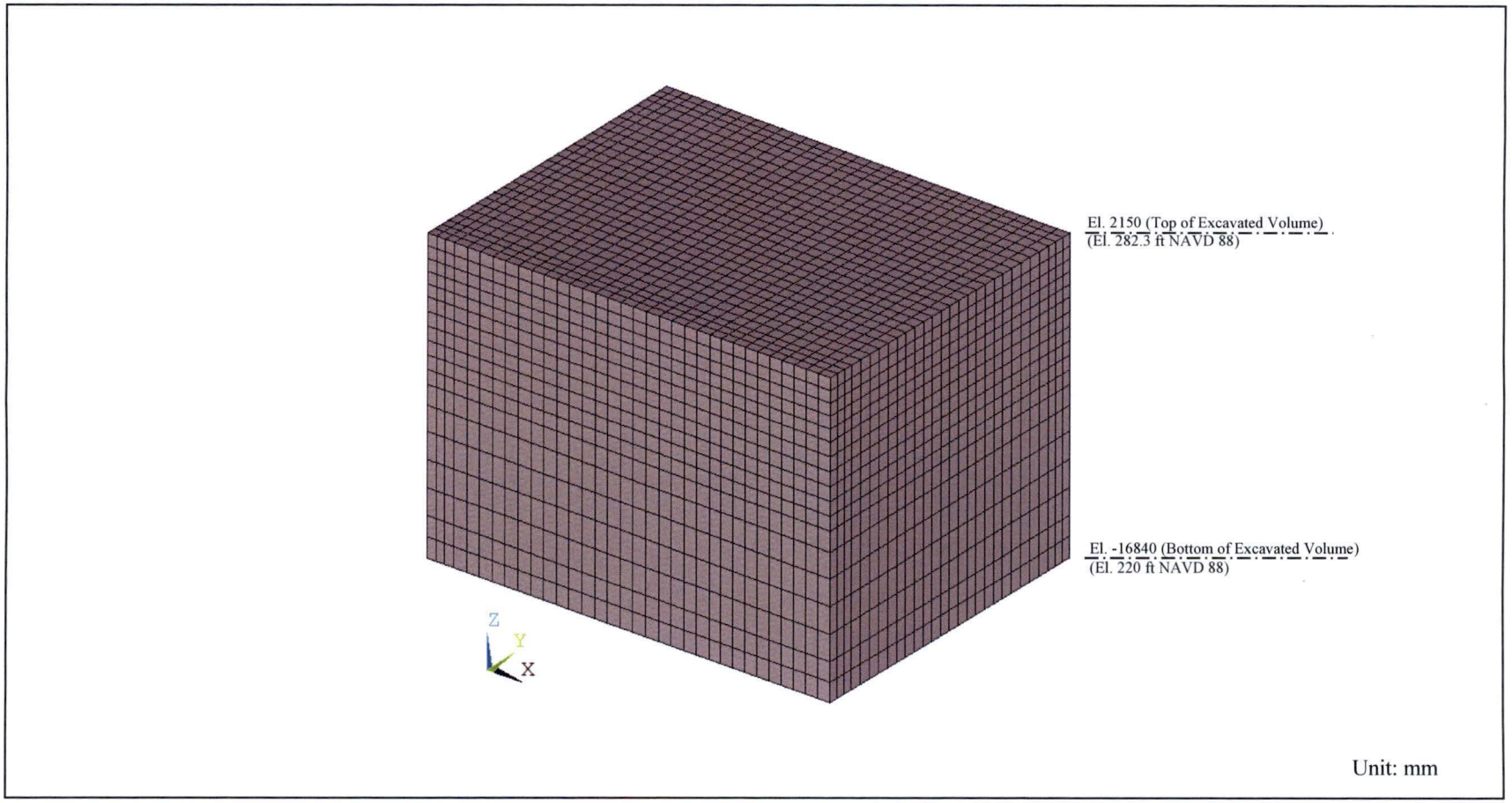

Figure 4.3-3: SASSI2010 Solid Elements for FWSC Concrete Fill and or Excavated Volume

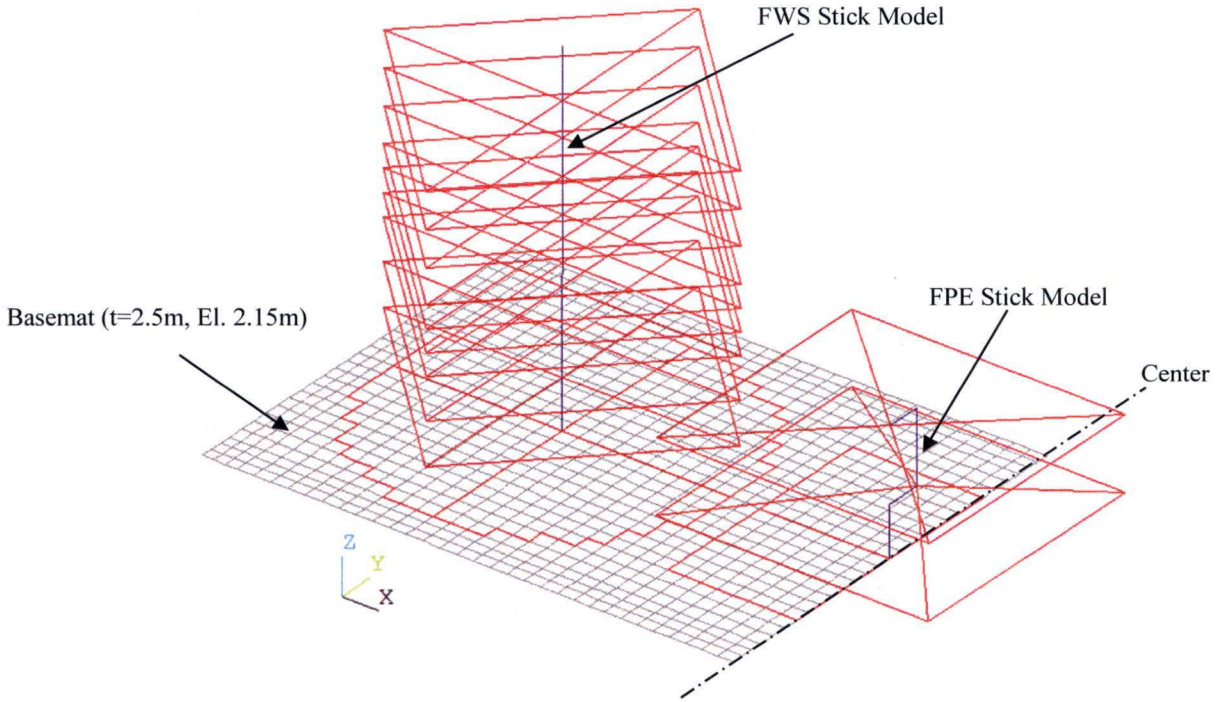

(a) Overview without Concrete Fill

Note: Basemat is modeled with shell elements.

Figure 4.3-4: Overview of SASSI2010 SSI FWSC Half Model

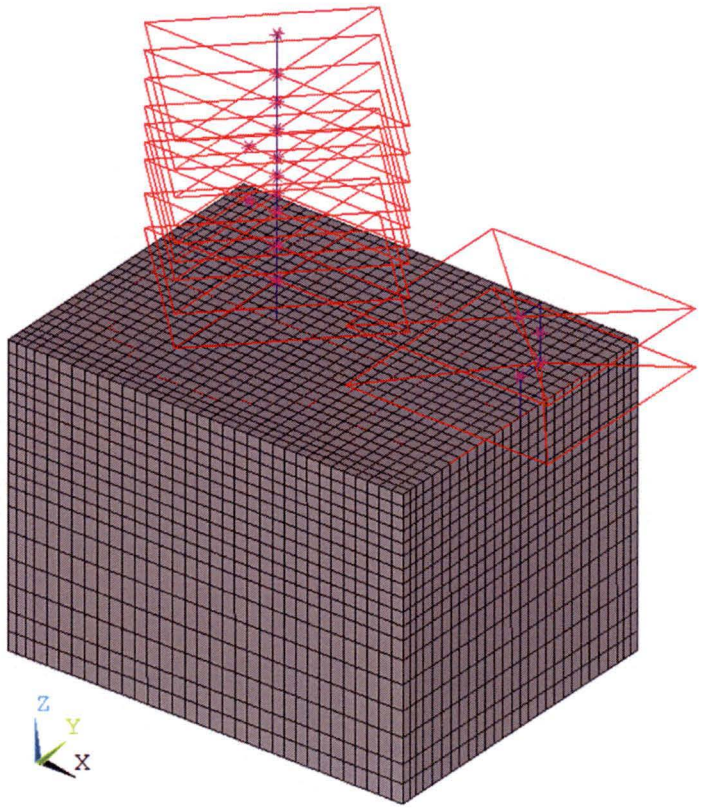

(b) Overview with Concrete Fill

Note: Basemat is modeled with shell elements.

Unit: mm

Figure 4.3-4: Overview of SASSI2010 SSI FWSC Half Model (Continued)

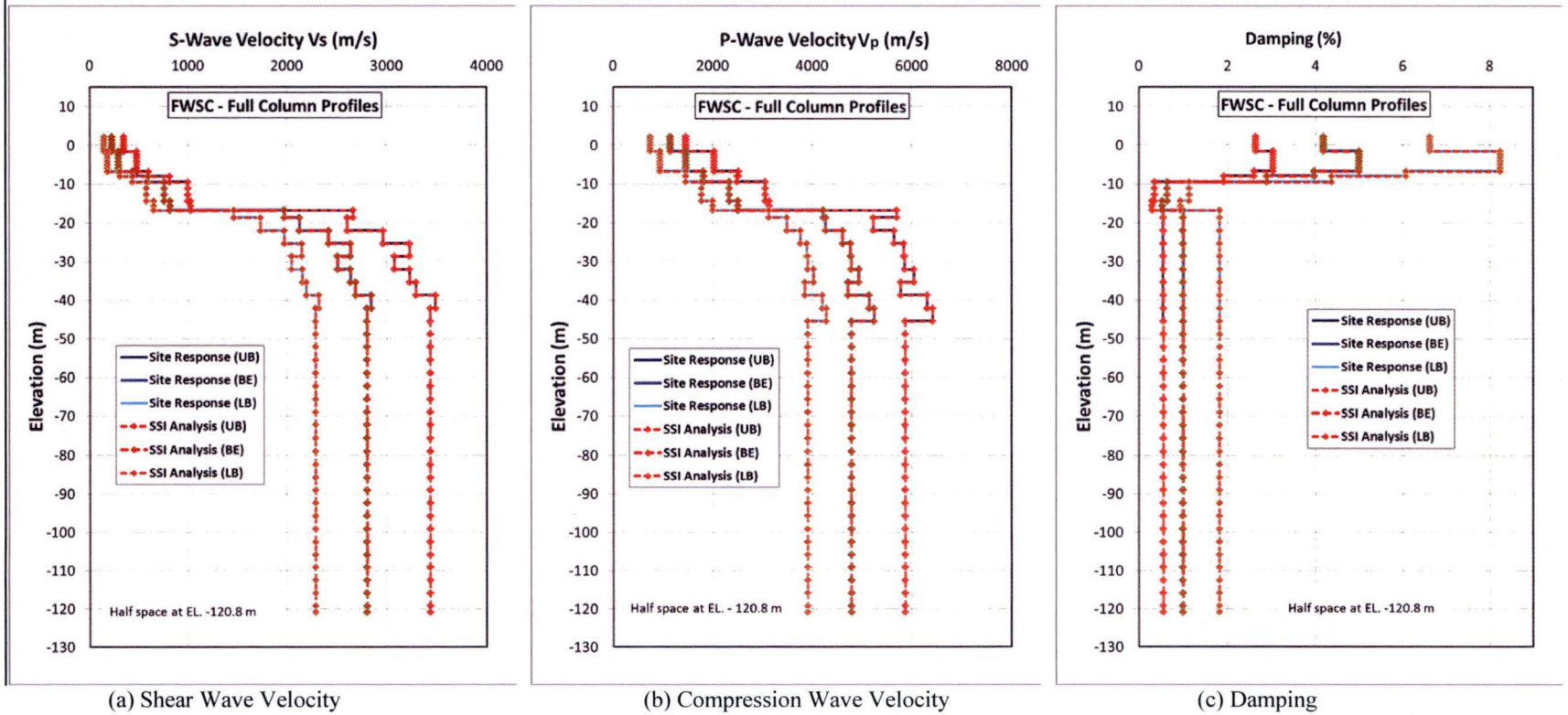

(a) Shear Wave Velocity (b) Compression Wave Velocity (c) Damping

Figure 4.3-5: SSI Input Strain-Compatible Subgrade Properties

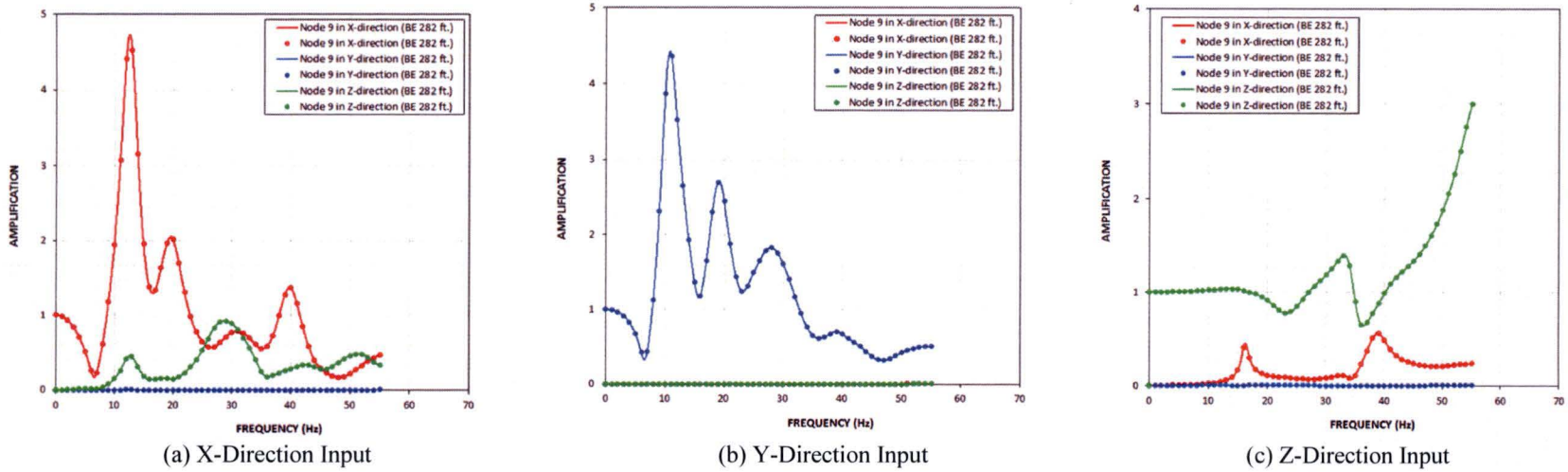

(a) X-Direction Input (b) Y-Direction Input (c) Z-Direction Input

Figure 5.1-1a: Transfer Functions for FWS Wall Top Response from Analysis of UC_{OBE} Model of BE Profile and Surface Input Motion at El. 282 ft

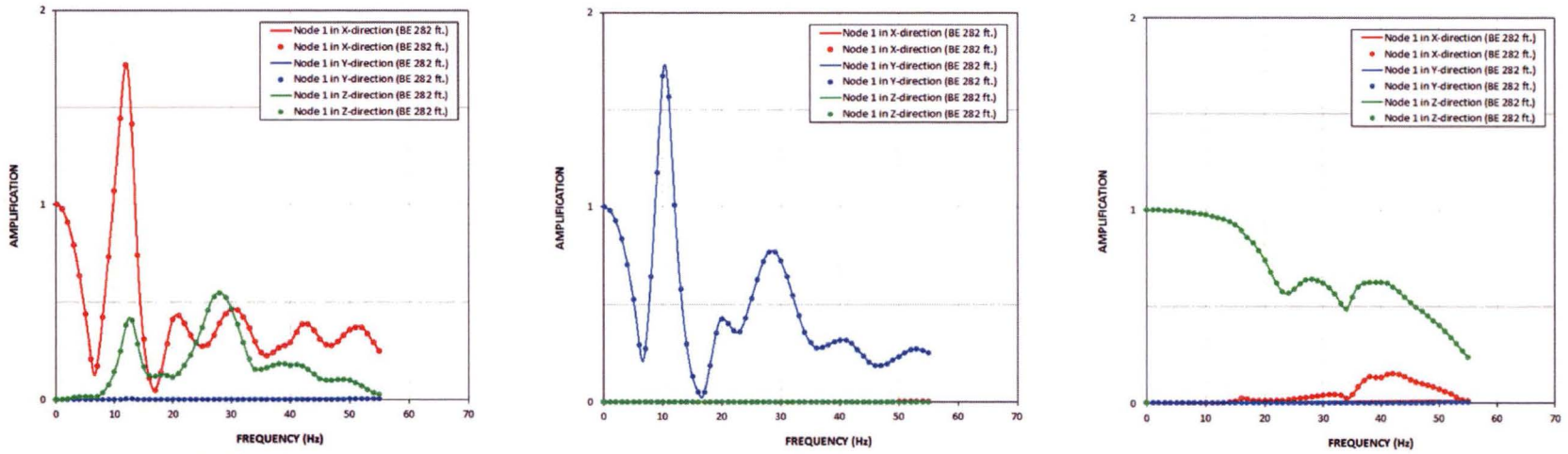

(a) X-Direction Input (b) Y-Direction Input (c) Z-Direction Input

Figure 5.1-1b: Transfer Functions for FWS Basemat Response from Analysis of UC_{OBE} Model of BE Profile and Surface Input Motion at El. 282 ft

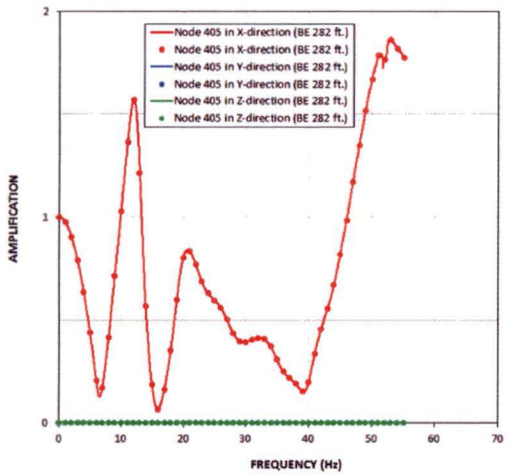

(a) X-Direction Input

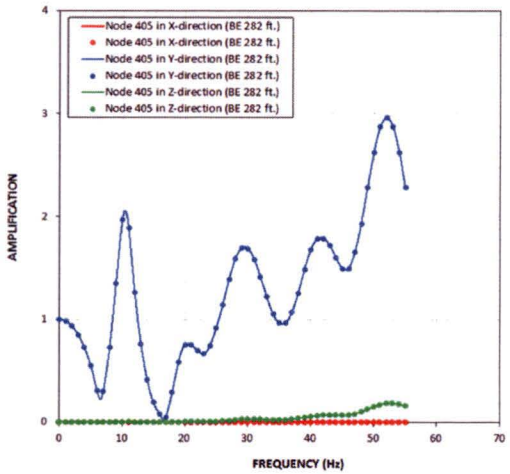

(b) Y-Direction Input

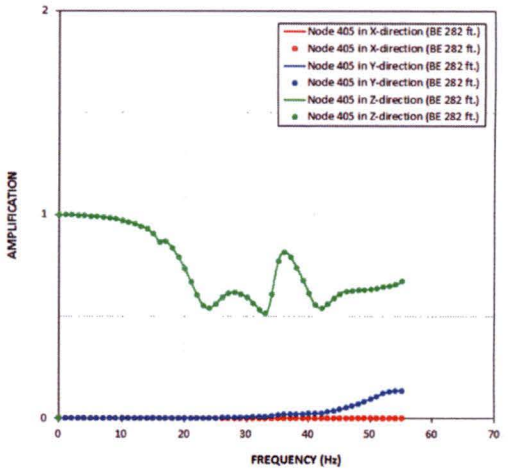

(c) Z-Direction Input

Figure 5.1-1c: Transfer Functions for FPE Top Response from Analysis of UC_{OBE} Model of BE Profile and Surface Input Motion at El. 282 ft

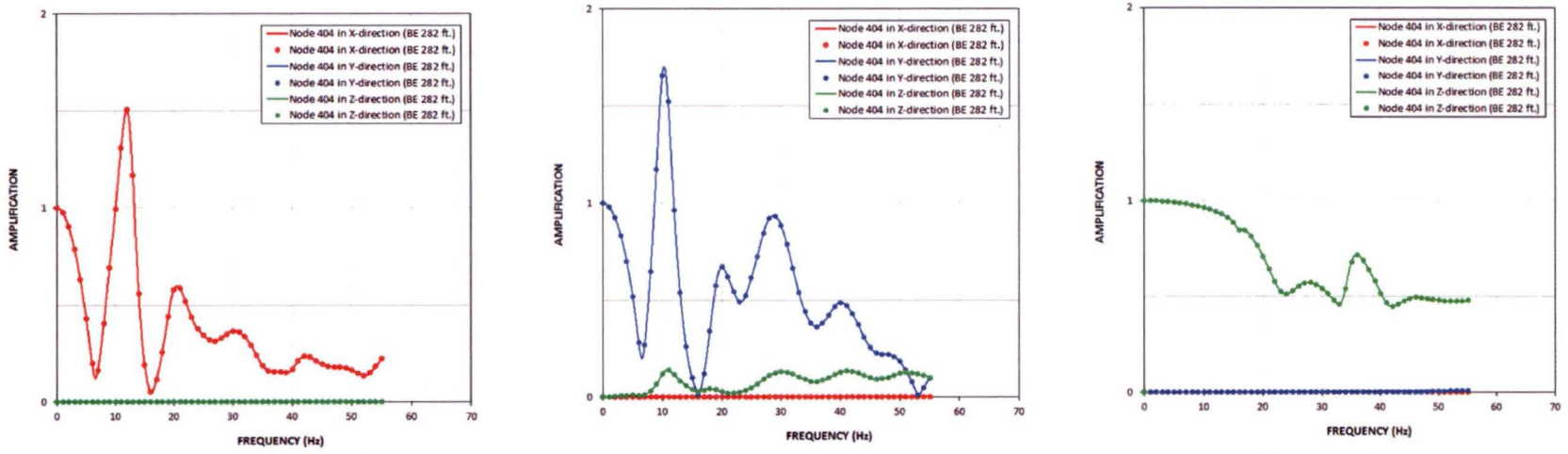

(a) X-Direction Input (b) Y-Direction Input (c) Z-Direction Input

Figure 5.1-1d: Transfer Functions for FPE Basemat Response from Analysis of UC_{OBE} Model of BE Profile and Surface Input Motion at El. 282 ft

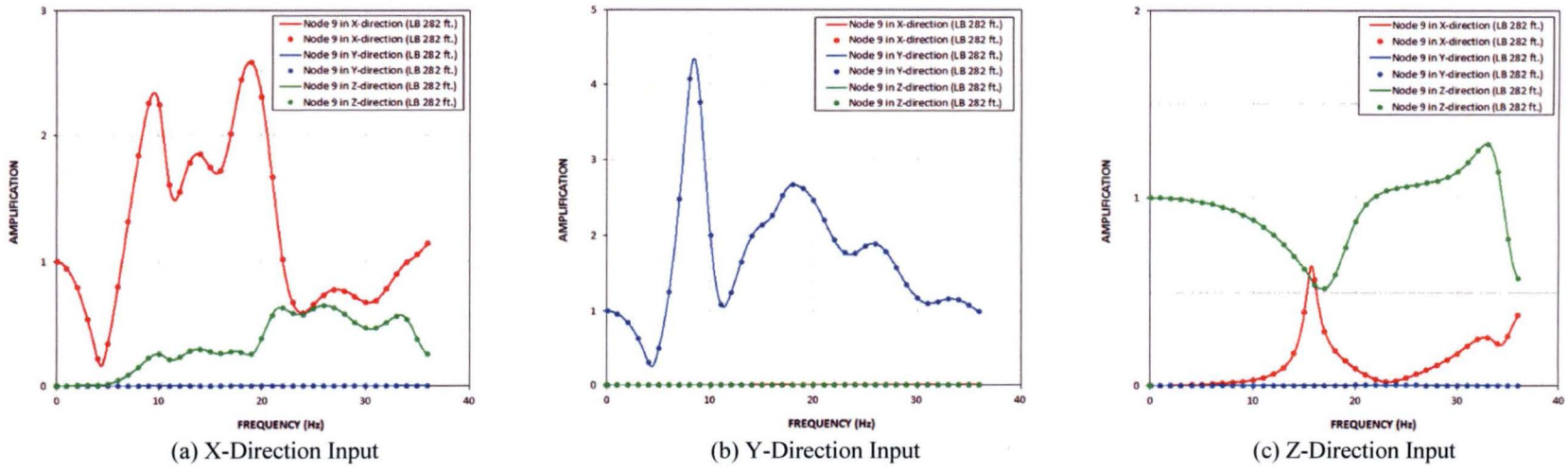

(a) X-Direction Input (b) Y-Direction Input (c) Z-Direction Input

Figure 5.1-2a: Transfer Functions for FWS Wall Top Response from Analysis of UC_{OBE} Model of LB Profile and Surface Input Motion at El. 282 ft

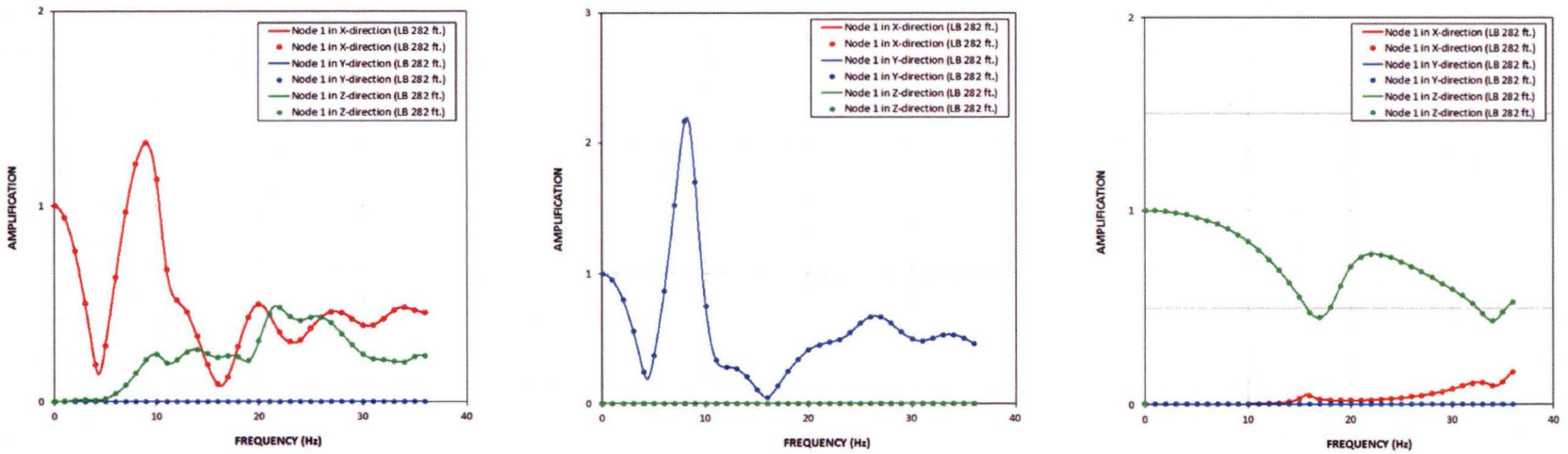

(a) X-Direction Input (b) Y-Direction Input (c) Z-Direction Input

Figure 5.1-2b: Transfer Functions for FWS Basemat Response from Analysis of UC_{OBE} Model of LB Profile and Surface Input Motion at El. 282 ft

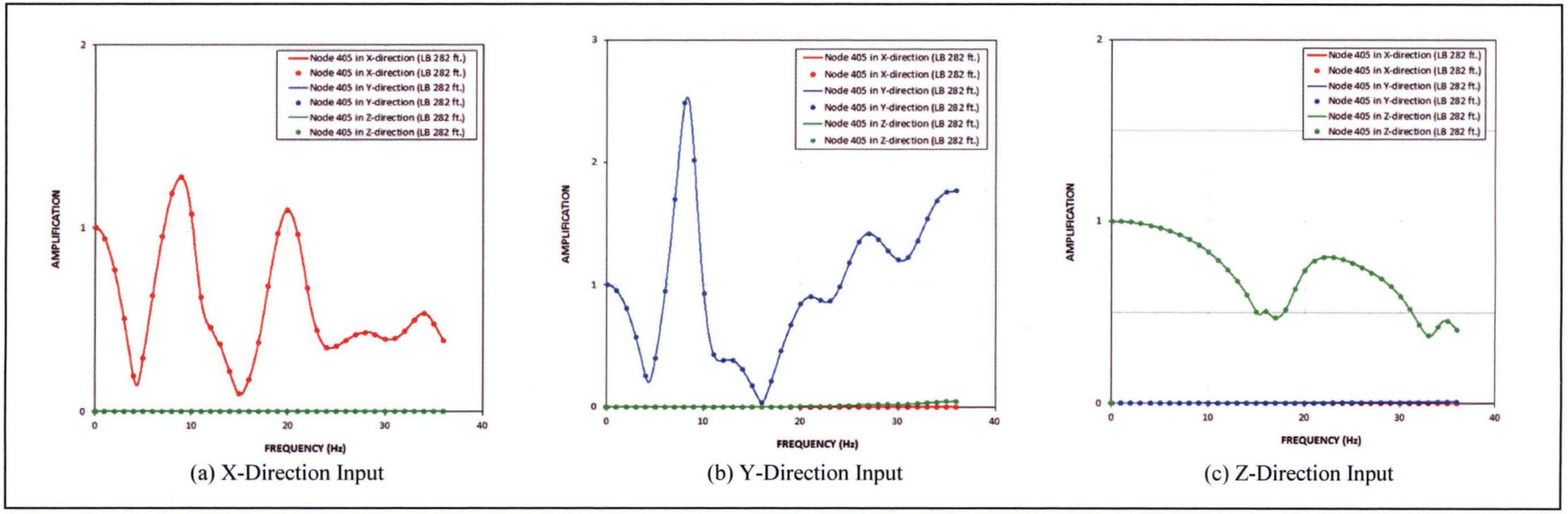

(a) X-Direction Input (b) Y-Direction Input (c) Z-Direction Input

Figure 5.1-2c: Transfer Functions for FPE Top Response from Analysis of UC_{OBE} Model of LB Profile and Surface Input Motion at El. 282 ft

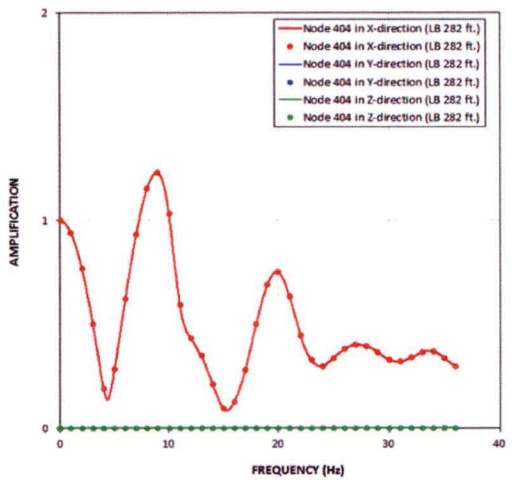

(a) X-Direction Input

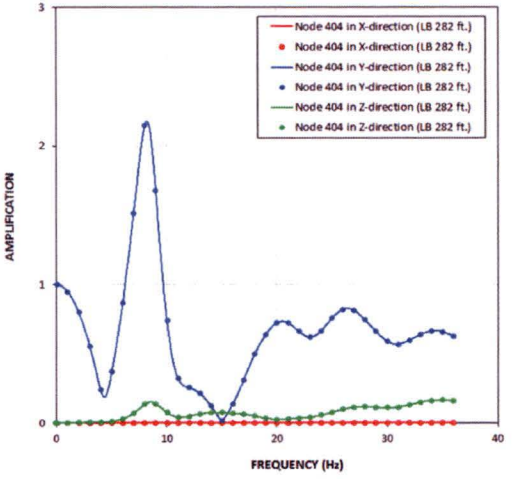

(b) Y-Direction Input

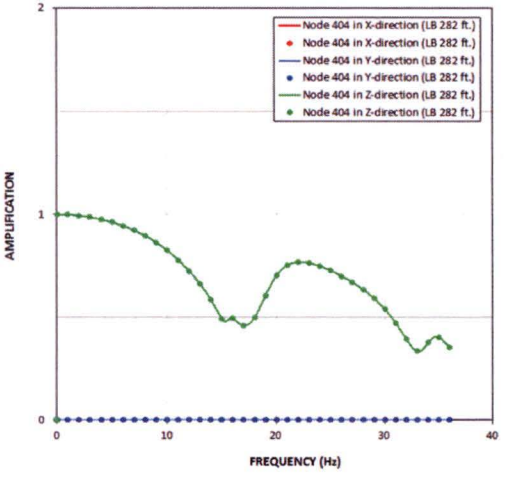

(c) Z-Direction Input

Figure 5.1-2d: Transfer Functions for FPE Basemat Response from Analysis of UC_{OBE} Model of LB Profile and Surface Input Motion at El. 282 ft

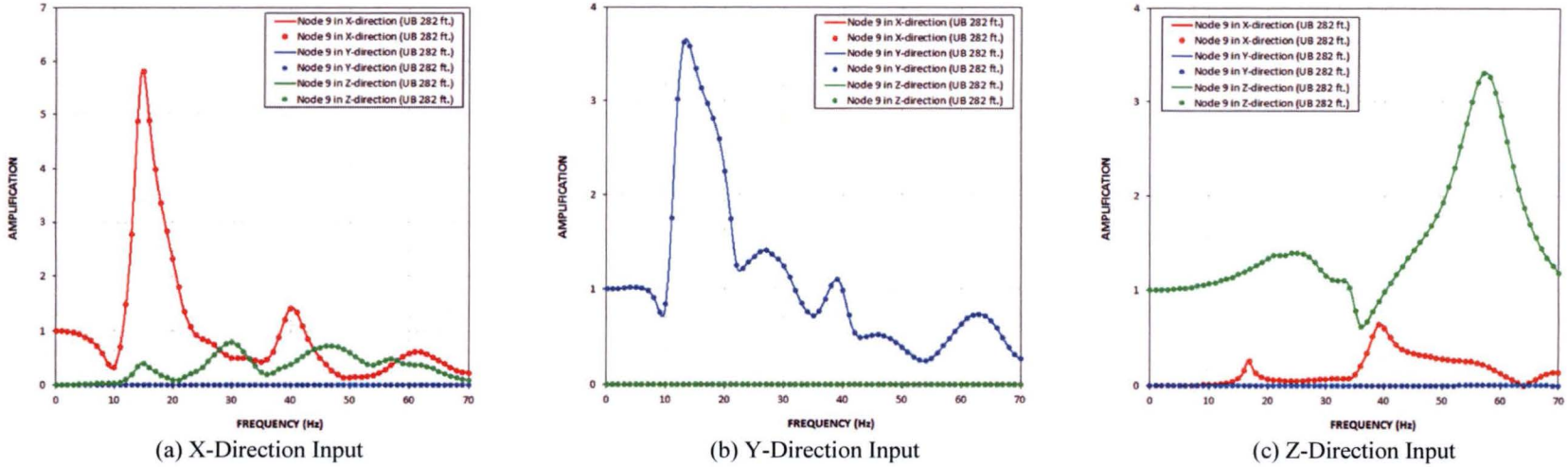

(a) X-Direction Input (b) Y-Direction Input (c) Z-Direction Input

Figure 5.1-3a: Transfer Functions for FWS Wall Top Response from Analysis of UC_{OBE} Model of UB Profile and Surface Input Motion at El. 282 ft

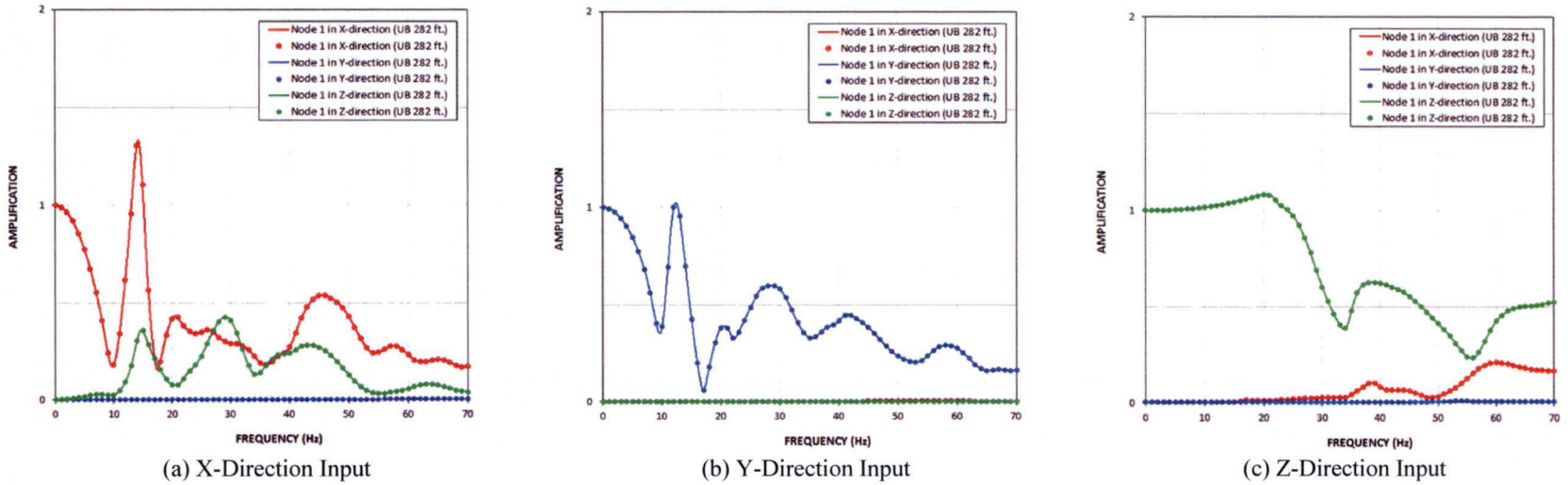

(a) X-Direction Input (b) Y-Direction Input (c) Z-Direction Input

Figure 5.1-3b: Transfer Functions for FWS Basemat Response from Analysis of UC_{OBE} Model of UB Profile and Surface Input Motion at El. 282 ft

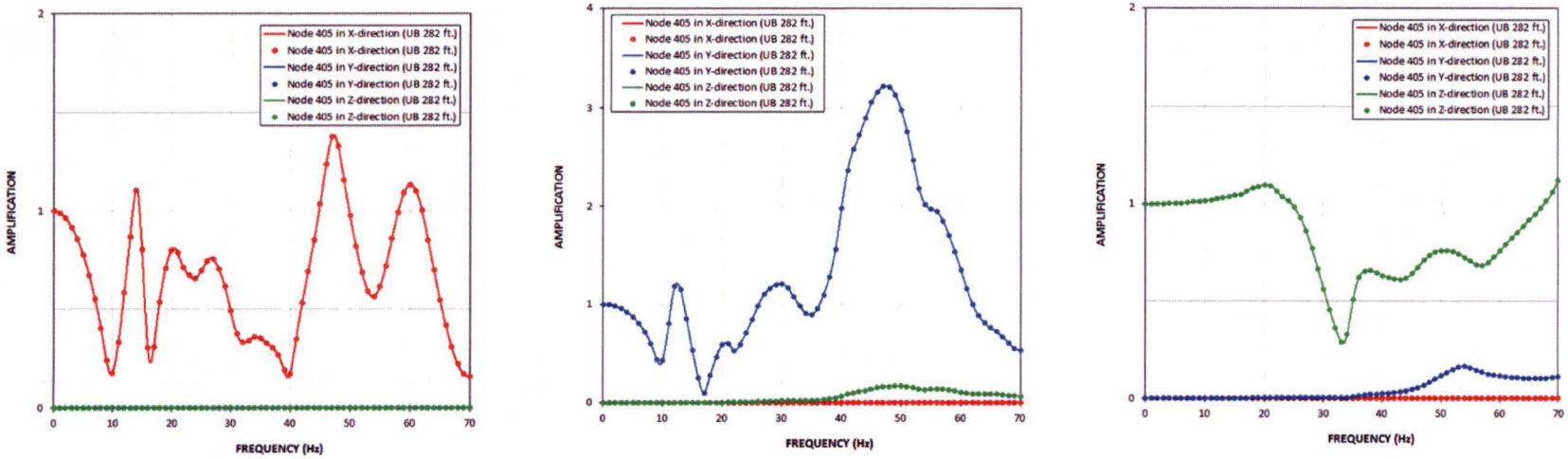

(a) X-Direction Input (b) Y-Direction Input (c) Z-Direction Input

Figure 5.1-3c: Transfer Functions for FPE Top Response from Analysis of UC_{OBE} Model of UB Profile and Surface Input Motion at El. 282 ft

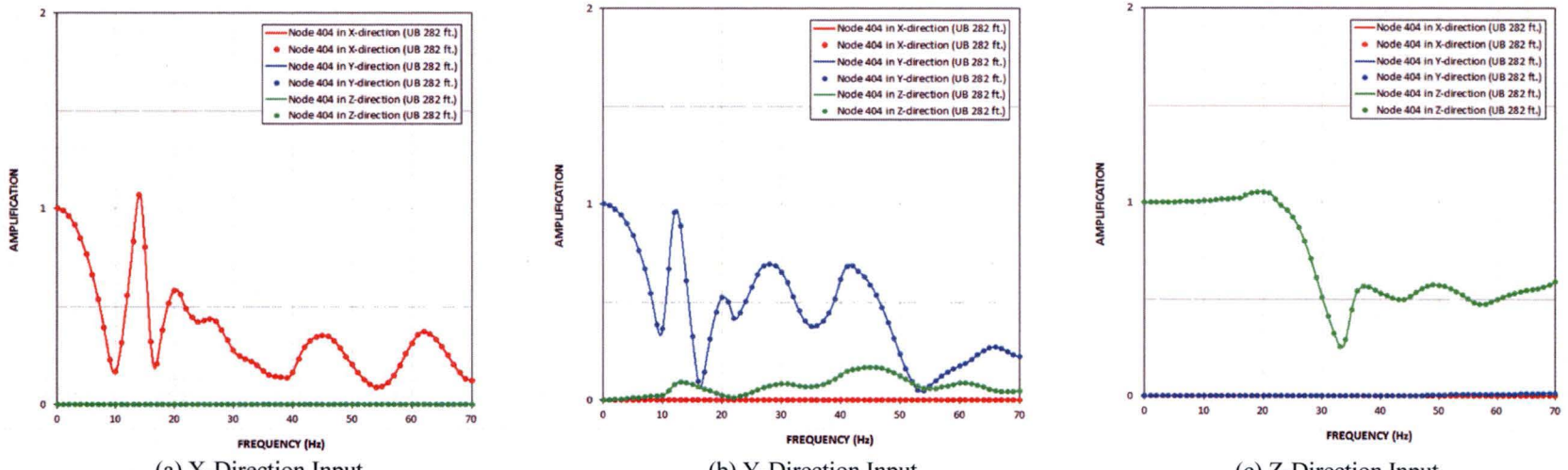

(a) X-Direction Input (b) Y-Direction Input (c) Z-Direction Input

Figure 5.1-3d: Transfer Functions for FPE Basemat Response from Analysis of UC_{OBE} Model of UB Profile and Surface Input Motion at El. 282 ft

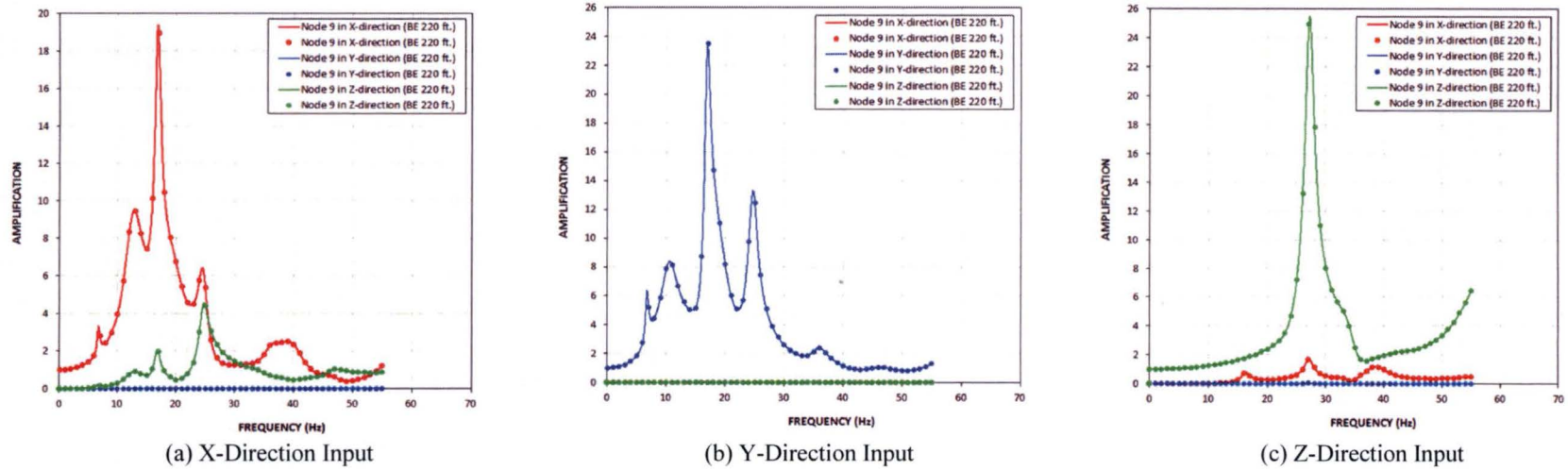

(a) X-Direction Input (b) Y-Direction Input (c) Z-Direction Input

Figure 5.1-4a: Transfer Functions for FWS Wall Top Response from Analysis of UC_{OBE} Model of BE Profile and Surface Input Motion at El. 220 ft

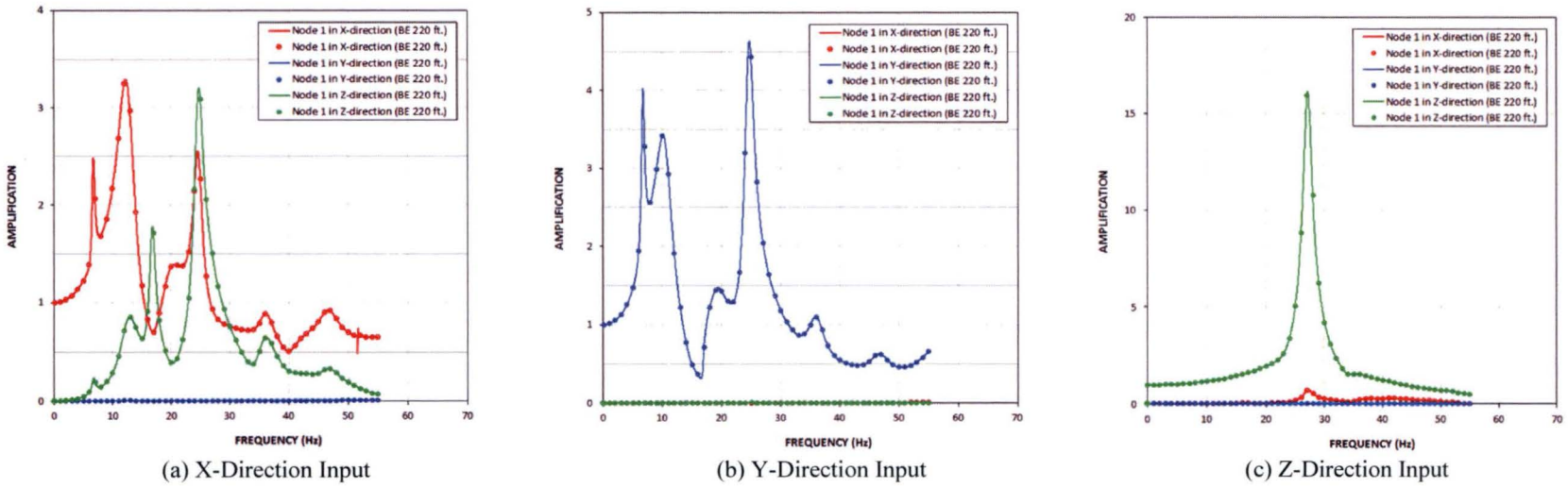

(a) X-Direction Input (b) Y-Direction Input (c) Z-Direction Input

Figure 5.1-4b: Transfer Functions for FWS Basemat Response from Analysis of UC_{OBE} Model of BE Profile and Surface Input Motion at El. 220 ft

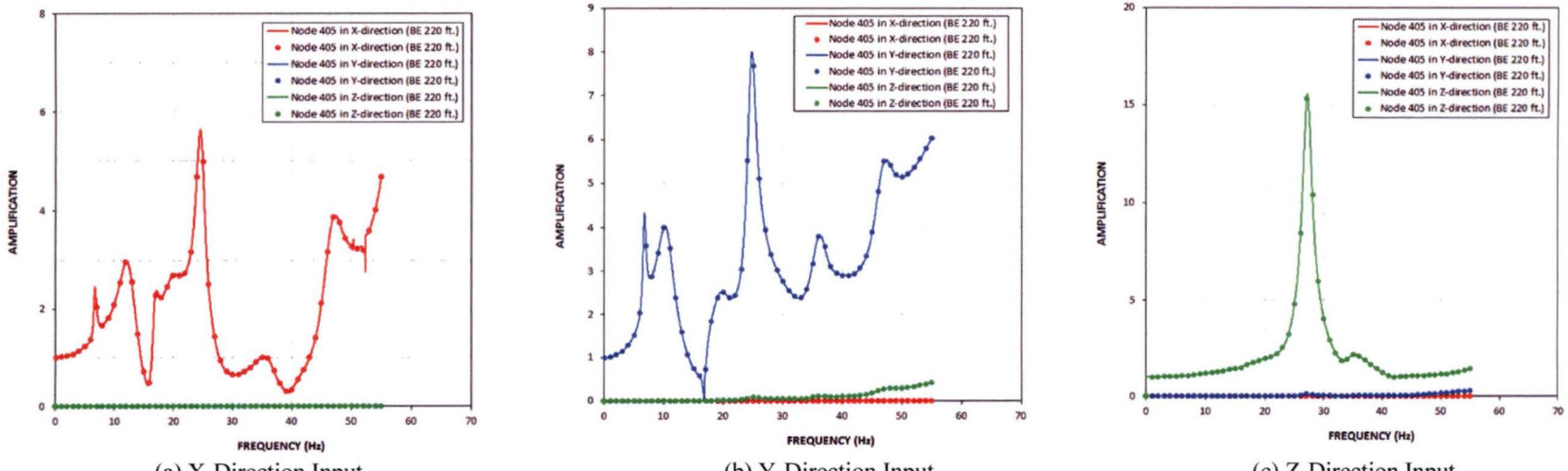

(a) X-Direction Input (b) Y-Direction Input (c) Z-Direction Input

Figure 5.1-4c: Transfer Functions for FPE Top Response from Analysis of UC_{OBE} Model of BE Profile and Surface Input Motion at El. 220 ft

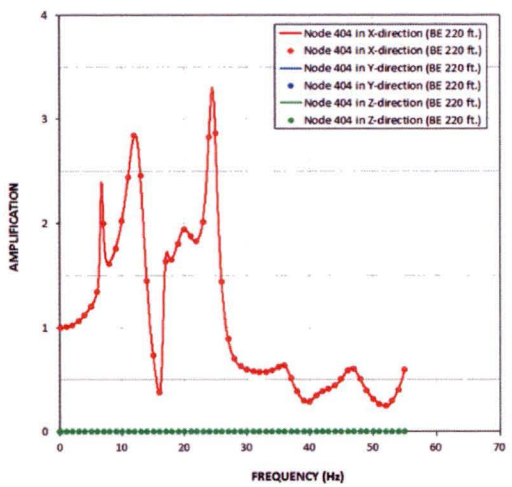

(a) X-Direction Input

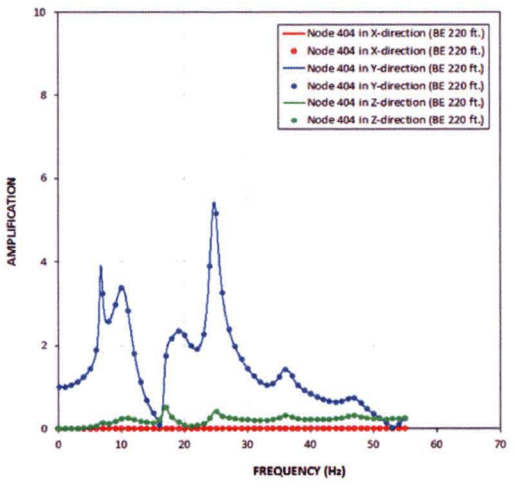

(b) Y-Direction Input

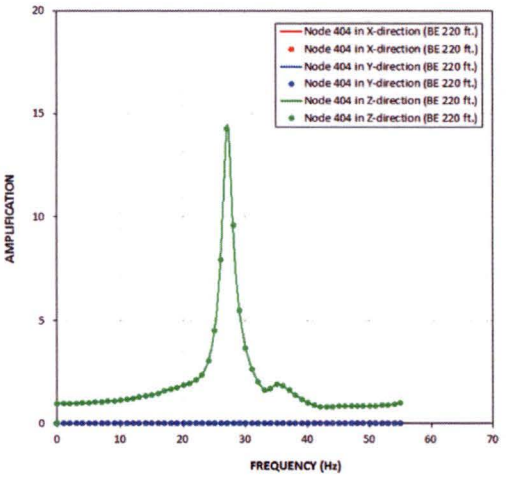

(c) Z-Direction Input

Figure 5.1-4d: Transfer Functions for FPE Basemat from Analysis of UC_{OBE} Model of BE Profile and Surface Input Motion at El. 220 ft

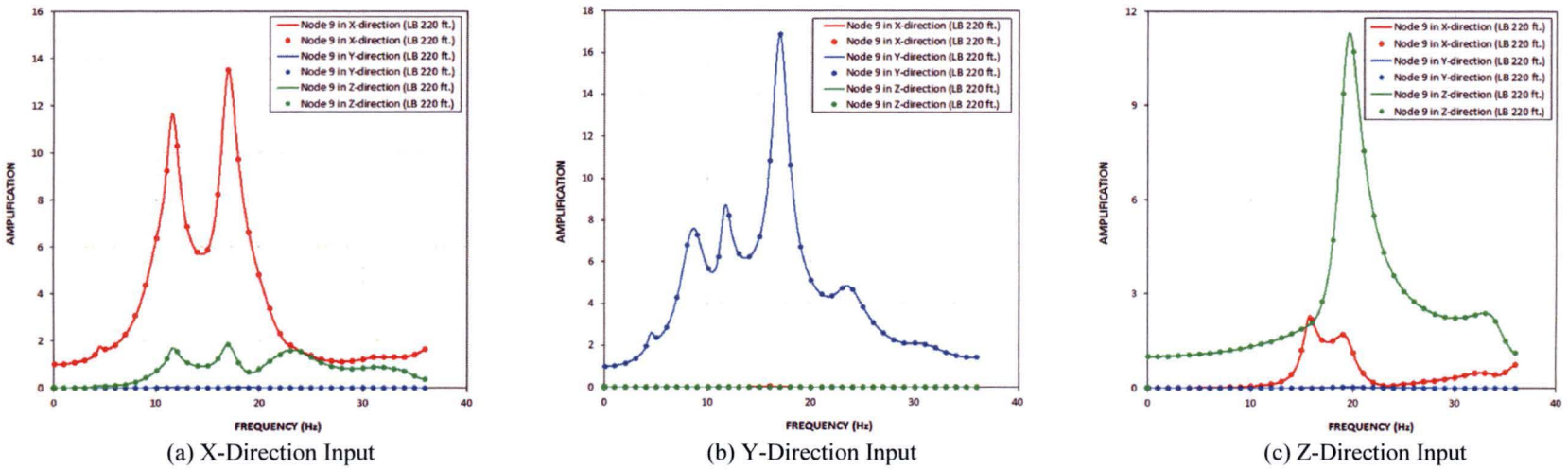

(a) X-Direction Input (b) Y-Direction Input (c) Z-Direction Input

Figure 5.1-5a: Transfer Functions for FWS Wall Top Response from Analysis of UC_{OBE} Model of LB Profile and Surface Input Motion at El. 220 ft

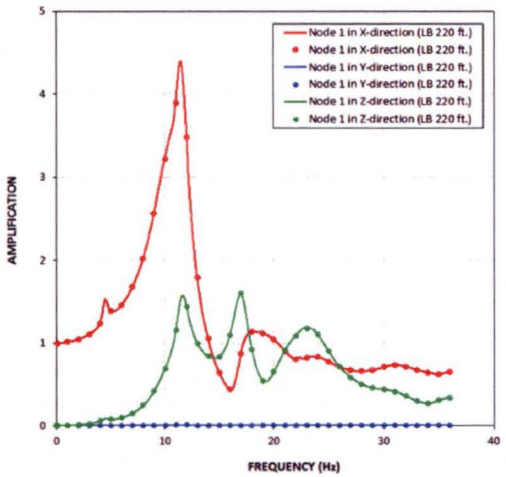

(a) X-Direction Input

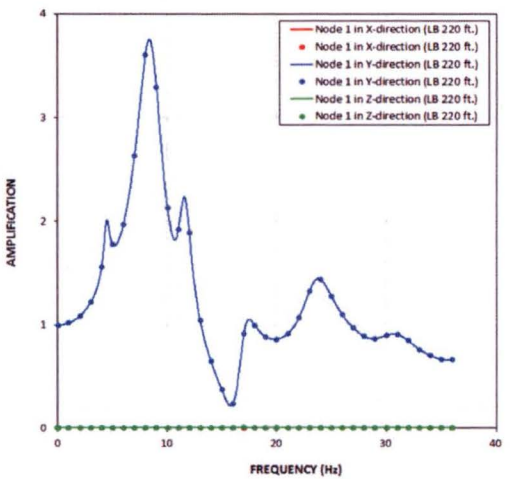

(b) Y-Direction Input

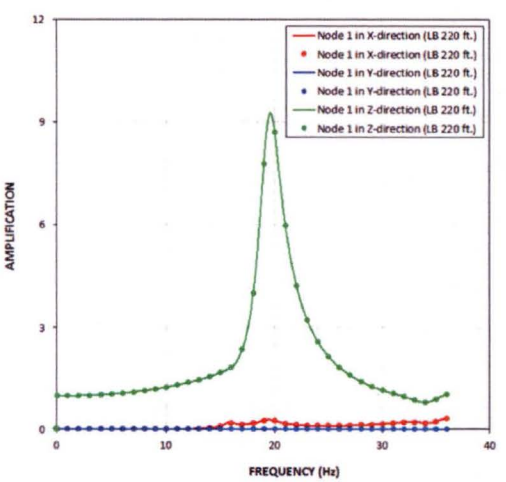

(c) Z-Direction Input

Figure 5.1-5b: Transfer Functions for FWS Basemat Response from Analysis of UC_{OBE} Model of LB Profile and Surface Input Motion at El. 220 ft

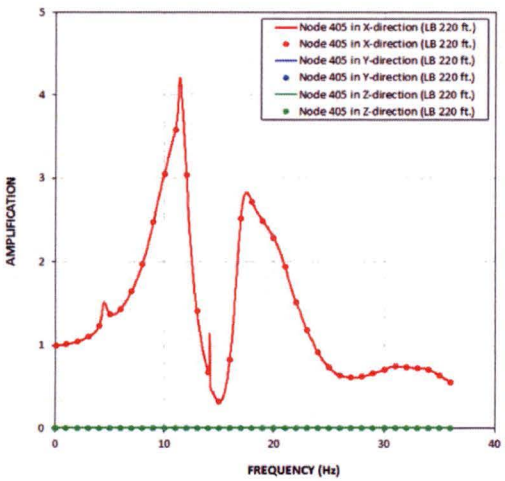

(a) X-Direction Input

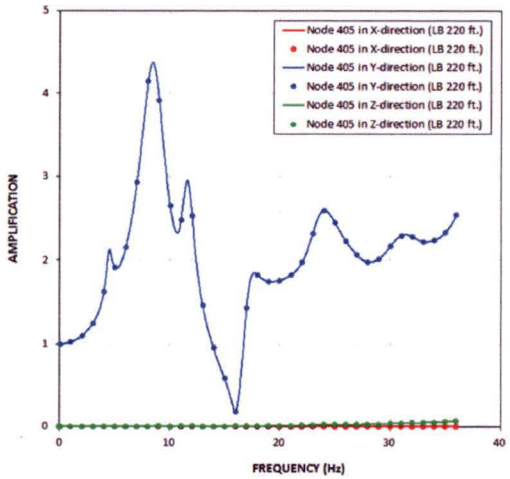

(b) Y-Direction Input

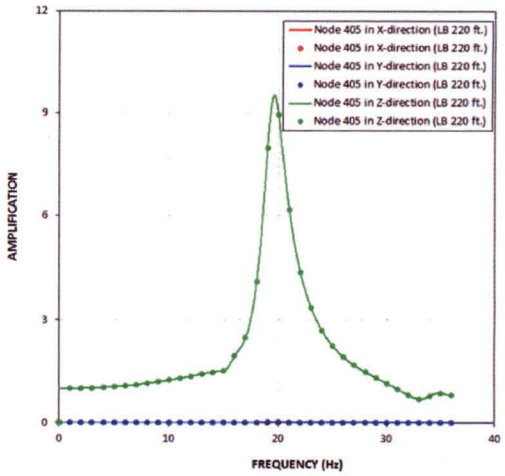

(c) Z-Direction Input

Figure 5.1-5c: Transfer Functions for FPE Top Response from Analysis of UC_{OBE} Model of LB Profile and Surface Input Motion at El. 220 ft

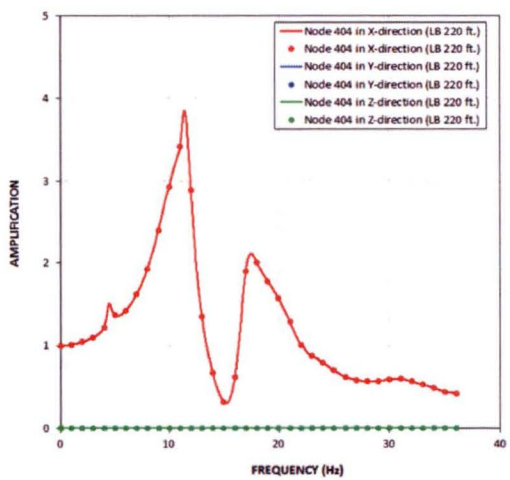

(a) X-Direction Input

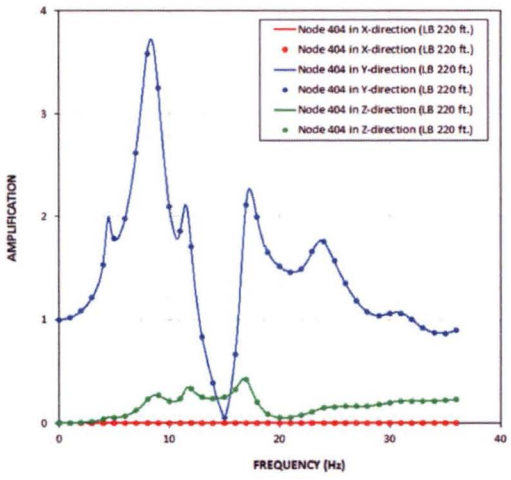

(b) Y-Direction Input

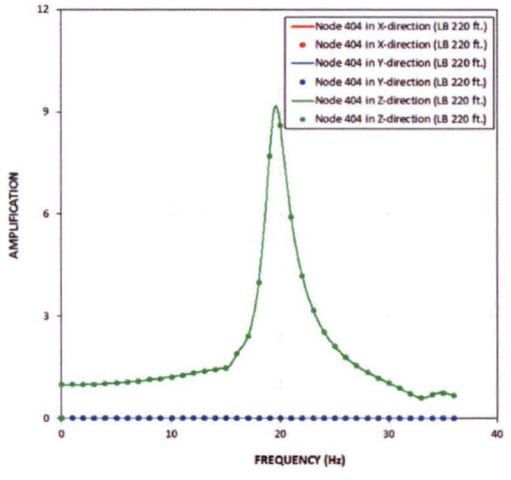

(c) Z-Direction Input

Figure 5.1-5d: Transfer Functions for FPE Basemat Response from Analysis of UC_{OBE} Model of LB Profile and Surface Input Motion at El. 220 ft

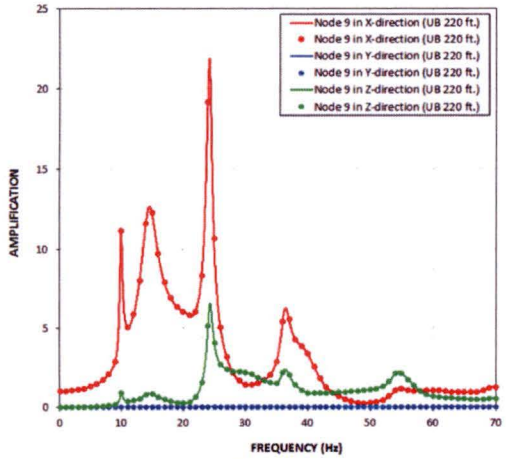

(a) X-Direction Input

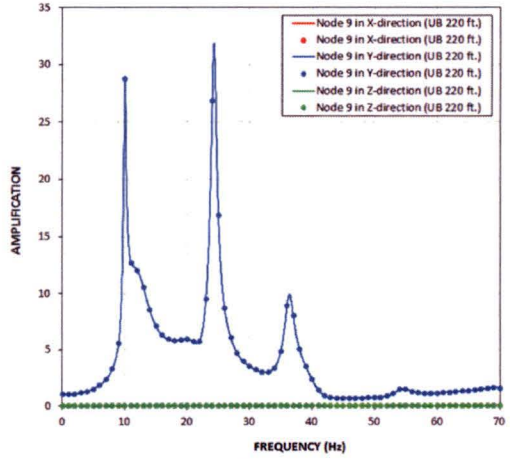

(b) Y-Direction Input

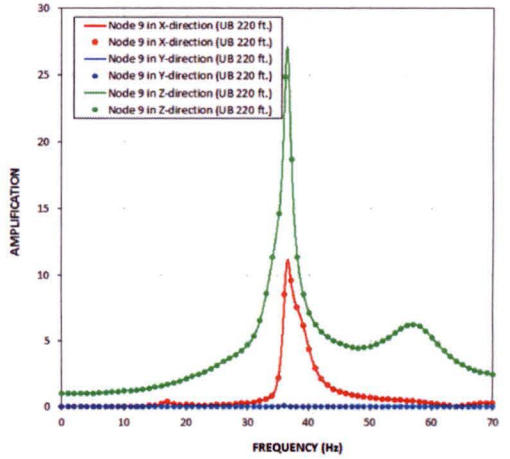

(c) Z-Direction Input

Figure 5.1-6a: Transfer Functions for FWS Wall Top Response from Analysis of UC_{OBE} Model of UB Profile and Surface Input Motion at El. 220 ft

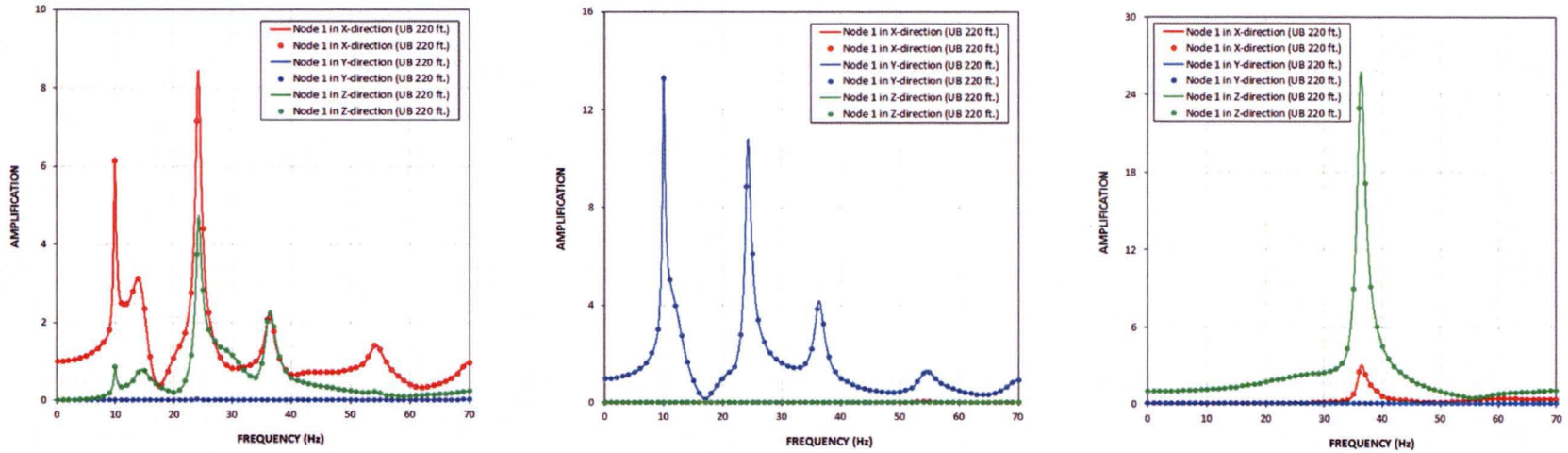

(a) X-Direction Input (b) Y-Direction Input (c) Z-Direction Input

Figure 5.1-6b: Transfer Functions for FWS Basemat Response from Analysis of UC_{OBE} Model of UB Profile and Surface Input Motion at El. 220 ft

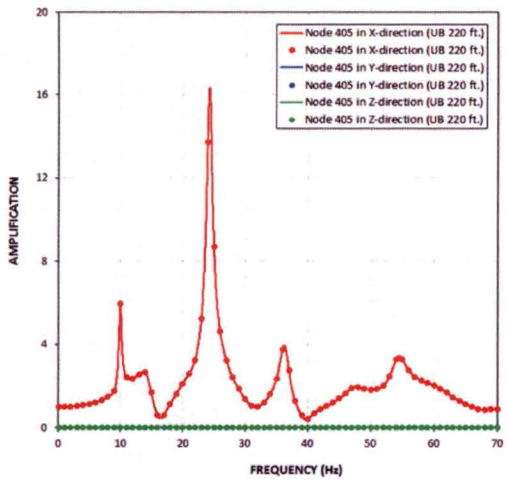

(a) X-Direction Input

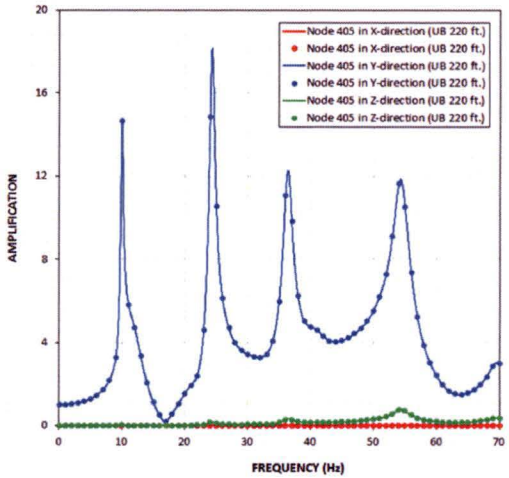

(b) Y-Direction Input

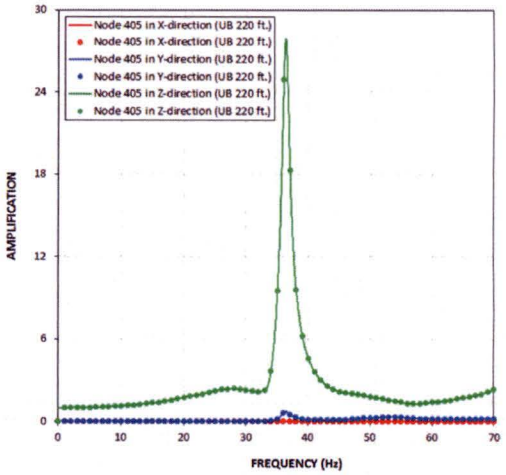

(c) Z-Direction Input

Figure 5.1-6c: Transfer Functions for FPE Top Response from Analysis of UC_{OBE} Model of UB Profile and Surface Input Motion at El. 220 ft

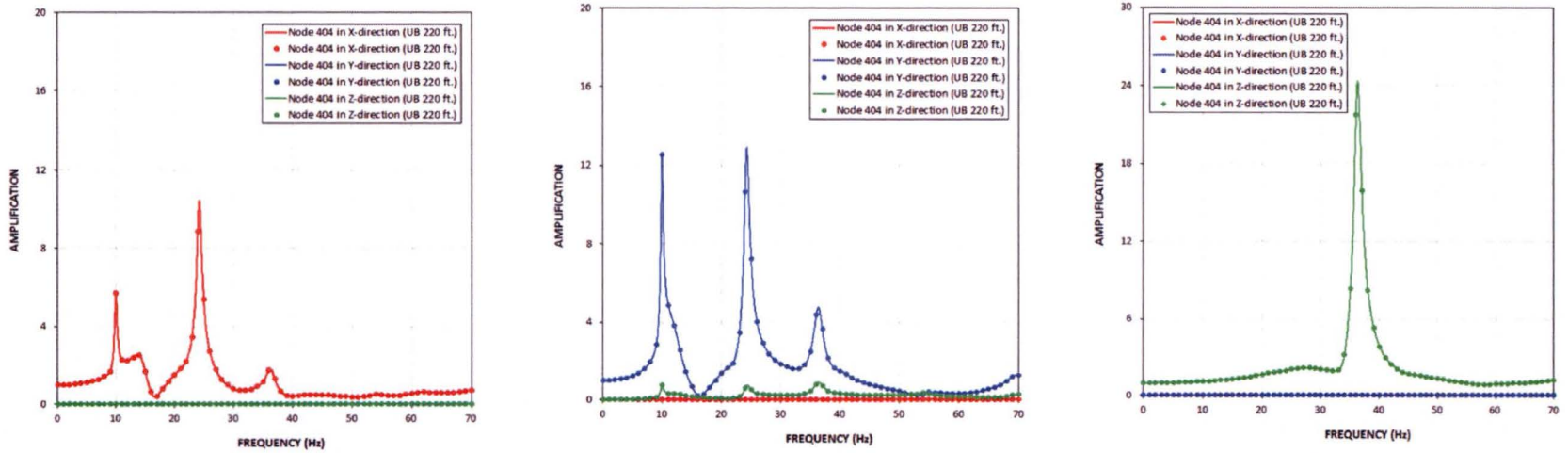

(a) X-Direction Input (b) Y-Direction Input (c) Z-Direction Input

Figure 5.1-6d: Transfer Functions for FPE Basemat Response from Analysis of UC_{OBE} Model of UB Profile and Surface Input Motion at El. 220 ft

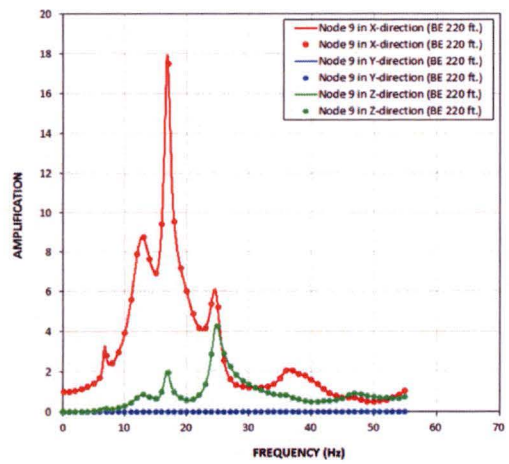

(a) X-Direction Input

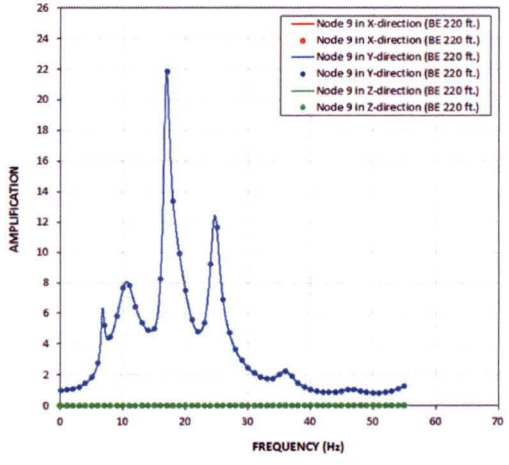

(b) Y-Direction Input

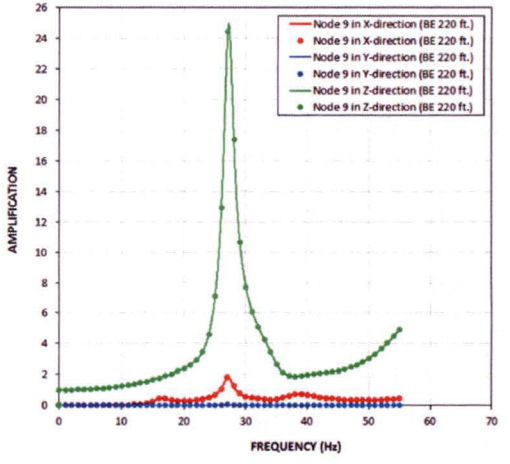

(c) Z-Direction Input

Figure 5.1-7a: Transfer Functions for FWS Wall Top Response from Analysis of UC_{SSE} Model of BE Profile and Surface Input Motion at El. 220 ft

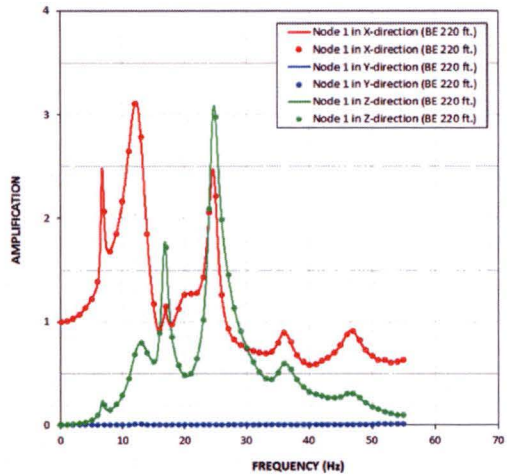

(a) X-Direction Input

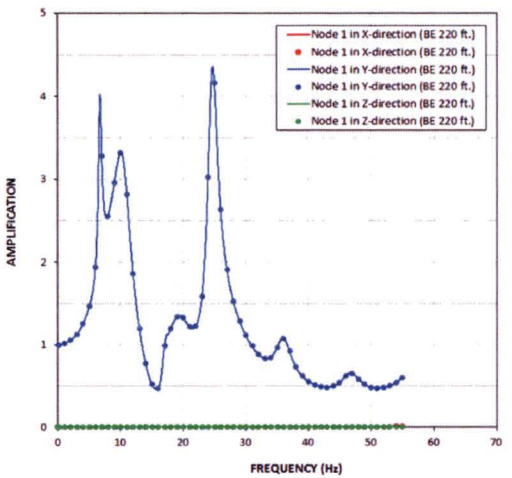

(b) Y-Direction Input

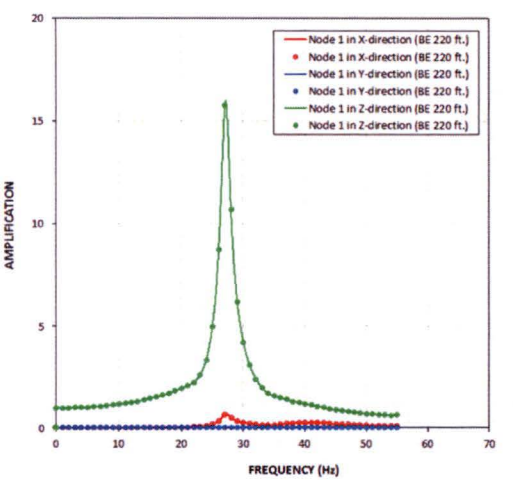

(c) Z-Direction Input

Figure 5.1-7b: Transfer Functions for FWS Basemat Response from Analysis of UC_{SSE} Model of BE Profile and Surface Input Motion at El. 220 ft

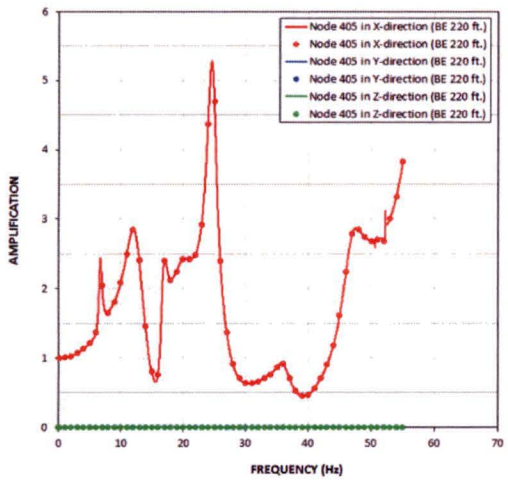

(a) X-Direction Input

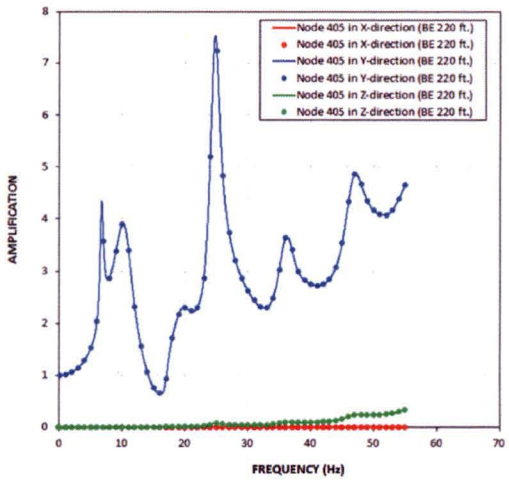

(b) Y-Direction Input

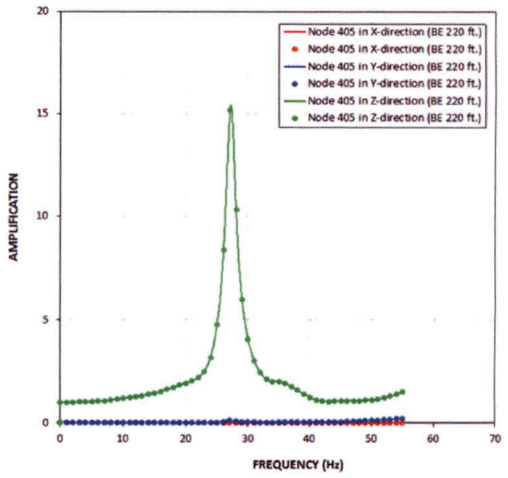

(c) Z-Direction Input

Figure 5.1-7c: Transfer Functions for FPE Top Response from Analysis of UC_{SSE} Model of BE Profile and Surface Input Motion at El. 220 ft

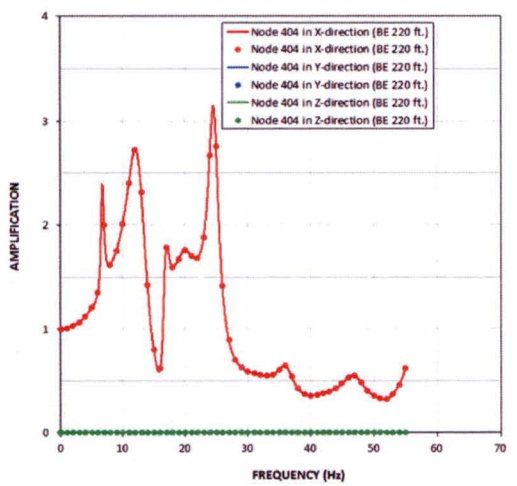

(a) X-Direction Input

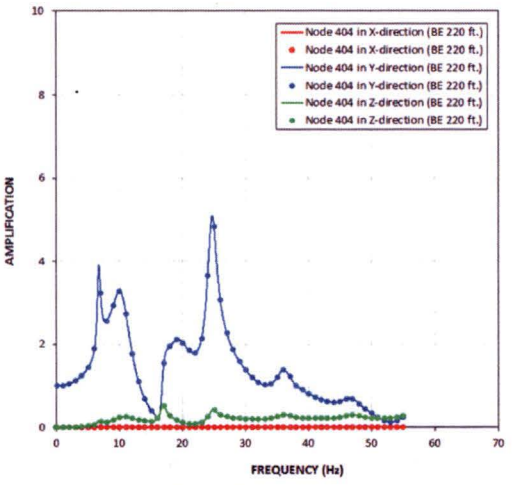

(b) Y-Direction Input

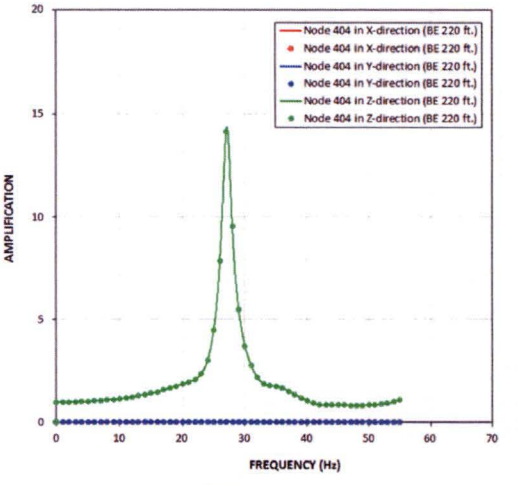

(c) Z-Direction Input

Figure 5.1-7d: Transfer Functions for FPE Basemat Response from Analysis of UC_{SSE} Model of BE Profile and Surface Input Motion at El. 220 ft

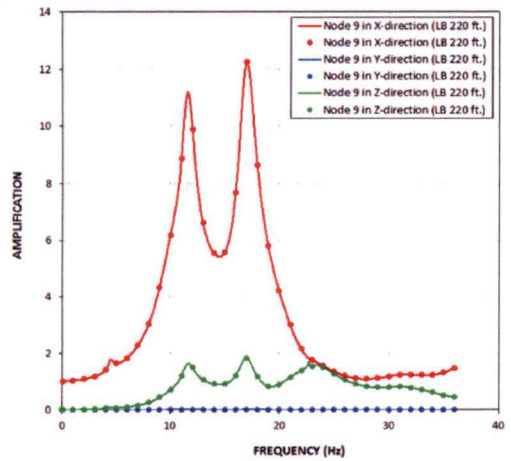

(a) X-Direction Input

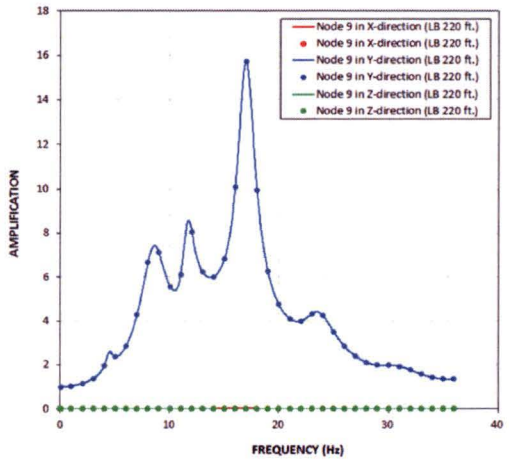

(b) Y-Direction Input

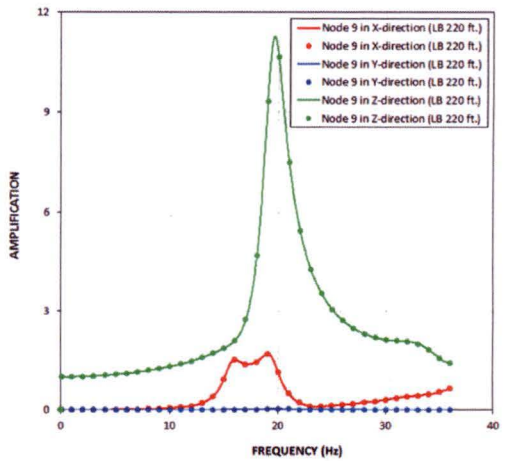

(c) Z-Direction Input

Figure 5.1-8a: Transfer Functions for FWS Wall Top Response from Analysis of UC_{SSE} Model of LB Profile and Surface Input Motion at El. 220 ft

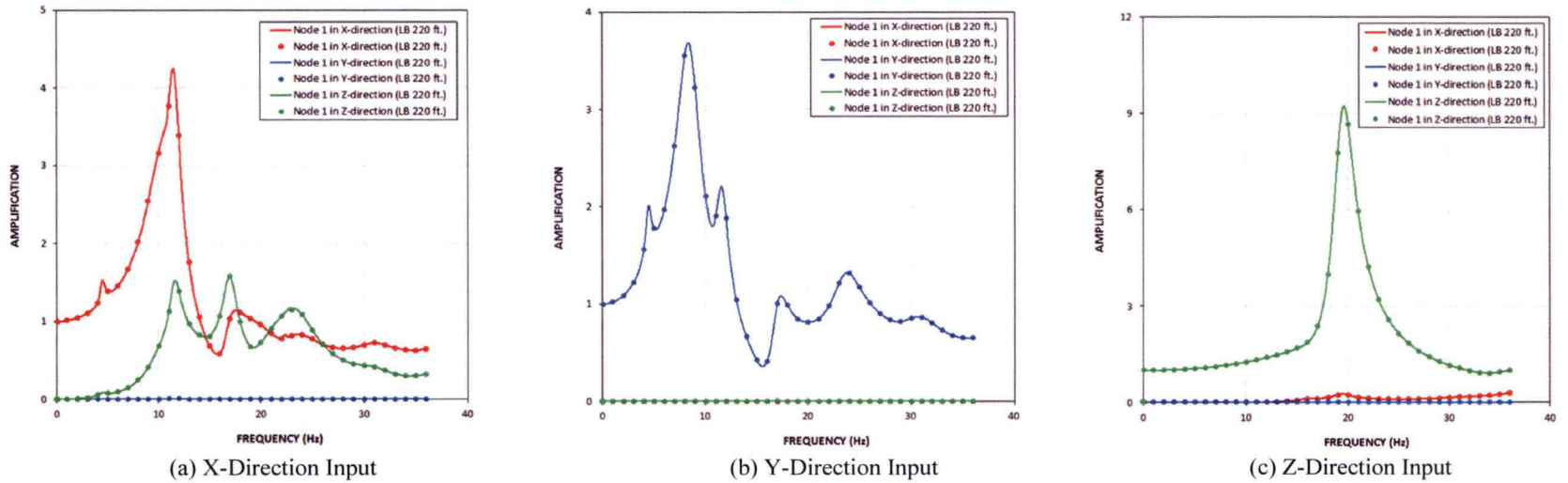

(a) X-Direction Input (b) Y-Direction Input (c) Z-Direction Input

Figure 5.1-8b: Transfer Functions for FWS Basemat Response from Analysis of UC_{SSE} Model of LB Profile and Surface Input Motion at El. 220 ft

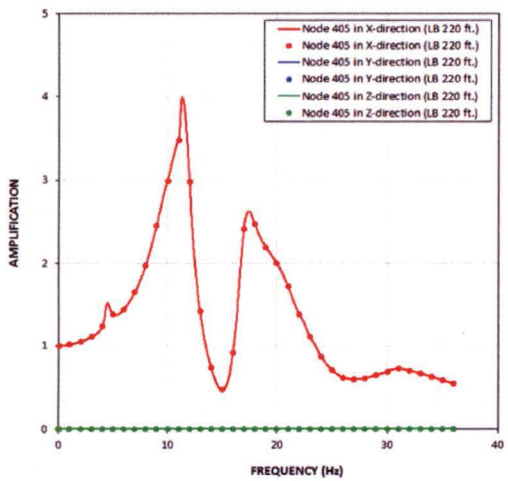

(a) X-Direction Input

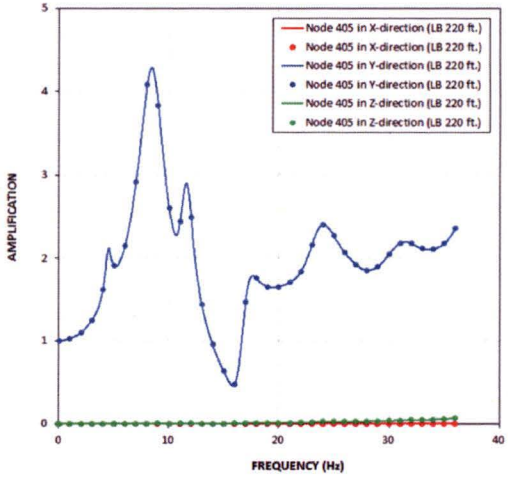

(b) Y-Direction Input

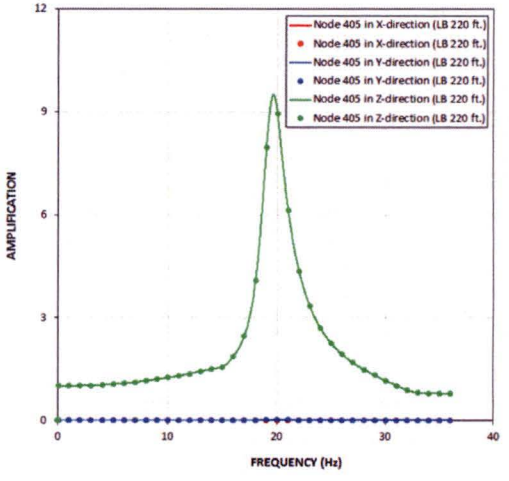

(c) Z-Direction Input

Figure 5.1-8c: Transfer Functions for FPE Top Response from Analysis of UC_{SSE} Model of LB Profile and Surface Input Motion at El. 220 ft

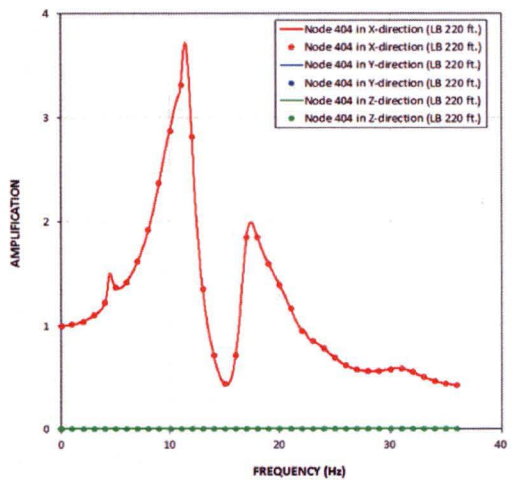

(a) X-Direction Input

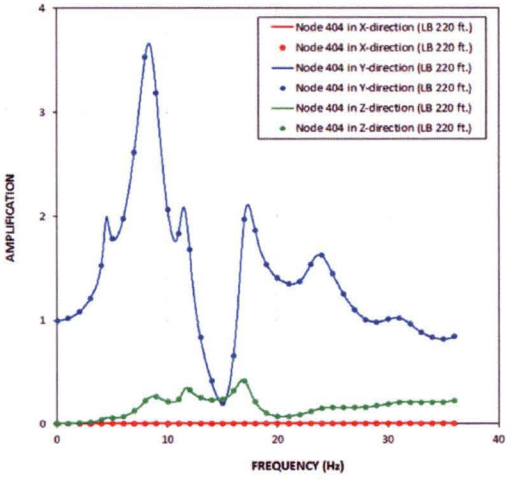

(b) Y-Direction Input

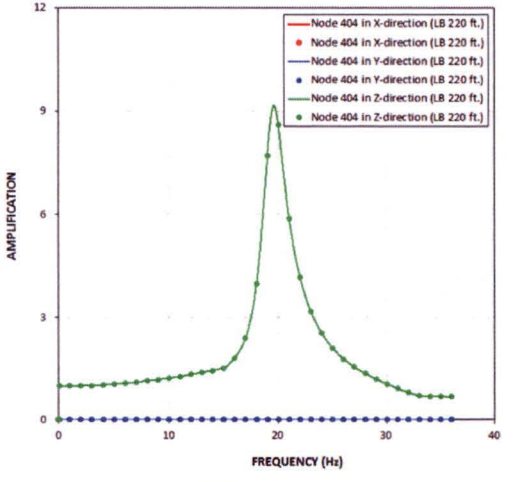

(c) Z-Direction Input

Figure 5.1-8d: Transfer Functions for FPE Basemat Response from Analysis of UC_{SSE} Model of LB Profile and Surface Input Motion at El. 220 ft

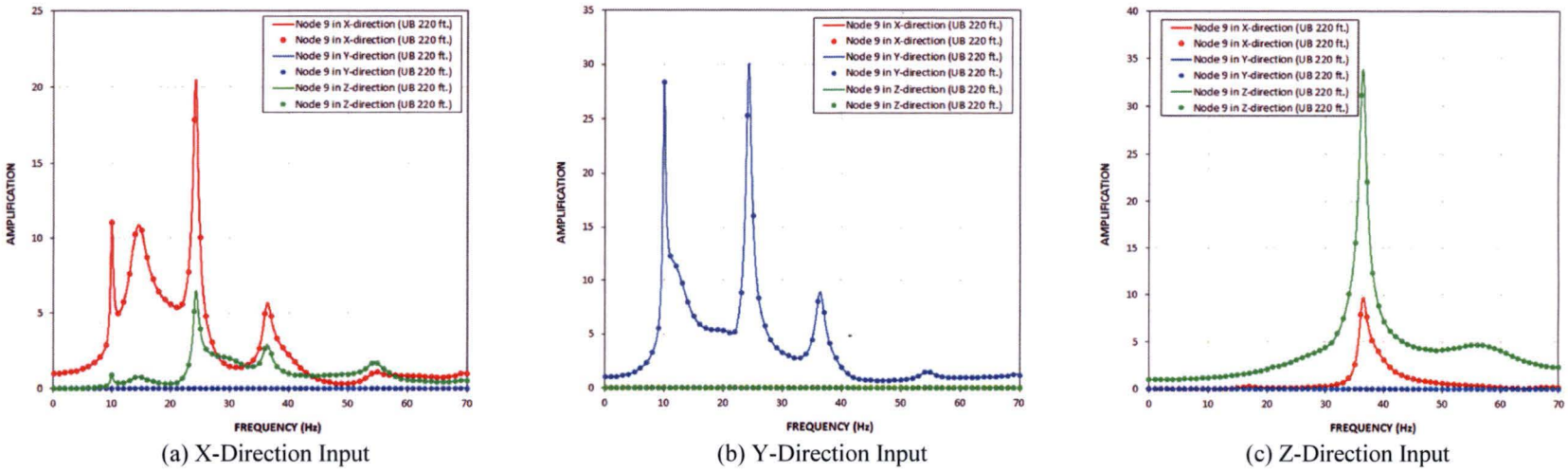

(a) X-Direction Input (b) Y-Direction Input (c) Z-Direction Input

Figure 5.1-9a: Transfer Functions for FWS Wall Top Response from Analysis of UC_{SSE} Model of UB Profile and Surface Input Motion at El. 220 ft

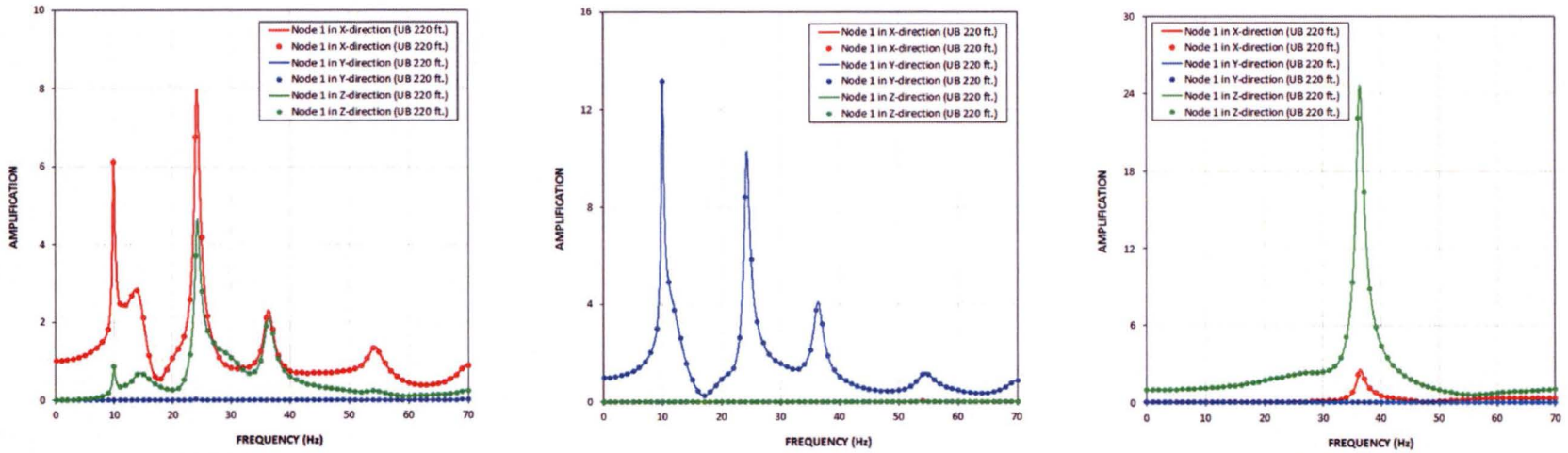

(a) X-Direction Input (b) Y-Direction Input (c) Z-Direction Input

Figure 5.1-9b: Transfer Functions for FWS Basemat Response from Analysis of UC_{SSE} Model of UB Profile and Surface Input Motion at El. 220 ft

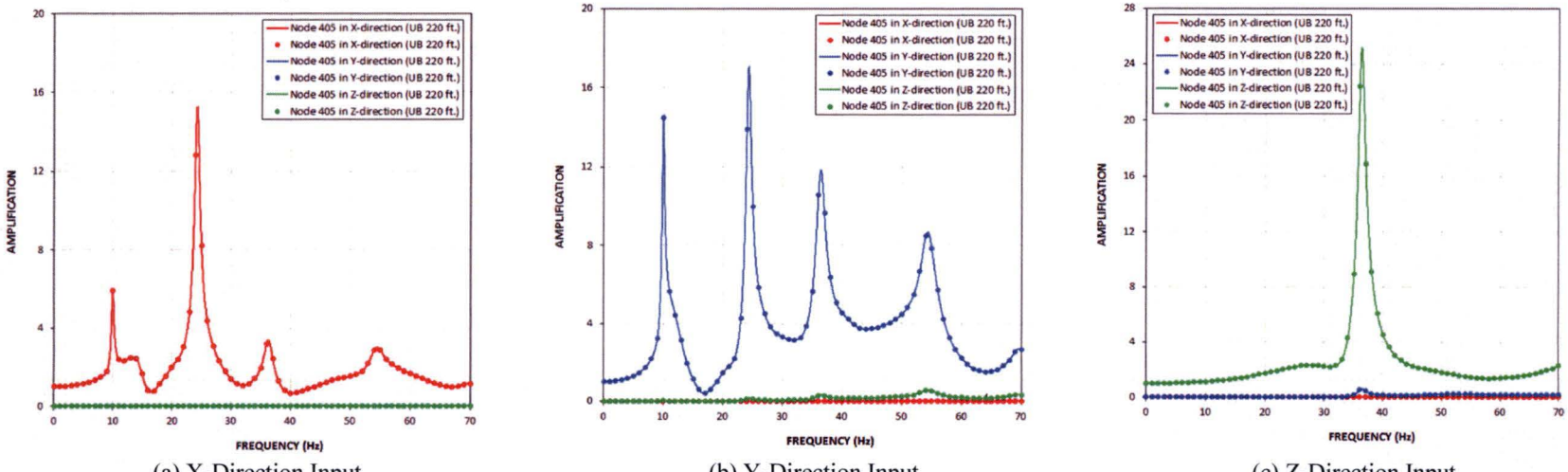

(a) X-Direction Input (b) Y-Direction Input (c) Z-Direction Input

Figure 5.1-9c: Transfer Functions for FPE Top Response from Analysis of UC_{SSE} Model of UB Profile and Surface Input Motion at El. 220 ft

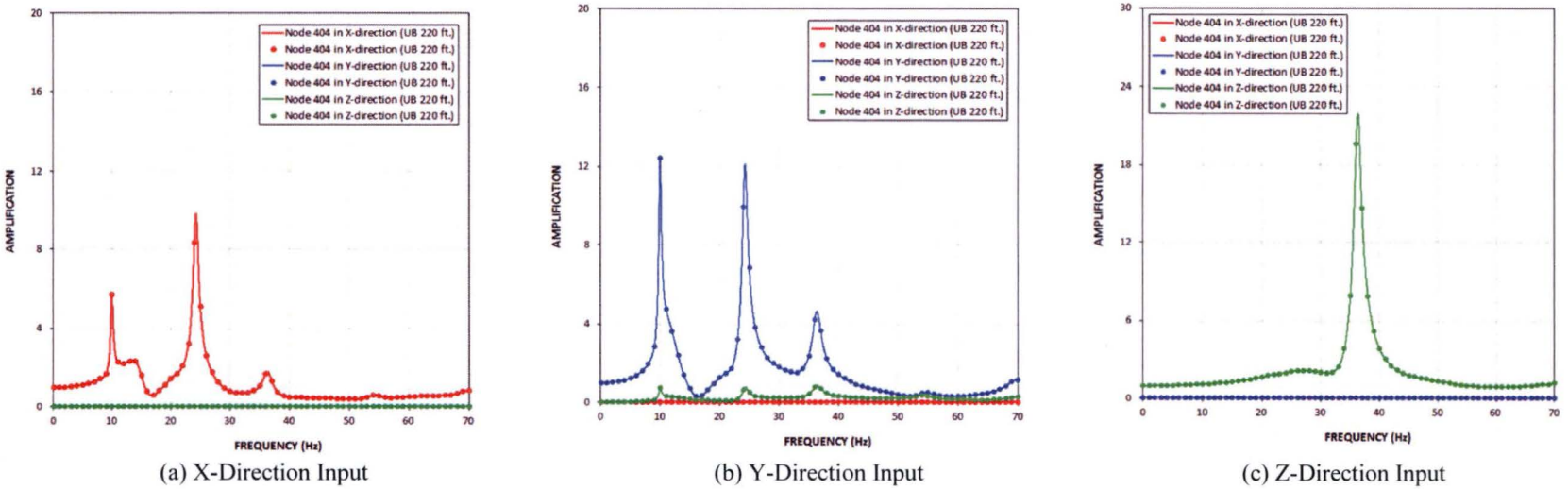

(a) X-Direction Input (b) Y-Direction Input (c) Z-Direction Input

Figure 5.1-9d: Transfer Functions for FPE Basemat Response from Analysis of UC_{SSE} Model of UB Profile and Surface Input Motion at El. 220 ft

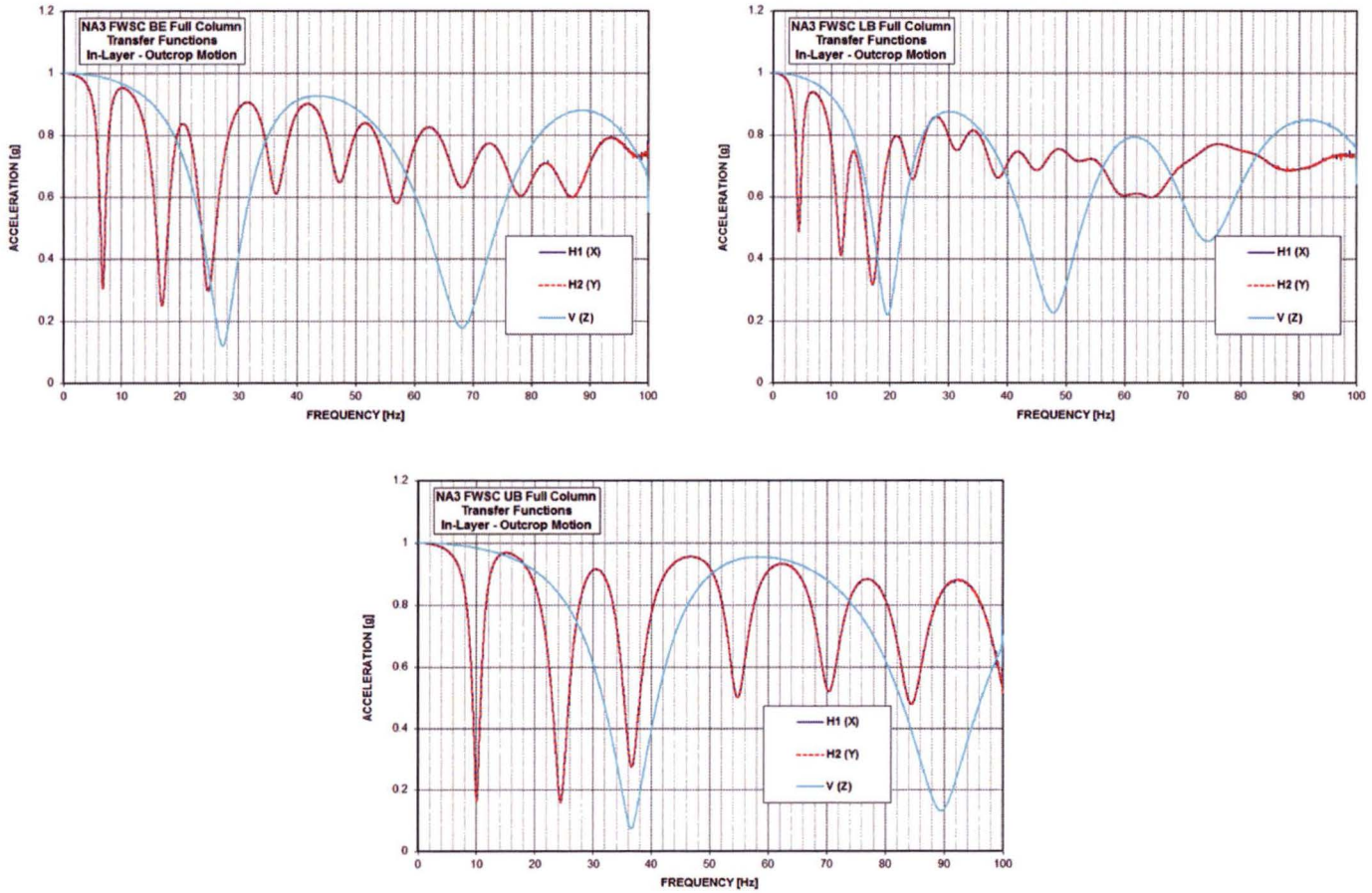

Figure 5.1-10: Transfer Functions for Transformation of FWSC In-Layer Motion into Outcrop Motion

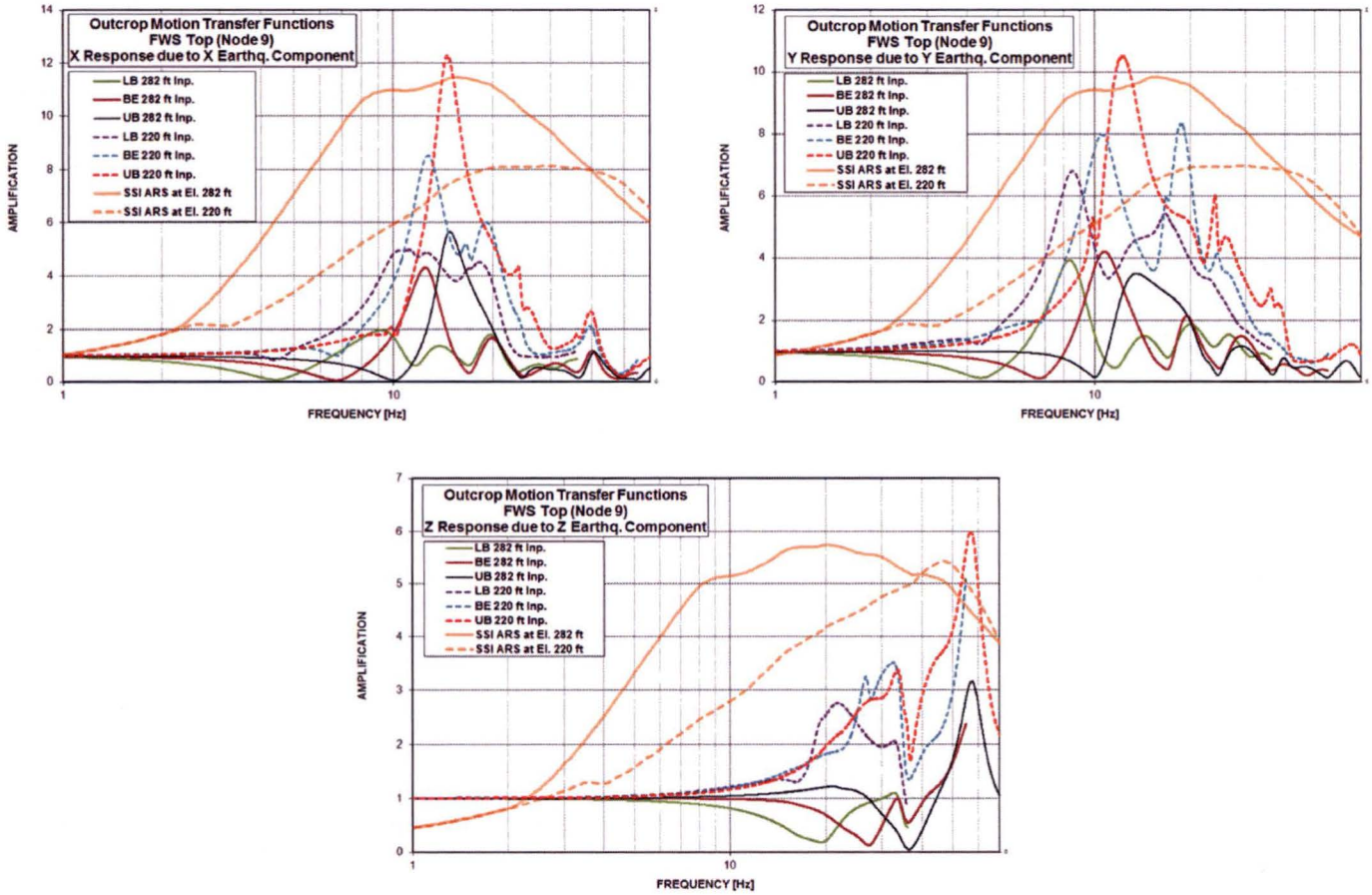

Figure 5.1-11: Outcrop Transfer Functions for Response of FWS Wall Top

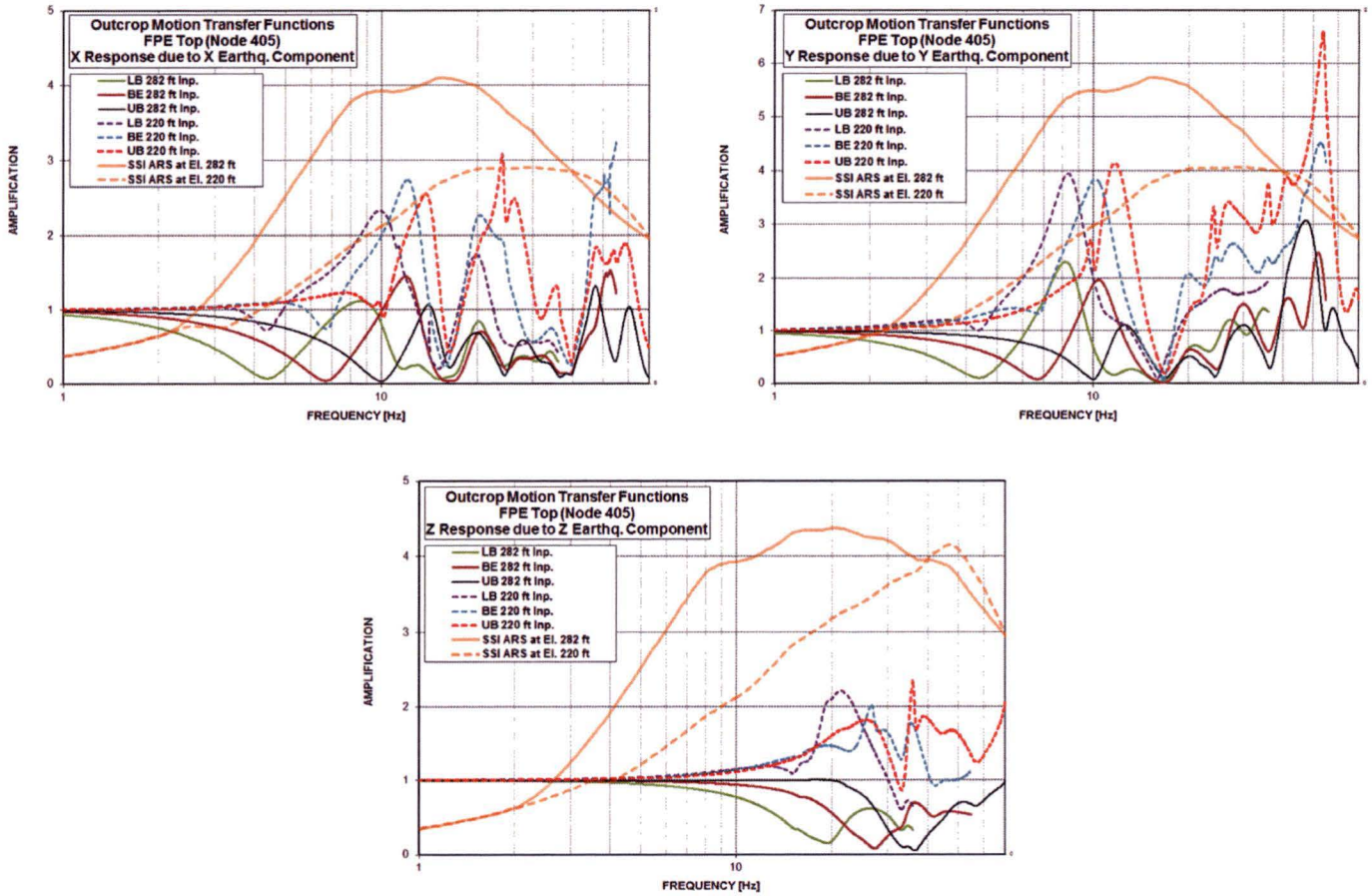

Figure 5.1-12: Outcrop Transfer Functions for Response of FPE Top

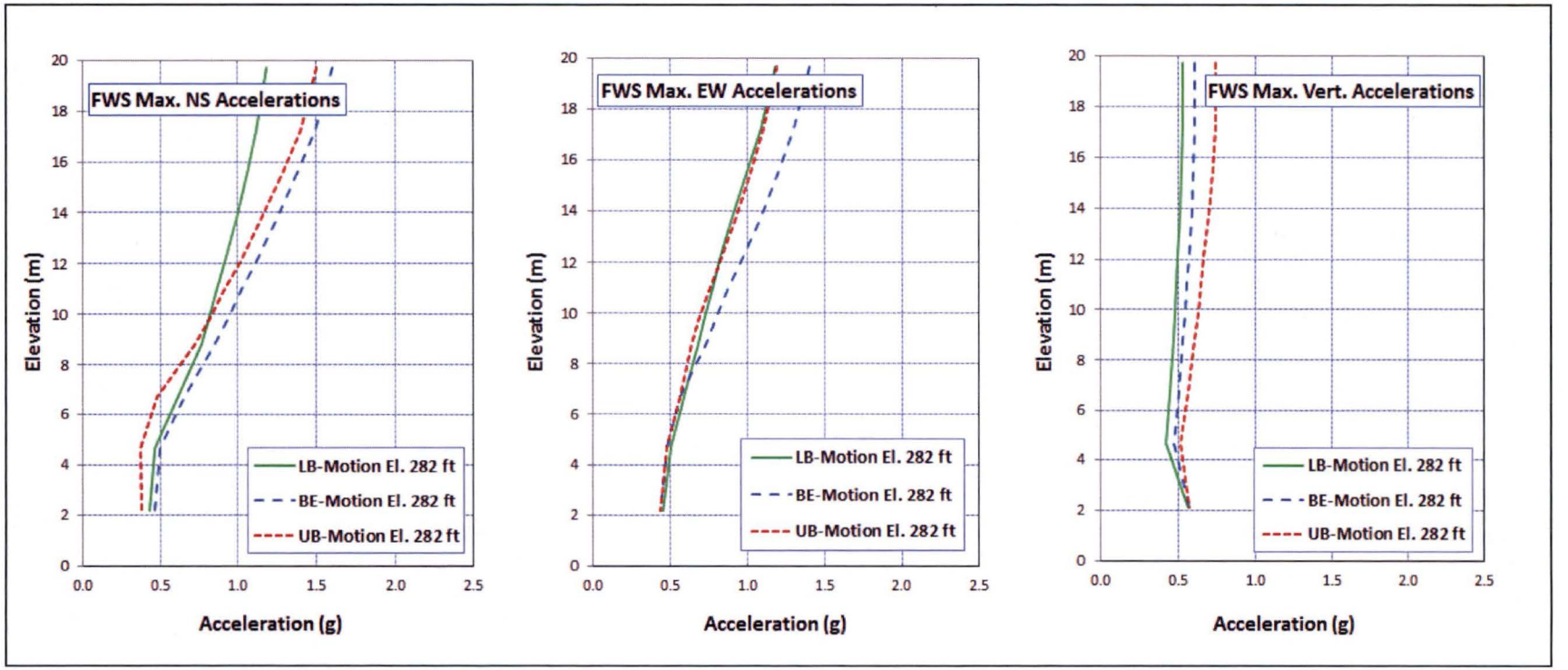

Figure 5.2-1a: FWS Maximum Accelerations from Analyses of FWSC UC_{OBE} Model with Surface Input Motion at El. 282 ft

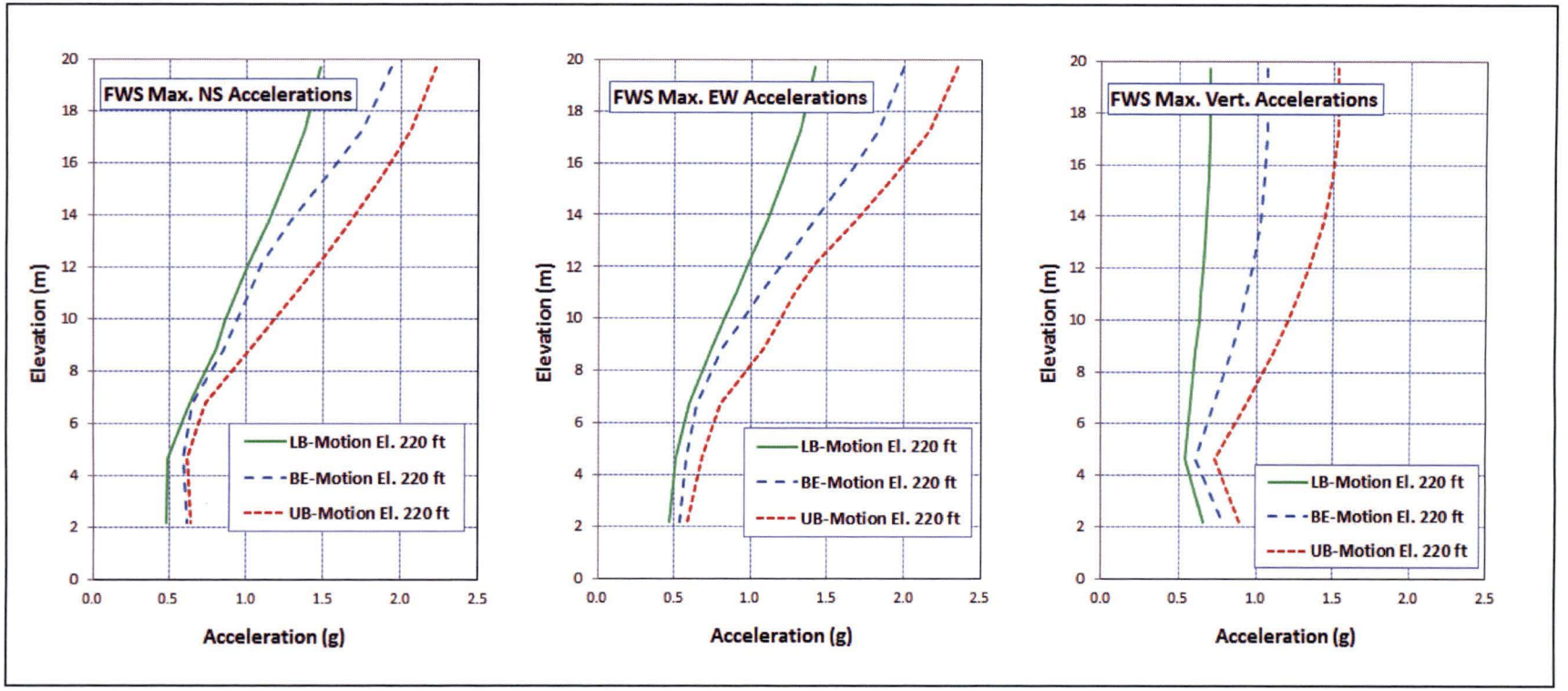

Figure 5.2-1b: FWS Maximum Accelerations from Analyses of FWSC UC_{OBE} Model with Deep Input Motion at El. 220 ft

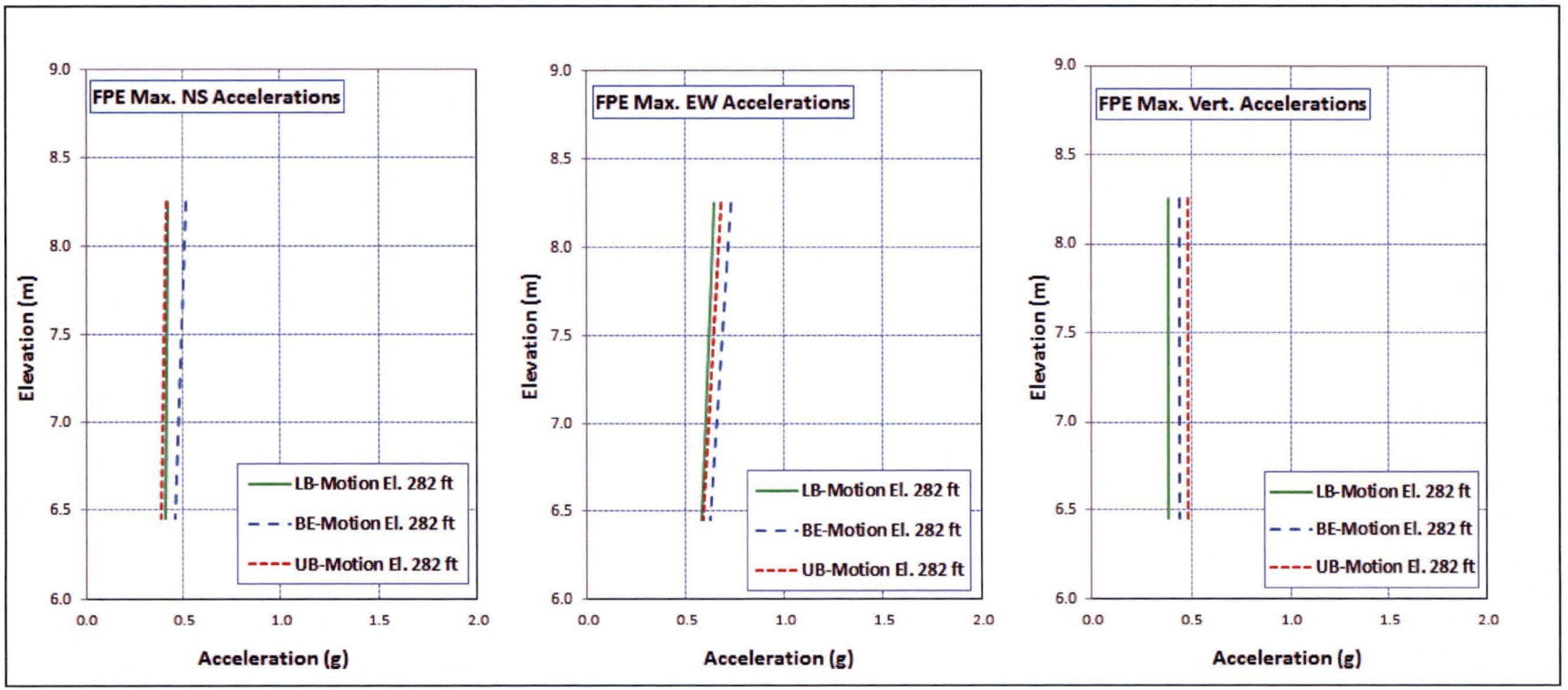

Figure 5.2-2a: FPE Maximum Accelerations from Analyses of FWSC UC_{OBE} Model with Surface Input Motion at El. 282 ft

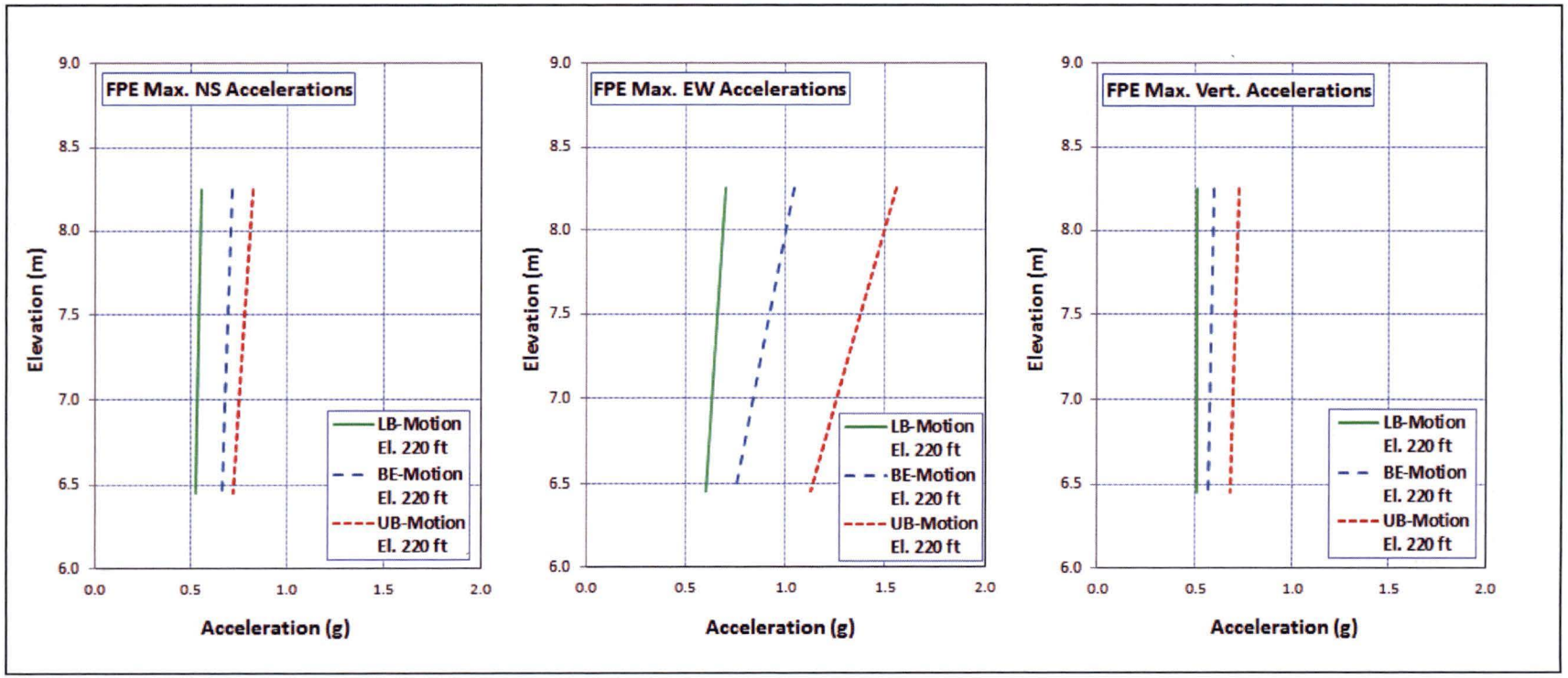

Figure 5.2-2b: FPE Maximum Accelerations from Analyses of FWSC UC_{OBE} Model with Deep Input Motion at El. 220 ft

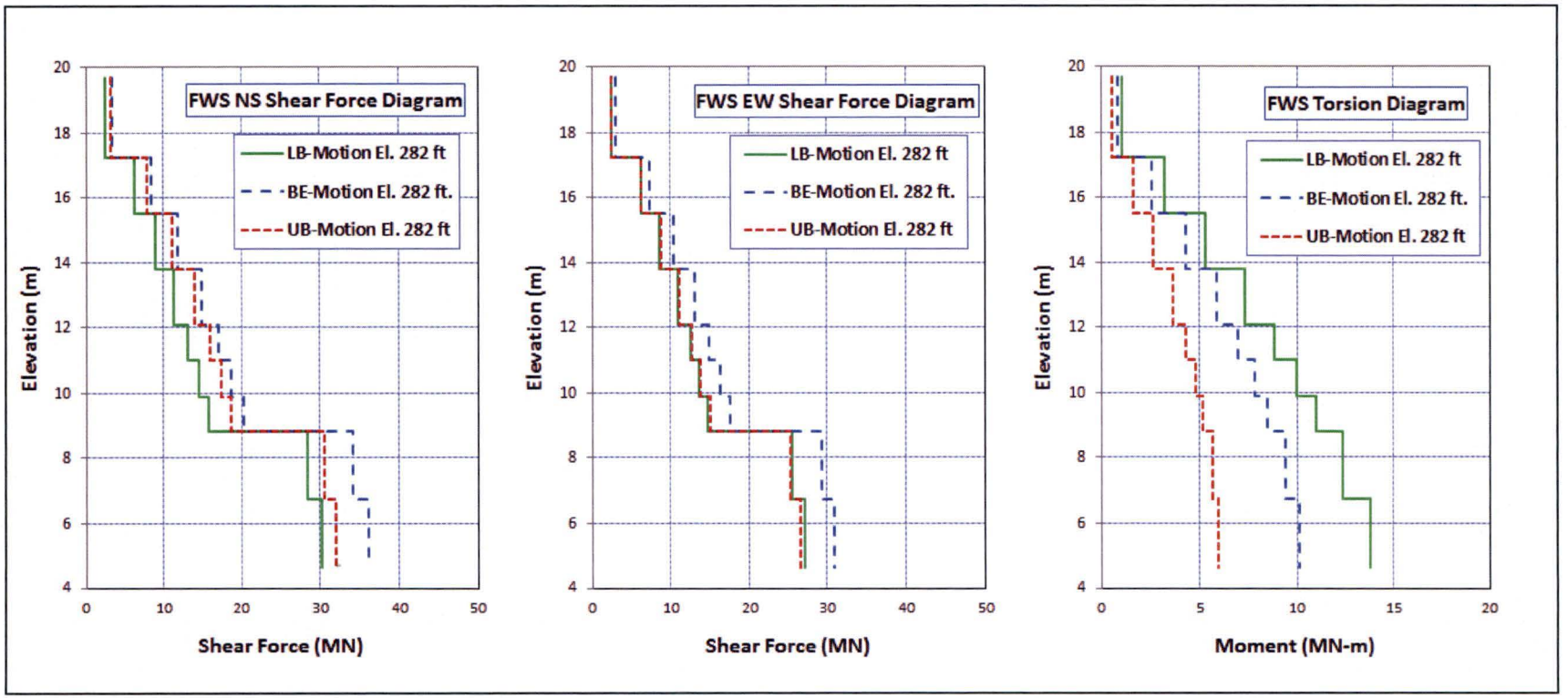

Figure 5.2-3a: FWS Maximum Shear Forces and Torsion from Analyses of FWSC UC_{OBE} Model with Surface Input Motion at El. 282 ft

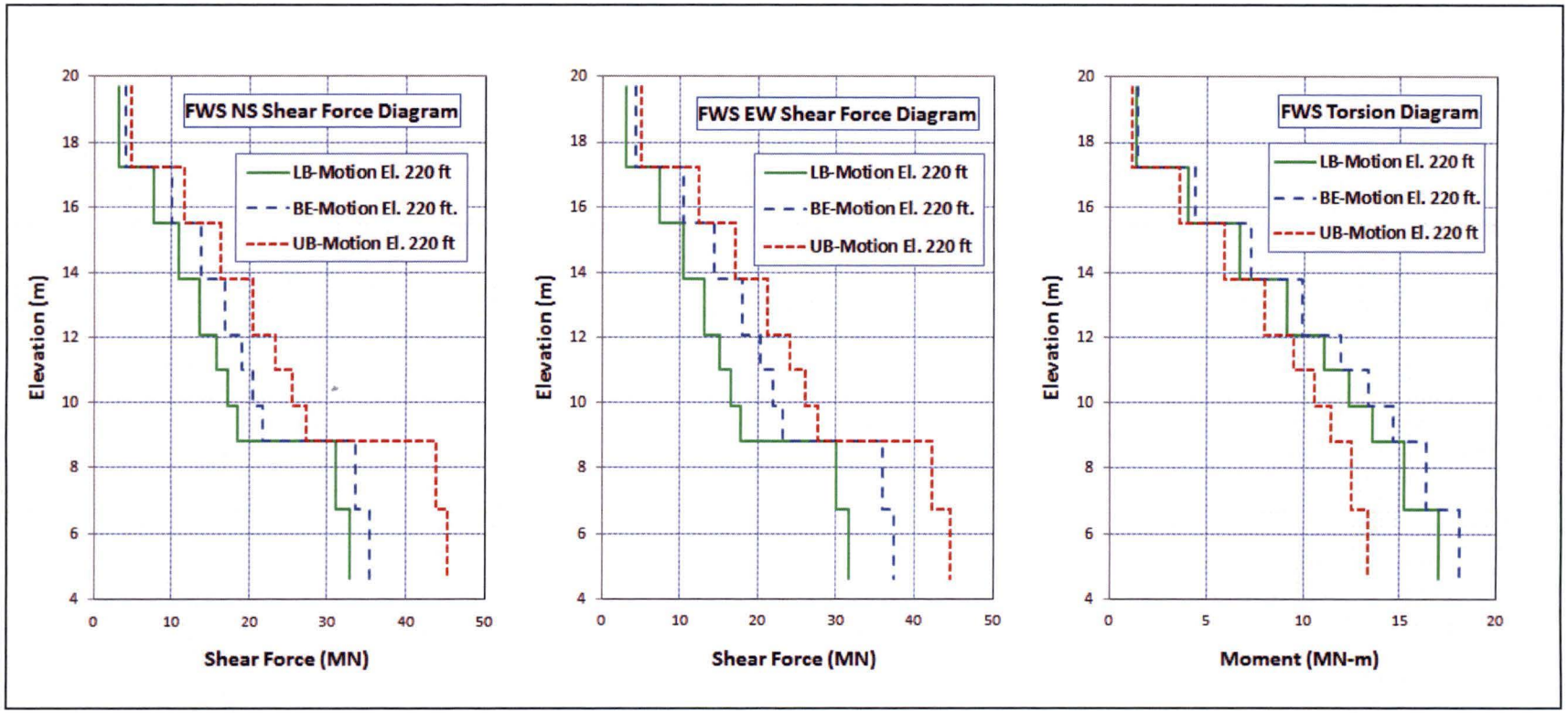

Figure 5.2-3b: FWS Maximum Shear Forces and Torsion from Analyses of FWSC UC_{OBE} Model with Deep Input Motion at El. 220 ft

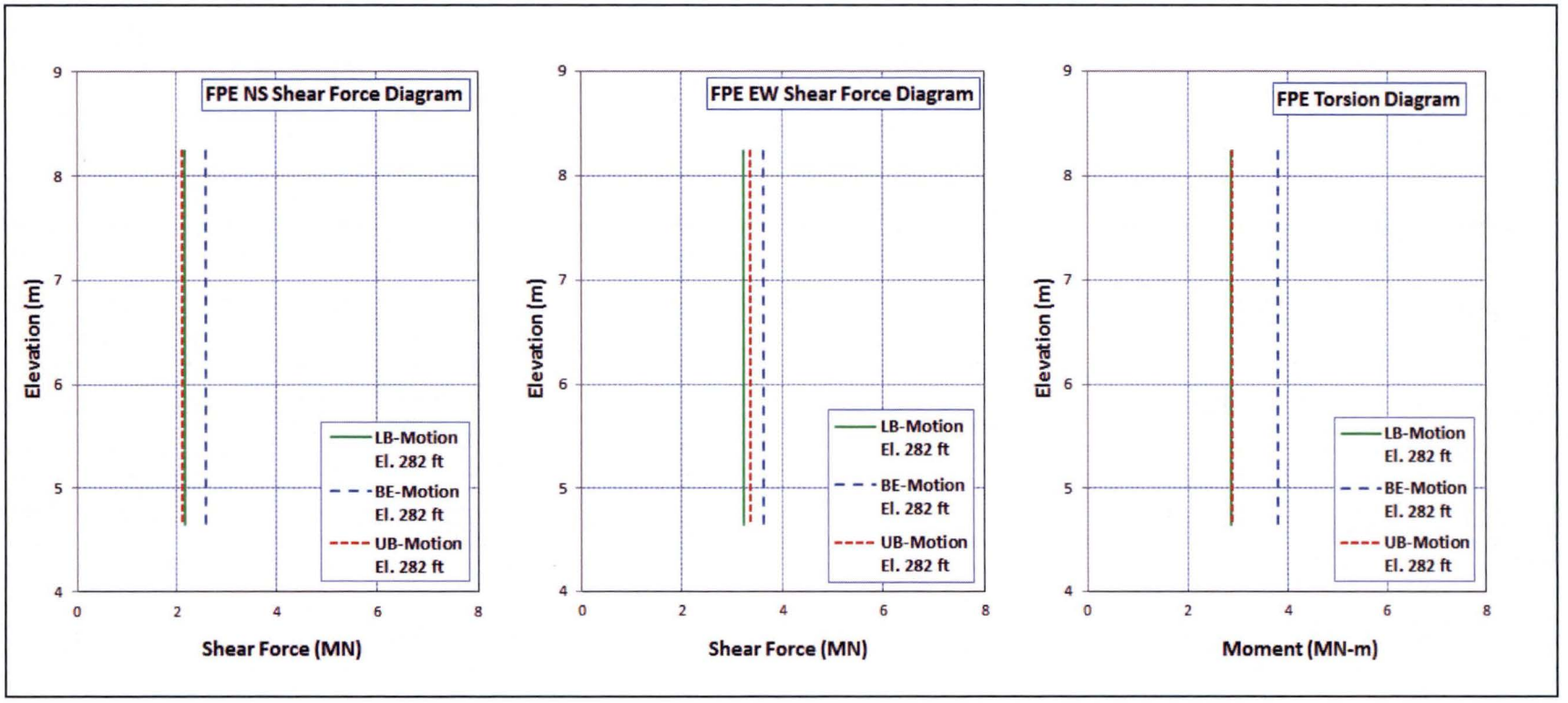

Figure 5.2-4a: FPE Maximum Shear Forces and Torsion from Analyses of FWSC UC_{OBE} Model with Surface Input Motion at El. 282 ft

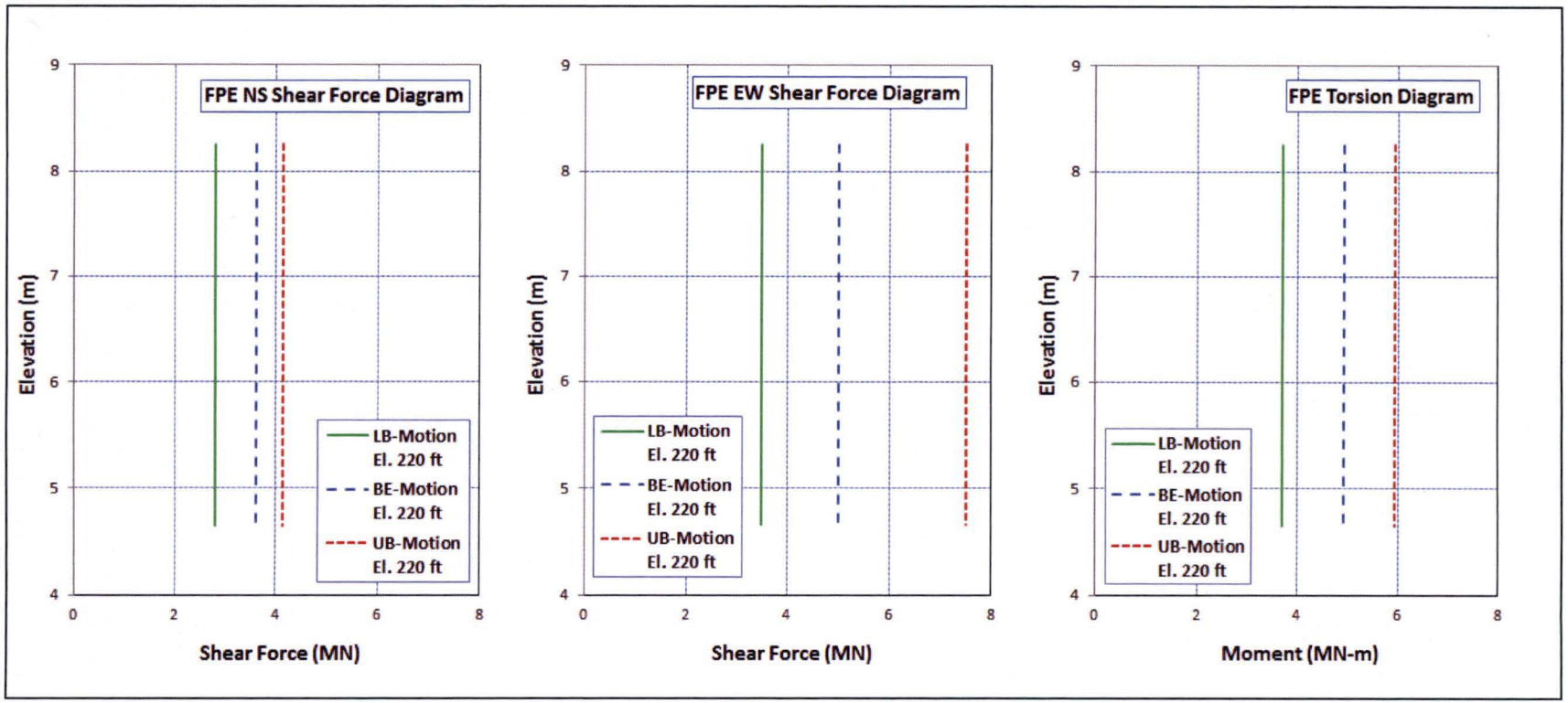

Figure 5.2-4b: FPE Maximum Shear Forces and Torsion from Analyses of FWSC UC_{OBE} Model with Deep Input Motion at El. 220 ft

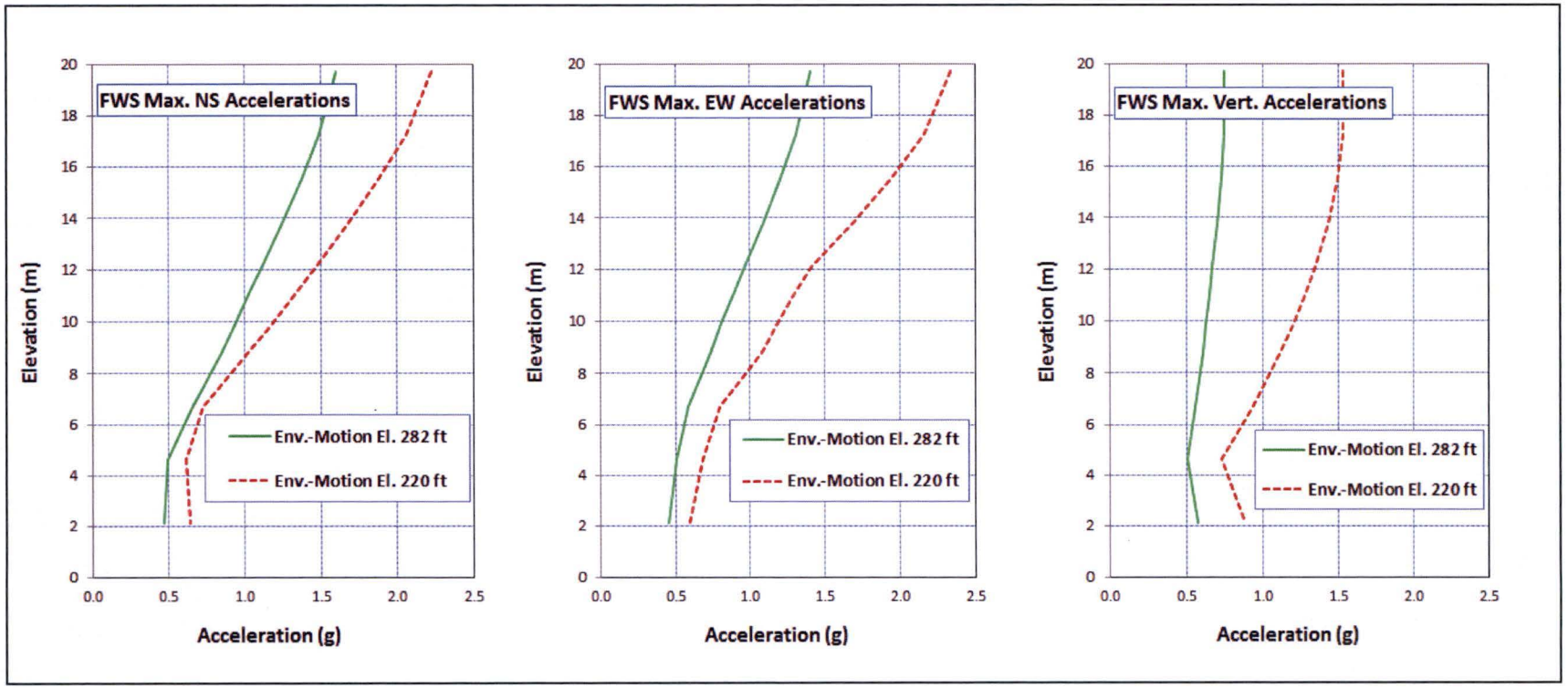

Figure 5.2-5a: Effects of Input Control Motion Elevation on FWS Maximum Accelerations

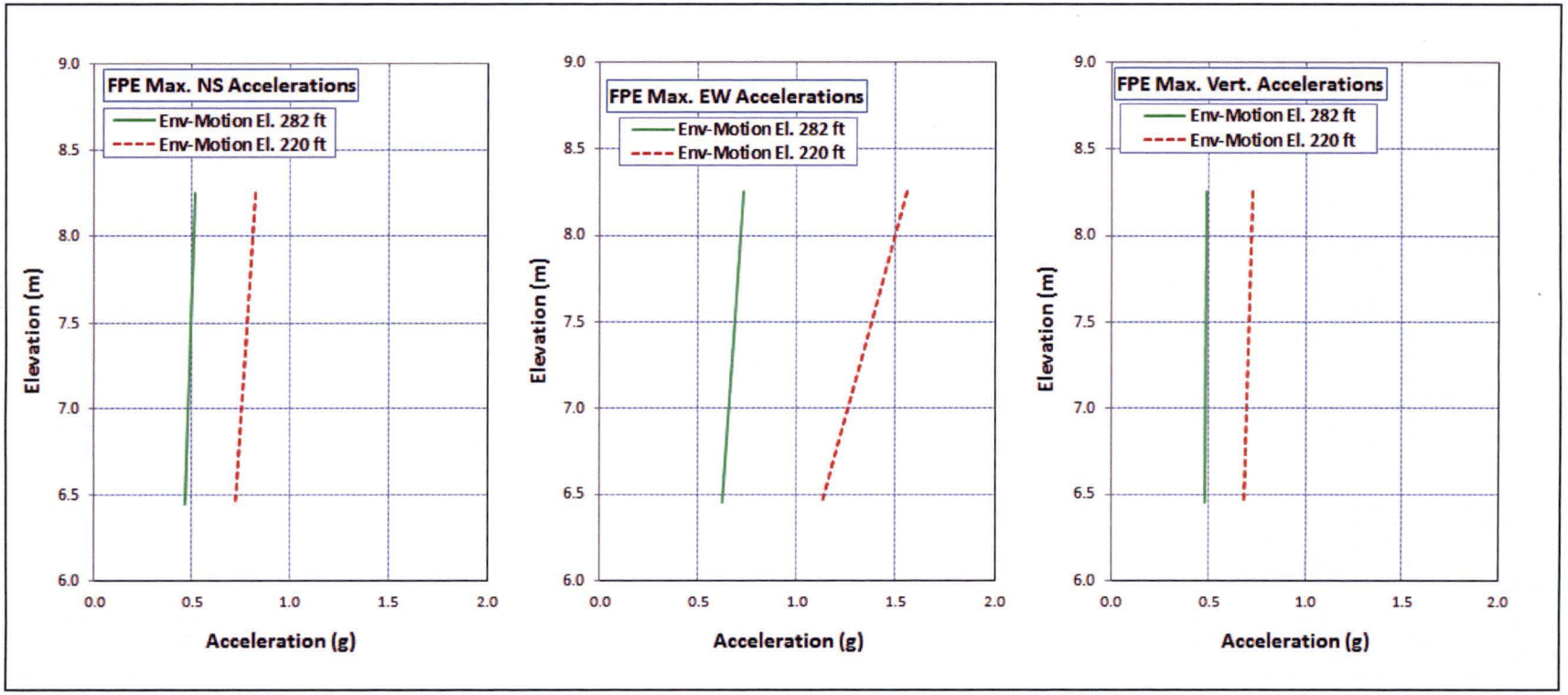

Figure 5.2-5b: Effects of Input Control Motion Elevation on FPE Maximum Accelerations

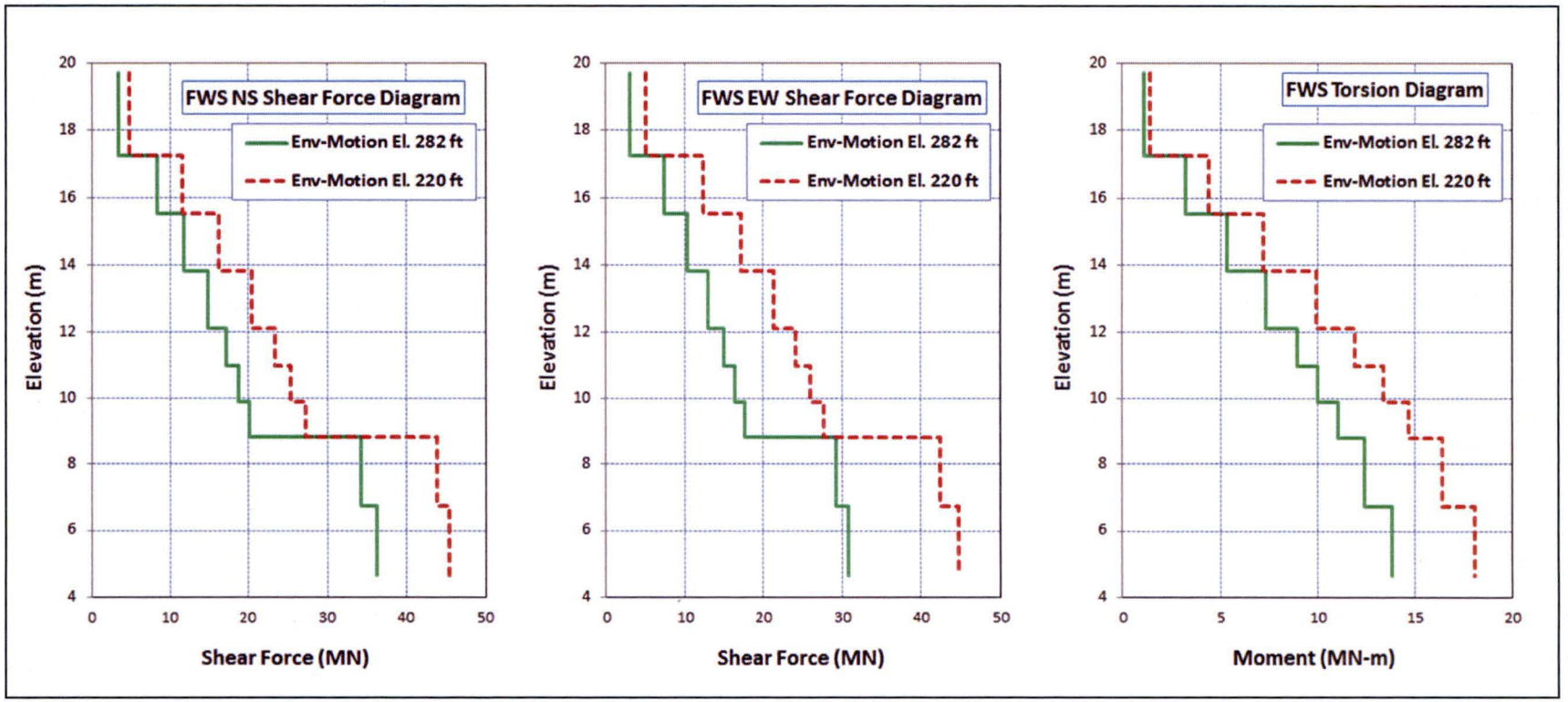

Figure 5.2-6a: Effects of Input Control Motion Elevation on FWS Maximum Shear Forces and Torsion

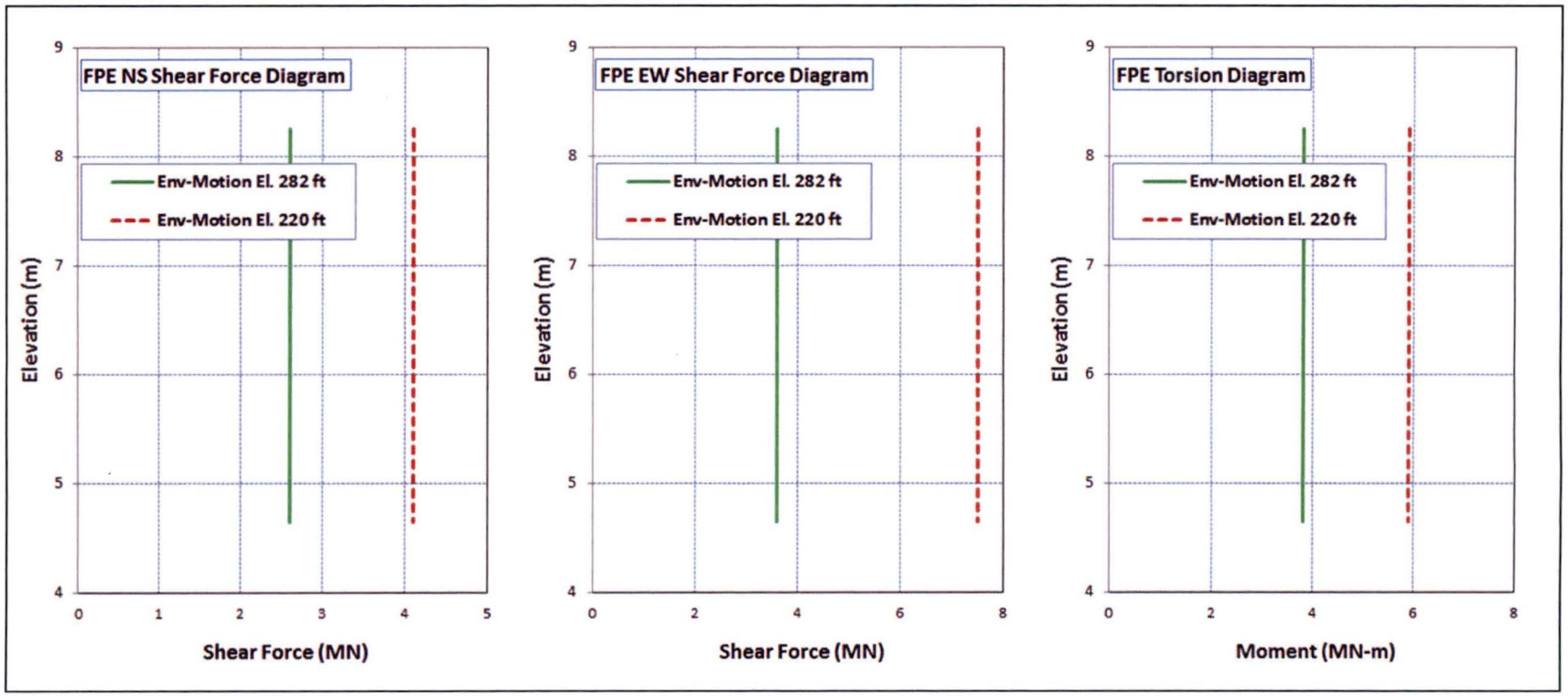

Figure 5.2-6b: Effects of Input Control Motion Elevation on FWS Maximum Shear Forces and Torsion

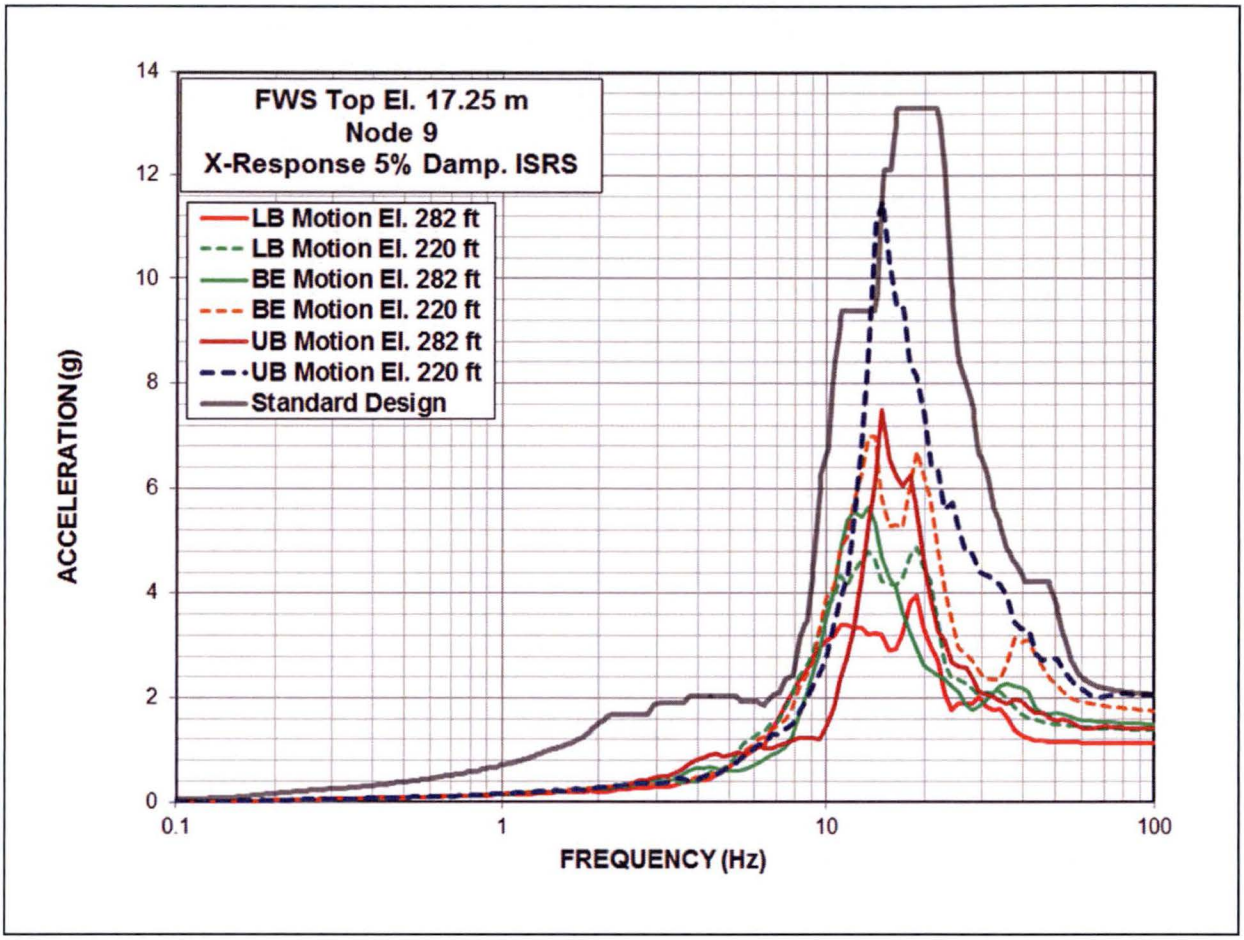

Figure 5.3-1a: Comparison of ISRS for Response of FWS Wall Top in NS (X) Direction

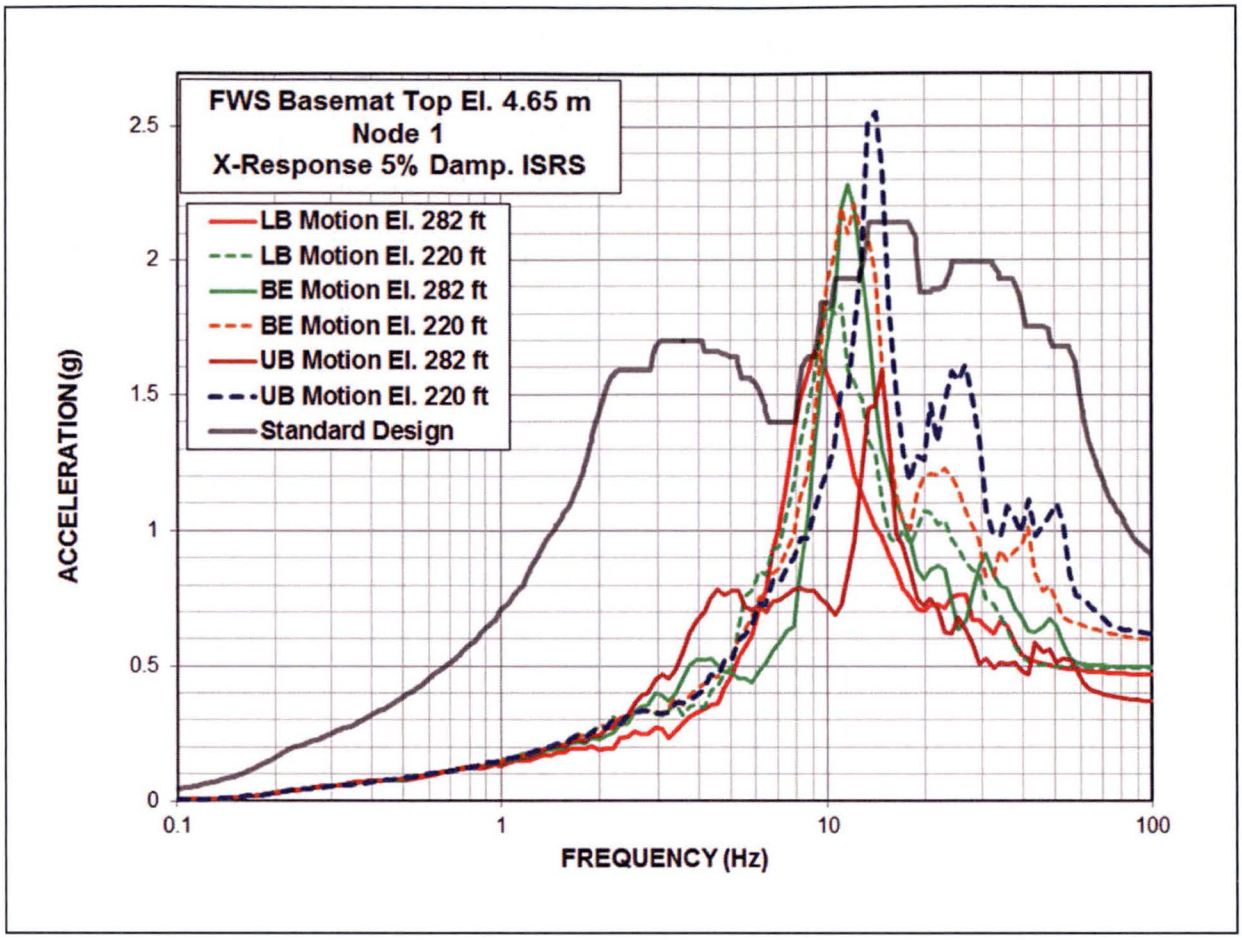

Figure 5.3-1b: Comparison of ISRS for Response of FWS Basemat in NS (X) Direction

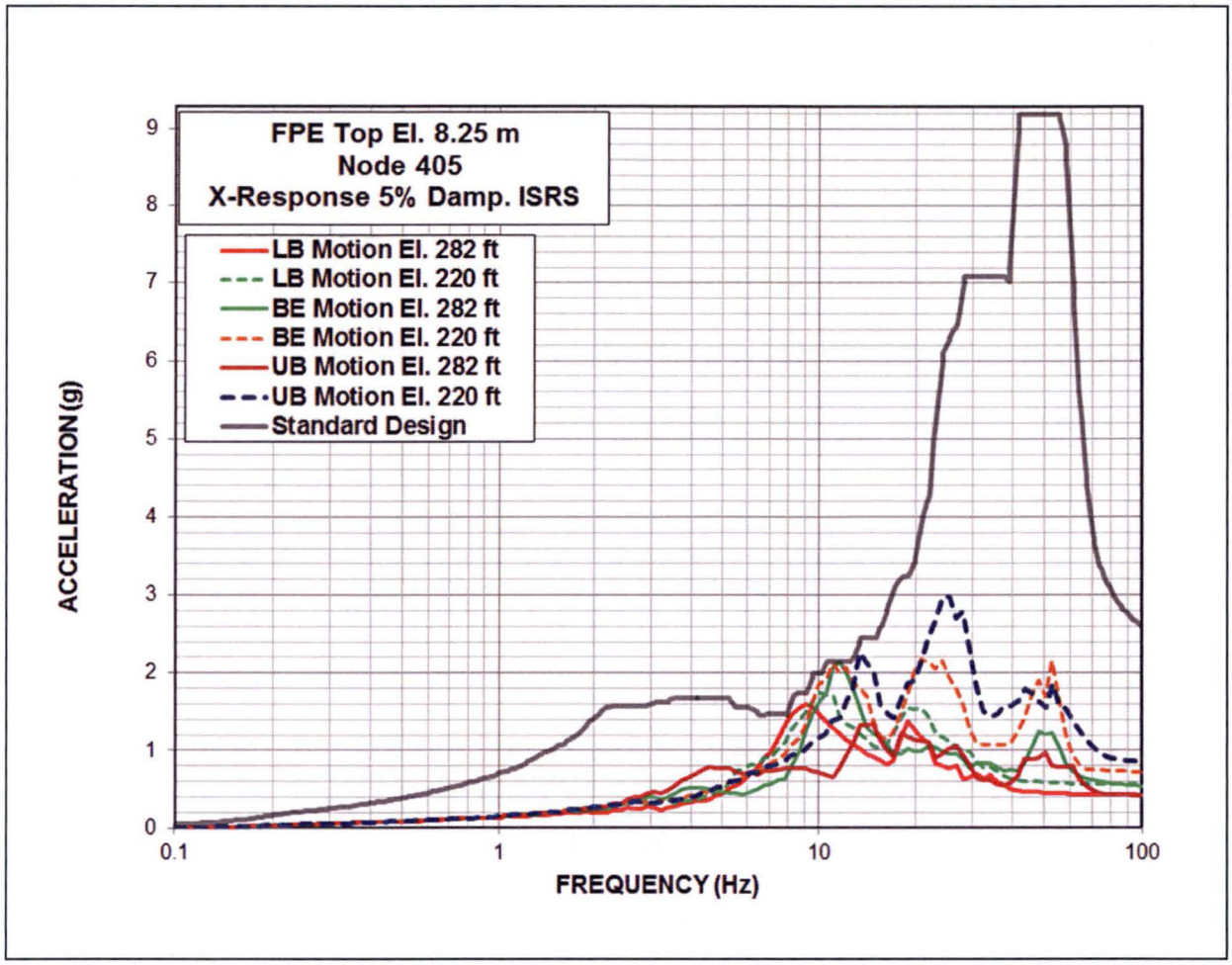

Figure 5.3-1c: Comparison of ISRS for Response of FPE Top in NS (X) Direction

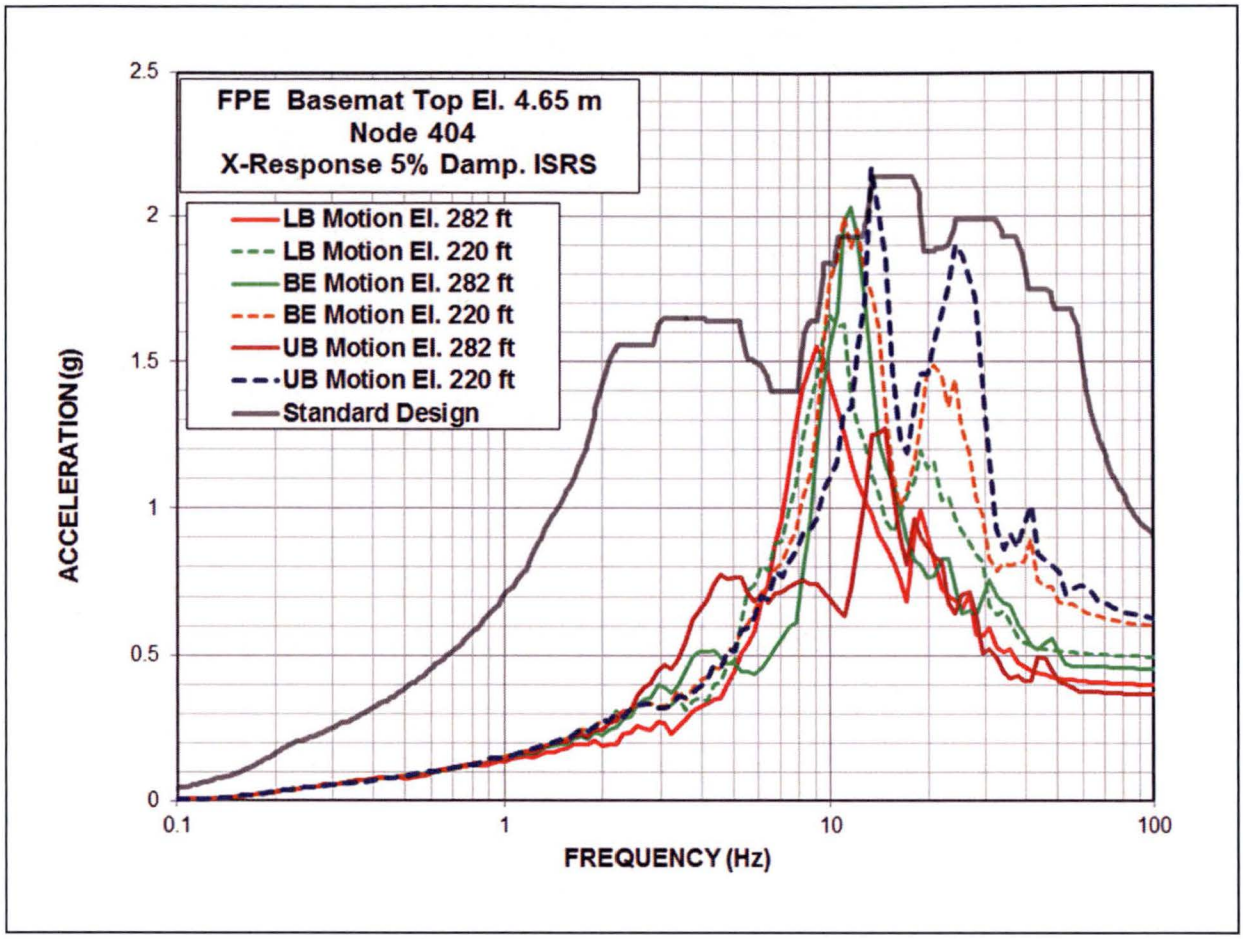

Figure 5.3-1d: Comparison of ISRS for Response of FPE Basemat in NS (X) Direction

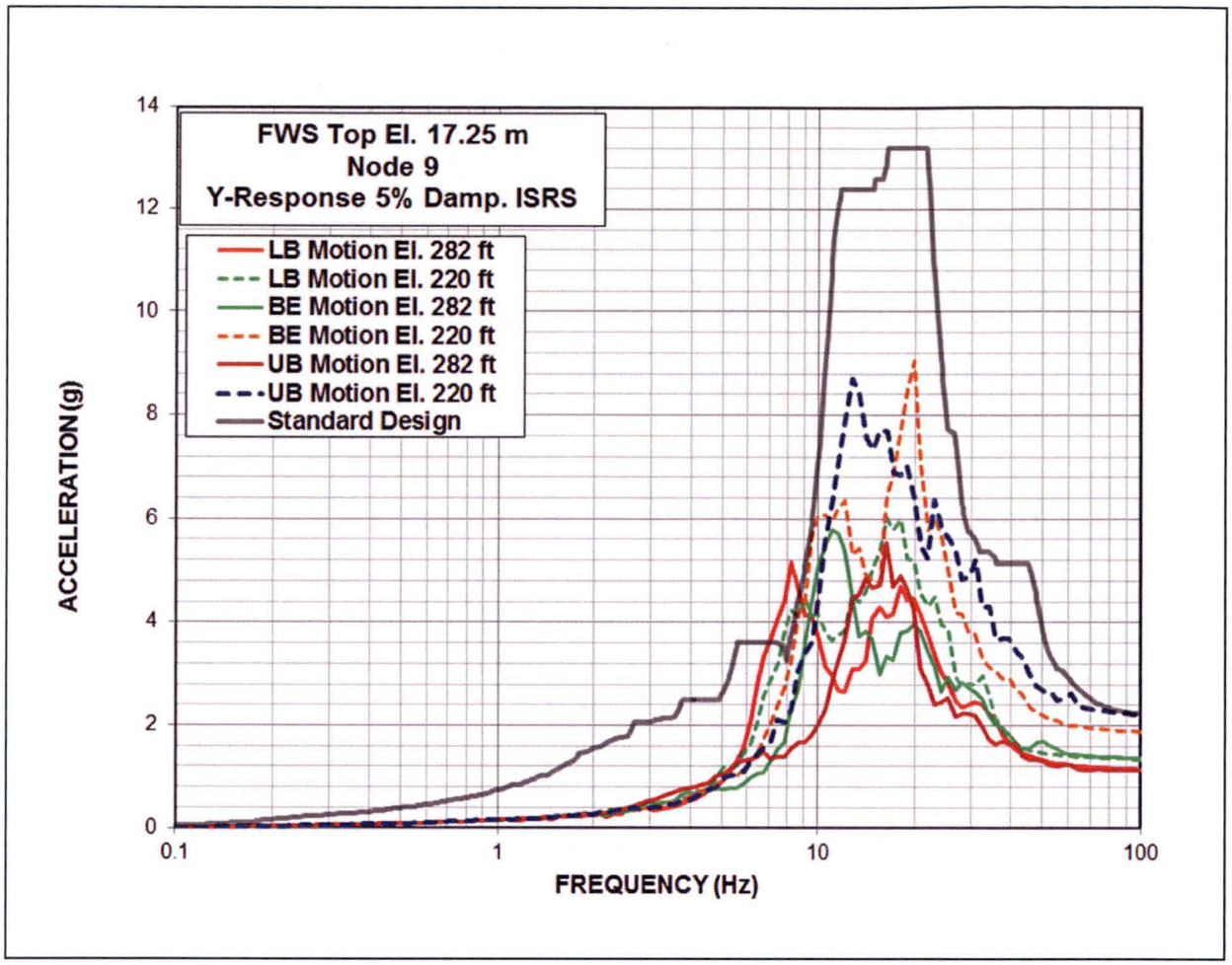

Figure 5.3-2a: Comparison of ISRS for Response of FWS Wall Top in EW (Y) Direction

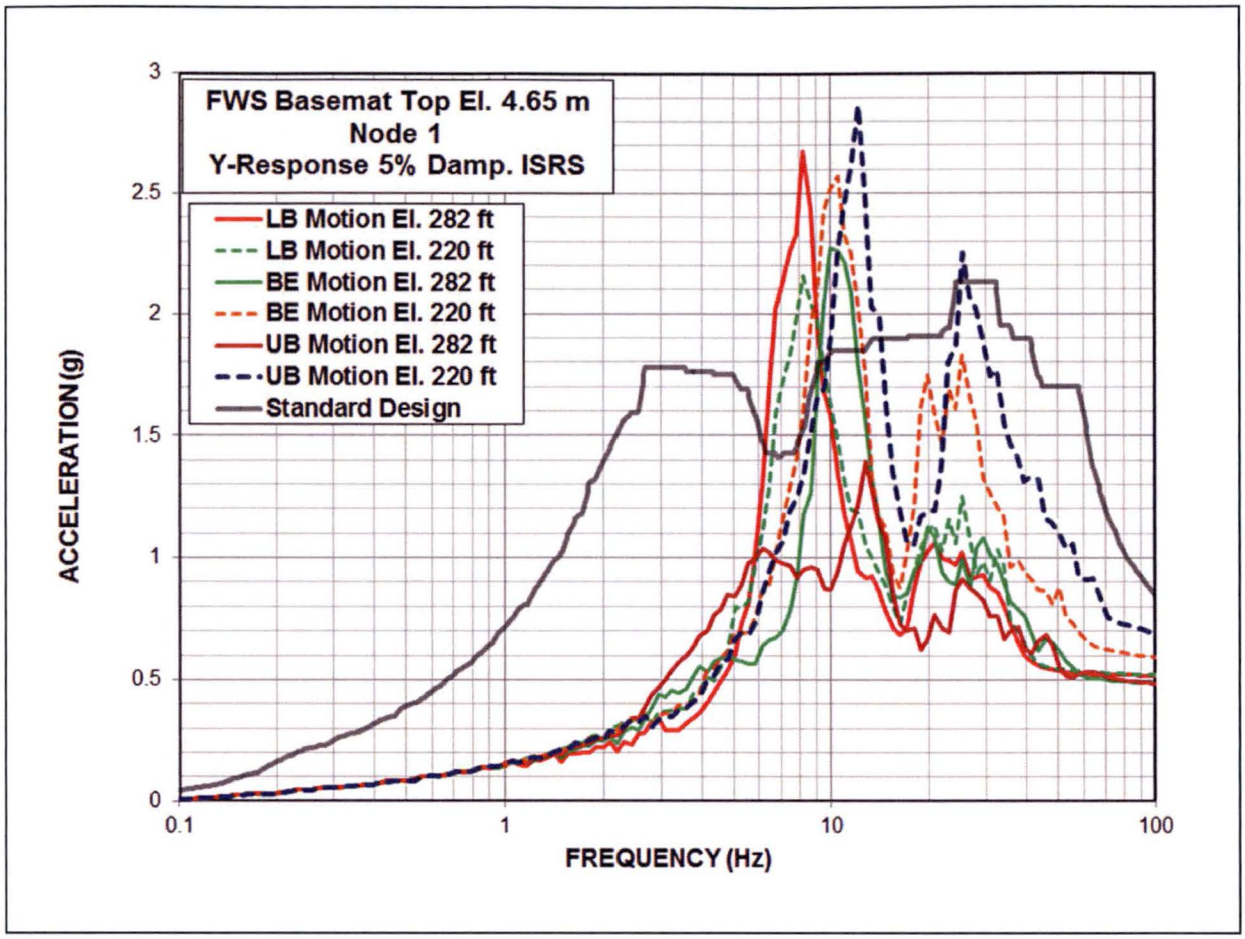

Figure 5.3-2b: Comparison of ISRS for Response of FWS Basemat in EW (Y) Direction

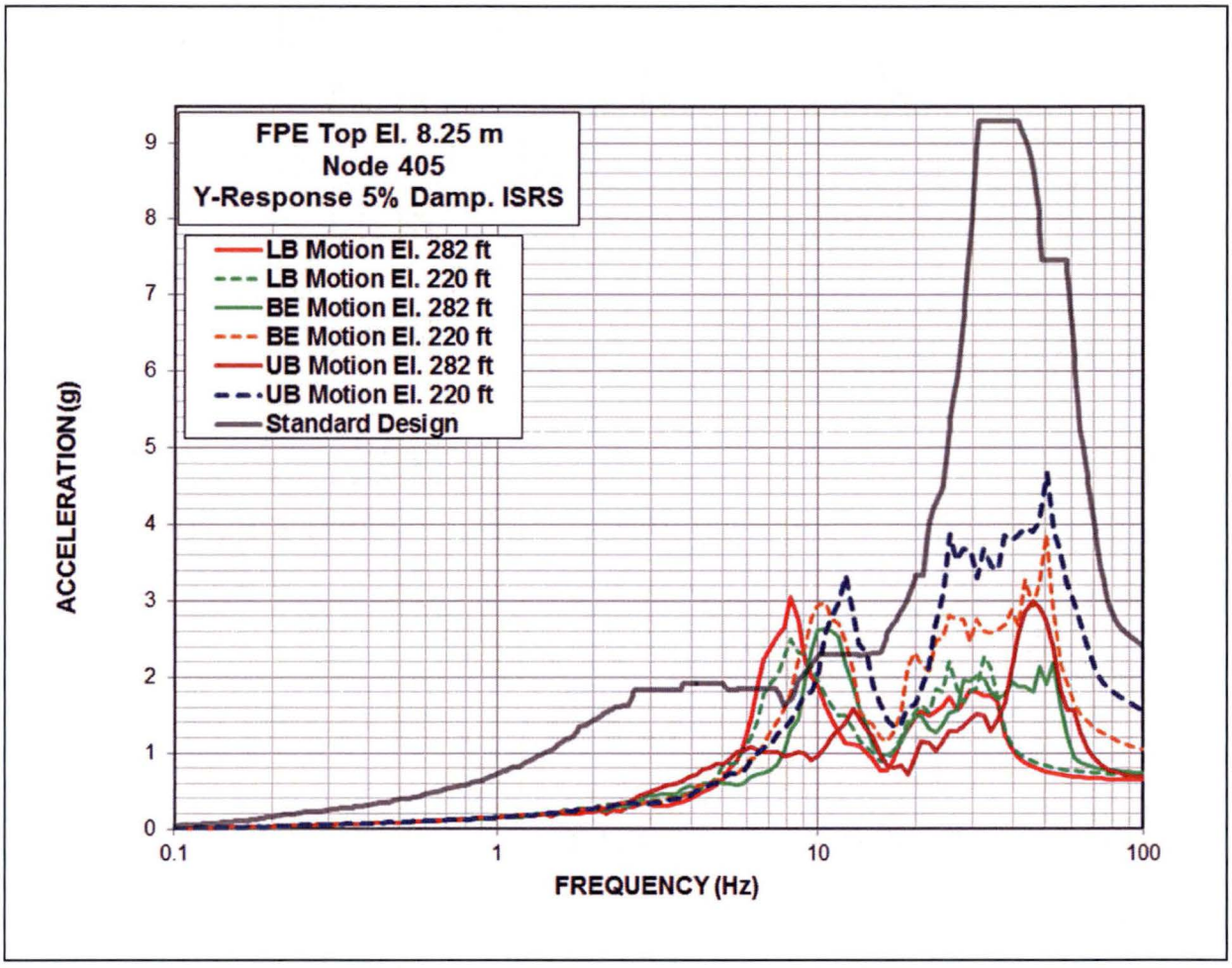

Figure 5.3-2c: Comparison of ISRS for Response of FPE Top in EW (Y) Direction

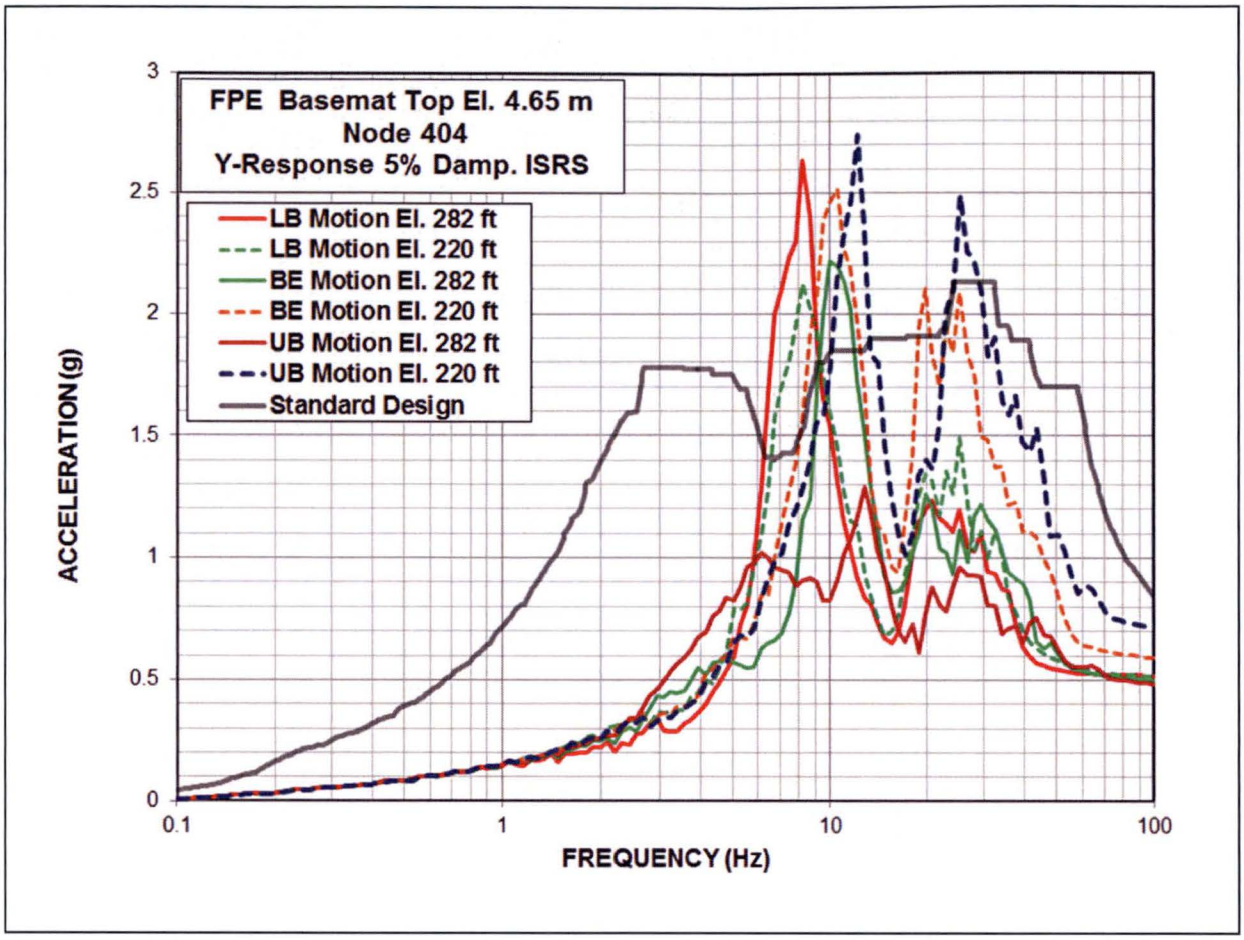

Figure 5.3-2d: Comparison of ISRS for Response of FPE Basemat in EW (Y) Direction

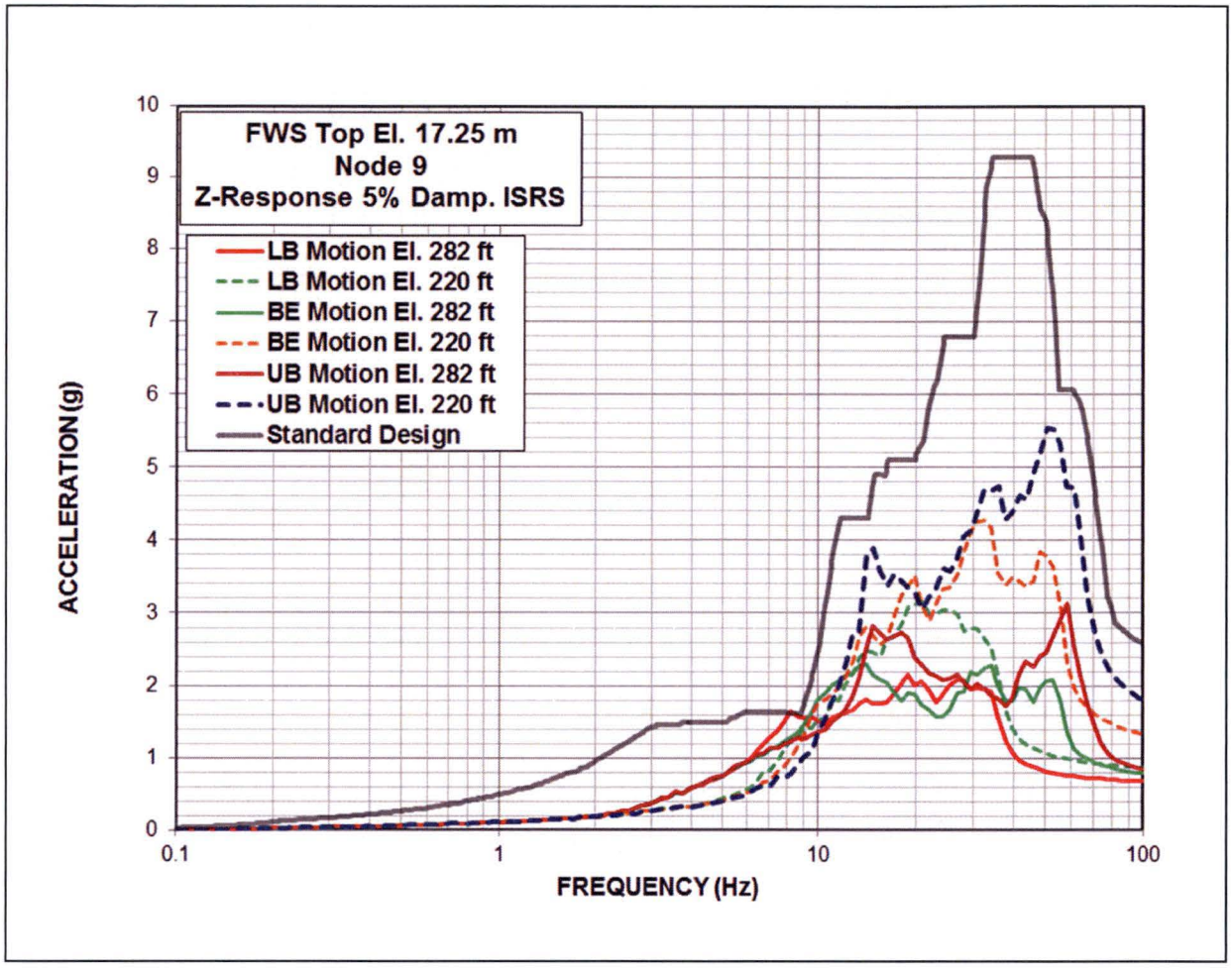

Figure 5.3-3a: Comparison of ISRS for Response of FWS Wall Top in Vert. (Z) Direction

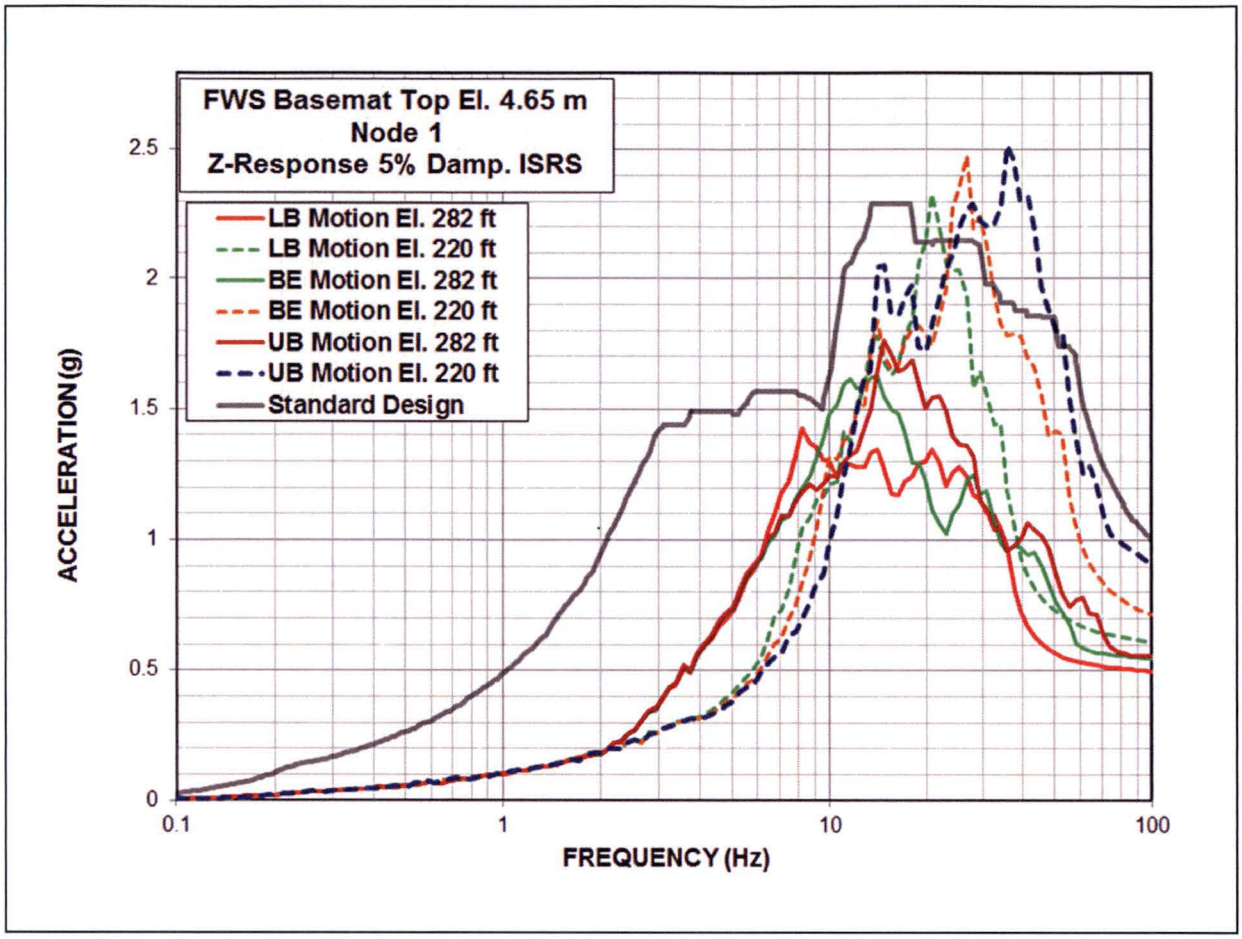

Figure 5.3-3b: Comparison of ISRS for Response of FWS Basemat in Vert. (Z) Direction

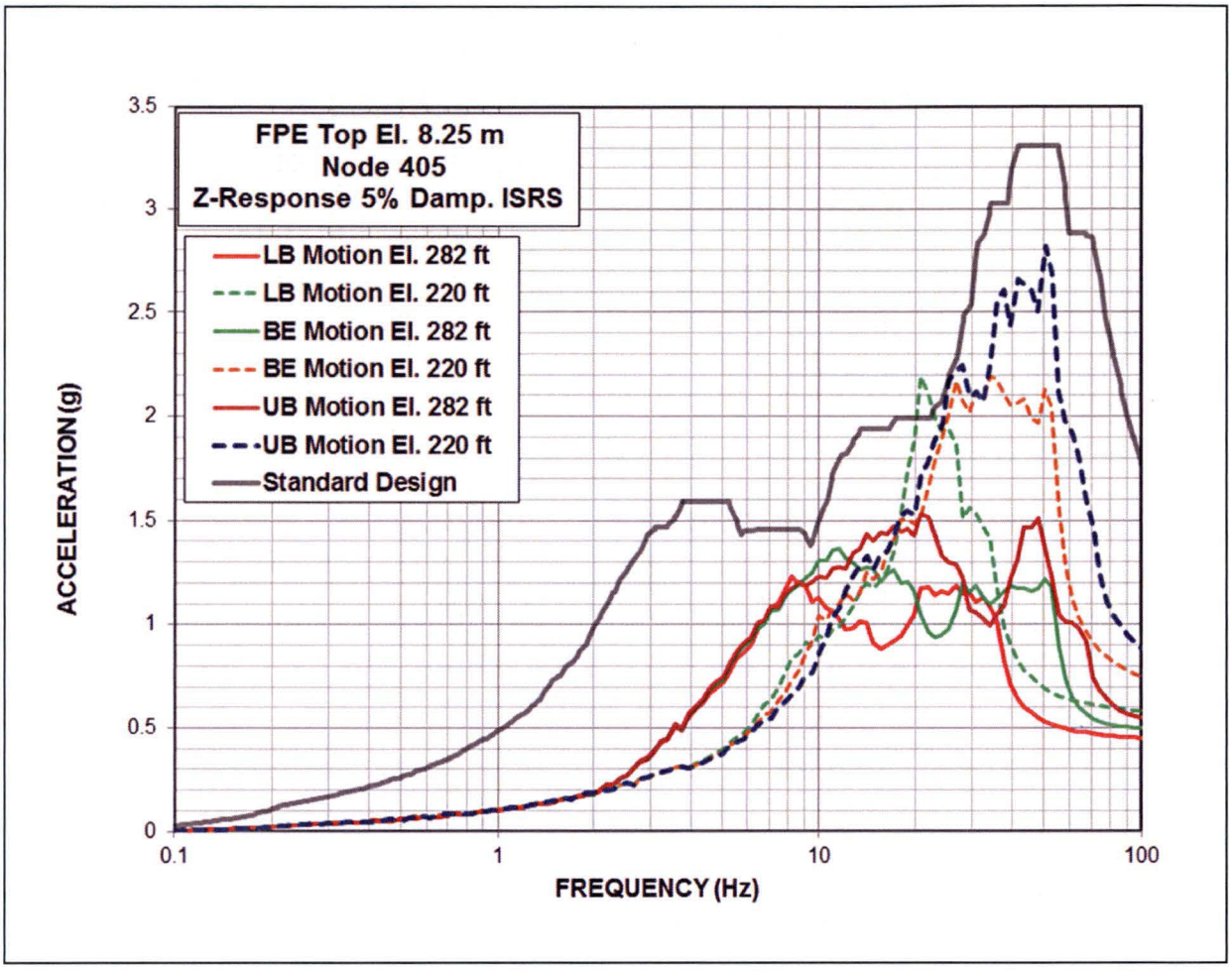

Figure 5.3-3c: Comparison of ISRS for Response of FPE Top in Vert. (Z) Direction

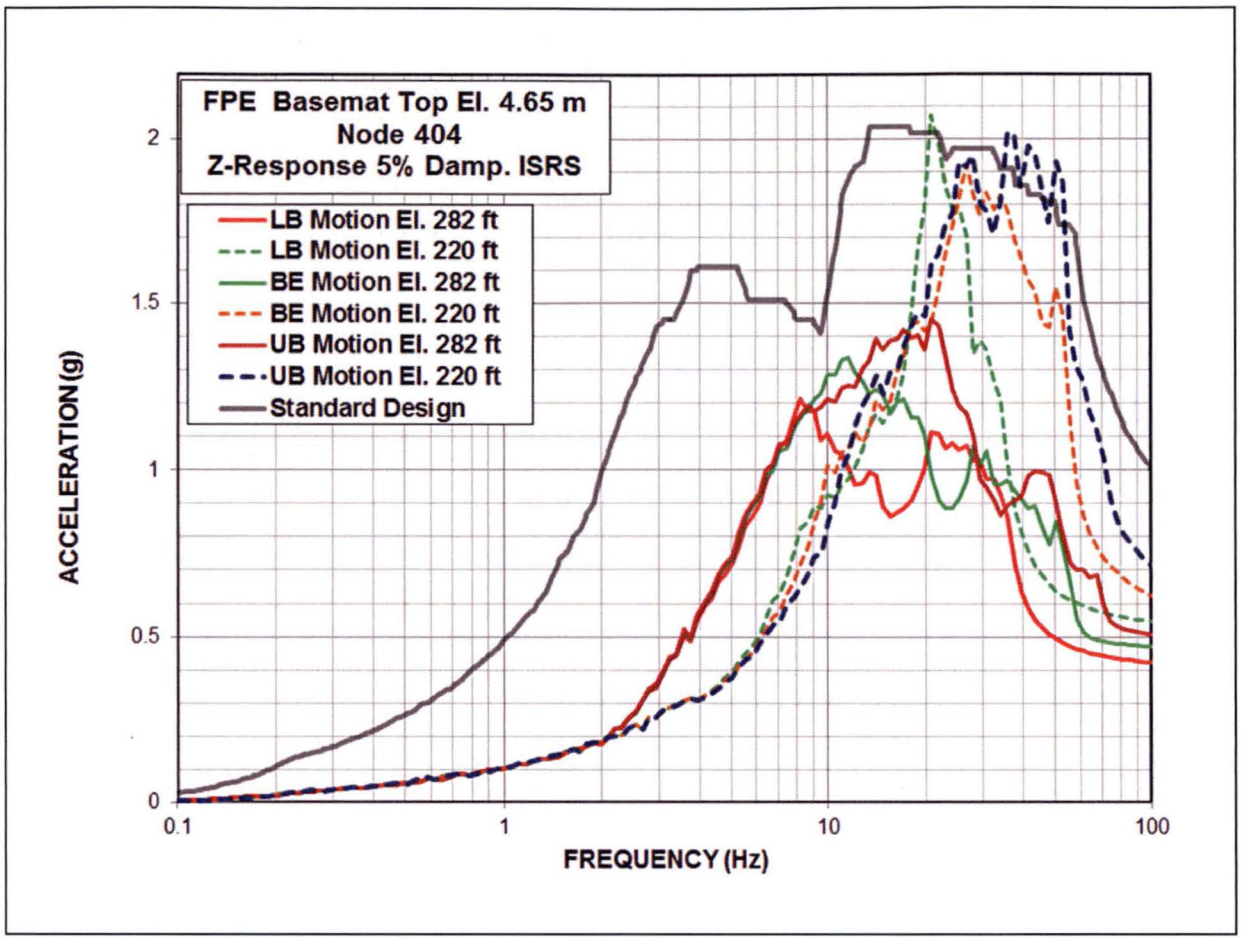

Figure 5.3-3d: Comparison of ISRS for Response of FPE Basemat in Vert. (Z) Direction

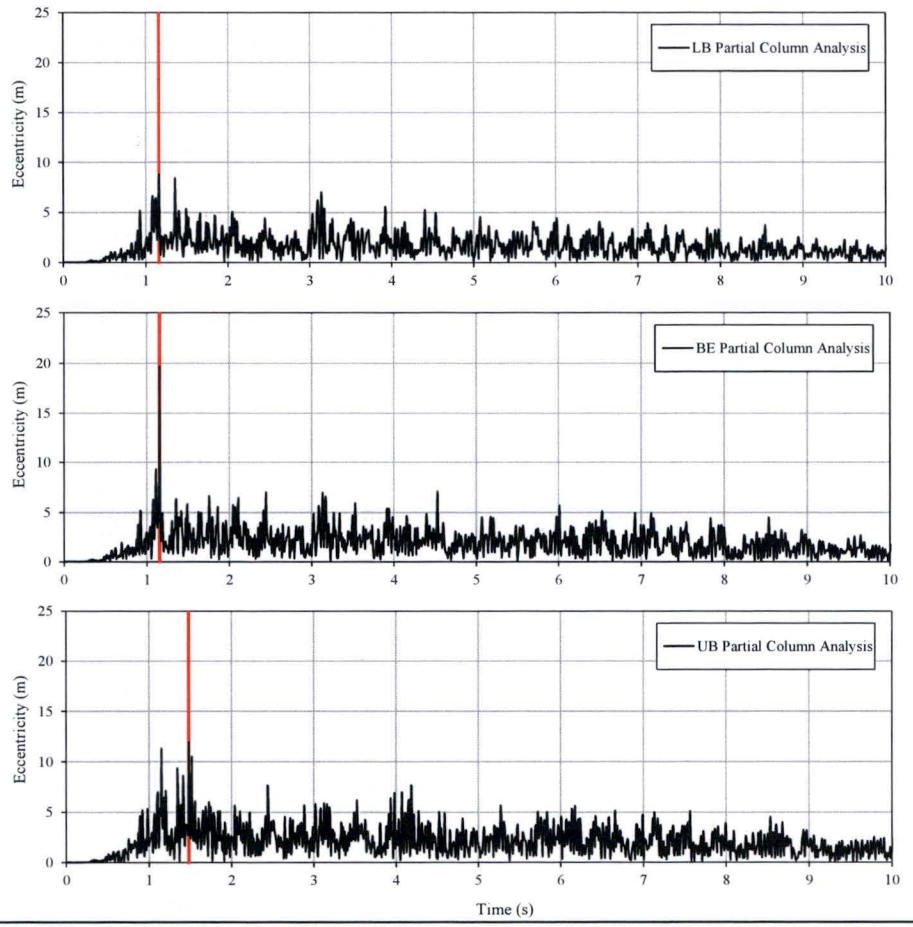

Note: The critical instances of time when the eccentricity of the vertical base reaction has maximum value are identified with red lines.

Figure 5.5-1: FWSC Base Reaction Eccentricity(+Ex+Ey+Ez)

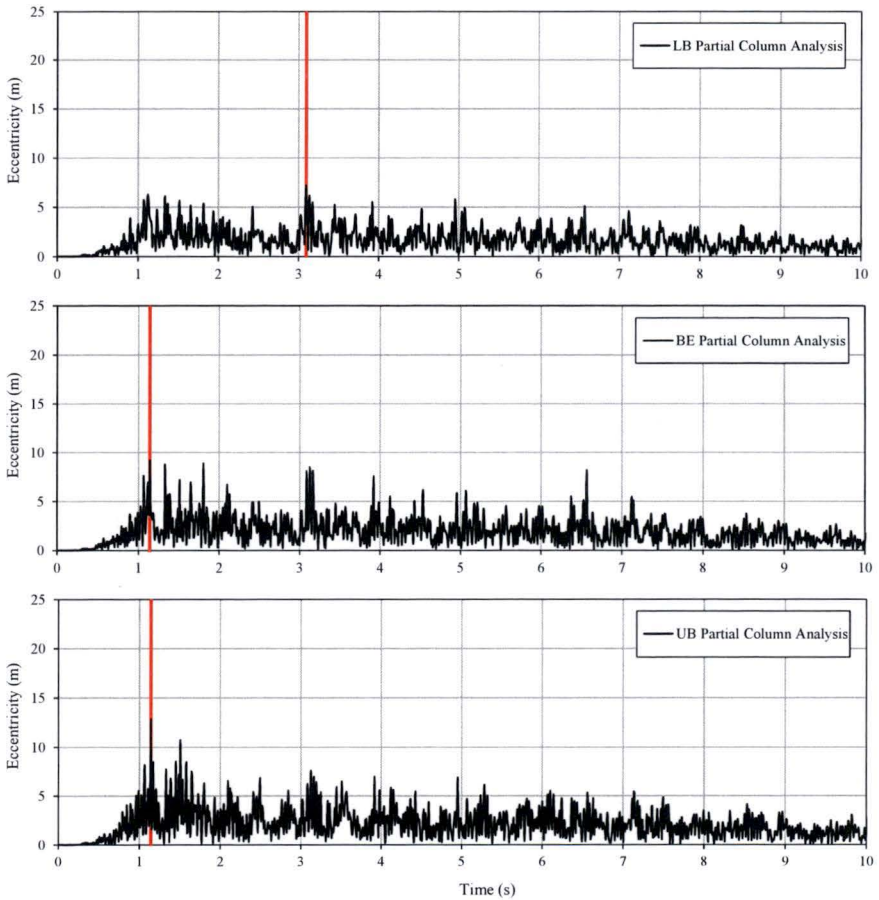

Note: The critical instances of time when the eccentricity of the vertical base reaction has maximum value are identified with red lines.

Figure 5.5-2: FWSC Base Reaction Eccentricity(-Ex-Ey-Ez)

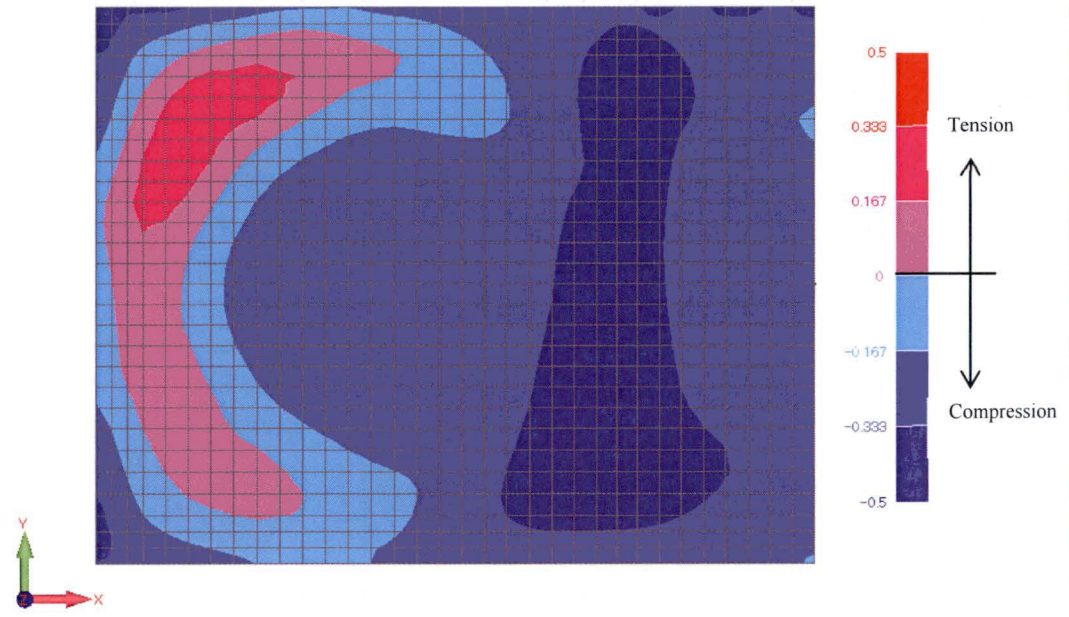

(a) Base Contact Pressures

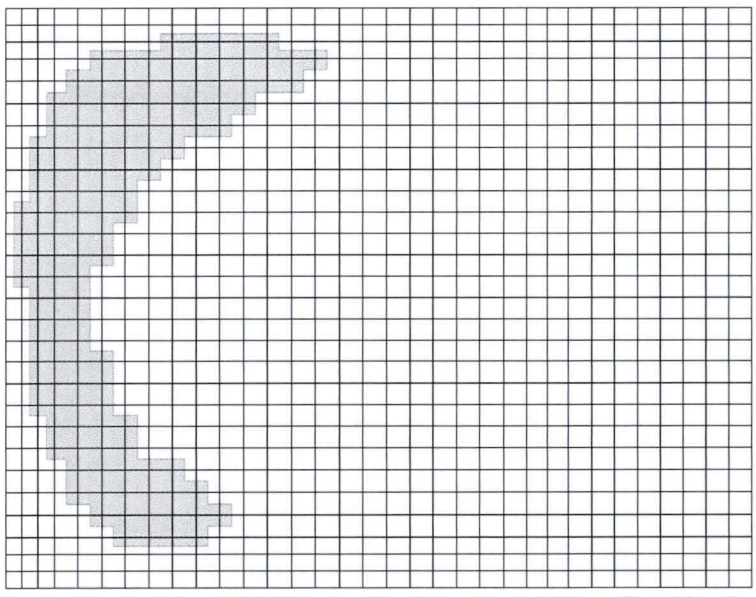

(b) Minimum Contact Area (85.8% at critical time t = 1.155 sec Combination +Ex+Ey+Ez)

Figure 5.5-3: FWSC Base Contact Area (BE Profile Analysis Case 8)

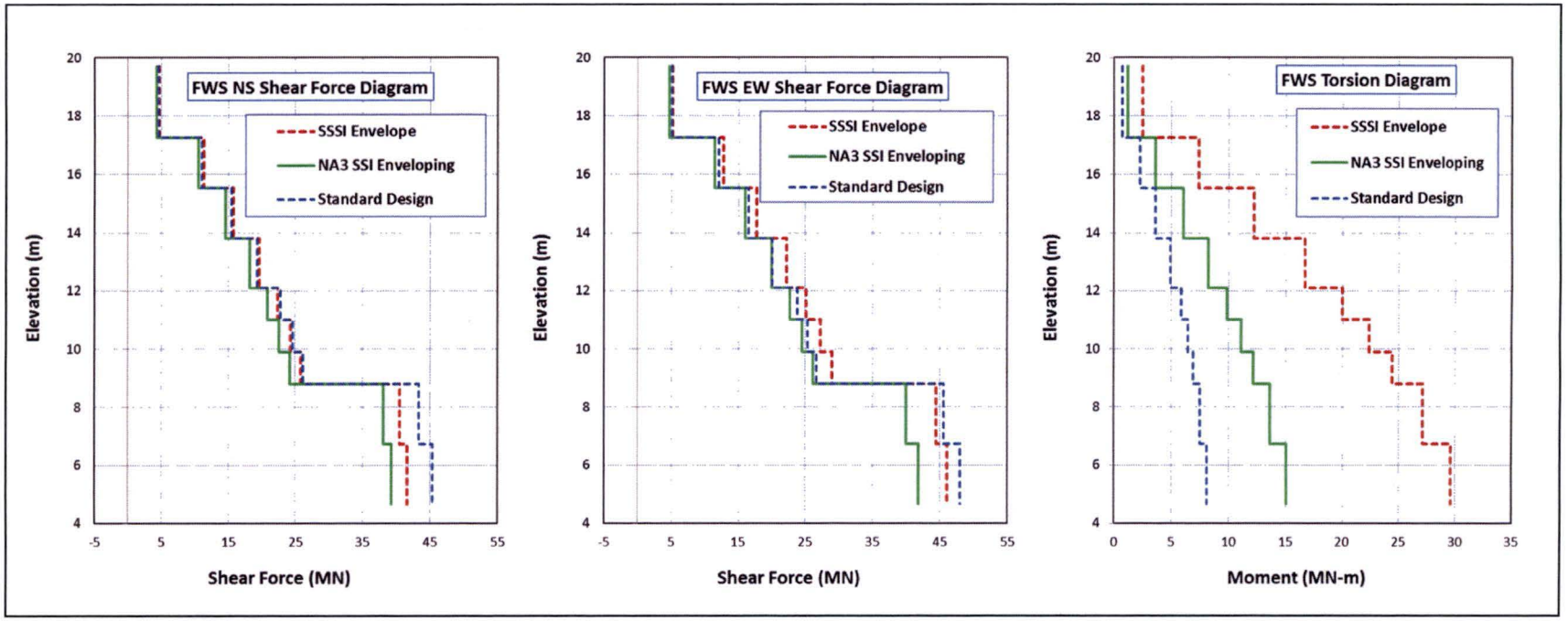

Figure 6.1-1: Comparison of Horizontal Seismic Load Demands on FWS Structure

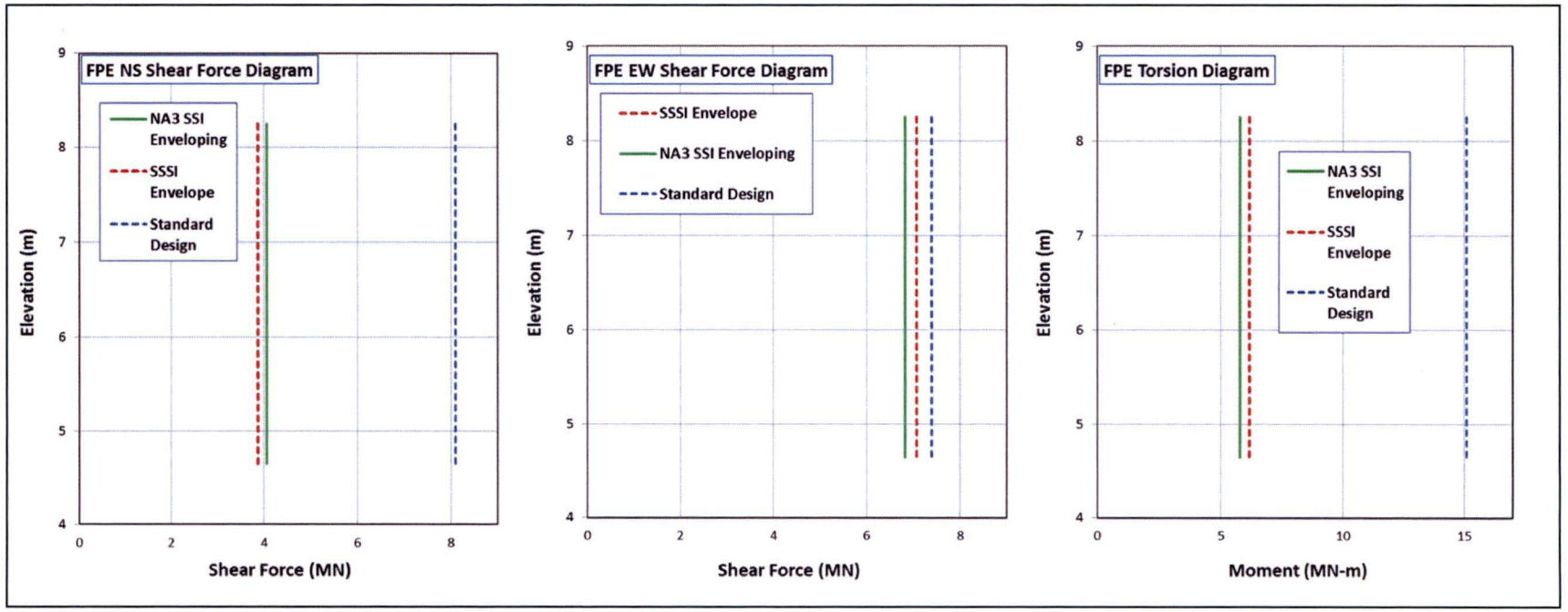

Figure 6.1-2: Comparison of Horizontal Seismic Load Demands on FPE Structure

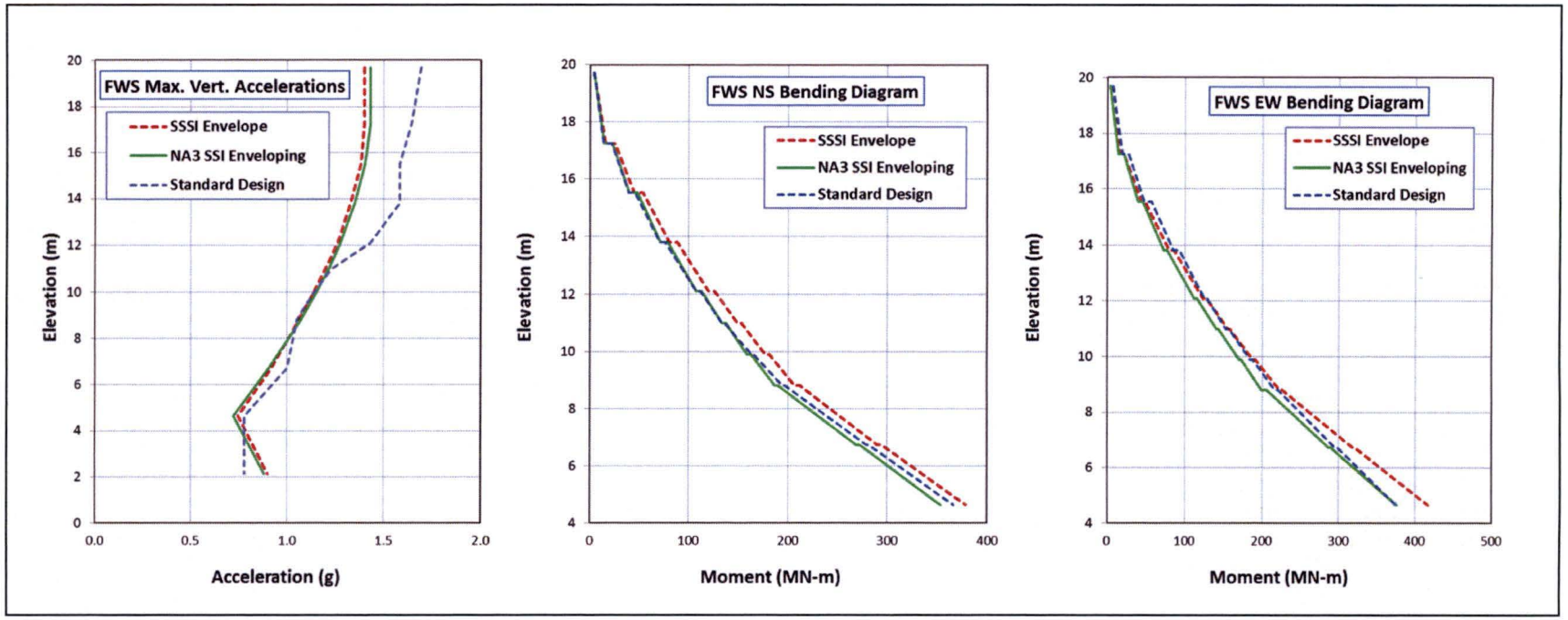

Figure 6.1-3: Comparison of Vertical Seismic Load Demands on FWS Structure

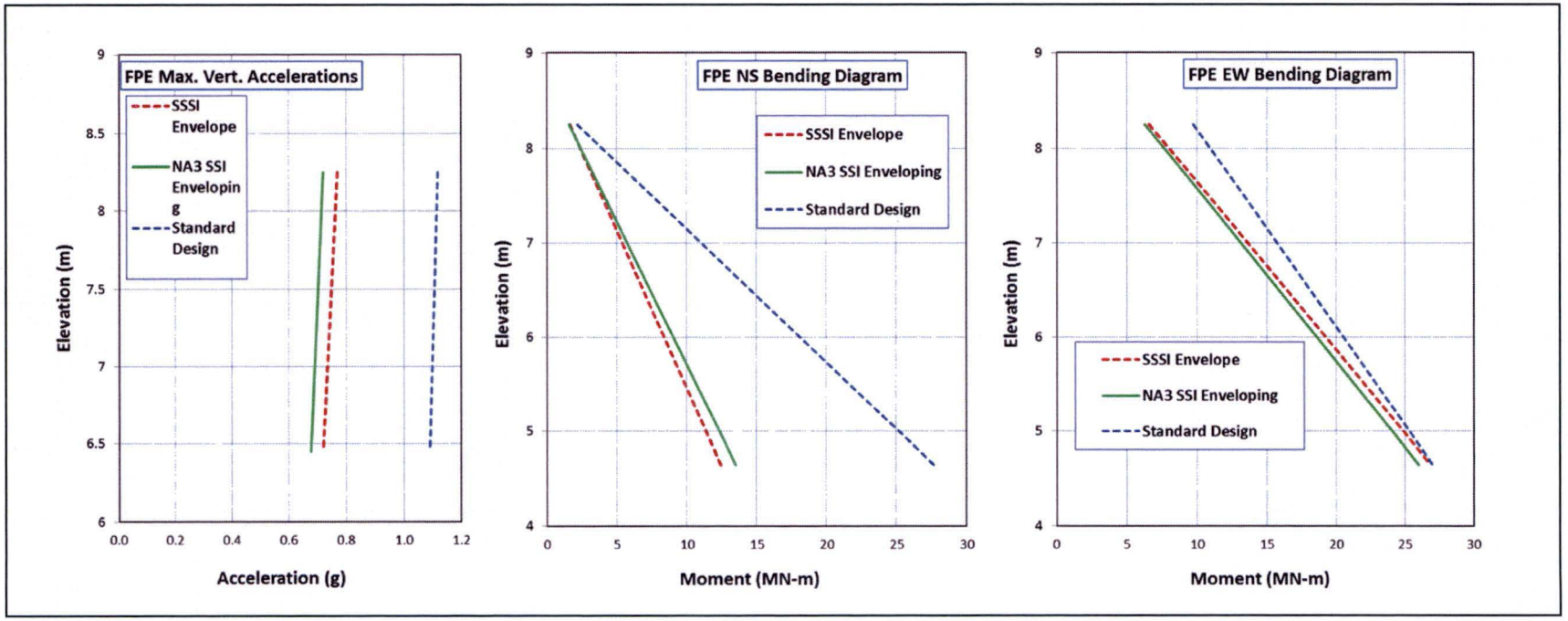

Figure 6.1-4: Comparison of Vertical Seismic Load Demands on FPE Structure

APPENDIX A
Results for Maximum Seismic Forces, Accelerations and Displacements

LIST OF TABLES

Table A-1: FWSC Maximum LMSM Member Forces and Moments (BE)

a) UC_{OBE} Model with Full Stiffness OBE-Damping Motion El. at 282 ft

Structure	Element			BE-UC_{OBE} Motion El. 282 ft				
	Elevation (m)	No.	Node No.	Shear (MN)		Bending (MN-m)		Torsion
				NS	EW	NS	EW	(MN-m)
FWS	19.70	9	10	3.4	3.0	2	2	0.9
			9			10	9	
	17.25	8	9	8.4	7.4	14	13	2.6
			8			28	25	
	15.53	7	8	11.8	10.4	32	29	4.3
			7			52	46	
	13.81	6	7	14.9	13.0	56	50	5.9
			6			81	72	
	12.10	5	6	17.2	15.0	84	75	7.0
			5			103	91	
	11.00	4	5	18.8	16.4	105	93	7.8
			4			126	111	
	9.90	3	4	20.2	17.6	128	113	8.5
			3			150	132	
	8.81	2	3	34.2	29.3	152	135	9.4
			2			223	196	
	6.73	1	2	36.2	30.9	226	199	10.2
	4.65		8002			301	263	
FPE	8.25	402	405	2.6	3.6	1	4	3.8
	4.65	401	404			8	14	

Table A-1: FWSC Maximum LMSM Member Forces and Moments (BE) (Continued)

b) UC_{OBE} Model with Full Stiffness OBE-Damping Motion El. at 220 ft

Structure	Element			BE-UC_{OBE} Motion El. 220 ft				
	Elevation (m)	No.	Node No.	Shear (MN)		Bending (MN-m)		Torsion
				NS	EW	NS	EW	(MN-m)
FWS	19.70	9	10	4.1	4.3	3	3	1.4
			9			13	13	
	17.25	8	9	10.0	10.4	20	19	4.4
			8			37	37	
	15.53	7	8	13.8	14.5	43	42	7.2
			7			67	67	
	13.81	6	7	16.9	17.9	73	72	9.9
			6			101	103	
	12.10	5	6	19.1	20.3	106	107	11.9
			5			127	129	
	11.00	4	5	20.5	21.9	130	132	13.4
			4			152	156	
	9.90	3	4	21.7	23.2	155	159	14.7
			3			179	184	
	8.81	2	3	33.6	36.0	183	187	16.4
			2			249	259	
	6.73	1	2	35.5	37.4	252	263	18.1
	4.65		8002			322	341	
FPE	8.25	402	405	3.6	5.0	2	5	4.9
	4.65	401	404			12	20	

Table A-1: FWSC Maximum LMSM Member Forces and Moments (BE) (Continued)

c) UC_{SSE} Model with Full Stiffness SSE-Damping Motion El. at 220 ft

Structure	Element			BE-UC_{SSE} Motion El. 220 ft				
	Elevation (m)	No.	Node No.	Shear (MN)		Bending (MN-m)		Torsion
				NS	EW	NS	EW	(MN-m)
FWS	19.70	9	10	3.7	3.9	3	3	1.2
			9			12	12	
	17.25	8	9	9.1	9.6	17	18	3.6
			8			33	34	
	15.53	7	8	12.5	13.4	38	39	6.0
			7			59	62	
	13.81	6	7	15.5	16.6	64	67	8.2
			6			91	95	
	12.10	5	6	17.6	18.7	95	98	9.9
			5			114	119	
	11.00	4	5	19.0	20.2	117	122	11.1
			4			137	144	
	9.90	3	4	20.1	21.5	140	146	12.2
			3			162	170	
	8.81	2	3	31.8	33.9	165	173	13.6
			2			229	244	
	6.73	1	2	33.7	35.3	232	248	15.0
	4.65		8002			299	322	
FPE	8.25	402	405	3.6	4.7	1	5	4.8
	4.65	401	404			12	19	

Table A-2: FWSC Maximum LMSM Member Forces and Moments (LB)

a) UC_{OBE} Model with Full Stiffness OBE-Damping Motion El. at 282 ft

Structure	Element			LB-UC_{OBE} Motion El. 282 ft				
	Elevation (m)	No.	Node No.	Shear (MN)		Bending (MN-m)		Torsion
				NS	EW	NS	EW	(MN-m)
FWS	19.70	9	10	2.5	2.5	1	2	1.1
			9			7	8	
	17.25	8	9	6.3	6.2	10	11	3.2
			8			20	22	
	15.53	7	8	8.9	8.7	23	25	5.3
			7			38	40	
	13.81	6	7	11.3	10.9	40	43	7.3
			6			60	62	
	12.10	5	6	13.2	12.5	62	64	8.9
			5			76	78	
	11.00	4	5	14.5	13.6	77	80	10.0
			4			93	95	
	9.90	3	4	15.8	14.7	95	97	11.0
			3			112	113	
	8.81	2	3	28.4	25.5	114	115	12.4
			2			173	166	
	6.73	1	2	30.2	27.2	175	169	13.8
	4.65		8002			238	222	
FPE	8.25	402	405	2.2	3.2	1	3	2.8
	4.65	401	404			7	12	

Table A-2: FWSC Maximum LMSM Member Forces and Moments (LB) (Continued)

b) UC_{OBE} Model with Full Stiffness OBE-Damping Motion El. at 220 ft

Structure	Element			LB-UC_{OBE} Motion El. 220 ft				
	Elevation (m)	No.	Node No.	Shear (MN)		Bending (MN-m)		Torsion
				NS	EW	NS	EW	(MN-m)
FWS	19.70	9	10	3.2	3.0	2	2	1.3
			9			9	9	
	17.25	8	9	7.8	7.5	13	14	4.1
			8			26	26	
	15.53	7	8	10.9	10.4	30	31	6.7
			7			49	48	
	13.81	6	7	13.7	13.1	52	52	9.2
			6			76	73	
	12.10	5	6	15.7	15.1	78	76	11.0
			5			96	92	
	11.00	4	5	17.2	16.5	98	94	12.4
			4			116	112	
	9.90	3	4	18.5	17.8	118	114	13.6
			3			139	133	
	8.81	2	3	31.1	30.0	141	136	15.2
			2			206	198	
	6.73	1	2	32.8	31.6	208	201	17.0
	4.65		8002			276	267	
FPE	8.25	402	405	2.8	3.5	1	4	3.7
	4.65	401	404			9	13	

Table A-2: FWSC Maximum LMSM Member Forces and Moments (LB) (Continued)

c) UC_{SSE} Model with Full Stiffness SSE-Damping Motion El. at 220 ft

Structure	Element			LB-UC_{SSE} Motion El. 220 ft				
	Elevation (m)	No.	Node No.	Shear (MN)		Bending (MN-m)		Torsion
				NS	EW	NS	EW	(MN-m)
FWS	19.70	9	10	3.0	2.9	2	2	1.1
			9			9	9	
	17.25	8	9	7.3	7.2	12	13	3.4
			8			25	25	
	15.53	7	8	10.2	10.1	28	29	5.6
			7			46	45	
	13.81	6	7	12.9	12.7	49	49	7.7
			6			71	70	
	12.10	5	6	14.8	14.5	73	72	9.3
			5			90	88	
	11.00	4	5	16.2	15.9	92	90	10.5
			4			109	107	
	9.90	3	4	17.5	17.2	111	109	11.6
			3			130	128	
	8.81	2	3	29.7	29.0	133	130	13.1
			2			194	191	
	6.73	1	2	31.4	30.6	196	194	14.7
	4.65		8002			261	257	
FPE	8.25	402	405	2.8	3.4	1	4	3.6
	4.65	401	404			9	13	

Table A-3: FWSC Maximum LMSM Member Forces and Moments (UB)

a) UC_{OBE} Model with Full Stiffness OBE-Damping Motion El. at 282 ft

Structure	Element			UB-UC_{OBE} Motion El. 282 ft				
	Elevation (m)	No.	Node No.	Shear (MN)		Bending (MN-m)		Torsion
				NS	EW	NS	EW	(MN-m)
FWS	19.70	9	10	3.2	2.5	2	2	0.5
			9			10	8	
	17.25	8	9	7.9	6.3	13	11	1.6
			8			27	21	
	15.53	7	8	11.1	8.8	30	24	2.7
			7			49	40	
	13.81	6	7	13.9	11.1	53	42	3.7
			6			76	61	
	12.10	5	6	16.0	12.7	79	64	4.3
			5			97	78	
	11.00	4	5	17.4	13.9	99	79	4.8
			4			118	95	
	9.90	3	4	18.7	15.0	120	96	5.2
			3			140	113	
	8.81	2	3	30.6	25.3	142	115	5.7
			2			206	167	
	6.73	1	2	32.0	26.7	208	170	6.0
	4.65		8002			275	225	
FPE	8.25	402	405	2.1	3.4	1	4	2.9
	4.65	401	404			7	13	

Table A-3: FWSC Maximum LMSM Member Forces and Moments (UB) (Continued)

b) UC_{OBE} Model with Full Stiffness OBE-Damping Motion El. at 220 ft

Structure	Element			UB-UC_{OBE} Motion El. 220 ft				
	Elevation (m)	No.	Node No.	Shear (MN)		Bending (MN-m)		Torsion
				NS	EW	NS	EW	(MN-m)
FWS	19.70	9	10	4.8	5.0	5	4	1.2
			9			16	15	
	17.25	8	9	11.7	12.3	25	23	3.6
			8			45	42	
	15.53	7	8	16.3	17.1	54	49	5.9
			7			80	78	
	13.81	6	7	20.4	21.3	88	83	8.0
			6			120	120	
	12.10	5	6	23.4	24.1	127	124	9.5
			5			149	150	
	11.00	4	5	25.5	26.1	154	153	10.6
			4			178	182	
	9.90	3	4	27.3	27.7	182	185	11.5
			3			208	214	
	8.81	2	3	43.9	42.2	212	218	12.5
			2			303	306	
	6.73	1	2	45.3	44.6	306	309	13.4
	4.65		8002			400	400	
FPE	8.25	402	405	4.1	7.5	2	6	5.9
	4.65	401	404			14	28	

Table A-3: FWSC Maximum LMSM Member Forces and Moments (UB) (Continued)

c) UC_{SSE} Model with Full Stiffness SSE-Damping Motion El. at 220 ft

Structure	Element			UB-UC_{SSE} Motion El. 220 ft				
	Elevation (m)	No.	Node No.	Shear (MN)		Bending (MN-m)		Torsion
				NS	EW	NS	EW	(MN-m)
FWS	19.70	9	10	4.3	4.7	4	3	0.8
			9			14	14	
	17.25	8	9	10.5	11.5	23	21	2.5
			8			40	39	
	15.53	7	8	14.6	16.0	48	46	4.2
			7			71	72	
	13.81	6	7	18.3	20.0	79	77	5.7
			6			107	112	
	12.10	5	6	20.8	22.7	113	115	6.7
			5			133	141	
	11.00	4	5	22.6	24.5	137	143	7.5
			4			159	170	
	9.90	3	4	24.2	26.1	163	173	8.1
			3			187	199	
	8.81	2	3	38.1	40.0	190	206	8.9
			2			269	287	
	6.73	1	2	39.3	41.9	272	290	9.5
	4.65		8002			354	376	
FPE	8.25	402	405	4.1	6.8	2	6	5.8
	4.65	401	404			14	26	

Table A-4: FWSC Maximum Absolute Accelerations (BE)

a) UC_{OBE} Model with Full Stiffness OBE-Damping Motion El. at 282 ft

Elev. (m)	Node No.	Location	BE-UC_{OBE} Motion El. 282 ft		
			NS (g)	EW (g)	Vert. (g)
19.70	10	FWS	1.60	1.41	0.61
17.25	9	FWS	1.49	1.31	0.61
15.53	8	FWS	1.38	1.20	0.60
13.81	7	FWS	1.25	1.09	0.59
12.10	6	FWS	1.12	0.97	0.57
11.00	5	FWS	1.03	0.88	0.56
9.90	4	FWS	0.94	0.81	0.55
8.81	3	FWS	0.85	0.73	0.53
6.73	2	FWS	0.66	0.56	0.50
4.65	8002	Basemat Top	0.50	0.48	0.47
2.15	8001	Basemat Bottom	0.47	0.44	0.57
8.25	405	FPE	0.52	0.73	0.44
6.45	402	FPE	0.46	0.62	0.44

b) UC_{OBE} Model with Full Stiffness OBE-Damping Motion El. at 220 ft

Elev. (m)	Node No.	Location	BE-UC_{OBE} Motion El. 220 ft		
			NS (g)	EW (g)	Vert. (g)
19.70	10	FWS	1.93	1.99	1.07
17.25	9	FWS	1.75	1.83	1.07
15.53	8	FWS	1.53	1.64	1.05
13.81	7	FWS	1.29	1.41	1.02
12.10	6	FWS	1.10	1.20	0.97
11.00	5	FWS	1.02	1.07	0.93
9.90	4	FWS	0.94	0.93	0.89
8.81	3	FWS	0.85	0.81	0.84
6.73	2	FWS	0.65	0.65	0.73
4.65	8002	Basemat Top	0.59	0.58	0.61
2.15	8001	Basemat Bottom	0.62	0.54	0.78
8.25	405	FPE	0.71	1.04	0.59
6.45	402	FPE	0.66	0.75	0.56

Table A-4: FWSC Maximum Absolute Accelerations (BE) (Continued)

c) UC_{SSE} Model with Full Stiffness SSE-Damping Motion El. at 220 ft

Elev. (m)	Node No.	Location	BE-UC_{SSE} Motion El. 220 ft		
			NS (g)	EW (g)	Vert. (g)
19.70	10	FWS	1.74	1.84	1.03
17.25	9	FWS	1.59	1.69	1.03
15.53	8	FWS	1.41	1.51	1.02
13.81	7	FWS	1.21	1.31	0.99
12.10	6	FWS	1.04	1.13	0.95
11.00	5	FWS	0.96	1.01	0.91
9.90	4	FWS	0.89	0.88	0.87
8.81	3	FWS	0.81	0.78	0.82
6.73	2	FWS	0.62	0.64	0.71
4.65	8002	Basemat Top	0.59	0.57	0.60
2.15	8001	Basemat Bottom	0.61	0.53	0.77
8.25	405	FPE	0.70	0.97	0.59
6.45	402	FPE	0.65	0.73	0.56

Table A-5: FWSC Maximum Absolute Accelerations (LB)

a) UC_{OBE} Model with Full Stiffness OBE-Damping Motion El. at 282 ft

Elev. (m)	Node No.	Location	LB-UC_{OBE} Motion El. 282 ft		
			NS (g)	EW (g)	Vert. (g)
19.70	10	FWS	1.18	1.19	0.53
17.25	9	FWS	1.12	1.09	0.53
15.53	8	FWS	1.06	1.00	0.52
13.81	7	FWS	0.99	0.90	0.51
12.10	6	FWS	0.92	0.82	0.50
11.00	5	FWS	0.87	0.78	0.49
9.90	4	FWS	0.82	0.73	0.48
8.81	3	FWS	0.76	0.68	0.47
6.73	2	FWS	0.62	0.59	0.45
4.65	8002	Basemat Top	0.47	0.51	0.42
2.15	8001	Basemat Bottom	0.43	0.46	0.57
8.25	405	FPE	0.42	0.64	0.39
6.45	402	FPE	0.41	0.58	0.38

b) UC_{OBE} Model with Full Stiffness OBE-Damping Motion El. at 220 ft

Elev. (m)	Node No.	Location	LB-UC_{OBE} Motion El. 220 ft		
			NS (g)	EW (g)	Vert. (g)
19.70	10	FWS	1.48	1.42	0.70
17.25	9	FWS	1.37	1.32	0.70
15.53	8	FWS	1.26	1.22	0.69
13.81	7	FWS	1.14	1.10	0.67
12.10	6	FWS	1.02	0.98	0.66
11.00	5	FWS	0.94	0.90	0.64
9.90	4	FWS	0.86	0.82	0.63
8.81	3	FWS	0.80	0.74	0.61
6.73	2	FWS	0.63	0.59	0.57
4.65	8002	Basemat Top	0.49	0.51	0.54
2.15	8001	Basemat Bottom	0.48	0.46	0.66
8.25	405	FPE	0.55	0.70	0.51
6.45	402	FPE	0.52	0.60	0.50

Table A-5: FWSC Maximum Absolute Accelerations (LB) (Continued)

c) UC_{SSE} Model with Full Stiffness SSE-Damping Motion El. at 220 ft

Elev. (m)	Node No.	Location	LB- UC_{SSE} Motion El. 220 ft		
			NS (g)	EW (g)	Vert. (g)
19.70	10	FWS	1.39	1.36	0.70
17.25	9	FWS	1.29	1.27	0.70
15.53	8	FWS	1.19	1.17	0.69
13.81	7	FWS	1.08	1.06	0.67
12.10	6	FWS	0.97	0.95	0.65
11.00	5	FWS	0.90	0.87	0.64
9.90	4	FWS	0.83	0.80	0.62
8.81	3	FWS	0.77	0.72	0.61
6.73	2	FWS	0.62	0.58	0.57
4.65	8002	Basemat Top	0.49	0.50	0.54
2.15	8001	Basemat Bottom	0.48	0.45	0.64
8.25	405	FPE	0.54	0.67	0.51
6.45	402	FPE	0.52	0.58	0.51

Table A-6: FWSC Maximum Absolute Accelerations (UB)

a) UC_{OBE} Model with Full Stiffness OBE-Damping Motion El. at 282 ft

Elev. (m)	Node No.	Location	UB-UC_{OBE} Motion El. 282 ft		
			NS (g)	EW (g)	Vert. (g)
19.70	10	FWS	1.50	1.19	0.74
17.25	9	FWS	1.40	1.11	0.74
15.53	8	FWS	1.29	1.02	0.73
13.81	7	FWS	1.16	0.93	0.70
12.10	6	FWS	1.01	0.83	0.67
11.00	5	FWS	0.92	0.76	0.65
9.90	4	FWS	0.82	0.69	0.63
8.81	3	FWS	0.72	0.64	0.61
6.73	2	FWS	0.48	0.56	0.56
4.65	8002	Basemat Top	0.37	0.48	0.51
2.15	8001	Basemat Bottom	0.38	0.44	0.58
8.25	405	FPE	0.41	0.68	0.49
6.45	402	FPE	0.39	0.59	0.48

b) UC_{OBE} Model with Full Stiffness OBE-Damping Motion El. at 220 ft.

Elev. (m)	Node No.	Location	UB-UC_{OBE} Motion El. 220 ft.		
			NS (g)	EW (g)	Vert. (g)
19.70	10	FWS	2.23	2.34	1.53
17.25	9	FWS	2.06	2.17	1.53
15.53	8	FWS	1.88	1.94	1.49
13.81	7	FWS	1.68	1.69	1.43
12.10	6	FWS	1.47	1.41	1.35
11.00	5	FWS	1.33	1.29	1.28
9.90	4	FWS	1.18	1.19	1.20
8.81	3	FWS	1.02	1.08	1.12
6.73	2	FWS	0.74	0.80	0.93
4.65	8002	Basemat Top	0.62	0.68	0.73
2.15	8001	Basemat Bottom	0.64	0.59	0.89
8.25	405	FPE	0.82	1.56	0.72
6.45	402	FPE	0.73	1.13	0.68

Table A-6: FWSC Maximum Absolute Accelerations (UB) (Continued)

c) UC_{SSE} Model with Full Stiffness SSE-Damping Motion El. at 220 ft

Elev. (m)	Node No.	Location	UB-UC_{SSE} Motion El. 220 ft		
			NS (g)	EW (g)	Vert. (g)
19.70	10	FWS	2.00	2.18	1.43
17.25	9	FWS	1.85	2.02	1.43
15.53	8	FWS	1.68	1.83	1.40
13.81	7	FWS	1.49	1.60	1.35
12.10	6	FWS	1.28	1.35	1.27
11.00	5	FWS	1.14	1.21	1.21
9.90	4	FWS	1.00	1.11	1.15
8.81	3	FWS	0.87	1.01	1.07
6.73	2	FWS	0.66	0.76	0.91
4.65	8002	Basemat Top	0.62	0.65	0.72
2.15	8001	Basemat Bottom	0.63	0.57	0.88
8.25	405	FPE	0.81	1.42	0.72
6.45	402	FPE	0.72	1.04	0.68

Table A-7: FWSC Maximum Displacement Relative to Free-Field (BE)

a) UC_{OBE} Model with Full Stiffness OBE-Damping Motion El. at 282 ft

Structure Location	Elev. (m)	Node No.	Location	BE-UC_{OBE} Motion El. 282 ft		
				NS (cm)	EW (cm)	Vert. (cm)
FWS	19.70	10	FWS	0.38	0.28	0.02
	17.25	9	FWS	0.37	0.27	0.07
	15.53	8	FWS	0.36	0.27	0.07
	13.81	7	FWS	0.35	0.27	0.07
	12.10	6	FWS	0.34	0.27	0.07
	11.00	5	FWS	0.34	0.26	0.07
	9.90	4	FWS	0.33	0.26	0.07
	8.81	3	FWS	0.33	0.26	0.06
	6.73	2	FWS	0.31	0.26	0.06
	4.65	8002	Basemat Top	0.30	0.26	0.05
	2.15	8001	Basemat Bottom	0.30	0.25	0.06
FPE	8.25	405	FPE	0.30	0.25	0.03
	6.45	402	FPE	0.30	0.25	0.01

b) UC_{OBE} Model with Full Stiffness OBE-Damping Motion El. at 220 ft

Structure Location	Elev. (m)	Node No.	Location	BE-UC_{OBE} Motion El. 220 ft		
				NS (cm)	EW (cm)	Vert. (cm)
FWS	19.70	10	FWS	0.25	0.33	0.04
	17.25	9	FWS	0.23	0.31	0.09
	15.53	8	FWS	0.22	0.29	0.09
	13.81	7	FWS	0.20	0.27	0.08
	12.10	6	FWS	0.18	0.25	0.08
	11.00	5	FWS	0.17	0.23	0.08
	9.90	4	FWS	0.16	0.22	0.08
	8.81	3	FWS	0.15	0.20	0.08
	6.73	2	FWS	0.12	0.16	0.07
	4.65	8002	Basemat Top	0.09	0.13	0.06
	2.15	8001	Basemat Bottom	0.09	0.12	0.07
FPE	8.25	405	FPE	0.09	0.15	0.04
	6.45	402	FPE	0.09	0.14	0.02

Table A-7: FWSC Maximum Displacement Relative to Free-Field (BE) (Continued)

c) UC_{SSE} Model with Full Stiffness SSE-Damping Motion El. at 220 ft

Structure Location	Elev. (m)	Node No.	Location	BE-UC_{SSE} Motion El. 220 ft		
				NS (cm)	EW (cm)	Vert. (cm)
FWS	19.70	10	FWS	0.24	0.32	0.04
	17.25	9	FWS	0.23	0.30	0.08
	15.53	8	FWS	0.21	0.28	0.08
	13.81	7	FWS	0.20	0.26	0.08
	12.10	6	FWS	0.18	0.24	0.08
	11.00	5	FWS	0.17	0.23	0.08
	9.90	4	FWS	0.16	0.21	0.08
	8.81	3	FWS	0.15	0.20	0.07
	6.73	2	FWS	0.12	0.16	0.07
	4.65	8002	Basemat Top	0.09	0.13	0.06
	2.15	8001	Basemat Bottom	0.09	0.12	0.07
FPE	8.25	405	FPE	0.09	0.15	0.04
	6.45	402	FPE	0.09	0.14	0.02

Table A-8: FWSC Maximum Displacement Relative to Free-Field (LB)

a) UC_{OBE} Model with Full Stiffness OBE-Damping Motion El. at 282 ft

Structure Location	Elev. (m)	Node No.	Location	LB-UC_{OBE} Motion El. 282 ft		
				NS (cm)	EW (cm)	Vert. (cm)
FWS	19.70	10	FWS	0.59	0.59	0.03
	17.25	9	FWS	0.57	0.59	0.10
	15.53	8	FWS	0.56	0.58	0.10
	13.81	7	FWS	0.55	0.57	0.10
	12.10	6	FWS	0.54	0.55	0.09
	11.00	5	FWS	0.54	0.55	0.09
	9.90	4	FWS	0.54	0.54	0.09
	8.81	3	FWS	0.53	0.53	0.09
	6.73	2	FWS	0.52	0.51	0.09
	4.65	8002	Basemat Top	0.52	0.50	0.08
	2.15	8001	Basemat Bottom	0.51	0.48	0.10
FPE	8.25	405	FPE	0.52	0.51	0.05
	6.45	402	FPE	0.52	0.50	0.03

b) UC_{OBE} Model with Full Stiffness OBE-Damping Motion El. at 220 ft

Structure Location	Elev. (m)	Node No.	Location	LB-UC_{OBE} Motion El. 220 ft		
				NS (cm)	EW (cm)	Vert. (cm)
FWS	19.70	10	FWS	0.28	0.39	0.05
	17.25	9	FWS	0.27	0.36	0.10
	15.53	8	FWS	0.25	0.34	0.10
	13.81	7	FWS	0.24	0.32	0.10
	12.10	6	FWS	0.22	0.30	0.10
	11.00	5	FWS	0.21	0.29	0.10
	9.90	4	FWS	0.20	0.27	0.09
	8.81	3	FWS	0.18	0.26	0.09
	6.73	2	FWS	0.15	0.22	0.09
	4.65	8002	Basemat Top	0.12	0.19	0.08
	2.15	8001	Basemat Bottom	0.12	0.17	0.10
FPE	8.25	405	FPE	0.12	0.22	0.06
	6.45	402	FPE	0.11	0.20	0.03

Table A-8: FWSC Maximum Displacement Relative to Free-Field (LB) (Continued)

c) UC_{SSE} Model with Full Stiffness SSE-Damping Motion El. at 220 ft

Structure Location	Elev. (m)	Node No.	Location	LB-UC_{SSE} Motion El. 220 ft		
				NS (cm)	EW (cm)	Vert. (cm)
FWS	19.70	10	FWS	0.28	0.38	0.05
	17.25	9	FWS	0.26	0.36	0.10
	15.53	8	FWS	0.25	0.34	0.10
	13.81	7	FWS	0.23	0.32	0.10
	12.10	6	FWS	0.22	0.30	0.10
	11.00	5	FWS	0.20	0.28	0.10
	9.90	4	FWS	0.19	0.27	0.09
	8.81	3	FWS	0.18	0.25	0.09
	6.73	2	FWS	0.15	0.22	0.09
	4.65	8002	Basemat Top	0.12	0.19	0.08
	2.15	8001	Basemat Bottom	0.11	0.17	0.10
FPE	8.25	405	FPE	0.12	0.22	0.06
	6.45	402	FPE	0.11	0.20	0.03

Table A-9: FWSC Maximum Displacement Relative to Free-Field (UB)

a) UC_{OBE} Model with Full Stiffness OBE-Damping Motion El. at 282 ft

Structure Location	Elev. (m)	Node No.	Location	UB-UC_{OBE} Motion El. 282 ft		
				NS (cm)	EW (cm)	Vert. (cm)
FWS	19.70	10	FWS	0.17	0.11	0.01
	17.25	9	FWS	0.15	0.11	0.05
	15.53	8	FWS	0.14	0.10	0.05
	13.81	7	FWS	0.13	0.09	0.05
	12.10	6	FWS	0.12	0.08	0.05
	11.00	5	FWS	0.13	0.08	0.05
	9.90	4	FWS	0.13	0.08	0.05
	8.81	3	FWS	0.13	0.07	0.04
	6.73	2	FWS	0.14	0.07	0.04
	4.65	8002	Basemat Top	0.14	0.08	0.03
	2.15	8001	Basemat Bottom	0.14	0.08	0.04
FPE	8.25	405	FPE	0.14	0.08	0.02
	6.45	402	FPE	0.15	0.08	0.01

b) UC_{OBE} Model with Full Stiffness OBE-Damping Motion El. at 220 ft

Structure Location	Elev. (m)	Node No.	Location	UB-UC_{OBE} Motion El. 220 ft		
				NS (cm)	EW (cm)	Vert. (cm)
FWS	19.70	10	FWS	0.22	0.33	0.03
	17.25	9	FWS	0.20	0.31	0.08
	15.53	8	FWS	0.19	0.29	0.08
	13.81	7	FWS	0.17	0.26	0.08
	12.10	6	FWS	0.15	0.24	0.08
	11.00	5	FWS	0.14	0.22	0.07
	9.90	4	FWS	0.13	0.21	0.07
	8.81	3	FWS	0.12	0.19	0.07
	6.73	2	FWS	0.09	0.15	0.06
	4.65	8002	Basemat Top	0.07	0.11	0.05
	2.15	8001	Basemat Bottom	0.07	0.10	0.06
FPE	8.25	405	FPE	0.07	0.13	0.03
	6.45	402	FPE	0.07	0.12	0.02

Table A-9: FWSC Maximum Displacement Relative to Free-Field (UB) (Continued)

c) UC_{SSE} Model with Full Stiffness SSE-Damping Motion El. at 220 ft

Structure Location	Elev. (m)	Node No.	Location	UB-UC_{SSE} Motion El. 220 ft		
				NS (cm)	EW (cm)	Vert. (cm)
FWS	19.70	10	FWS	0.20	0.31	0.03
	17.25	9	FWS	0.18	0.29	0.08
	15.53	8	FWS	0.17	0.27	0.08
	13.81	7	FWS	0.16	0.25	0.08
	12.10	6	FWS	0.14	0.23	0.07
	11.00	5	FWS	0.14	0.21	0.07
	9.90	4	FWS	0.13	0.20	0.07
	8.81	3	FWS	0.12	0.18	0.06
	6.73	2	FWS	0.09	0.14	0.06
	4.65	8002	Basemat Top	0.07	0.11	0.05
	2.15	8001	Basemat Bottom	0.07	0.10	0.05
FPE	8.25	405	FPE	0.07	0.13	0.03
	6.45	402	FPE	0.06	0.12	0.02

APPENDIX B
Evaluation of Concrete Cracking Effects

TABLE OF CONTENTS

LIST OF TABLES

LIST OF FIGURES

B.1. SCOPE

This appendix presents the site-specific sensitivity evaluations of the effects of concrete cracking on the SSI response of the NA3 FWSC. The evaluation is based on the comparisons of the results obtained from:

- The FWSC $\mathbf{UC_{OBE}}$ and $\mathbf{UC_{SSE}}$ models with upper bound structural stiffness properties representing the condition when all members of the FWSC reinforced concrete structures are assigned full (uncracked concrete) stiffness properties. The results from the site-specific SSI analyses of the $\mathbf{UC_{OBE}}$ and $\mathbf{UC_{SSE}}$ models (analysis Cases 1 to 9 in Table 4.2-1) are presented in Sections 5.0 and 6.0.
- The FWSC $\mathbf{CR_{SSE}}$ model with lower bound structural stiffness properties representing the condition when all members of the FWSC reinforced concrete structures are fully cracked. The results from the site-specific SSI analyses of the $\mathbf{CR_{SSE}}$ model with reduced stiffness properties (analyses Cases S1 to S6 in Table 4.2 - 1) are presented in Sections B.3 and B.4 of this appendix.

The evaluation considers the effects of concrete cracking on the response of the FWSC reinforced concrete members and the out-of-plane vibrations of the FWS roof. The effect of the concrete cracking on the site-specific seismic demands on the FWSC structures are evaluated by comparing the results from the analyses of the $\mathbf{CR_{SSE}}$ model with reduced (cracked concrete) stiffness properties with the enveloping maximum member forces and accelerations results from the site-specific SSI analyses of the FWSC $\mathbf{UC_{SSE}}$ model with full stiffness properties and SSE damping (analysis Cases 7 to 9 in Table 4.2-1). The effect of the concrete cracking on the FWSC site-specific ISRS are evaluated by comparing the 5% ISRS obtained from the sensitivity analysis Cases S1 to S6 in Table 4.2-1 that are performed on the $\mathbf{CR_{SSE}}$ models with the 5% damped broadened and valley filled ISRS obtained as an envelope of results from the SSI analyses of the FWSC $\mathbf{UC_{OBE}}$ models with full stiffness properties and OBE damping (analysis Cases 1 to 6 in Table 4.2-1).

B.2. ANALYSES

The site-specific evaluations of structural stiffness variations on the response of the FWSC are based on the results of the sensitivity seismic response analyses of the $\mathbf{CR_{SSE}}$ model representing fully cracked concrete condition, i.e., conditions where all of the FWSC reinforced concrete structural members are cracked. SSE damping values are assigned to this model in conjunction with the reduced (cracked concrete) stiffness properties to represent the higher dissipation of energy in the FWSC structures when subjected to high stresses corresponding to the fully cracked concrete condition.

Six analyses of the reduced stiffness $\mathbf{CR_{SSE}}$ models are performed for the LB, UB, and BE subgrade profiles using the surface input motion at the bottom of the FWSC basemat and the deep input motion at the bottom of the concrete fill located at El. 282 ft and El. 220 ft NAVD 88, respectively. The consideration of the LB, UB, and BE subgrade profiles representing

three subgrade stiffness conditions captures the effect of subgrade dynamic property variations on the response of the FWSC structures under fully cracked concrete conditions.

Tables B.2-1 through B.2-3 present the frequencies used for the six sensitivity analysis cases (Cases S1 through S6 in Table 4.2-1) performed for the evaluation of the effects of concrete cracking on the seismic response of the FWSC.

In accordance with ASCE 43-05 (Reference 2-x), the effects of concrete cracking on the shear and flexural stiffness of the reinforced concrete walls are captured by reducing the section properties for the shear areas, torsional moment of inertia, and flexural moments of inertia of the stick elements by 50%. In order to simulate the full (100%) axial stiffness of the cracked walls, as recommended by ASCE 43-05 (Reference 2-x), the axial areas of the stick members are the same as the areas of the stick members in the FWSC $\mathbf{UC_{OBE}}$ and $\mathbf{UC_{SSE}}$ models with full stiffness properties (Section 4.3). The overall stiffness of the shell elements modeling the basemat are reduced by 50%.

The cracking of the concrete also reduces the flexural stiffness of the walls and slabs thus lowering their natural frequencies of out-of-plane vibrations. ASCE 43-05 (Reference 2-x) recommends a 50% reduction of the flexural stiffness of the slabs and walls under fully cracked conditions resulting in the reduction of the natural frequencies of the out-of-plane vibrations of the FWSC slabs and walls by $\sqrt{2}$. One SDOF oscillator is used in the $\mathbf{UC_{OBE}}$ and $\mathbf{UC_{SSE}}$ models with full (uncracked concrete) properties described in Section 4.3 to capture the out-of-plane modes of vibration of the FWS roof with frequencies up to 50 Hz under full (uncracked) stiffness conditions. Therefore, besides applying the 50% reduction to the stiffness of the existing FWS roof SDOF oscillator in the $\mathbf{UC_{SSE}}$ and $\mathbf{UC_{OBE}}$ models, two additional SDOF oscillators are added to the $\mathbf{CR_{SSE}}$ models to capture the modes of out-of-plane vibrations of the cracked FWS and FPE roofs with frequencies ranging from 35 Hz $(\frac{50}{\sqrt{2}})$ to 50 Hz. Figure B.2-1 depicts the configuration of the FWSC $\mathbf{CR_{SSE}}$ LMSMs showing the additional vertical SDOF oscillators attached to the FWS and FPE LMSMs in red.

The development of these additional SDOF oscillators, representing the out-of-plane vibrations of the FWS and FPE roofs under fully cracked conditions, is presented in Reference 2-aa. The properties of the additional oscillators are developed based on the results of the eigenvalue analyses following the same methodology as the one used in the standard design for the development of oscillators for the out-of-plane vibrations of slabs under uncracked concrete conditions. The floor lumped mass inertia properties are adjusted to account for the mass of the additional oscillators as described in Reference 2-aa. The results of the eigenvalue analyses described in Reference 2-aa demonstrate that the frequencies of the out-of-plane vibrations of the FWSC walls under fully cracked conditions are all above the rigid threshold frequency of 50 Hz. Therefore, no SDOF oscillators are added to the FWSC $\mathbf{CR_{SSE}}$ model to represent out-of-plane vibrations of cracked walls.

The other characteristics of the $\mathbf{CR_{SSE}}$ model, such as the locations of interaction nodes in the HOUSE module input file, wave types and location of input control motion in the SITE

module input file, and the point radius value in the POINT module input file, are the same as the ones used for the $\mathbf{UC_{SSE}}$ and $\mathbf{UC_{OBE}}$ models presented in Section 4.2.

B.3. RESULTS FROM SENSITIVITY SSI ANALYSES OF $\mathbf{CR_{SSE}}$ MODEL

This section presents the results of the site-specific sensitivity analyses of the FWSC $\mathbf{CR_{SSE}}$ model for acceleration transfer functions, outcrop motion transfer functions, maximum accelerations, and maximum displacements. The plots of the interpolated and calculated acceleration transfer functions demonstrate adequate numerical accuracy of results obtained from the SSI analyses of the FWSC $\mathbf{CR_{SSE}}$ model. The comparisons of the outcrop transfer functions obtained from the analyses of the $\mathbf{CR_{SSE}}$ model with those obtained from the analysis of the $\mathbf{UC_{OBE}}$ model illustrate how the concrete cracking affects the seismic response of the FWSC structures.

Figures B.3-1 (a through d) and B.3-2 (a through d) present plots of the amplitudes of the acceleration transfer functions obtained from the analysis of the FWSC $\mathbf{CR_{SSE}}$ model for the LB subgrade profile using the surface input motion at El. 282 ft NAVD 88 and the deep input motion at El. 220 ft NAVD 88, respectively. Figures B.3-3 (a through d) and B.3-4 (a through d) present plots of the amplitudes of the acceleration transfer functions obtained from the analysis of the FWSC $\mathbf{CR_{SSE}}$ model for the UB subgrade profile using the surface input motion and the deep input motion, respectively. Figures B.3-5 (a through d) and B.3-6 (a through d) present plots of the amplitudes of the acceleration transfer functions obtained from the analysis of the FWSC $\mathbf{CR_{SSE}}$ model for the BE subgrade profile using the surface input motion and the deep input motion, respectively. The plots present the responses of the FWSC at the same four key locations as the ones listed in Section 5.1. Each figure includes three plots presenting the FWSC responses in the three orthogonal directions due to the three earthquake components. The computed values of the transfer functions in these plots are depicted with dots. The interpolated values of the transfer functions are depicted by solid lines. The plots generally show no numerical anomalies in the interpolated transfer functions (e.g., sharp narrow spikes) that can potentially impact the accuracy of the frequency domain SSI analyses results.

Figures B.3-7 (a through c) and B.3-8 (a through c) present the transfer functions of the responses relative to the outcrop design motion at the top of the FWS LMSM (Node 9) and FPE LMSM (Node 405). These outcrop motion transfer functions represent the responses of the FWSC structures in the direction of the applied input ground motion. In Figures B.3-7(a) and B.3-8(a), the outcrop motion transfer functions obtained from the sensitivity analyses of the $\mathbf{CR_{SSE}}$ model for LB profile (analysis Cases S1 and S2 in Table 4.2-1) are compared with the outcrop transfer functions in Section 5.1. These are obtained from the LB profile analyses of the $\mathbf{UC_{OBE}}$ model with full stiffness properties and OBE damping (analysis Cases 1 and 4 in Table 4.2-1). Figures B.3-7(b) and B.3-8(b) compare the outcrop motion transfer functions obtained from the sensitivity analyses of the $\mathbf{CR_{SSE}}$ model for UB profile (analysis Cases S3 and S4 in Table 4.2-1) with the outcrop transfer functions obtained from the UB profile analyses of the $\mathbf{UC_{OBE}}$ model (analysis Cases 3 and 6 in Table 4.2-1). Figures B.3-7(c) and B.3-8(c) compare the outcrop motion transfer functions obtained from the sensitivity

analyses of the $\mathbf{CR_{SSE}}$ model for BE profile (analysis Cases S5 and S6 in Table 4.2-1) with the outcrop transfer functions obtained from the BE profile analyses of the $\mathbf{UC_{OBE}}$ model (analysis Cases 2 and 5 in Table 4.2-1). In order to illustrate how the peak frequency shifts affect the responses of the FWSC structures, the plots in Figures B.3-7 and B.3-8 also include the spectra defining the surface and deep SSI design ground motion at El. 282 ft and El. 220 ft NAVD 88, respectively. The solid line curves in the figures present the input motion spectra and transfer function results of the analyses performed with surface input motion. The input motion spectra and results of the analyses performed with deep input motion are presented with dashed lines.

The comparison in Figures B.3-7(a) and B.3-8(a) of the outcrop motion transfer functions obtained from the LB subgrade profile analyses of the $\mathbf{CR_{SSE}}$ model and the $\mathbf{UC_{OBE}}$ model illustrate the shifts of the structural peak responses to lower frequencies resulting in SSI resonance amplifications. The frequency shifts of the horizontal peak responses are more pronounced in the results obtained from the analyses of the stiff UB subgrade profile, presented in Figures B.3-7(b) and B.3-8(b). The comparison in Figure B.3-7(b) of the outcrop transfer functions obtained from the analyses of the UB profile with deep input motion show that the concrete cracking shifts the FWS peak responses to lower frequencies where the amplitude of the input motion is lower. The outcrop function results in Figure B.3-8(b) indicate that the concrete cracking can amplify the response of the FPE structure by shifting the FPE peak responses closer to the input motion peak frequency.

Tables B.3-1 through B.3-6 present the results for maximum member forces and moments obtained from the six sensitivity analyses of the $\mathbf{CR_{SSE}}$ model for the LB, UB and BE subgrade profiles using surface and deep input motions (analysis Cases S1 through S6 in Table 4.2-1). The results for maximum accelerations at lumped mass locations from these six sensitivity analyses are presented in Tables B.3-7 through B.3-12. Tables B.3-7, B.3-9 and B.3-11 compare the results obtained from the sensitivity analyses of the $\mathbf{CR_{SSE}}$ model with surface input motion (Cases S1, S3 and S5 in Table 4.2-1) with the results of the corresponding analyses of the $\mathbf{UC_{OBE}}$ model for the LB, UB, and BE subgrade profiles and surface input motion (Cases 1, 3 and 2 in Table 4.2-1). Tables B.3-8, B.3-10 and B.3-12 compare the results obtained from the sensitivity analyses of the $\mathbf{CR_{SSE}}$ model for the LB, UB, and BE subgrade profiles with deep input motion (Cases S2, S4 and S6 in Table 4.2-1) with the results of the corresponding LB, UB, and BE profile analyses of the $\mathbf{UC_{SSE}}$ model with deep input motion (Cases 7, 9 and 8 in Table 4.2-1). Tables B.3-13 through B.3-15 provide the comparisons of the maximum accelerations of the FWSC SDOF oscillators obtained from the analyses of $\mathbf{CR_{SSE}}$, $\mathbf{UC_{OBE}}$, and $\mathbf{UC_{SSE}}$ models for the LB, UB, and BE subgrade profiles, respectively. The bold red numbers in the tables are the node numbers of the additional SDOF oscillators added to the $\mathbf{CR_{SSE}}$ to capture the flexible modes of vibration of the FWS and FPE roofs under cracked concrete conditions.

Tables B.3-1 through B.3-15 also present comparisons of the $\mathbf{CR_{SSE}}$ model results with the envelope of maximum force, moment, and acceleration results obtained from the analyses of the $\mathbf{UC_{SSE}}$ model for the LB, BE, and UB subgrade profiles using the deep input motion at El. 220 ft NAVD 88. As described in Section 6.1, these serve as a basis for the development of

the NA3 site-specific load demands on the FWSC structures. These tables identify the maximum response results of the FWSC $\mathbf{CR_{SSE}}$ model sensitivity analyses that exceed the envelope of results from the SSI analyses of the $\mathbf{UC_{SSE}}$ model. The comparisons indicate that the analyses of the $\mathbf{CR_{SSE}}$ model with reduced (cracked concrete) stiffness properties can amplify the maximum responses of the FWSC structures. The comparisons with the envelope of the results from the analyses of the full stiffness $\mathbf{UC_{SSE}}$ model show that these exceedances are enveloped by the governing licensing basis SSI analysis of the UB profile with deep input motion (analysis Case 9 in Table 4.2-1) with exception of the exceedances identified in Tables B.3-4, B.3-6, B.3-10, B.3-12, and B.3-14. These exceedances are observed in the results of the sensitivity analyses of the $\mathbf{CR_{SSE}}$ models for the UB and BE subgrade profiles with deep input motion (Cases S4 and S6 in Table 4.2-1) and mainly affect the maximum responses of the FPE structure. The exceedances identified in Table B.3-14 for the maximum acceleration in the EW direction of the impulsive mode of vibration of the water contained in the FWSC is less than 10% and is enveloped by the hydrodynamic load used for the standard design of the FWSC.

Tables B.3-16 through B.3-24 present the results of the sensitivity analyses of the $\mathbf{CR_{SSE}}$ model for the LB, UB, and BE subgrade profiles (Cases S1 through S6 in Table 4.2-1) for the maximum displacements of the FWSC structures relative to the free-field motion. These results for the maximum displacements of the fully cracked FWSC structures are compared with the envelope of the results of the analyses of the $\mathbf{UC_{OBE}}$ model with full stiffness properties and OBE damping for the LB, BE, and UB profiles using surface and deep input motions (Cases 1 through 6 in Table 4.2-1) that form the basis of the NA3 site-specific design. Comparisons are also made with the enveloping maximum displacements used for the standard design of the FWSC. The comparisons show that the analysis of the $\mathbf{CR_{SSE}}$ model for the LB subgrade profile with surface input motion yields maximum horizontal displacements of the FWS structure in NS direction above elevation 15.53 m that exceed both the displacements of the $\mathbf{UC_{OBE}}$ model and those used for the standard design. However, the slightly larger displacements above elevation 15.53 m are inconsequential because no piping or other components are attached to the tank above this elevation that are interconnected with other buildings.

B.4. EVALUATION OF STRUCTURAL STIFFNESS VARIATION EFFECTS

Section 6.0 presents the site-specific enveloping responses that form the basis for site-specific design and evaluation of the NA3 FWSC. These enveloping responses are obtained as an envelope of the results from the SSI and SSSI analyses of the FWSC standalone model and FWSC-CB combined model, respectively, with full (uncracked concrete) stiffness properties. The responses obtained from the sensitivity SSI analyses of the **CR_{SSE}** model are compared with the envelope of results obtained from the SSI analyses of the FWSC models with full (uncracked concrete) stiffness properties to evaluate the effects of concrete cracking on the FWSC site-specific design basis.

B.4.1 Effect of Stiffness Variation on Site-Specific Structural Load Demands

Figures B.4-1 through B.4-6 present, with dashed red lines, the results of the sensitivity analyses of the **CR_{SSE}** model for the LB, UB, and BE subgrade profiles for the shear and torsion load demands on the FWS and FPE reinforced concrete structures under fully cracked conditions. The sensitivity analysis results of the vertical load demands on the fully cracked FWS and FPE structures are presented in Figures B.4-7 through B.4-12. These results are compared with the results of the corresponding analyses of FWSC models with full (uncracked concrete) stiffness properties that are presented with solid green lines in Figures B.4-1 through B.4-12. The figures also provide, with solid blue lines, the envelopes of the results for seismic load demands from the analyses of the FWSC standalone model with full stiffness and SSE damping (**UC_{SSE}** model) for the LB, BE, and UB subgrade profiles (analysis Cases 7 through 9 in Table 4.2-1).

The comparisons presented in Figures B.4-1, B.4-2, B.4-3, B.4-7, and B.4-8, and B.4-9 show that the site-specific FWSC SSI analysis of the **UC_{SSE}** model with full (uncracked concrete) stiffness and SSE damping envelope the effects of concrete cracking on the site-specific load demands on the FWS structure. The only exception is the torsional moment demands on the FWS tank wall that, as shown in Figure B.4-2 and Table B.4-4, can exceed the results of the **UC_{SSE}** model by 25% to 30%. Table B.4-4 presents the values of the total torsional moment demand on the FWS and FPE structures that are obtained as a sum of the calculated and accidental torsion. These total torsional moments are then used in Table B.4-5 to calculate the total shear demands on the FWS and FPE reinforced concrete walls in the NS and EW directions. Tables B.4-4 and B.4-5 present the calculations of the total torsion and shear demands for the critical sensitivity analysis of the **CR_{SSE}** model for the UB profile and deep input motion (Case S4 in Table 4.2-1) that yield calculated torsion demands that exceed the torsion calculated as an envelope of the SSI analyses of the full stiffness **UC_{SSE}** model (Cases 7 to 9 in Table 4.2-1). Tables B.4-6 and B.4-7 also present the calculations of the total torsion and shear demands of the **CR_{SSE}** model for the BE profile and deep input motion (Case S6 in Table 4.2-1). These calculations demonstrate that the exceedances in torsional moments observed in Figure B.4-2 do not affect the total shear demand on the FWS wall since the contribution of the torsion on the overall shear stress demands on the FWS wall is small.

The comparisons in Figures B.4-4, B.4-5, B.4-6, B.4-10, B.4-11, and B.4-12 show that the cracking of the concrete can amplify the response of the FPE structure resulting in horizontal

load demands that exceed those calculated from the analyses of the $\mathbf{UC_{SSE}}$ model with full (uncracked concrete) stiffness and SSE damping. The comparisons in Figure B.4-5 show that the horizontal load demands on the cracked FPE structure exceed those obtained from the full stiffness $\mathbf{UC_{SSE}}$ model with exceedance of the NS and EW shear loads being 15% and 10%, respectively. As shown in Table B.4-5, the exceedances in the total shear demands on the FPE walls that include the contribution from the torsional response of the cracked FPE structure are 18% and 12% in the NS and EW directions, respectively. The comparisons in Figures B.4-10, B.4-11 and B.4-12 show that the full stiffness $\mathbf{UC_{SSE}}$ model provides vertical load demands on the FPE structure that bound the effects of concrete cracking. The exceedances of the bending moments observed in Figure B.4-11 are due to the exceedances in the FPE horizontal loads and will be addressed by using amplified horizontal loads for the site-specific evaluation of the FWSC structure. As shown in Table B.3-4, the concrete cracking will only slightly affect the rocking response of the FPE, increasing the EW bending moment at the FPE top by less than 1 MN-m. When translated to the increase in axial force applied to the FPE walls, this amplification of the rocking response of the FPE top is negligibly small (less than 0.05 MN).

Tables B.4-1, B.4-2 and B.4-3 present the calculations of the site-specific out-of-plane loads on the FWS and FPE roof slabs under fully cracked conditions that are based on the maximum acceleration results obtained from the sensitivity analyses of the FWSC $\mathbf{CR_{SSE}}$ model. In Table B.4-1, the out-of-plane loads on the cracked FWS and FPE roofs are compared with the out-of-plane loads obtained as an envelope of the results from SSI analysis of the $\mathbf{UC_{SSE}}$ model for the LB, BE, and UB profiles presented in Section 6.1 and for the out-of-plane loads used for the standard design of the FWSC structures. The comparisons show that the sensitivity analyses of the $\mathbf{CR_{SSE}}$ model with cracked FWS roof slab provided site-specific out-of-plane loads that are bounded by the envelope of the results from the SSI analyses of the FWSC $\mathbf{UC_{SSE}}$ model that represent the dynamic properties of the FWSC structures under full (uncracked concrete) stiffness conditions. Tables B.4-2 and B.4-3 show that the cracking of the concrete can amplify the out-of-plane load demand on the FPE roof by approximately 51% and 26%, respectively.

The comparisons of the results from the analyses of the $\mathbf{CR_{SSE}}$ model and SSI envelope $\mathbf{UC_{SSE}}$ model for the seismic horizontal forces and overturning moments on the top of the basemat along with the vertical accelerations are also used to evaluate the effects of concrete cracking on the FWSC stability and dynamic bearing pressures. The seismic demands that govern the stability evaluations and the calculations of the dynamic bearing pressures are proportional to the sum of the corresponding forces and moments that the two LMSMs representing the FWS and the FPE (see Figure 4.3-4) transfer to the basemat.

The comparisons in Figure B.4-1 through B.4-12 show that:

- The concrete cracking reduces the horizontal shear force demands on the top of the FWSC basemat (elevation 4.65 m) by 3% to 50%.
- The concrete cracking also reduces the overturning moment demands on the top of the FWSC basemat in by 5% to 50%.

- The vertical accelerations obtained from the cracked cases ($\mathbf{CR_{SSE}}$) are all bounded by the envelope of the SSI analyses of the model representing uncracked concrete ($\mathbf{UC_{SSE}}$ SSI envelope) for both the FWS and the FPE LMSMs (Figures B.4-7 and B.4-8 and Figures B.4-10 through B.4-12). An exception is the maximum acceleration at the bottom of the FWS stick obtained from the analysis of the FWSC $\mathbf{CR_{SSE}}$ model for the BE profile that slightly exceed the $\mathbf{UC_{SSE}}$ SSI envelope acceleration as shown in Figure B.4-9. Since this mass node represents only a portion of the total weight of the FWSC, the effect of this exceedance on the total vertical seismic demand on the supporting subgrade is negligible.

The seismic driving forces used for the evaluation of the FWSC stability are proportional to the shear force, vertical force and bending moment demands on the top of the FWSC basemat. The dynamic bearing pressure demands are proportional to the overturning moment and vertical seismic force demands. Therefore, it can be concluded, based on the observations above, that the site-specific SSI analyses of the models with full (uncracked concrete) stiffness and SSE damping provide seismic demands for the evaluation of the FWSC foundation stability and dynamic bearing pressures that bound effects of concrete cracking.

B.4.2 Effect of Stiffness Variation on ISRS

Following the procedure described in Section 5.3, 5% damped ISRS are developed from the results of the six sensitivity SSI analyses of the $\mathbf{CR_{SSE}}$ model with reduced stiffness and SSE damping values. Figures B.4-13 through B.4-24 present the ISRS results obtained from the sensitivity analyses of the $\mathbf{CR_{SSE}}$ model for the responses at the four key locations within the FWSC. These spectra are compared with the 5% damped ISRS obtained from the analyses of the full stiffness $\mathbf{UC_{OBE}}$ model for the LB, BE, and UB profiles (analysis Cases 1 through 6 in Table 4.2-1). The comparisons illustrate how the horizontal response ISRS shifts the ISRS peaks to lower frequencies. The figures also show that the effect of the concrete cracking on the vertical ISRS are small.

Figures B.4-13 through B.4-24 also compare the results of the sensitivity analyses of the $\mathbf{CR_{SSE}}$ model with the ±15% broadened ISRS obtained as the envelope of results from the site-specific FWSC SSI analyses of the $\mathbf{UC_{OBE}}$ model with full (uncracked concrete) stiffness and OBE damping and the corresponding standard design ISRS. The comparisons show that the ±15% broadened ISRS obtained as the envelope of results from the analyses of the $\mathbf{UC_{OBE}}$ model for LB, BE, and UB profiles (analysis Cases 1 through 6 in Table 4.2-1) envelop the concrete cracking effects with small (< 10%) exceedances. The only significant (>10%) exceedances can be observed in the ISRS representing the response of the FPE top for frequencies between 15 and 40 Hz. All significant exceedances in the ISRS for the horizontal response of FPE top are enveloped by the standard design ISRS.

Figures B.4-25, B.4-26 and B.4-27 present the 5% damped spectra of the SDOF oscillators representing the out-of-plane responses of the FWS roof under cracked concrete conditions obtained from the sensitivity analyses of the FWSC $\mathbf{CR_{SSE}}$ model for the LB, UB, and BE

subgrade profiles (analysis Cases S1 through S6 in Table 4.2-1). To illustrate how the cracking of the FWS roof slab shifts the oscillator ISRS peaks to lower frequencies, the ISRS results are compared with the 5% damped ISRS of the SDOF oscillators representing out-of-plane response of the roofs under uncracked concrete conditions. These are obtained from the analyses of the FWSC $\mathbf{UC_{OBE}}$ model for the LB, UB, and BE subgrade profiles (analysis Cases 1 through 6 in Table 4.2-1). Figures B.4-25, B.4-26, and B.4-27 also compare the 5% damped ISRS of the cracked FWS roof with the ±15% broadened SDOF oscillator ISRS obtained as the envelope of results from the analyses of the $\mathbf{UC_{OBE}}$ model for LB, BE, and UB profiles. The comparisons show that this broadened ISRS envelops the results of the sensitivity analyses of the FWSC $\mathbf{CR_{SSE}}$ model. The small exceedance in low (< 15 Hz) frequencies that can be observed in the results obtained from the analyses of the $\mathbf{CR_{SSE}}$ model for the LB, UB, and BE profiles and deep input motion (sensitivity analysis Cases S2 and S4 in Table 4.2-1) are enveloped by the standard design ISRS.

Figures B.4-28, B.4-29, and B.4-30 present the 5% damped ISRS results of the sensitivity analysis for the vertical response of the SDOF oscillators representing the flexible mode of out-of-plane vibration of the FPE roof under cracked concrete conditions. These spectra are compared with the ±15% broadened ISRS and the standard design ISRS representing the vertical response of the FPE roof which is rigid under full (uncracked concrete) stiffness conditions. The broadened site-specific ISRS in Figures B.4-28, B.4-29, and B.4-30 are obtained as the envelope of results from the analyses of the $\mathbf{UC_{OBE}}$ model for LB, BE, and UB profiles. The comparisons show that the cracking of the concrete amplifies the out-of-plane response of the FPE roof that results in ISRS peak exceedances both of the broadened and enveloped site-specific ISRS and the standard design ISRS. These exceedances occur at frequencies close to the frequency of the SDOF oscillator that represent the flexible mode of out-of-plane vibration of the FPE roof under cracked concrete conditions and are bounded by the results of the sensitivity analysis of the FWSC $\mathbf{CR_{SSE}}$ model for the UB profile with deep input motion (Case S4 in Table 4.2-1).

B.5. CONCLUSIONS

The results of the NA3 site-specific evaluation presented in this appendix show that the site-specific SSI analyses of the models with full (uncracked concrete) stiffness and SSE damping provide site-specific seismic demands on the FWS structures that envelop the effects of concrete cracking. The sensitivity evaluation presented in this appendix also shows that the cracking of the concrete amplifies the horizontal load demands on the FPE structure and the local vertical out-of-plane load on the FPE roof. The site-specific evaluation of the FWSC structures will address the effects of concrete cracking by using amplified input seismic loads that bound the exceedances of:

- The horizontal hydrodynamic load from the water contained in the FWSC tank
- The horizontal loads on the FPE structure
- The out-of-plane vertical load on the FPE roof

In Section 3.2 of Reference 2-n, these seismic loads are enhanced to bound the exceedances due to the concrete cracking effects. Concrete cracking amplification factors (CR_{amp}) larger than 1.0 are applied to the enveloping loads presented in Section 6.1 after being enhanced to address effects of separation between the concrete fill and the surrounding soil as described in Section 7 of Reference 2-dd. These amplification factors are calculated as the ratios of :

- the enveloped results of the sensitivity SSI analyses of FWSC CR_{SSE} standalone model with reduced (cracked concrete) stiffness and SSE damping (analysis Cases S1 through S6 in Table 4.2-1) over,
- the enveloped results of the licensing basis SSI analyses of FWSC UC_{SSE} standalone model with full (uncracked concrete) stiffness and SSE damping (analysis Cases 7 through 9 in Table 4.2-1)

The use of concrete cracking amplification factors helps capture the combined effects of concrete cracking, soil separation and SSSI of CB on the seismic response of the FWSC structures.

The site-specific evaluation presented in this appendix also shows that the site-specific SSI analyses of the models with full (uncracked concrete) stiffness and SSE damping provide seismic demands for the evaluation of the FSWC foundation stability and dynamic bearing pressures that bound effects of structural stiffness variations.

The site-specific SSI analyses of the FWSC model with full (uncracked concrete) stiffness properties and OBE damping values provide site-specific design ISRS that envelop the concrete cracking effects with the only significant (>10%) exceedances in the ISRS representing the response of the FPE top that are otherwise enveloped by the standard design ISRS. If any of the sensitivity SSI analyses of the FWSC model with reduced stiffness (analysis Cases S1 through S6) yield 5% damped ARS results that exceed the 5% damped broadened design ISRS by more than 10% for any frequency smaller than or equal to 50 Hz,

that ISRS is to be enhanced for the purposes of design and qualification of equipment and components.

The 10% exceedance criterion that is used for the enhancement of the site-specific ISRS is reasonable considering the conservatisms introduced in these evaluations of concrete cracking effects. Due to the impracticality of performing an analysis that accurately considers the variations of concrete stiffness as a function of the member stresses, a conservative approach is used to address the effects of concrete cracking. The conditions considered in the sensitivity analyses, where the stiffness of all concrete elements throughout their length is reduced by 50%, is conservative because during an SSE event, many concrete elements will not crack and, for most cracked elements, cracking will be limited to the vicinity of the highly stressed portions of the element length. ISG-01 (Reference 2-v) requires the design ISRS to accurately represent the response of the structures up to 50 Hz. Therefore, exceedances occurring at frequencies higher than 50 Hz have no impact on the design or evaluations of the equipment.

In order to combine together the effects of concrete cracking, separation between concrete fill and surrounding soil and the CB SSSI on the FWSC response, for each damping ratio required, the ISRS is to be enhanced as follows:

a. Develop an uncracked SSI ISRS as the envelope of the results from the licensing basis SSI analyses of the FWSC $\mathbf{UC_{OBE}}$ standalone model with full stiffness and OBE damping representing fully bonded conditions at concrete fill-to-soil interfaces (analysis Cases 1 through 6 in Table 4.2-1 of this report).

b. Develop an uncracked response ISRS as the envelope of the results from:

   — Licensing basis SSI analyses of the FWSC $\mathbf{UC_{OBE}}$ standalone model (Step a.)

   — Licensing basis SSSI analyses of the FWSC-CB $\mathbf{UC_{OBE}}$ combined model representing fully bonded conditions at concrete fill-to-soil interfaces (analysis Cases FC1 through FC6 in Table 4.2-2 of Reference 2-r).

   — SSI sensitivity analyses of FWSC $\mathbf{SUC_{SSE}}$ standalone model representing maximum separation between concrete fill and surrounding soil (analysis Cases SF1 through SF3 in Table 4.2-1 of Reference 2-dd)

   — SSSI sensitivity analyses of FWSC-CB $\mathbf{SUC_{SSE}}$ combined model representing maximum separation between concrete fill and surrounding soil (analysis Cases SF4 through SF6 in Table 4.2-2 of Reference 2-dd)

c. Develop a cracked SSI ISRS as the envelope of the results from the SSI analyses of the FWSC model with reduced stiffness and SSE damping (analysis Cases S1 through S6 in Table 4.2-1 of this report).

d. Determine the concrete cracking amplification factors $CR_{amp} > 1.0$ for frequencies up to 50 Hz based on the ratio of the cracked SSI ISRS from Step c. over the SSI ISRS from the licensing basis SSI analyses developed in Step a.

e. Apply the concrete cracking amplification factor determined in Step d. on the uncracked response ISRS developed in Step b. representing the enveloping response of FWSC structures with full (uncracked concrete) stiffness properties.

f. Broaden the peaks of the amplified ISRS obtained in Step e. by ±15% and then fill the valleys to obtain the enhanced design ISRS that bound the effects of both the concrete cracking and CB SSSI on the FWSC response.

ISRS results for the response of the additional SDOF Oscillator 13 obtained from the SSI analyses of the FWSC model with reduced stiffness and SSE damping (analysis Cases S1 through S6 in Table 4.2-1) will be enveloped and broadened by ±15%. This ISRS is to be used for the site-specific design and qualification of equipment or components supported by FPE roof.

Table B.2-1: List of Frequencies of Analyses (Analysis Cases S1 and S2)

Frequency No.	Frequency (Hz)
	LB
1	0.0244
41	1.0010
82	2.0020
123	3.0029
164	4.0039
205	5.0049
246	6.0059
287	7.0068
328	8.0078
369	9.0088
410	10.0098
451	11.0107
492	12.0117
532	12.9883
573	13.9893
614	14.9902
655	15.9912
696	16.9922
737	17.9932
778	18.9941
819	19.9951
860	20.9961
901	21.9971
942	22.9980
983	23.9990
1024	25.0000
1065	26.0010
1106	27.0020
1147	28.0029
1188	29.0039
1229	30.0049
1270	31.0059
1311	32.0068
1352	33.0078
1393	34.0088
1434	35.0098
1475	36.0107

Table B.2-2: List of Frequencies of Analyses (Analysis Cases S3 and S4)

Frequency No.	Frequency (Hz)	Frequency No.	Frequency (Hz)
	UB		UB
1	0.0244	1516	37.0117
41	1.0010	1557	38.0127
82	2.0020	1598	39.0137
123	3.0029	1639	40.0146
164	4.0039	1680	41.0156
205	5.0049	1721	42.0166
246	6.0059	1762	43.0176
287	7.0068	1803	44.0186
328	8.0078	1844	45.0195
369	9.0088	1885	46.0205
410	10.0098	1926	47.0215
451	11.0107	1966	47.9980
492	12.0117	2007	48.9990
532	12.9883	2048	50.0000
573	13.9893	2089	51.0010
614	14.9902	2130	52.0020
655	15.9912	2171	53.0029
696	16.9922	2212	54.0039
737	17.9932	2253	55.0049
778	18.9941	2294	56.0059
819	19.9951	2335	57.0068
860	20.9961	2376	58.0078
901	21.9971	2417	59.0088
942	22.9980	2458	60.0098
983	23.9990	2499	61.0107
1024	25.0000	2540	62.0117
1065	26.0010	2581	63.0127
1106	27.0020	2622	64.0137
1147	28.0029	2663	65.0146
1188	29.0039	2703	65.9912
1229	30.0049	2744	66.9922
1270	31.0059	2785	67.9932
1311	32.0068	2826	68.9941
1352	33.0078	2867	69.9951
1393	34.0088		
1434	35.0098		
1475	36.0107		

Table B.2-3: List of Frequencies of Analyses (Analysis Cases S5 and S6)

Frequency No.	Frequency (Hz) BE	Frequency No.	Frequency (Hz) BE
1	0.0244	1516	37.0117
41	1.0010	1557	38.0127
82	2.0020	1598	39.0137
123	3.0029	1639	40.0146
164	4.0039	1680	41.0156
205	5.0049	1721	42.0166
246	6.0059	1762	43.0176
287	7.0068	1803	44.0186
328	8.0078	1844	45.0195
369	9.0088	1885	46.0205
410	10.0098	1926	47.0215
451	11.0107	1966	47.9980
492	12.0117	2007	48.9990
532	12.9883	2048	50.0000
573	13.9893	2089	51.0010
614	14.9902	2130	52.0020
655	15.9912	2171	53.0029
696	16.9922	2212	54.0039
737	17.9932	2253	55.0049
778	18.9941		
819	19.9951		
860	20.9961		
901	21.9971		
942	22.9980		
983	23.9990		
1024	25.0000		
1065	26.0010		
1106	27.0020		
1147	28.0029		
1188	29.0039		
1229	30.0049		
1270	31.0059		
1311	32.0068		
1352	33.0078		
1393	34.0088		
1434	35.0098		
1475	36.0107		

Table B.3-1: Maximum Member Forces and Moments - LB Profile Analysis with Surface Input Motion (Case S1)

Structure	Element			CR_{SSE} Model					UC_{OBE} Model					UC_{SSE} Model SSI Envelope				
	Elev. (m)	No.	Node No.	Shear (MN)		Bending (MN-m)		Torsion (MN-m)	Shear (MN)		Bending (MN-m)		Torsion (MN-m)	Shear (MN)		Bending (MN-m)		Torsion (MN-m)
				NS	EW	NS	EW		NS	EW	NS	EW		NS	EW	NS	EW	
FWS	19.70	9	10	3.4	2.7	2	2	0.8	2.5	2.5	1	2	1.1	4.3	4.7	4	3	1.2
			9			10	8				7	8				14	14	
	17.25	8	9	8.5	6.6	14	11	2.4	6.3	6.2	10	11	3.2	10.5	11.5	23	21	3.6
			8			29	22				20	22				40	39	
	15.53	7	8	11.8	9.3	33	25	4.0	8.9	8.7	23	25	5.3	14.6	16.0	48	46	6.0
			7			53	41				38	40				71	72	
	13.81	6	7	14.8	11.8	57	44	5.4	11.3	10.9	40	43	7.3	18.3	20.0	79	77	8.2
			6			82	64				60	62				107	112	
	12.10	5	6	17.0	13.6	85	66	6.4	13.2	12.5	62	64	8.9	20.8	22.7	113	115	9.9
			5			104	81				76	78				133	141	
	11.00	4	5	18.5	15.0	106	82	7.1	14.5	13.6	77	80	10.0	22.6	24.5	137	143	11.1
			4			126	99				93	95				159	170	
	9.90	3	4	19.9	16.3	128	100	7.6	15.8	14.7	95	97	11.0	24.2	26.1	163	173	12.2
			3			150	118				112	113				187	199	
	8.81	2	3	32.5	28.5	153	120	8.3	28.4	25.5	114	115	12.4	38.1	40.0	190	206	13.6
			2			220	179				173	166				269	287	
	6.73	1	2	34.0	30.3	223	181	8.7	30.2	27.2	175	169	13.8	39.3	41.9	272	290	15.0
	4.65		8002			293	244				238	222				354	376	
FPE	8.25	402	405	2.5	4.1	1.1	3.8	3.5	2.2	3.2	0.7	3.2	2.8	4.1	6.8	2	6	5.8
	4.65	401	404			8.4	15.9				6.7	12.1				14	26	

Table B.3-2: Maximum Member Forces and Moments - LB Profile Analysis with Deep Input Motion (Case S2)

Structure	Element			CR_{SSE} Model					UC_{SSE} Model					UC_{SSE} Model SSI Envelope				
	Elev. (m)	No.	Node No.	Shear (MN)		Bending (MN-m)		Torsion (MN-m)	Shear (MN)		Bending (MN-m)		Torsion (MN-m)	Shear (MN)		Bending (MN-m)		Torsion (MN-m)
				NS	EW	NS	EW		NS	EW	NS	EW		NS	EW	NS	EW	
FWS	19.70	9	10	4.0	3.2	3	2	0.9	3.0	2.9	2	2	1.1	4.3	4.7	4	3	1.2
			9			12	10				9	9				14	14	
	17.25	8	9	9.7	7.9	18	15	2.8	7.3	7.2	12	13	3.4	10.5	11.5	23	21	3.6
			8			34	28				25	25				40	39	
	15.53	7	8	13.5	11.0	39	33	4.6	10.2	10.1	28	29	5.6	14.6	16.0	48	46	6.0
			7			63	52				46	45				71	72	
	13.81	6	7	16.7	13.7	68	56	6.4	12.9	12.7	49	49	7.7	18.3	20.0	79	77	8.2
			6			96	79				71	70				107	112	
	12.10	5	6	19.0	15.7	100	83	7.7	14.8	14.5	73	72	9.3	20.8	22.7	113	115	9.9
			5			121	100				90	88				133	141	
	11.00	4	5	20.5	17.0	124	102	8.8	16.2	15.9	92	90	10.5	22.6	24.5	137	143	11.1
			4			147	121				109	107				159	170	
	9.90	3	4	21.8	18.2	149	123	9.3	17.5	17.2	111	109	11.6	24.2	26.1	163	173	12.2
			3			173	143				130	128				187	199	
	8.81	2	3	33.2	29.1	176	146	10.4	29.7	29.0	133	130	13.1	38.1	40.0	190	206	13.6
			2			245	206				194	191				269	287	
	6.73	1	2	34.5	30.7	249	209	11.4	31.4	30.6	196	194	14.7	39.3	41.9	272	290	15.0
	4.65		8002			320	271				261	257				354	376	
FPE	8.25	402	405	2.9	4.3	1.5	4.7	3.9	2.8	3.4	0.9	4.1	3.6	4.1	6.8	2	6	5.8
	4.65	401	404			10.1	17.1				9.3	12.8				14	26	

Table B.3-3: Maximum Member Forces and Moments - UB Profile Analysis with Surface Input Motion (Case S3)

Structure	Element			CR_{SSE} Model					UC_{OBE} Model					UC_{SSE} Model SSI Envelope				
	Elev. (m)	No.	Nodes No.	Shear (MN)		Bending (MN-m)		Torsion (MN-m)	Shear (MN)		Bending (MN-m)		Torsion (MN-m)	Shear (MN)		Bending (MN-m)		Torsion (MN-m)
				NS	EW	NS	EW		NS	EW	NS	EW		NS	EW	NS	EW	
FWS	19.70	9	10	2.4	2.8	2	2	0.7	3.2	2.5	2	2	0.5	4.3	4.7	4	3	1.2
			9			8	8				10	8				14	14	
	17.25	8	9	6.0	7.0	11	11	2.1	7.9	6.3	13	11	1.6	10.5	11.5	23	21	3.6
			8			21	23				27	21				40	39	
	15.53	7	8	8.3	9.7	24	27	3.4	11.1	8.8	30	24	2.7	14.6	16.0	48	46	6.0
			7			38	43				49	40				71	72	
	13.81	6	7	10.2	12.0	41	46	4.6	13.9	11.1	53	42	3.7	18.3	20.0	79	77	8.2
			6			58	67				76	61				107	112	
	12.10	5	6	11.4	13.6	60	69	5.5	16.0	12.7	79	64	4.3	20.8	22.7	113	115	9.9
			5			73	84				97	78				133	141	
	11.00	4	5	12.2	14.7	74	85	6.1	17.4	13.9	99	79	4.8	22.6	24.5	137	143	11.1
			4			88	102				118	95				159	170	
	9.90	3	4	12.8	15.6	89	103	6.6	18.7	15.0	120	96	5.2	24.2	26.1	163	173	12.2
			3			103	120				140	113				187	199	
	8.81	2	3	18.0	23.4	105	122	7.2	30.6	25.3	142	115	5.7	38.1	40.0	190	206	13.6
			2			141	171				206	167				269	287	
	6.73	1	2	19.1	24.2	142	172	7.7	32.0	26.7	208	170	6.0	39.3	41.9	272	290	15.0
	4.65		8002			179	223				275	225				354	376	
FPE	8.25	402	405	2.1	3.4	1	4	3.2	2.1	3.4	1	4	2.9	4.1	6.8	2	6	5.8
	4.65	401	404			7	13				7	13				14	26	

Table B.3-4: Maximum Member Forces and Moments - UB Profile Analysis with Deep Input Motion (Case S4)

Structure	Element			CR_{SSE} Model					UC_{SSE} Model					UC_{SSE} Model SSI Envelope				
	Elev. (m)	No.	Nodes No.	Shear (MN)		Bending (MN-m)		Torsion (MN-m)	Shear (MN)		Bending (MN-m)		Torsion (MN-m)	Shear (MN)		Bending (MN-m)		Torsion (MN-m)
				NS	EW	NS	EW		NS	EW	NS	EW		NS	EW	NS	EW	
FWS	19.70	9	10	3.7	4.4	4	5	1.9	4.3	4.7	4	3	0.8	4.3	4.7	4	3	1.2
			9			12	15				14	14				14	14	
	17.25	8	9	9.2	10.8	19	25	5.8	10.5	11.5	23	21	2.5	10.5	11.5	23	21	3.6
			8			32	42				40	39				40	39	
	15.53	7	8	12.7	14.9	38	52	9.6	14.6	16.0	48	46	4.2	14.6	16.0	48	46	6.0
			7			58	75				71	72				71	72	
	13.81	6	7	15.8	18.6	64	84	13.0	18.3	20.0	79	77	5.7	18.3	20.0	79	77	8.2
			6			89	112				107	112				107	112	
	12.10	5	6	17.8	21.1	92	118	15.5	20.8	22.7	113	115	6.7	20.8	22.7	113	115	9.9
			5			112	138				133	141				133	141	
	11.00	4	5	19.2	22.9	114	142	17.2	22.6	24.5	137	143	7.5	22.6	24.5	137	143	11.1
			4			135	163				159	170				159	170	
	9.90	3	4	20.4	24.3	137	167	18.7	24.2	26.1	163	173	8.1	24.2	26.1	163	173	12.2
			3			159	191				187	199				187	199	
	8.81	2	3	30.9	38.0	162	195	20.6	38.1	40.0	190	206	8.9	38.1	40.0	190	206	13.6
			2			225	265				269	287				269	287	
	6.73	1	2	32.2	39.9	228	270	22.0	39.3	41.9	272	290	9.5	39.3	41.9	272	290	15.0
	4.65		8002			293	346				354	376				354	376	
FPE	8.25	402	405	4.7	7.5	2	7	8.5	4.1	6.8	2	6	5.8	4.1	6.8	2	6	5.8
	4.65	401	404			17	29				14	26				14	26	

Note: Shaded cells identify exceedances due to concrete cracking effects.

Table B.3-5: Maximum Member Forces and Moments - BE Profile Analysis with Surface Input Motion (Case S5)

Structure	Element			CR_{SSE} Model					UC_{OBE} Model					UC_{SSE} Model SSI Envelope				
	Elev. (m)	No.	Nodes No.	Shear (MN)		Bending (MN-m)		Torsion (MN-m)	Shear (MN)		Bending (MN-m)		Torsion (MN-m)	Shear (MN)		Bending (MN-m)		Torsion (MN-m)
				NS	EW	NS	EW		NS	EW	NS	EW		NS	EW	NS	EW	
FWS	19.70	9	10	4.0	3.2	3	2	0.7	3.4	3.0	2	2	0.9	4.3	4.7	4	3	1.2
			9			13	10				10	9				14	14	
	17.25	8	9	9.8	8.0	18	14	2.2	8.4	7.4	14	13	2.6	10.5	11.5	23	21	3.6
			8			35	28				28	25				40	39	
	15.53	7	8	13.6	11.2	40	32	3.6	11.8	10.4	32	29	4.3	14.6	16.0	48	46	6.0
			7			63	51				52	46				71	72	
	13.81	6	7	17.0	14.0	68	55	4.8	14.9	13.0	56	50	5.9	18.3	20.0	79	77	8.2
			6			97	78				81	72				107	112	
	12.10	5	6	19.4	16.0	101	81	5.7	17.2	15.0	84	75	7.0	20.8	22.7	113	115	9.9
			5			122	98				103	91				133	141	
	11.00	4	5	21.0	17.3	125	100	6.3	18.8	16.4	105	93	7.8	22.6	24.5	137	143	11.1
			4			147	118				126	111				159	170	
	9.90	3	4	22.5	18.5	149	120	6.8	20.2	17.6	128	113	8.5	24.2	26.1	163	173	12.2
			3			173	140				150	132				187	199	
	8.81	2	3	35.5	28.3	176	142	7.4	34.2	29.3	152	135	9.4	38.1	40.0	190	206	13.6
			2			249	197				223	196				269	287	
	6.73	1	2	37.0	29.6	252	200	7.8	36.2	30.9	226	199	10.2	39.3	41.9	272	290	15.0
	4.65		8002			329	260				301	263				354	376	
FPE	8.25	402	405	2.4	4.4	1	4	3.6	2.6	3.6	1	4	3.8	4.1	6.8	2	6	5.8
	4.65	401	404			8	17				8	14				14	26	

Table B.3-6: Maximum Member Forces and Moments - BE Profile Analysis with Deep Input Motion (Case S6)

Structure	Element			CR_{SSE} Model					UC_{SSE} Model					UC_{SSE} Model SSI Envelope				
	Elev. (m)	No.	Nodes No.	Shear (MN)		Bending (MN-m)		Torsion (MN-m)	Shear (MN)		Bending (MN-m)		Torsion (MN-m)	Shear (MN)		Bending (MN-m)		Torsion (MN-m)
				NS	EW	NS	EW		NS	EW	NS	EW		NS	EW	NS	EW	
FWS	19.70	9	10	4.2	4.2	3	3	1.4	3.7	3.9	3	3	1.2	4.3	4.7	4	3	1.2
			9			13	13				12	12				14	14	
	17.25	8	9	10.1	10.4	20	20	4.1	9.1	9.6	17	18	3.6	10.5	11.5	23	21	3.6
			8			37	38				33	34				40	39	
	15.53	7	8	13.9	14.3	43	44	6.8	12.5	13.4	38	39	6.0	14.6	16.0	48	46	6.0
			7			67	68				59	62				71	72	
	13.81	6	7	17.4	17.7	73	74	9.2	15.5	16.6	64	67	8.2	18.3	20.0	79	77	8.2
			6			102	103				91	95				107	112	
	12.10	5	6	19.8	19.8	107	108	11.0	17.6	18.7	95	98	9.9	20.8	22.7	113	115	9.9
			5			128	128				114	119				133	141	
	11.00	4	5	21.5	21.2	132	132	12.2	19.0	20.2	117	122	11.1	22.6	24.5	137	143	11.1
			4			155	154				137	144				159	170	
	9.90	3	4	23.0	22.4	157	157	13.2	20.1	21.5	140	146	12.2	24.2	26.1	163	173	12.2
			3			182	180				162	170				187	199	
	8.81	2	3	36.5	34.5	186	184	14.5	31.8	33.9	165	173	13.6	38.1	40.0	190	206	13.6
			2			258	247				229	244				269	287	
	6.73	1	2	38.0	36.0	262	249	15.5	33.7	35.3	232	248	15.0	39.3	41.9	272	290	15.0
	4.65		8002			337	314				299	322				354	376	
FPE	8.25	402	405	4.1	6.2	2	6	6.1	3.6	4.7	1	5	4.8	4.1	6.8	2	6	5.8
	4.65	401	404			14	25				12	19				14	26	

Note: Shaded cells identify exceedances due to concrete cracking effects.

Table B.3-7: Maximum Lumped Mass Accelerations - LB Profile Analysis with Surface Input Motion (Case S1)

Elev. (m)	Node No.	Location	CR_{SSE} Model			UC_{OBE} Model			UC_{SSE} Model SSI Envelope		
			NS (g)	EW (g)	Vert. (g)	NS (g)	EW (g)	Vert. (g)	NS (g)	EW (g)	Vert. (g)
19.70	10	FWS	1.62	1.25	0.51	1.18	1.19	0.53	2.00	2.18	1.43
17.25	9	FWS	1.50	1.18	0.51	1.12	1.09	0.53	1.85	2.02	1.43
15.53	8	FWS	1.38	1.10	0.51	1.06	1.00	0.52	1.68	1.83	1.40
13.81	7	FWS	1.24	1.02	0.50	0.99	0.90	0.51	1.49	1.60	1.35
12.10	6	FWS	1.08	0.93	0.49	0.92	0.82	0.50	1.28	1.35	1.27
11.00	5	FWS	0.98	0.87	0.48	0.87	0.78	0.49	1.14	1.21	1.21
9.90	4	FWS	0.87	0.81	0.47	0.82	0.73	0.48	1.00	1.11	1.15
8.81	3	FWS	0.76	0.75	0.46	0.76	0.68	0.47	0.87	1.01	1.07
6.73	2	FWS	0.51	0.62	0.44	0.62	0.59	0.45	0.66	0.76	0.91
4.65	8002	Basemat Top	0.43	0.53	0.42	0.47	0.51	0.42	0.62	0.65	0.72
2.15	8001	Basemat Bottom	0.43	0.48	0.53	0.43	0.46	0.57	0.63	0.57	0.88
8.25	405	FPE	0.50	0.84	0.38	0.42	0.64	0.39	0.81	1.42	0.72
6.45	402	FPE	0.45	0.63	0.38	0.41	0.58	0.38	0.72	1.04	0.68

Table B.3-8: Maximum Lumped Mass Accelerations - LB Profile Analysis with Deep Input Motion (Case S2)

Elev. (m)	Node No.	Location	CR_{SSE} Model			UC_{SSE} Model			UC_{SSE} Model SSI Envelope		
			NS (g)	EW (g)	Vert. (g)	NS (g)	EW (g)	Vert. (g)	NS (g)	EW (g)	Vert. (g)
19.70	10	FWS	1.87	1.52	0.69	1.39	1.36	0.70	2.00	2.18	1.43
17.25	9	FWS	1.71	1.39	0.69	1.29	1.27	0.70	1.85	2.02	1.43
15.53	8	FWS	1.53	1.26	0.68	1.19	1.17	0.69	1.68	1.83	1.40
13.81	7	FWS	1.32	1.11	0.66	1.08	1.06	0.67	1.49	1.60	1.35
12.10	6	FWS	1.11	0.96	0.65	0.97	0.95	0.65	1.28	1.35	1.27
11.00	5	FWS	0.98	0.88	0.63	0.90	0.87	0.64	1.14	1.21	1.21
9.90	4	FWS	0.85	0.80	0.62	0.83	0.80	0.62	1.00	1.11	1.15
8.81	3	FWS	0.73	0.73	0.60	0.77	0.72	0.61	0.87	1.01	1.07
6.73	2	FWS	0.54	0.55	0.57	0.62	0.58	0.57	0.66	0.76	0.91
4.65	8002	Basemat Top	0.47	0.48	0.54	0.49	0.50	0.54	0.62	0.65	0.72
2.15	8001	Basemat Bottom	0.45	0.42	0.64	0.48	0.45	0.64	0.63	0.57	0.88
8.25	405	FPE	0.57	0.89	0.50	0.54	0.67	0.51	0.81	1.42	0.72
6.45	402	FPE	0.53	0.68	0.49	0.52	0.58	0.51	0.72	1.04	0.68

Table B.3-9: Maximum Lumped Mass Accelerations - UB Profile Analysis with Surface Input Motion (Case S3)

Elev. (m)	Node No.	Location	CR_{SSE} Model			UC_{OBE} Model			UC_{SSE} Model SSI Envelope		
			NS (g)	EW (g)	Vert. (g)	NS (g)	EW (g)	Vert. (g)	NS (g)	EW (g)	Vert. (g)
19.7	10	FWS	1.14	1.32	0.69	1.50	1.19	0.74	2.00	2.18	1.43
17.25	9	FWS	1.06	1.23	0.69	1.40	1.11	0.74	1.85	2.02	1.43
15.53	8	FWS	0.93	1.10	0.68	1.29	1.02	0.73	1.68	1.83	1.40
13.81	7	FWS	0.77	0.96	0.67	1.16	0.93	0.70	1.49	1.60	1.35
12.1	6	FWS	0.61	0.80	0.65	1.01	0.83	0.67	1.28	1.35	1.27
11	5	FWS	0.55	0.69	0.64	0.92	0.76	0.65	1.14	1.21	1.21
9.9	4	FWS	0.53	0.61	0.62	0.82	0.69	0.63	1.00	1.11	1.15
8.81	3	FWS	0.51	0.59	0.60	0.72	0.64	0.61	0.87	1.01	1.07
6.73	2	FWS	0.38	0.45	0.55	0.48	0.56	0.56	0.66	0.76	0.91
4.65	8002	Basemat Top	0.36	0.35	0.51	0.37	0.48	0.51	0.62	0.65	0.72
2.15	8001	Basemat Bottom	0.36	0.35	0.55	0.38	0.44	0.58	0.63	0.57	0.88
8.25	405	FPE	0.42	0.72	0.49	0.41	0.68	0.49	0.81	1.42	0.72
6.45	402	FPE	0.38	0.47	0.48	0.39	0.59	0.48	0.72	1.04	0.68

Table B.3-10: Maximum Lumped Mass Accelerations - UB Profile Analysis with Deep Input Motion (Case S4)

Elev. (m)	Node No.	Location	CR_{SSE} Model			UC_{SSE} Model			UC_{SSE} Model SSI Envelope		
			NS (g)	EW (g)	Vert. (g)	NS (g)	EW (g)	Vert. (g)	NS (g)	EW (g)	Vert. (g)
19.7	10	FWS	1.75	2.10	1.23	2.00	2.18	1.43	2.00	2.18	1.43
17.25	9	FWS	1.62	1.91	1.23	1.85	2.02	1.43	1.85	2.02	1.43
15.53	8	FWS	1.45	1.74	1.21	1.68	1.83	1.40	1.68	1.83	1.40
13.81	7	FWS	1.25	1.52	1.17	1.49	1.60	1.35	1.49	1.60	1.35
12.1	6	FWS	1.05	1.27	1.11	1.28	1.35	1.27	1.28	1.35	1.27
11	5	FWS	0.93	1.17	1.05	1.14	1.21	1.21	1.14	1.21	1.21
9.9	4	FWS	0.83	1.14	0.99	1.00	1.11	1.15	1.00	1.11	1.15
8.81	3	FWS	0.76	1.10	0.93	0.87	1.01	1.07	0.87	1.01	1.07
6.73	2	FWS	0.64	0.79	0.82	0.66	0.76	0.91	0.66	0.76	0.91
4.65	8002	Basemat Top	0.66	0.59	0.73	0.62	0.65	0.72	0.62	0.65	0.72
2.15	8001	Basemat Bottom	0.69	0.53	0.97	0.63	0.57	0.88	0.63	0.57	0.88
8.25	405	FPE	0.98	1.60	0.71	0.81	1.42	0.72	0.81	1.42	0.72
6.45	402	FPE	0.78	1.06	0.67	0.72	1.04	0.68	0.72	1.04	0.68

Note: Shaded cells identify exceedances due to concrete cracking effects.

Table B.3-11: Maximum Lumped Mass Accelerations - BE Profile Analysis with Surface Input Motion (Case S5)

Elev. (m)	Node No.	Location	CR_{SSE} Model			UC_{OBE} Model			UC_{SSE} Model SSI Envelope		
			NS (g)	EW (g)	Vert. (g)	NS (g)	EW (g)	Vert. (g)	NS (g)	EW (g)	Vert. (g)
19.7	10	FWS	1.88	1.50	0.56	1.60	1.41	0.61	2.00	2.18	1.43
17.25	9	FWS	1.72	1.42	0.56	1.49	1.31	0.61	1.85	2.02	1.43
15.53	8	FWS	1.56	1.30	0.55	1.38	1.20	0.60	1.68	1.83	1.40
13.81	7	FWS	1.38	1.15	0.55	1.25	1.09	0.59	1.49	1.60	1.35
12.1	6	FWS	1.18	0.98	0.54	1.12	0.97	0.57	1.28	1.35	1.27
11	5	FWS	1.05	0.87	0.53	1.03	0.88	0.56	1.14	1.21	1.21
9.9	4	FWS	0.92	0.77	0.52	0.94	0.81	0.55	1.00	1.11	1.15
8.81	3	FWS	0.81	0.69	0.51	0.85	0.73	0.53	0.87	1.01	1.07
6.73	2	FWS	0.54	0.51	0.49	0.66	0.56	0.50	0.66	0.76	0.91
4.65	8002	Basemat Top	0.37	0.36	0.59	0.50	0.48	0.47	0.62	0.65	0.72
2.15	8001	Basemat Bottom	0.37	0.36	0.43	0.47	0.44	0.57	0.63	0.57	0.88
8.25	405	FPE	0.49	0.92	0.44	0.52	0.73	0.44	0.81	1.42	0.72
6.45	402	FPE	0.43	0.62	0.44	0.46	0.62	0.44	0.72	1.04	0.68

Table B.3-12: Maximum Lumped Mass Accelerations - BE Profile Analysis with Deep Input Motion (Case S6)

Elev. (m)	Node No.	Location	CR_{SSE} Model			UC_{SSE} Model			UC_{SSE} Model SSI Envelope		
			NS (g)	EW (g)	Vert. (g)	NS (g)	EW (g)	Vert. (g)	NS (g)	EW (g)	Vert. (g)
19.7	10	FWS	1.95	1.98	0.86	1.74	1.84	1.03	2.00	2.18	1.43
17.25	9	FWS	1.76	1.83	0.86	1.59	1.69	1.03	1.85	2.02	1.43
15.53	8	FWS	1.60	1.61	0.86	1.41	1.51	1.02	1.68	1.83	1.40
13.81	7	FWS	1.42	1.35	0.86	1.21	1.31	0.99	1.49	1.60	1.35
12.1	6	FWS	1.22	1.16	0.84	1.04	1.13	0.95	1.28	1.35	1.27
11	5	FWS	1.09	1.05	0.82	0.96	1.01	0.91	1.14	1.21	1.21
9.9	4	FWS	0.96	0.94	0.80	0.89	0.88	0.87	1.00	1.11	1.15
8.81	3	FWS	0.83	0.83	0.77	0.81	0.78	0.82	0.87	1.01	1.07
6.73	2	FWS	0.63	0.65	0.71	0.62	0.64	0.71	0.66	0.76	0.91
4.65	8002	Basemat Top	0.61	0.55	0.81	0.59	0.57	0.60	0.62	0.65	0.72
2.15	8001	Basemat Bottom	0.56	0.51	0.53	0.61	0.53	0.77	0.63	0.57	0.88
8.25	405	FPE	0.83	1.32	0.59	0.70	0.97	0.59	0.81	1.42	0.72
6.45	402	FPE	0.69	0.88	0.57	0.65	0.73	0.56	0.72	1.04	0.68

Note: Shaded cells identify exceedances due to concrete cracking effects.

Table B.3-13: Maximum Accelerations of SDOF Oscillators for LB

SDOF Oscillator				Acceleration (g)					
Elev. (m)	Node No.	Description	Direction	LB Profile Analysis with Surface Input Motion		LB Profile Analysis with Deep Input Motion		UC_{SSE} Model SSI Envelope	Standard Design
				CR_{SSE} Model	UC_{OBE} Model	CR_{SSE} Model	UC_{SSE} Model		
19.70	11	FWS Roof	Vert. (Z)	1.30	1.34	2.20	1.64	3.36	3.26
	12			1.15	-	1.49	-	-	-
8.25	**13**	FPE Roof	Vert. (Z)	0.74	-	0.78	-	-	-
12.10	60	FWS Water Sloshing Mode	NS (X)	0.10	0.10	0.10	0.10	0.10	0.30
			EW (Y)	0.07	0.07	0.09	0.09	0.09	0.40
8.81	30	FWS Water Impulsive Mode	NS (X)	0.76	0.77	0.73	0.77	0.87	1.10
			EW (Y)	0.75	0.68	0.73	0.72	1.01	1.40

Note: Node No. in red show additional oscillators.

Table B.3-14: Maximum Accelerations of SDOF Oscillators for UB

SDOF Oscillator				Acceleration (g)					
Elev. (m)	Node No.	Description	Direction	UB Profile Analysis with Surface Input Motion		UB Profile Analysis with Deep Input Motion		UC_{SSE} Model SSI Envelope	Standard Design
				CR_{SSE} Model	UC_{OBE} Model	CR_{SSE} Model	UC_{SSE} Model		
19.70	11	FWS Roof	Vert. (Z)	1.44	1.58	2.27	3.36	3.36	3.26
	12			1.15	-	2.78	-	-	-
8.25	**13**	FPE Roof	Vert. (Z)	0.74	-	1.88	-	-	-
12.10	60	FWS Water Sloshing Mode	NS (X)	0.10	0.10	0.10	0.10	0.10	0.30
			EW (Y)	0.07	0.07	0.09	0.09	0.09	0.40
8.81	30	FWS Water Impulsive Mode	NS (X)	0.51	0.72	0.76	0.87	0.87	1.10
			EW (Y)	0.59	0.64	1.10	1.01	1.01	1.40

Note: Shaded cell identifies exceedance due to concrete cracking effects.

Node No. in red show additional oscillators.

Table B.3-15: Maximum Accelerations of SDOF Oscillators for BE

SDOF Oscillator				Acceleration (g)					
Elev. (m)	Node No.	Description	Direction	BE Profile Analysis with Surface Input Motion		BE Profile Analysis with Deep Input Motion		UC_{SSE} Model SSI Envelope	Standard Design
				CR_{SSE} Model	UC_{OBE} Model	CR_{SSE} Model	UC_{SSE} Model		
19.70	11	FWS Roof	Vert. (Z)	1.11	1.62	2.35	2.56	3.36	3.26
	12			1.12	-	2.20	-	-	-
8.25	**13**	FPE Roof	Vert. (Z)	0.78	-	1.56	-	-	-
12.10	60	FWS Water Sloshing Mode	NS (X)	0.10	0.10	0.10	0.10	0.10	0.30
			EW (Y)	0.07	0.07	0.09	0.09	0.09	0.40
8.81	30	FWS Water Impulsive Mode	NS (X)	0.81	0.85	0.83	0.81	0.87	1.10
			EW (Y)	0.69	0.73	0.83	0.78	1.01	1.40

Note: Shaded cell identifies exceedance due to concrete cracking effects.

Node No. in red show additional oscillators.

Table B.3-16: Maximum Displacements Relative to Free-Field - LB Profile Analysis with Surface Input Motion (Case S1)

Elev. (m)	Node No.	Location	CR_{SSE} Model			UC_{OBE} Model SSI Envelope			Standard Design		
			NS (cm)	EW (cm)	Vert. (cm)	NS (cm)	EW (cm)	Vert. (cm)	NS (cm)	EW (cm)	Vert. (cm)
19.70	10	FWS	0.72	0.62	0.03	0.59	0.59	0.05	0.71	0.80	0.28
17.25	9	FWS	0.69	0.61	0.12	0.57	0.59	0.10	0.68	0.75	0.28
15.53	8	FWS	0.67	0.59	0.12	0.56	0.58	0.10	0.66	0.71	0.28
13.81	7	FWS	0.64	0.58	0.12	0.55	0.57	0.10	0.64	0.67	0.28
12.10	6	FWS	0.60	0.56	0.12	0.54	0.55	0.10	0.62	0.63	0.28
11.00	5	FWS	0.58	0.55	0.12	0.54	0.55	0.10	0.61	0.60	0.28
9.90	4	FWS	0.56	0.54	0.11	0.54	0.54	0.09	0.60	0.58	0.28
8.81	3	FWS	0.54	0.53	0.11	0.53	0.53	0.09	0.58	0.55	0.28
6.73	2	FWS	0.52	0.49	0.10	0.52	0.51	0.09	0.55	0.51	0.28
4.65	8002	Basemat Top	0.51	0.46	0.08	0.52	0.50	0.08	0.51	0.46	0.28
2.15	8001	Basemat Bottom	0.51	0.44	0.10	0.51	0.48	0.10	0.50	0.42	0.28
8.25	405	FPE	0.52	0.47	0.06	0.52	0.51	0.06	0.53	0.52	0.28
6.45	402	FPE	0.51	0.47	0.03	0.52	0.50	0.03	0.52	0.49	0.28

Note: Shaded cell identifies exceedance due to concrete cracking effects.

Table B.3-17: Maximum Displacements Relative to Free-Field - LB Profile Analysis with Deep Input Motion (Case S2)

Elev. (m)	Node No.	Location	CR_{SSE} Model			UC_{OBE} Model SSI Envelope			Standard Design		
			NS (cm)	EW (cm)	Vert. (cm)	NS (cm)	EW (cm)	Vert. (cm)	NS (cm)	EW (cm)	Vert. (cm)
19.70	10	FWS	0.38	0.48	0.05	0.59	0.59	0.05	0.71	0.80	0.28
17.25	9	FWS	0.36	0.45	0.12	0.57	0.59	0.10	0.68	0.75	0.28
15.53	8	FWS	0.34	0.42	0.12	0.56	0.58	0.10	0.66	0.71	0.28
13.81	7	FWS	0.31	0.39	0.12	0.55	0.57	0.10	0.64	0.67	0.28
12.10	6	FWS	0.28	0.36	0.12	0.54	0.55	0.10	0.62	0.63	0.28
11.00	5	FWS	0.26	0.33	0.11	0.54	0.55	0.10	0.61	0.60	0.28
9.90	4	FWS	0.24	0.31	0.11	0.54	0.54	0.09	0.60	0.58	0.28
8.81	3	FWS	0.22	0.28	0.10	0.53	0.53	0.09	0.58	0.55	0.28
6.73	2	FWS	0.17	0.22	0.09	0.52	0.51	0.09	0.55	0.51	0.28
4.65	8002	Basemat Top	0.12	0.17	0.08	0.52	0.50	0.08	0.51	0.46	0.28
2.15	8001	Basemat Bottom	0.11	0.15	0.10	0.51	0.48	0.10	0.50	0.42	0.28
8.25	405	FPE	0.12	0.20	0.05	0.52	0.51	0.06	0.53	0.52	0.28
6.45	402	FPE	0.11	0.19	0.03	0.52	0.50	0.03	0.52	0.49	0.28

Note: Shaded cell identifies exceedance due to concrete cracking effects.

Table B.3-18: Maximum Displacements Relative to Free-Field - UB Profile Analysis with Surface Input Motion (Case S3)

Elev. (m)	Node No.	Location	CR_{SSE} Model			UC_{OBE} Model SSI Envelope			Standard Design		
			NS (cm)	EW (cm)	Vert. (cm)	NS (cm)	EW (cm)	Vert. (cm)	NS (cm)	EW (cm)	Vert. (cm)
19.70	10	FWS	0.14	0.14	0.01	0.59	0.59	0.05	0.71	0.80	0.28
17.25	9	FWS	0.13	0.12	0.07	0.57	0.59	0.10	0.68	0.75	0.28
15.53	8	FWS	0.11	0.10	0.06	0.56	0.58	0.10	0.66	0.71	0.28
13.81	7	FWS	0.09	0.08	0.06	0.55	0.57	0.10	0.64	0.67	0.28
12.10	6	FWS	0.08	0.06	0.06	0.54	0.55	0.10	0.62	0.63	0.28
11.00	5	FWS	0.07	0.05	0.06	0.54	0.55	0.10	0.61	0.60	0.28
9.90	4	FWS	0.08	0.04	0.05	0.54	0.54	0.09	0.60	0.58	0.28
8.81	3	FWS	0.09	0.04	0.05	0.53	0.53	0.09	0.58	0.55	0.28
6.73	2	FWS	0.11	0.05	0.04	0.52	0.51	0.09	0.55	0.51	0.28
4.65	8002	Basemat Top	0.14	0.09	0.03	0.52	0.50	0.08	0.51	0.46	0.28
2.15	8001	Basemat Bottom	0.14	0.09	0.03	0.51	0.48	0.10	0.50	0.42	0.28
8.25	405	FPE	0.14	0.08	0.02	0.52	0.51	0.06	0.53	0.52	0.28
6.45	402	FPE	0.15	0.09	0.01	0.52	0.50	0.03	0.52	0.49	0.28

Table B.3-19: Maximum Displacements Relative to Free-Field - UB Profile Analysis with Deep Input Motion (Case S4)

Elev. (m)	Node No.	Location	CR_{SSE} Model			UC_{OBE} Model SSI Envelope			Standard Design		
			NS (cm)	EW (cm)	Vert. (cm)	NS (cm)	EW (cm)	Vert. (cm)	NS (cm)	EW (cm)	Vert. (cm)
19.70	10	FWS	0.30	0.40	0.03	0.59	0.59	0.05	0.71	0.80	0.28
17.25	9	FWS	0.28	0.38	0.10	0.57	0.59	0.10	0.68	0.75	0.28
15.53	8	FWS	0.26	0.35	0.10	0.56	0.58	0.10	0.66	0.71	0.28
13.81	7	FWS	0.23	0.32	0.10	0.55	0.57	0.10	0.64	0.67	0.28
12.10	6	FWS	0.20	0.29	0.09	0.54	0.55	0.10	0.62	0.63	0.28
11.00	5	FWS	0.18	0.27	0.09	0.54	0.55	0.10	0.61	0.60	0.28
9.90	4	FWS	0.16	0.25	0.08	0.54	0.54	0.09	0.60	0.58	0.28
8.81	3	FWS	0.15	0.22	0.08	0.53	0.53	0.09	0.58	0.55	0.28
6.73	2	FWS	0.10	0.16	0.06	0.52	0.51	0.09	0.55	0.51	0.28
4.65	8002	Basemat Top	0.07	0.10	0.05	0.52	0.50	0.08	0.51	0.46	0.28
2.15	8001	Basemat Bottom	0.07	0.09	0.05	0.51	0.48	0.10	0.50	0.42	0.28
8.25	405	FPE	0.08	0.12	0.03	0.52	0.51	0.06	0.53	0.52	0.28
6.45	402	FPE	0.07	0.10	0.02	0.52	0.50	0.03	0.52	0.49	0.28

Table B.3-20: Maximum Displacements Relative to Free-Field - BE Profile Analysis with Surface Input Motion (Case S5)

Elev. (m)	Node No.	Location	CR_{SSE} Model			UC_{OBE} Model SSI Envelope			Standard Design		
			NS (cm)	EW (cm)	Vert. (cm)	NS (cm)	EW (cm)	Vert. (cm)	NS (cm)	EW (cm)	Vert. (cm)
19.70	10	FWS	0.39	0.31	0.02	0.59	0.59	0.05	0.71	0.80	0.28
17.25	9	FWS	0.38	0.30	0.10	0.57	0.59	0.10	0.68	0.75	0.28
15.53	8	FWS	0.37	0.29	0.10	0.56	0.58	0.10	0.66	0.71	0.28
13.81	7	FWS	0.36	0.28	0.09	0.55	0.57	0.10	0.64	0.67	0.28
12.10	6	FWS	0.34	0.27	0.09	0.54	0.55	0.10	0.62	0.63	0.28
11.00	5	FWS	0.33	0.26	0.09	0.54	0.55	0.10	0.61	0.60	0.28
9.90	4	FWS	0.33	0.25	0.08	0.54	0.54	0.09	0.60	0.58	0.28
8.81	3	FWS	0.32	0.25	0.07	0.53	0.53	0.09	0.58	0.55	0.28
6.73	2	FWS	0.30	0.24	0.06	0.52	0.51	0.09	0.55	0.51	0.28
4.65	8002	Basemat Top	0.29	0.24	0.04	0.52	0.50	0.08	0.51	0.46	0.28
2.15	8001	Basemat Bottom	0.29	0.23	0.05	0.51	0.48	0.10	0.50	0.42	0.28
8.25	405	FPE	0.30	0.24	0.03	0.52	0.51	0.06	0.53	0.52	0.28
6.45	402	FPE	0.29	0.24	0.01	0.52	0.50	0.03	0.52	0.49	0.28

Table B.3-21: Maximum Displacements Relative to Free-Field - BE Profile Analysis with Deep Input Motion (Case S6)

Elev. (m)	Node No.	Location	CR_{SSE} Model			UC_{OBE} Model SSI Envelope			Standard Design		
			NS (cm)	EW (cm)	Vert. (cm)	NS (cm)	EW (cm)	Vert. (cm)	NS (cm)	EW (cm)	Vert. (cm)
19.70	10	FWS	0.37	0.44	0.04	0.59	0.59	0.05	0.71	0.80	0.28
17.25	9	FWS	0.34	0.41	0.11	0.57	0.59	0.10	0.68	0.75	0.28
15.53	8	FWS	0.31	0.38	0.11	0.56	0.58	0.10	0.66	0.71	0.28
13.81	7	FWS	0.28	0.35	0.11	0.55	0.57	0.10	0.64	0.67	0.28
12.10	6	FWS	0.25	0.32	0.10	0.54	0.55	0.10	0.62	0.63	0.28
11.00	5	FWS	0.23	0.30	0.10	0.54	0.55	0.10	0.61	0.60	0.28
9.90	4	FWS	0.21	0.28	0.09	0.54	0.54	0.09	0.60	0.58	0.28
8.81	3	FWS	0.19	0.25	0.09	0.53	0.53	0.09	0.58	0.55	0.28
6.73	2	FWS	0.14	0.20	0.08	0.52	0.51	0.09	0.55	0.51	0.28
4.65	8002	Basemat Top	0.09	0.14	0.06	0.52	0.50	0.08	0.51	0.46	0.28
2.15	8001	Basemat Bottom	0.09	0.13	0.07	0.51	0.48	0.10	0.50	0.42	0.28
8.25	405	FPE	0.10	0.15	0.04	0.52	0.51	0.06	0.53	0.52	0.28
6.45	402	FPE	0.09	0.14	0.02	0.52	0.50	0.03	0.52	0.49	0.28

Note: Shaded cell identifies exceedance due to concrete cracking effects.

Table B.3-22: Maximum Displacements of SDOF Oscillators Relative to Free-Field for LB

SDOF Oscillator				Displacement (cm)					
Elev. (m)	Node No.	Description	Direction	LB Profile Analysis with Surface Input Motion		LB Profile Analysis with Deep Input Motion		UC_{OBE} Model SSI Envelope	Standard Design
				CR_{SSE} Model	UC_{OBE} Model	CR_{SSE} Model	UC_{OBE} Model		
19.70	11	FWS Roof	Vert. (Z)	0.06	0.04	0.11	0.08	0.09	0.29
	12			0.03	-	0.07	-	-	-
8.25	**13**	FPE Roof		0.02	-	0.04	-	-	-
12.10	60	FWS Water Sloshing Mode	NS (X)	43.51	43.76	42.65	42.79	44.05	142.3
			EW (Y)	28.66	28.68	37.30	37.35	37.66	142.3
8.81	30	FWS Water Impulsive Mode	NS (X)	0.54	0.53	0.22	0.18	0.53	0.58
			EW (Y)	0.52	0.53	0.28	0.26	0.53	0.55

Note: Shaded cell identifies exceedance due to concrete cracking effects.
Node No. in red show additional oscillators.

Table B.3-23: Maximum Displacements of SDOF Oscillators Relative to Free-Field for UB

SDOF Oscillator				Displacement (cm)					
Elev. (m)	Node No.	Description	Direction	UB Profile Analysis with Surface Input Motion		UB Profile Analysis with Deep Input Motion		UC_{OBE} Model SSI Envelope	Standard Design
				CR_{SSE} Model	UC_{OBE} Model	CR_{SSE} Model	UC_{OBE} Model		
19.70	11	FWS Roof	Vert. (Z)	0.06	0.04	0.10	0.09	0.09	0.29
	12			0.03	-	0.06	-	-	-
8.25	**13**	FPE Roof		0.01	-	0.04	-	-	-
12.10	60	FWS Water Sloshing Mode	NS (X)	43.99	44.05	43.14	43.19	44.05	142.3
			EW (Y)	28.72	28.74	37.63	37.66	37.66	142.3
8.81	30	FWS Water Impulsive Mode	NS (X)	0.09	0.13	0.15	0.12	0.53	0.58
			EW (Y)	0.04	0.07	0.22	0.19	0.53	0.55

Note: Shaded cell identifies exceedance due to concrete cracking effects.
Node No. in red show additional oscillators.

Table B.3-24: Maximum Displacements of SDOF Oscillators Relative to Free-Field for BE

SDOF Oscillator				Displacement (cm)					
Elev. (m)	Node No.	Description	Direction	BE Profile Analysis with Surface Input Motion		BE Profile Analysis with Deep Input Motion		UC_{OBE} Model SSI Envelope	Standard Design
				CR_{SSE} Model	UC_{OBE} Model	CR_{SSE} Model	UC_{OBE} Model		
19.70	11	FWS Roof	Vert. (Z)	0.05	0.04	0.10	0.08	0.09	0.29
	12			0.03	-	0.07	-	-	-
8.25	**13**	FPE Roof		0.01	-	0.04	-	-	-
12.10	60	FWS Water Sloshing Mode	NS (X)	43.95	44.01	43.14	43.19	44.05	142.3
			EW (Y)	28.70	28.72	37.62	37.65	37.66	142.3
8.81	30	FWS Water Impulsive Mode	NS (X)	0.32	0.33	0.19	0.15	0.53	0.58
			EW (Y)	0.25	0.26	0.25	0.20	0.53	0.55

Note: Shaded cell identifies exceedance due to concrete cracking effects.
Node No. in red show additional oscillators.

Table B.4-1: Vertical Out-of-Plane Loads on FWS and FPE Roofs LB

Slab		Flexible Mode (SDOF Oscillator)				Rigid Mode (LMSM)				Eq. Ave. Acc. (g)			
Elev. (m)	Location	Weight (kN)	Mass Node	Acceleration (g)		Mass Node	Weight (kN)	Acceleration (g)		CR_{SSE}		UC_{SSE} SSI Envel.	Stand. Design
				Surf. Motion (Case S1)	Deep Motion (Case S2)			Surf. Motion (Case S1)	Deep Motion (Case S2)	Surf. Motion (Case S1)	Deep Motion (Case S2)		
19.70	FWS Roof	1339	11	1.21	1.80	10	1610	0.51	0.69	0.97	1.42	2.11	1.74
		1743	12										
8.25	FPE Roof	758	13	0.74	0.78	405	1536	0.38	0.50	0.50	0.59	0.72	1.12

Table B.4-2: Vertical Out-of-Plane Loads on FWS and FPE Roofs UB

Slab		Flexible Mode (SDOF Oscillator)				Rigid Mode (LMSM)				Eq. Ave. Acc. (g)			
Elev. (m)	Location	Weight (kN)	Mass Node	Acceleration (g)		Mass Node	Weight (kN)	Acceleration (g)		CR_{SSE}		UC_{SSE} SSI Envel.	Stand. Design
				Surf. Motion (Case S3)	Deep Motion (Case S4)			Surf. Motion (Case S3)	Deep Motion (Case S4)	Surf. Motion (Case S3)	Deep Motion (Case S4)		
19.70	FWS Roof	1339	11	1.28	2.56	10	1610	0.69	1.23	1.07	2.10	2.11	1.74
		1743	12										
8.25	FPE Roof	758	13	0.74	1.88	405	1536	0.49	0.71	0.57	1.10	0.72	1.12

Note: Shaded cell identifies exceedance due to concrete cracking effects.

Table B.4-3: Vertical Out-of-Plane Loads on FWS and FPE Roofs BE

Slab		Flexible Mode (SDOF Oscillator)				Rigid Mode (LMSM)				Eq. Ave. Acc. (g)			
Elev. (m)	Location	Weight (kN)	Mass Node	Acceleration (g)		Mass Node	Weight (kN)	Acceleration (g)		CR_{SSE}		UC_{SSE} SSI Envel.	Stand. Design
				Surf. Motion (Case S5)	Deep Motion (Case S6)			Surf. Motion (Case S5)	Deep Motion (Case S6)	Surf. Motion (Case S5)	Deep Motion (Case S6)		
19.70	FWS Roof	1339	11	1.12	2.27	10	1610	0.56	0.86	0.92	1.78	2.11	1.74
		1743	12										
8.25	FPE Roof	758	13	0.78	1.56	405	1536	0.44	0.59	0.55	0.91	0.72	1.12

Note: Shaded cell identifies exceedance due to concrete cracking effects.

Table B.4-4: Total Torsion Demand - UB Profile Analysis with Deep Input Motion (Case S4)

Structure	Element			Torsion (MN-m)								
				CR_{SSE} Model			UC_{SSE} Model			UC_{SSE} Model SSI Envelope		
	Elev. (m)	No.	Nodes No.	SASSI	Accidental	Total	SASSI	Accidental	Total	SASSI	Accidental	Total
FWS	19.70	9	10	1.9	3.9	5.8	0.8	4.1	4.9	1.2	4.1	5.3
			9									
	17.25	8	9	5.8	9.5	15.2	2.5	10.1	12.6	3.6	10.1	13.7
			8									
	15.53	7	8	9.6	13.0	22.6	4.2	14.0	18.2	6.0	14.0	20.0
			7									
	13.81	6	7	13.0	16.3	29.3	5.7	17.5	23.1	8.2	17.5	25.7
			6									
	12.10	5	6	15.5	18.5	34.0	6.7	19.8	26.6	9.9	19.8	29.7
			5									
	11.00	4	5	17.2	20.0	37.3	7.5	21.5	28.9	11.1	21.5	32.5
			4									
	9.90	3	4	18.7	21.3	40.0	8.1	22.9	31.0	12.2	22.9	35.0
			3									
	8.81	2	3	20.6	33.2	53.8	8.9	35.0	43.9	13.6	35.0	48.6
			2									
	6.73	1	2	22.0	34.9	56.9	9.5	36.6	46.1	15.0	36.6	51.7
	4.65		8002									
FPE	8.25	402	405	8.5	5.0	13.5	5.8	4.5	10.3	5.8	4.5	10.3
	4.65	401	404									

Note: Shaded cells identify exceedances due to concrete cracking effects.

Table B.4-5: Total Shear Demand - UB Profile Analysis with Deep Input Motion (Case S4)

Structure	Element			CR_{SSE} Model					UC_{SSE} Model					UC_{SSE} Model SSI Envelope				
	Elev. (m)	No.	Nodes No.	Tors.*) (MN-m)	NS Shear (MN)		EW Shear(MN)		Tors.*) (MN-m)	NS Shear (MN)		EW Shear(MN)		Tors.*) (MN-m)	NS Shear (MN)		EW Shear(MN)	
					SASSI	Total	SASSI	Total		SASSI	Total	SASSI	Total		SASSI	Total	SASSI	Total
FWS	19.70	9	10	5.8	3.7	4.4	4.4	5.1	4.9	4.3	4.8	4.7	5.2	5.3	4.3	4.9	4.7	5.3
			9															
	17.25	8	9	15.2	9.2	10.9	10.8	12.5	12.6	10.5	11.9	11.5	12.9	13.7	10.5	12.1	11.5	13.1
			8															
	15.53	7	8	22.6	12.7	15.3	14.9	17.5	18.2	14.6	16.7	16.0	18.1	20.0	14.6	16.9	16.0	18.3
			7															
	13.81	6	7	29.3	15.8	19.1	18.6	21.9	23.1	18.3	20.9	20.0	22.6	25.7	18.3	21.2	20.0	22.9
			6															
	12.10	5	6	34.0	17.8	21.7	21.1	25.0	26.6	20.8	23.9	22.7	25.7	29.7	20.8	24.2	22.7	26.1
			5															
	11.00	4	5	37.3	19.2	23.5	22.9	27.1	28.9	22.6	25.9	24.5	27.9	32.5	22.6	26.3	24.5	28.3
			4															
	9.90	3	4	40.0	20.4	25.0	24.3	28.9	31.0	24.2	27.7	26.1	29.7	35.0	24.2	28.2	26.1	30.1
			3															
	8.81	2	3	53.8	30.9	37.1	38.0	44.1	43.9	38.1	43.1	40.0	45.0	48.6	38.1	43.6	40.0	45.5
			2															
	6.73	1	2	56.9	32.2	38.7	39.9	46.4	46.1	39.3	44.5	41.9	47.1	51.7	39.3	45.2	41.9	47.8
	4.65		8002															
FPE	8.25	402	405	13.5	4.7	5.8	7.5	8.6	10.3	4.1	4.9	6.8	7.7	10.3	4.1	4.9	6.8	7.7
	4.65	401	404															

Note: *) Total torsion demand from Table B.4-4.
Shaded cells identify exceedances due to concrete cracking effects.

Table B.4-6: Total Torsion Demand - BE Profile Analysis with Deep Input Motion (Case S6)

Structure	Element			Torsion (MN-m)								
				CR_{SSE} Model			UC_{SSE} Model			UC_{SSE} Model SSI Envelope		
	Elev. (m)	No.	Nodes No.	SASSI	Accidental	Total	SASSI	Accidental	Total	SASSI	Accidental	Total
FWS	19.70	9	10 / 9	1.4	3.7	5.1	1.2	3.4	4.6	1.2	4.1	5.3
	17.25	8	9 / 8	4.1	9.1	13.2	3.6	8.4	12.0	3.6	10.1	13.7
	15.53	7	8 / 7	6.8	12.5	19.3	6.0	11.7	17.7	6.0	14.0	20.0
	13.81	6	7 / 6	9.2	15.4	24.7	8.2	14.5	22.7	8.2	17.5	25.7
	12.10	5	6 / 5	11.0	17.3	28.3	9.9	16.4	26.3	9.9	19.8	29.7
	11.00	4	5 / 4	12.2	18.8	31.0	11.1	17.7	28.7	11.1	21.5	32.5
	9.90	3	4 / 3	13.2	20.1	33.4	12.2	18.8	31.0	12.2	22.9	35.0
	8.81	2	3 / 2	14.5	32.0	46.5	13.6	29.7	43.3	13.6	35.0	48.6
	6.73 / 4.65	1	2 / 8002	15.5	33.3	48.8	15.0	30.9	45.9	15.0	36.6	51.7
FPE	8.25 / 4.65	402 / 401	405 / 404	6.1	4.1	10.2	4.8	3.1	7.9	5.8	4.5	10.3

Note: Shaded cells identify exceedances due to concrete cracking effects.

Table B.4-7: Total Shear Demand - BE Profile Analysis with Deep Input Motion (Case S6)

Structure	Element			CR_{SSE} Model					UC_{SSE} Model					UC_{SSE} Model SSI Envelope				
	Elev. (m)	No.	Nodes No.	Tors.*) (MN-m)	NS Shear (MN)		EW Shear (MN)		Tors.*) (MN-m)	NS Shear (MN)		EW Shear (MN)		Tors.*) (MN-m)	NS Shear (MN)		EW Shear (MN)	
					SASSI	Total	SASSI	Total		SASSI	Total	SASSI	Total		SASSI	Total	SASSI	Total
FWS	19.70	9	10	5.1	4.2	4.7	4.2	4.8	4.6	3.7	4.3	3.9	4.5	5.3	4.3	4.9	4.7	5.3
			9															
	17.25	8	9	13.2	10.1	11.6	10.4	11.9	12.0	9.1	10.5	9.6	11.0	13.7	10.5	12.1	11.5	13.1
			8															
	15.53	7	8	19.3	13.9	16.1	14.3	16.5	17.7	12.5	14.6	13.4	15.4	20.0	14.6	16.9	16.0	18.3
			7															
	13.81	6	7	24.7	17.4	20.2	17.7	20.5	22.7	15.5	18.1	16.6	19.2	25.7	18.3	21.2	20.0	22.9
			6															
	12.10	5	6	28.3	19.8	23.0	19.8	23.1	26.3	17.6	20.6	18.7	21.7	29.7	20.8	24.2	22.7	26.1
			5															
	11.00	4	5	31.0	21.5	25.0	21.2	24.8	28.7	19.0	22.2	20.2	23.5	32.5	22.6	26.3	24.5	28.3
			4															
	9.90	3	4	33.4	23.0	26.8	22.4	26.2	31.0	20.1	23.7	21.5	25.0	35.0	24.2	28.2	26.1	30.1
			3															
	8.81	2	3	46.5	36.5	41.8	34.5	39.8	43.3	31.8	36.8	33.9	38.9	48.6	38.1	43.6	40.0	45.5
			2															
	6.73	1	2	48.8	38.0	43.6	36.0	41.6	45.9	33.7	38.9	35.3	40.6	51.7	39.3	45.2	41.9	47.8
	4.65		8002															
FPE	8.25	402	405	10.2	4.1	4.9	6.2	7.0	7.9	3.6	4.2	4.7	5.3	10.3	4.1	4.9	6.8	7.7
	4.65	401	404															

Note: *) Total torsion demand from Table B.4-3.
Shaded cells identify exceedances due to concrete cracking effects.

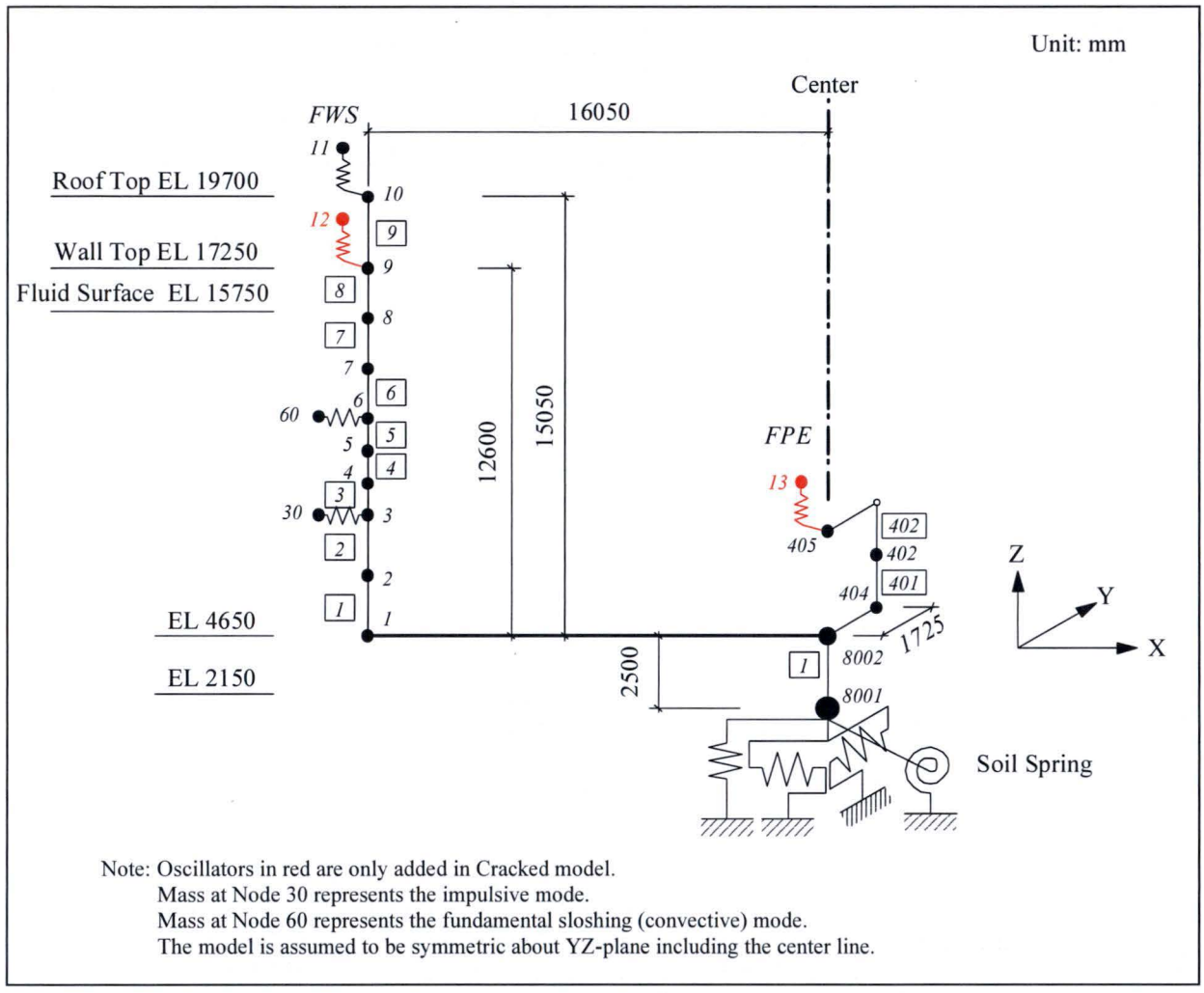

Note: Oscillators in red are only added in Cracked model.
Mass at Node 30 represents the impulsive mode.
Mass at Node 60 represents the fundamental sloshing (convective) mode.
The model is assumed to be symmetric about YZ-plane including the center line.

Figure B.2-1: FWSC Lumped Mass Stick CR_{SSE} Model

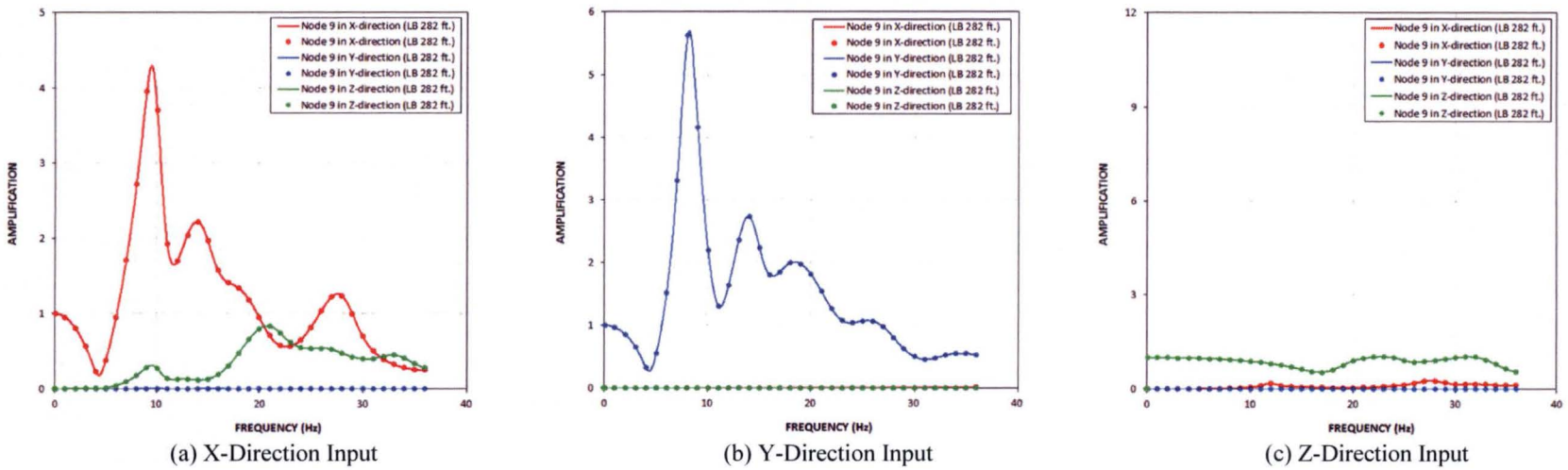

(a) X-Direction Input (b) Y-Direction Input (c) Z-Direction Input

Figure B.3-1a: Transfer Functions for FWS Wall Top Response from Analysis of CR_{SSE} Model of LB Profile and Surface Input Motion at El. 282 ft

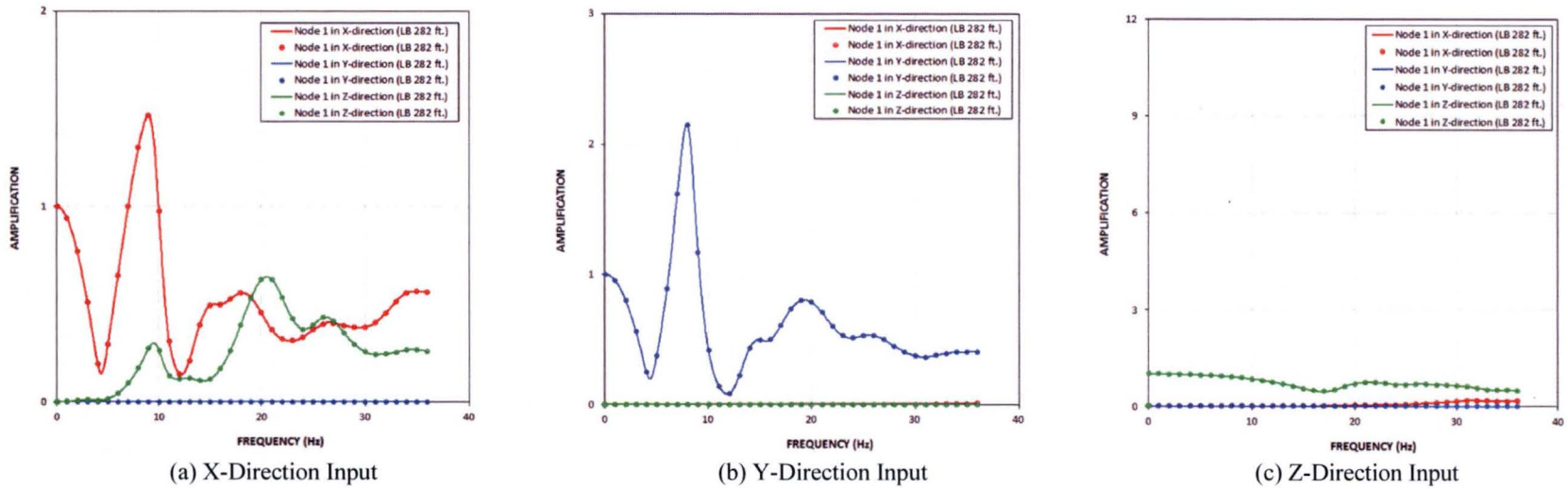

(a) X-Direction Input (b) Y-Direction Input (c) Z-Direction Input

Figure B.3-1b: Transfer Functions for FWS Basemat Response from Analysis of CR_{SSE} Model of LB Profile and Surface Input Motion at El. 282 ft

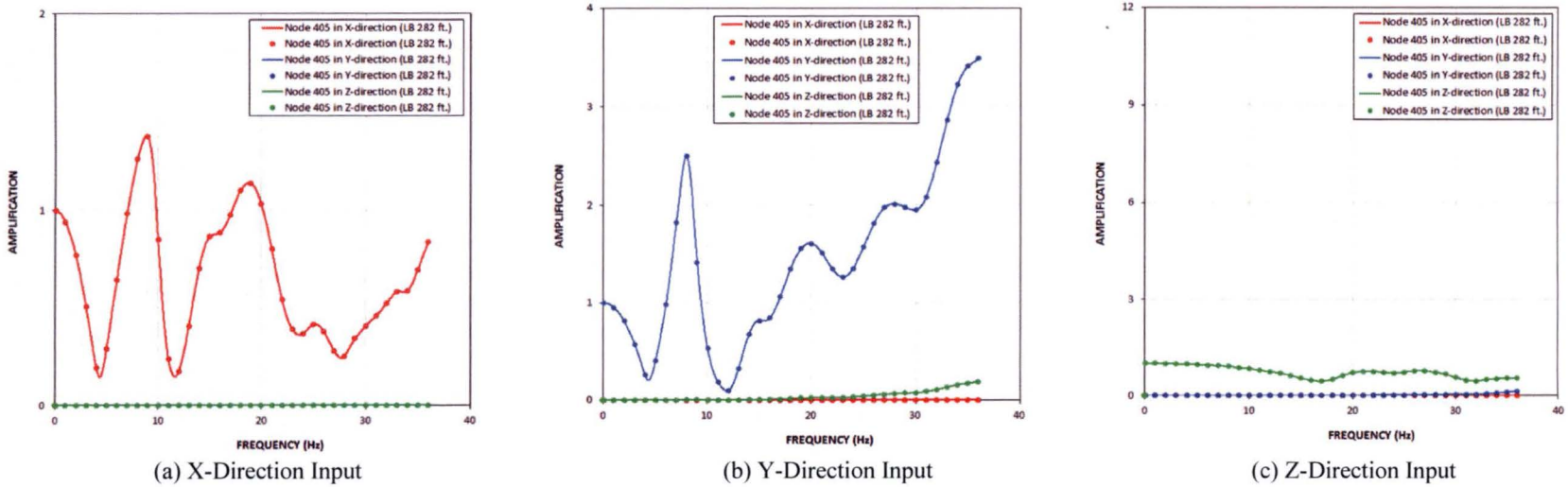

(a) X-Direction Input (b) Y-Direction Input (c) Z-Direction Input

Figure B.3-1c: Transfer Functions for FPE Top Response from Analysis of CR_{SSE} Model of LB Profile and Surface Input Motion at El. 282 ft

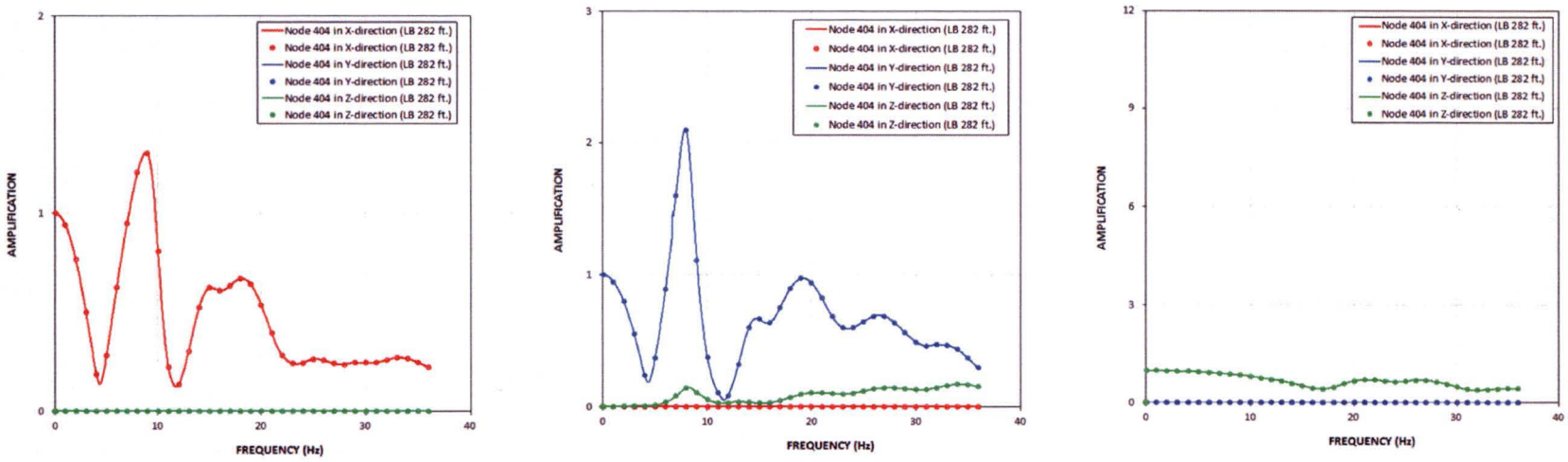

(a) X-Direction Input (b) Y-Direction Input (c) Z-Direction Input

Figure B.3-1d: Transfer Functions for FPE Basemat Response from Analysis of CR_{SSE} Model of LB Profile and Surface Input Motion at El. 282 ft

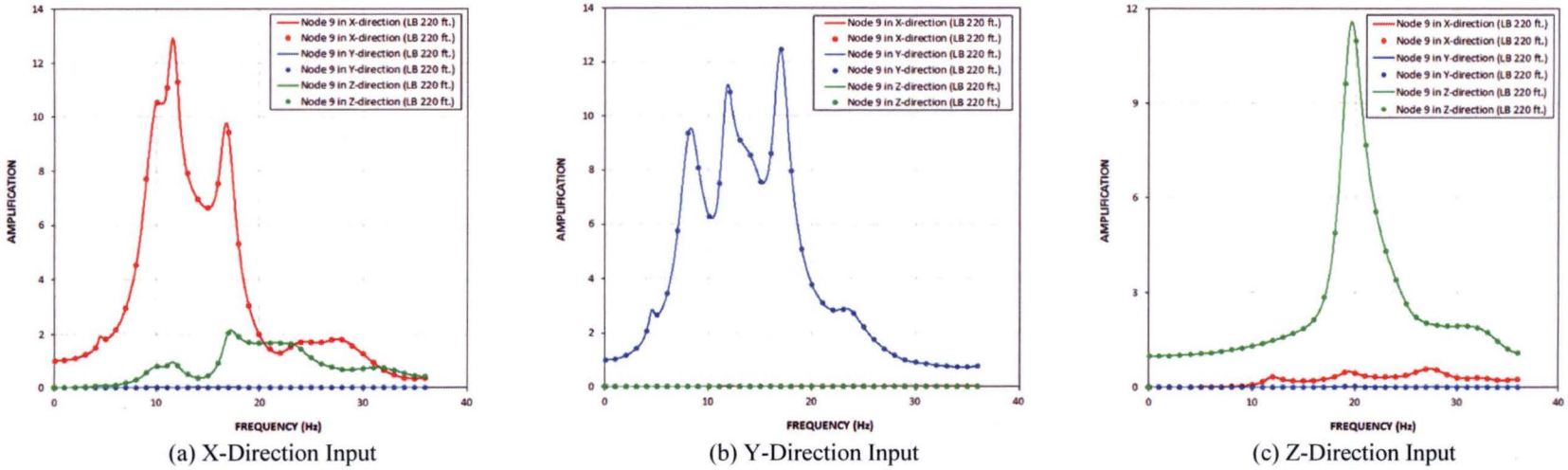

(a) X-Direction Input (b) Y-Direction Input (c) Z-Direction Input

Figure B.3-2a: Transfer Functions for FWS Wall Top Response from Analysis of CR_{SSE} Model of LB Profile and Deep Input Motion at El. 220 ft

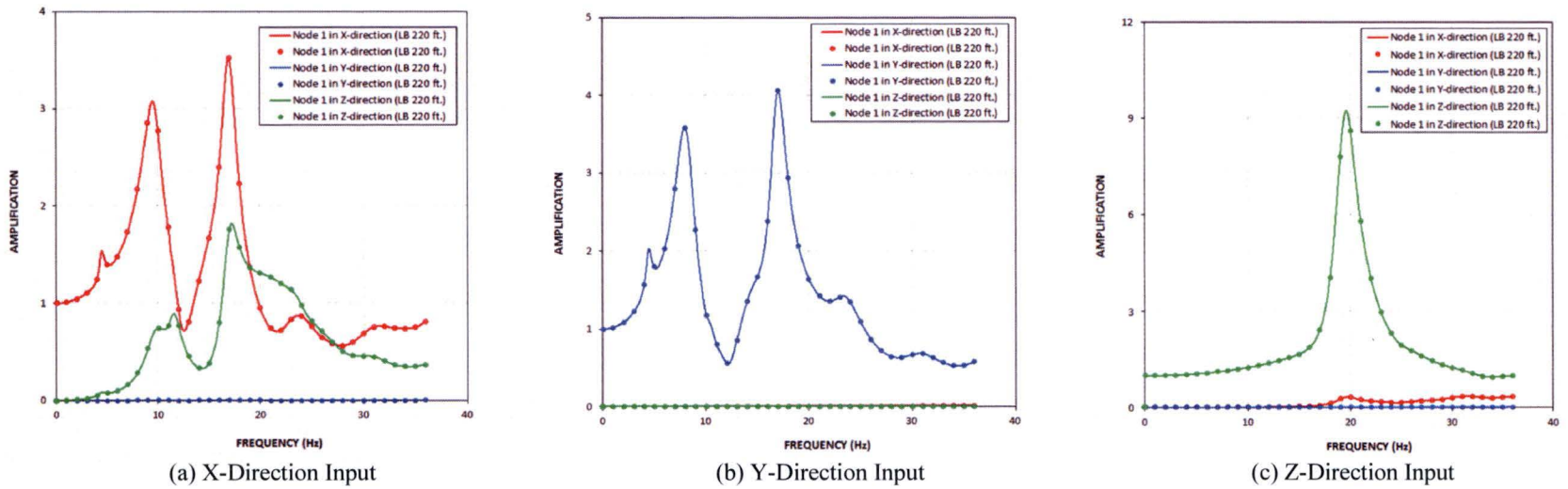

(a) X-Direction Input (b) Y-Direction Input (c) Z-Direction Input

Figure B.3-2b: Transfer Functions for FWS Basemat Response from Analysis of CR_{SSE} Model of LB Profile and Deep Input Motion at El. 220 ft

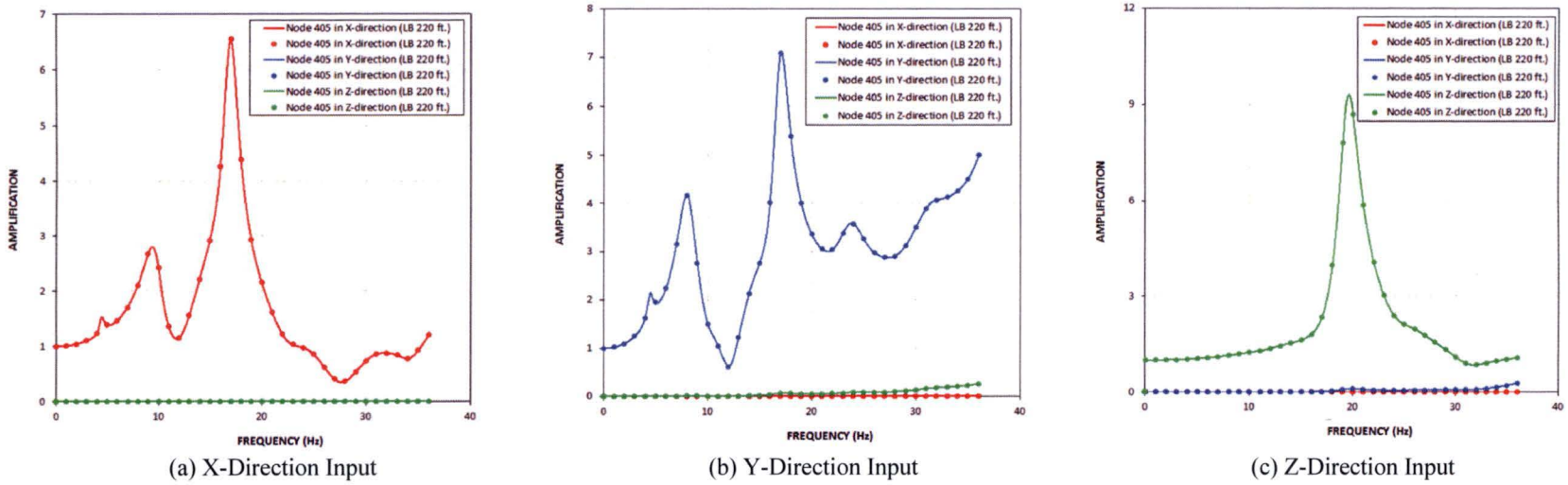

(a) X-Direction Input (b) Y-Direction Input (c) Z-Direction Input

Figure B.3-2c: Transfer Functions for FPE Top Response from Analysis of CR_{SSE} Model of LB Profile and Deep Input Motion at El. 220 ft

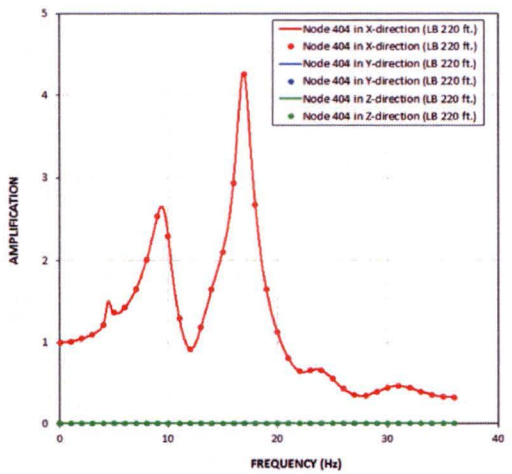

(a) X-Direction Input

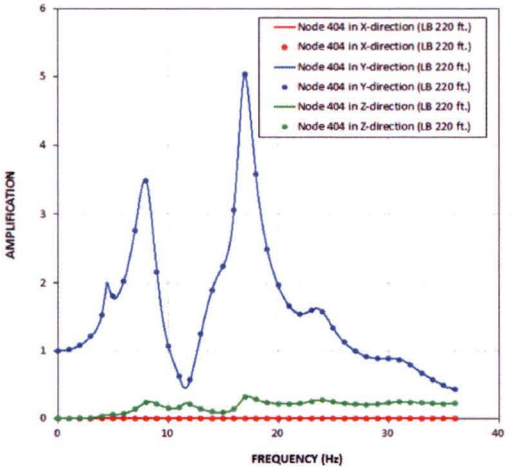

(b) Y-Direction Input

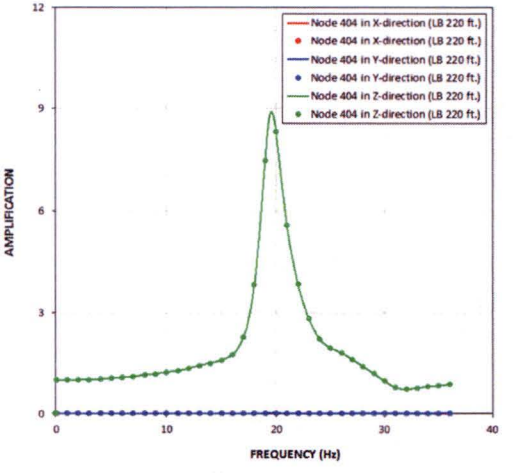

(c) Z-Direction Input

Figure B.3-2d: Transfer Functions for FPE Basemat Response from Analysis of CR_{SSE} Model of LB Profile and Deep Input Motion at El. 220 ft

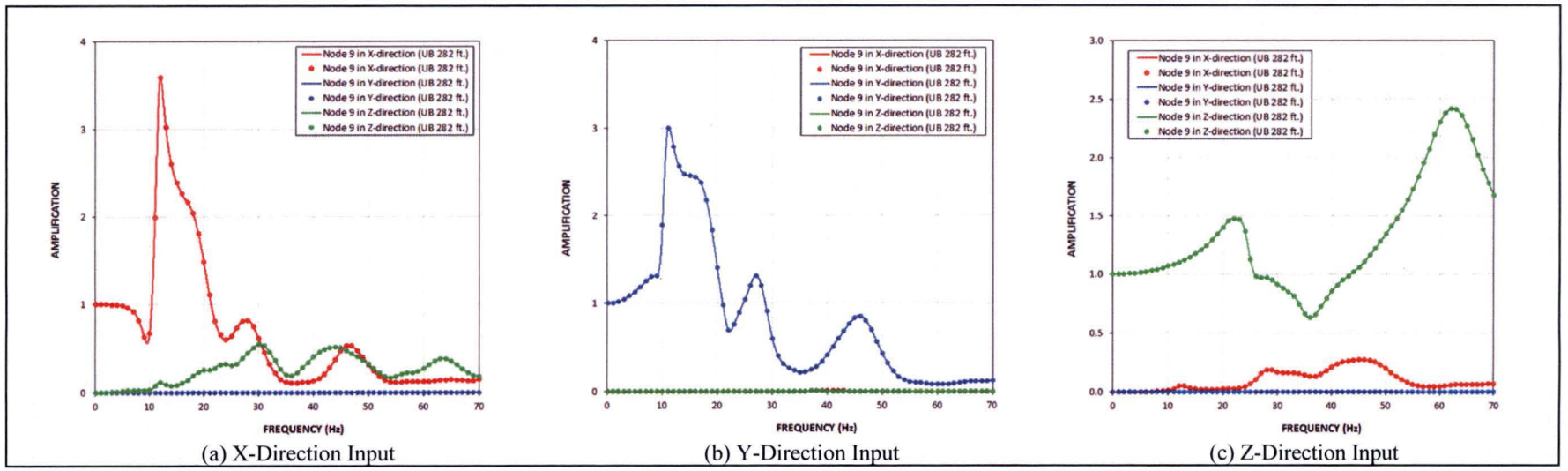

(a) X-Direction Input (b) Y-Direction Input (c) Z-Direction Input

Figure B.3-3a: Transfer Functions for FWS Wall Top Response from Analysis of CR_{SSE} Model of UB Profile and Surface Input Motion at El. 282 ft

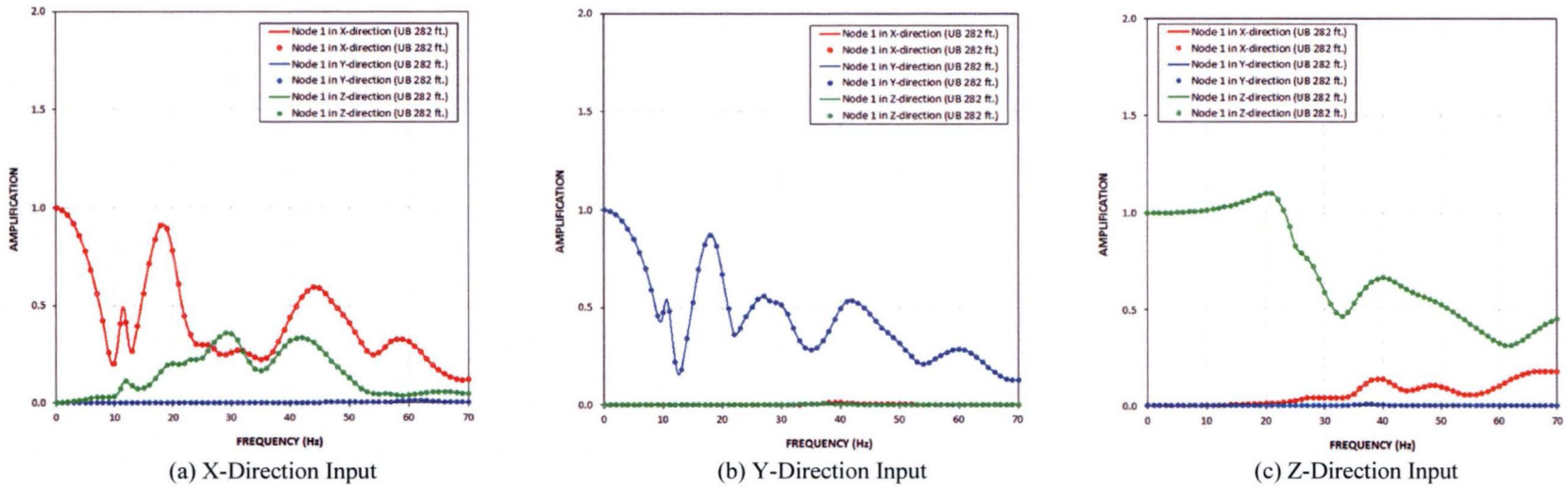

(a) X-Direction Input (b) Y-Direction Input (c) Z-Direction Input

Figure B.3-3b: Transfer Functions for FWS Basemat Response from Analysis of CR_{SSE} Model of UB Profile and Surface Input Motion at El. 282 ft

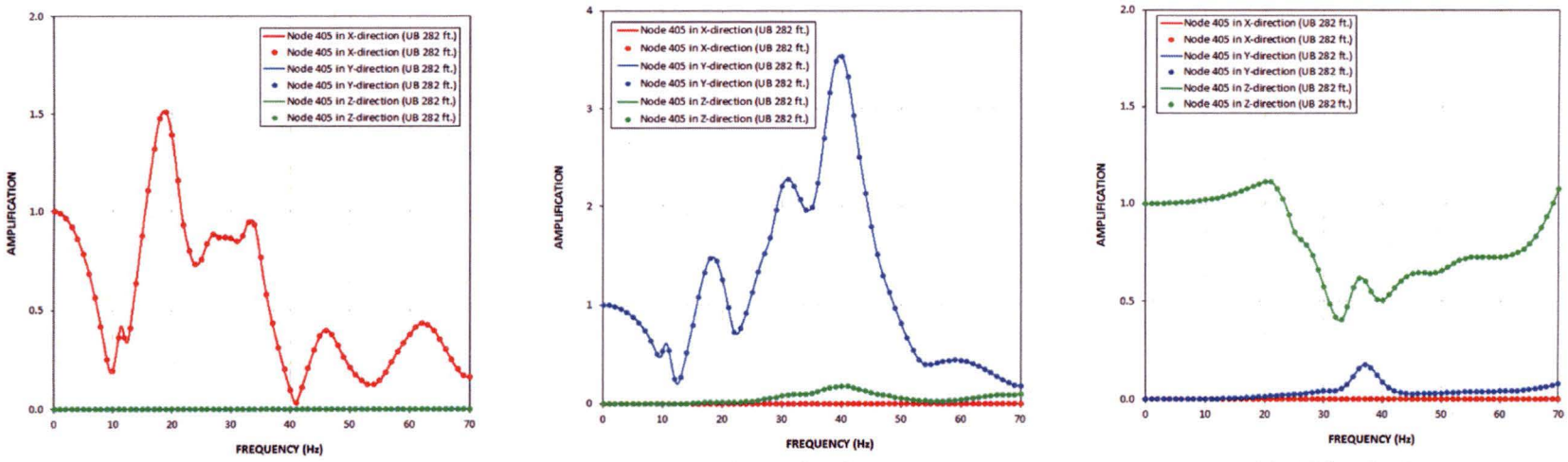

(a) X-Direction Input (b) Y-Direction Input (c) Z-Direction Input

Figure B.3-3c: Transfer Functions for FPE Top Response from Analysis of CR_{SSE} Model of UB Profile and Surface Input Motion at El. 282 ft

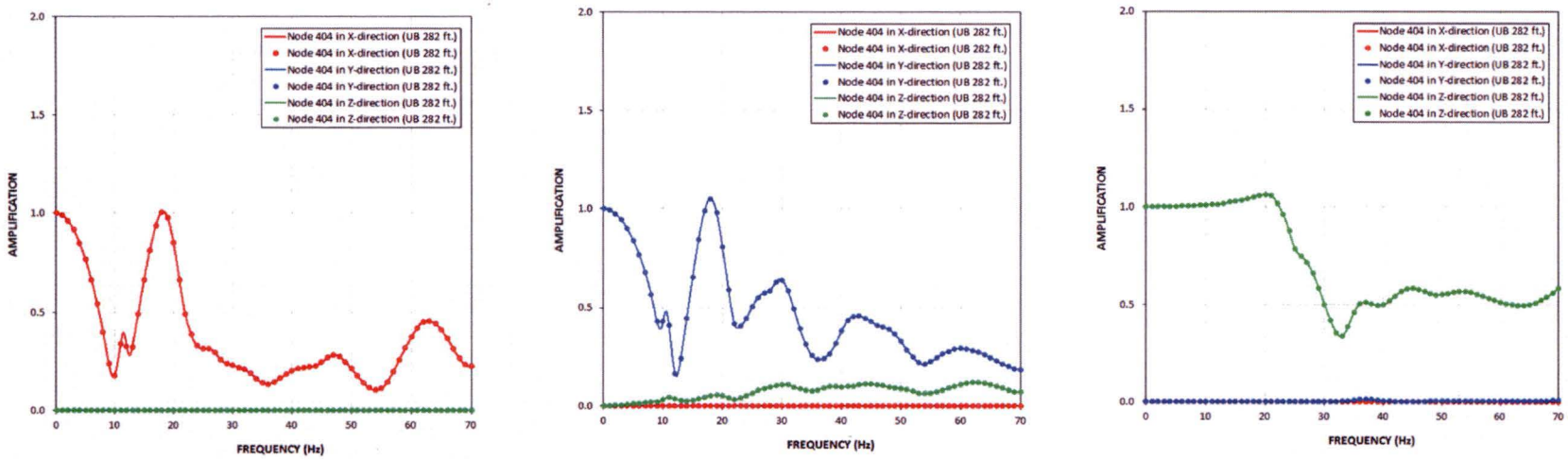

(a) X-Direction Input (b) Y-Direction Input (c) Z-Direction Input

Figure B.3-3d: Transfer Functions for FPE Basemat Response from Analysis of CR_{SSE} Model of UB Profile and Surface Input Motion at El. 282 ft

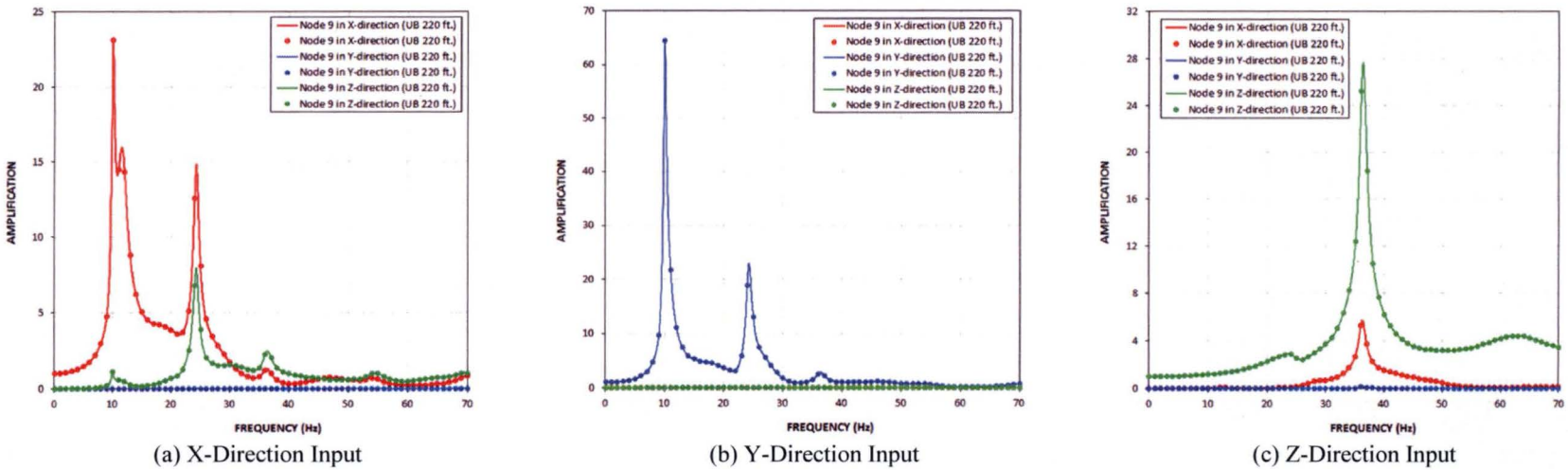

(a) X-Direction Input (b) Y-Direction Input (c) Z-Direction Input

Figure B.3-4a: Transfer Functions for FWS Wall Top Response from Analysis of CR_{SSE} Model of UB Profile and Deep Input Motion at El. 220 ft

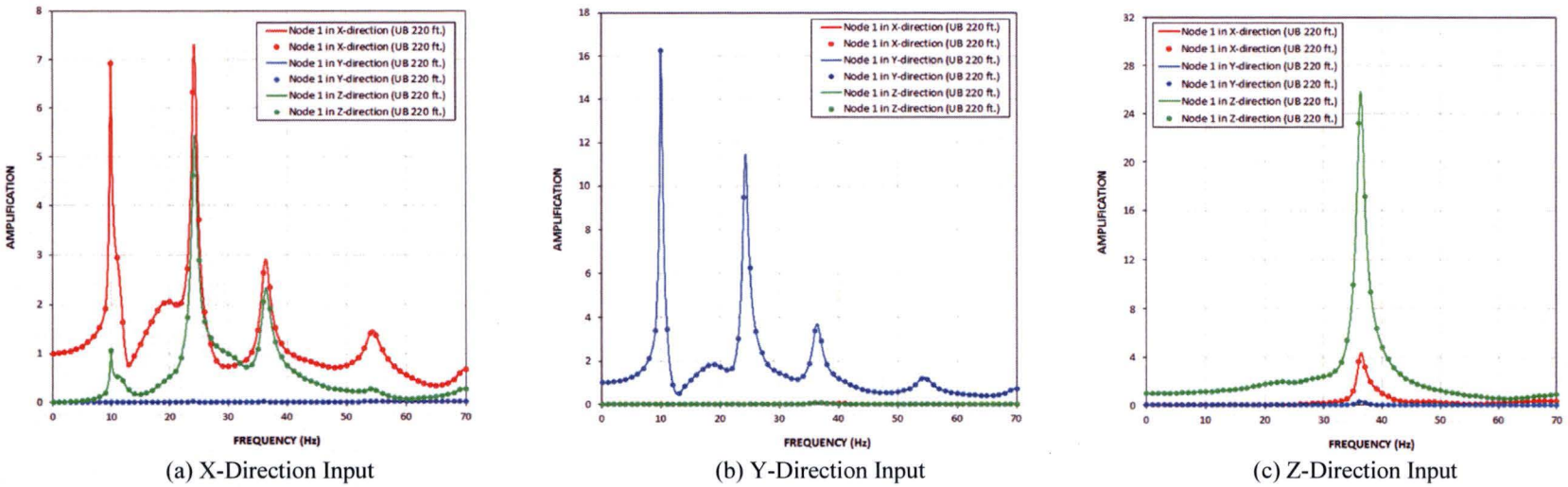

(a) X-Direction Input (b) Y-Direction Input (c) Z-Direction Input

Figure B.3-4b: Transfer Functions for FWS Basemat Response from Analysis of CR_{SSE} Model of UB Profile and Deep Input Motion at El. 220 ft

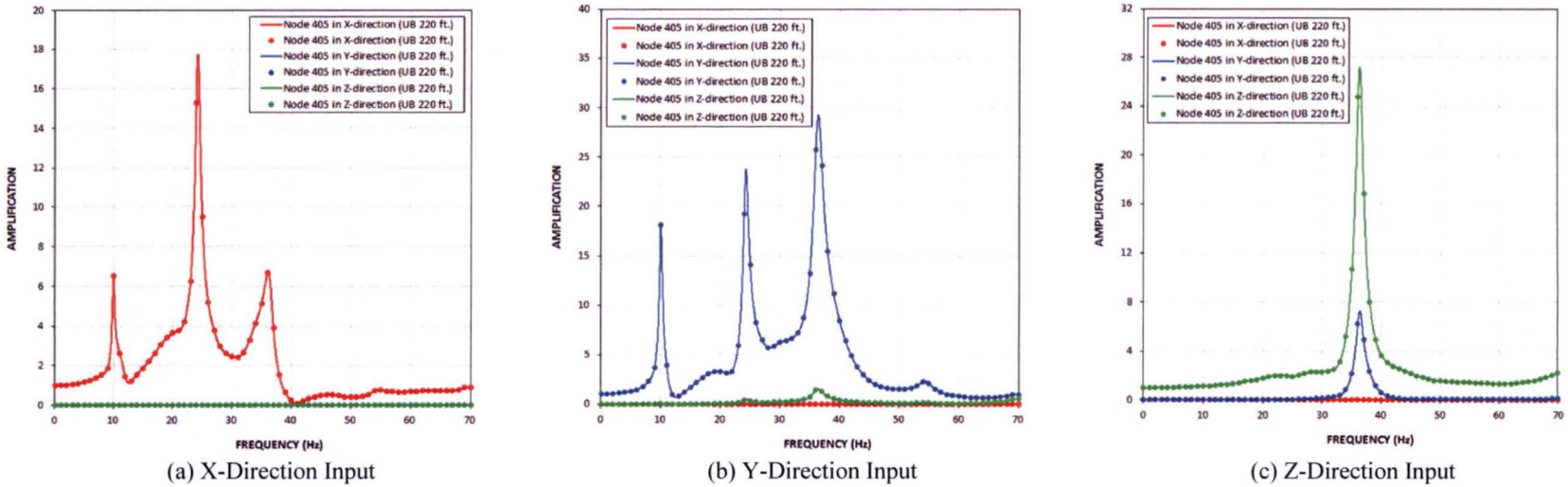

(a) X-Direction Input (b) Y-Direction Input (c) Z-Direction Input

Figure B.3-4c: Transfer Functions for FPE Top Response from Analysis of CR_{SSE} Model of UB Profile and Deep Input Motion at El. 220 ft

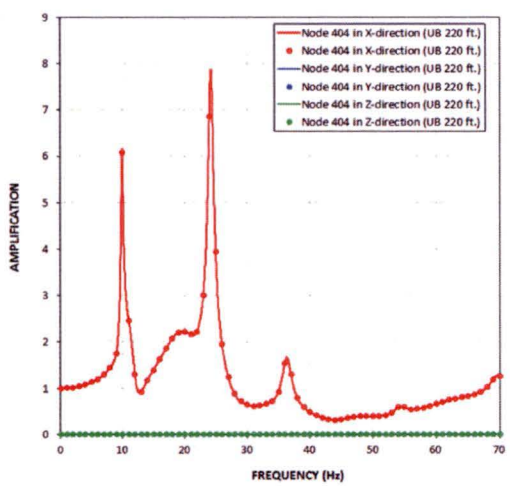

(a) X-Direction Input

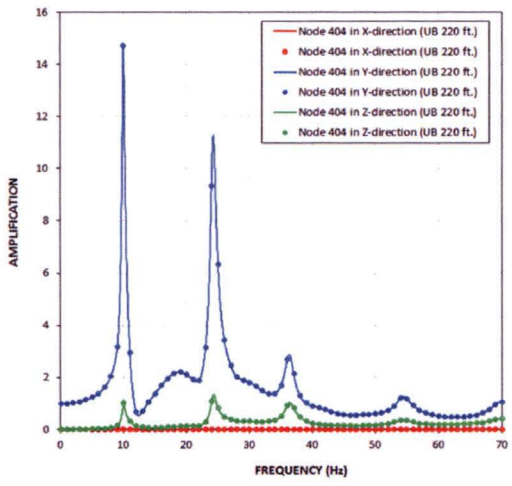

(b) Y-Direction Input

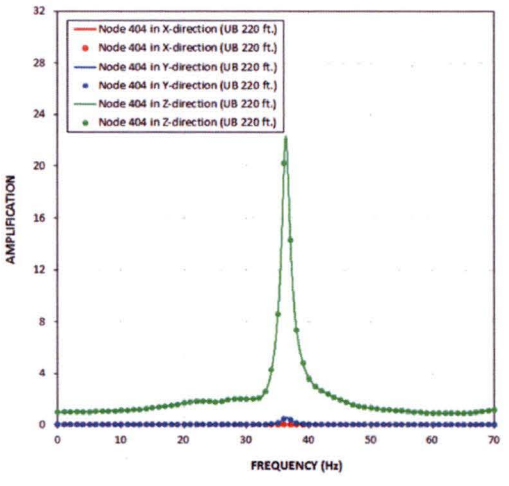

(c) Z-Direction Input

Figure B.3-4d: Transfer Functions for FPE Basemat Response from Analysis of CR_{SSE} Model of UB Profile and Deep Input Motion at El. 220 ft

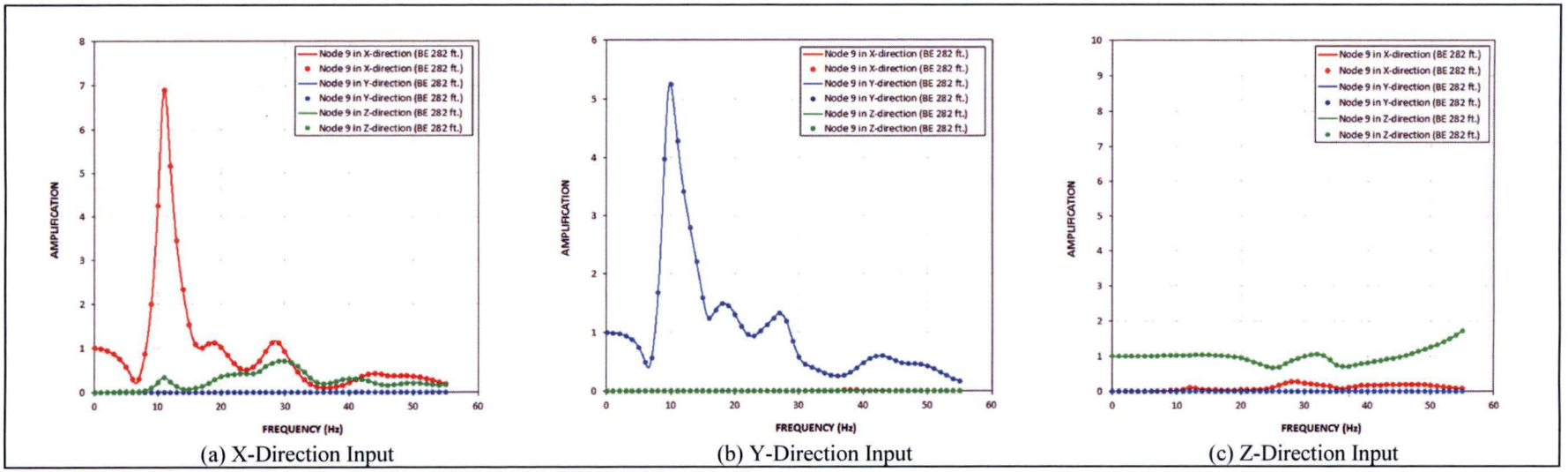

(a) X-Direction Input (b) Y-Direction Input (c) Z-Direction Input

Figure B.3-5a: Transfer Functions for FWS Wall Top Response from Analysis of CR_{SSE} Model of BE Profile and Surface Input Motion at El. 282 ft

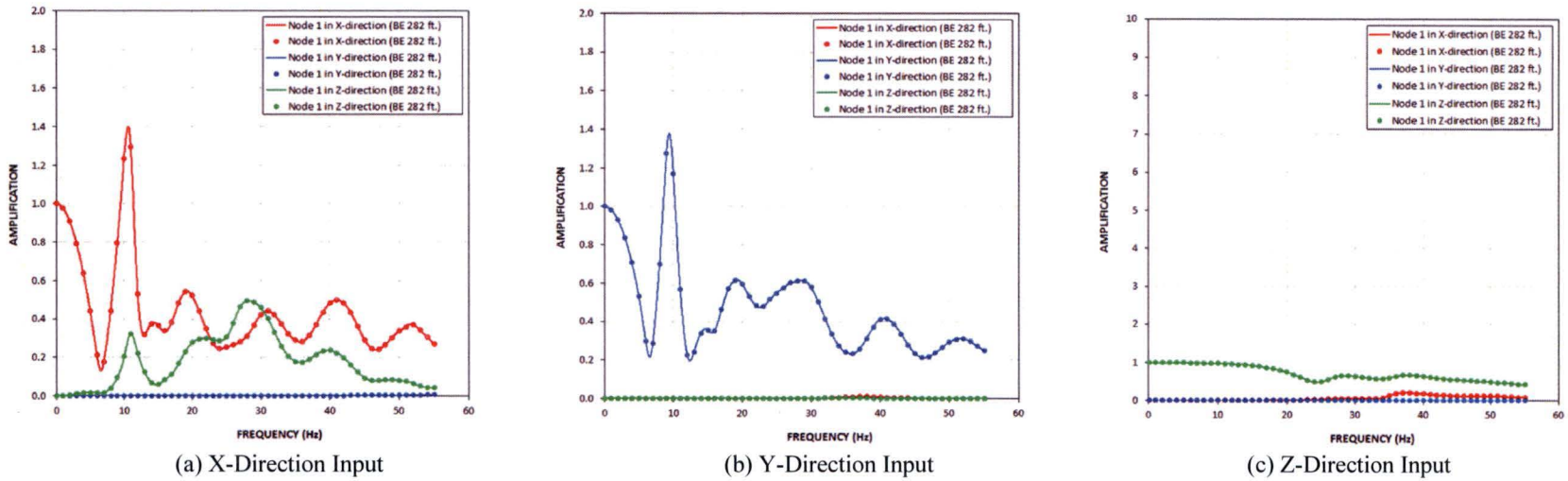

(a) X-Direction Input (b) Y-Direction Input (c) Z-Direction Input

Figure B.3-5b: Transfer Functions for FWS Basemat Response from Analysis of CR_{SSE} Model of BE Profile and Surface Input Motion at El. 282 ft

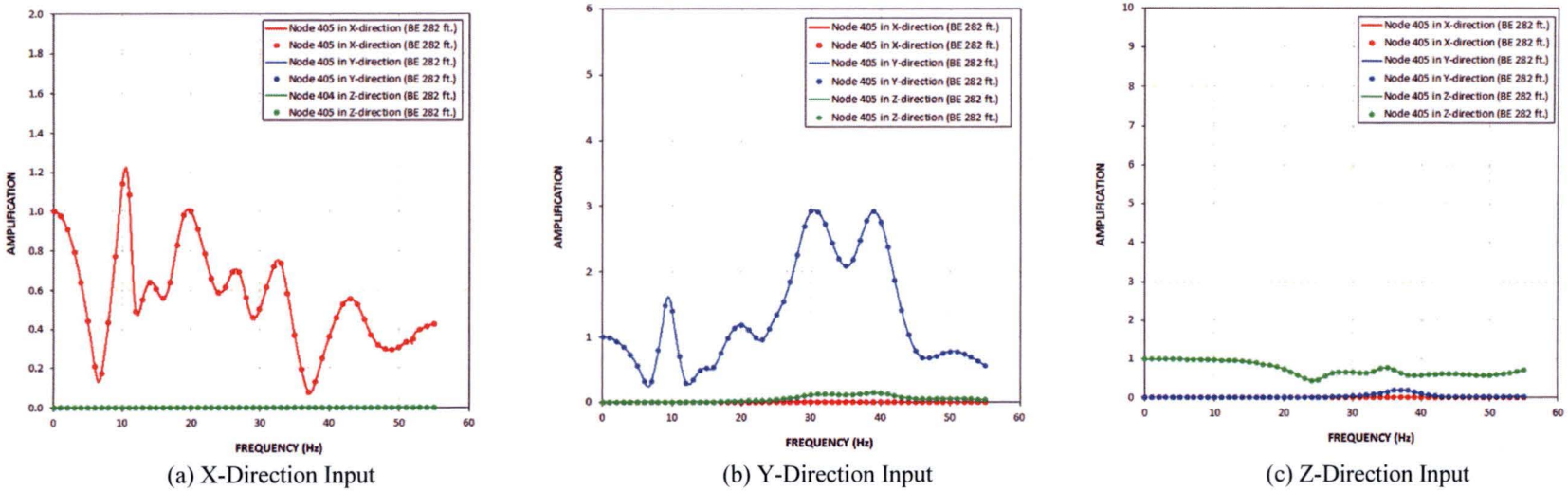

(a) X-Direction Input (b) Y-Direction Input (c) Z-Direction Input

Figure B.3-5c: Transfer Functions for FPE Top Response from Analysis of CR_{SSE} Model of BE Profile and Surface Input Motion at El. 282 ft

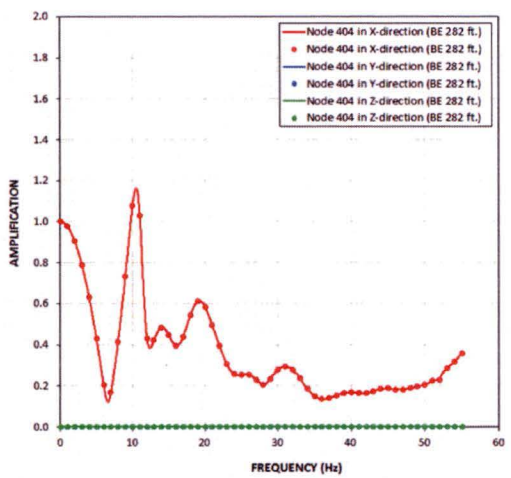

(a) X-Direction Input

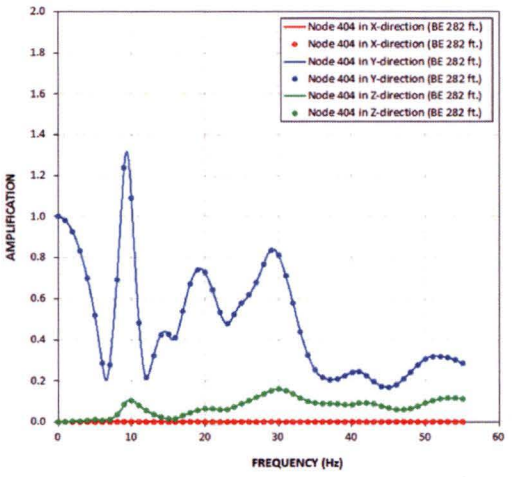

(b) Y-Direction Input

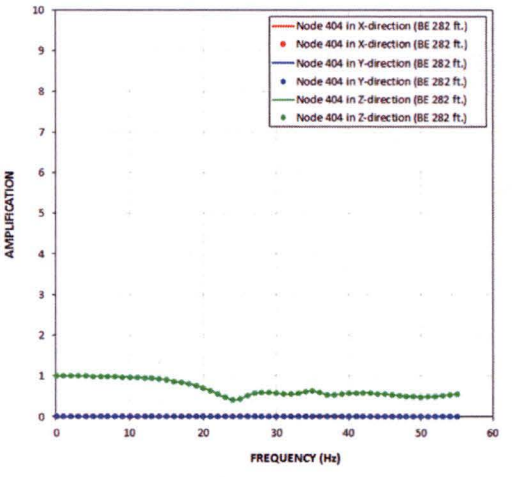

(c) Z-Direction Input

Figure B.3-5d: Transfer Functions for FPE Basemat Response from Analysis of CR_{SSE} Model of BE Profile and Surface Input Motion at El. 282 ft

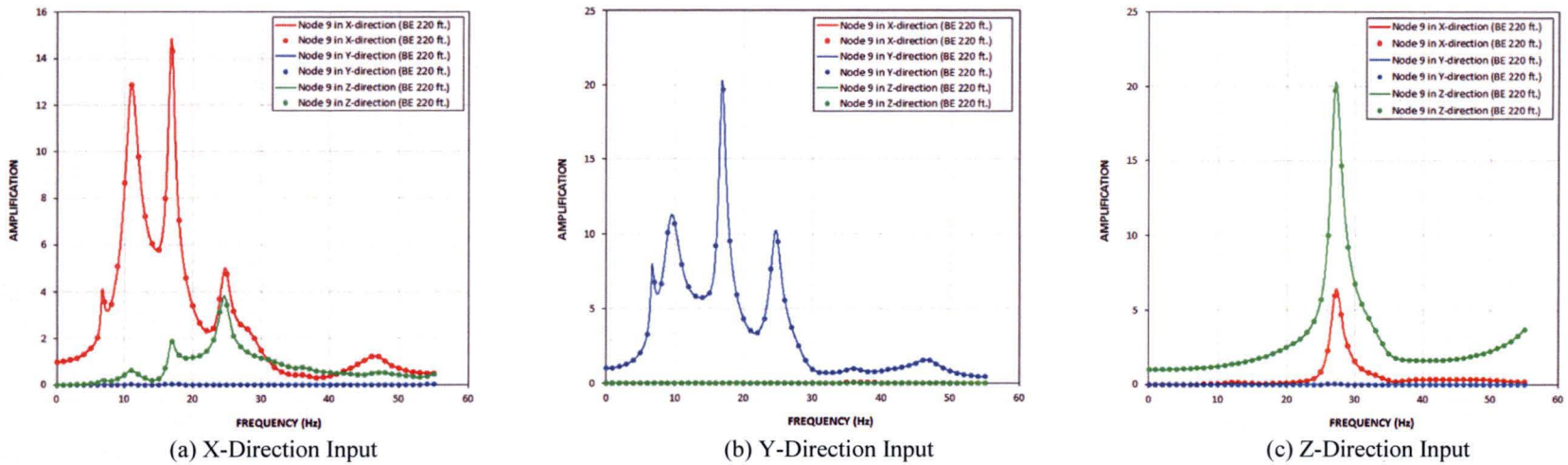

(a) X-Direction Input (b) Y-Direction Input (c) Z-Direction Input

Figure B.3-6a: Transfer Functions for FWS Wall Top Response from Analysis of CR_{SSE} Model of BE Profile and Deep Input Motion at El. 220 ft

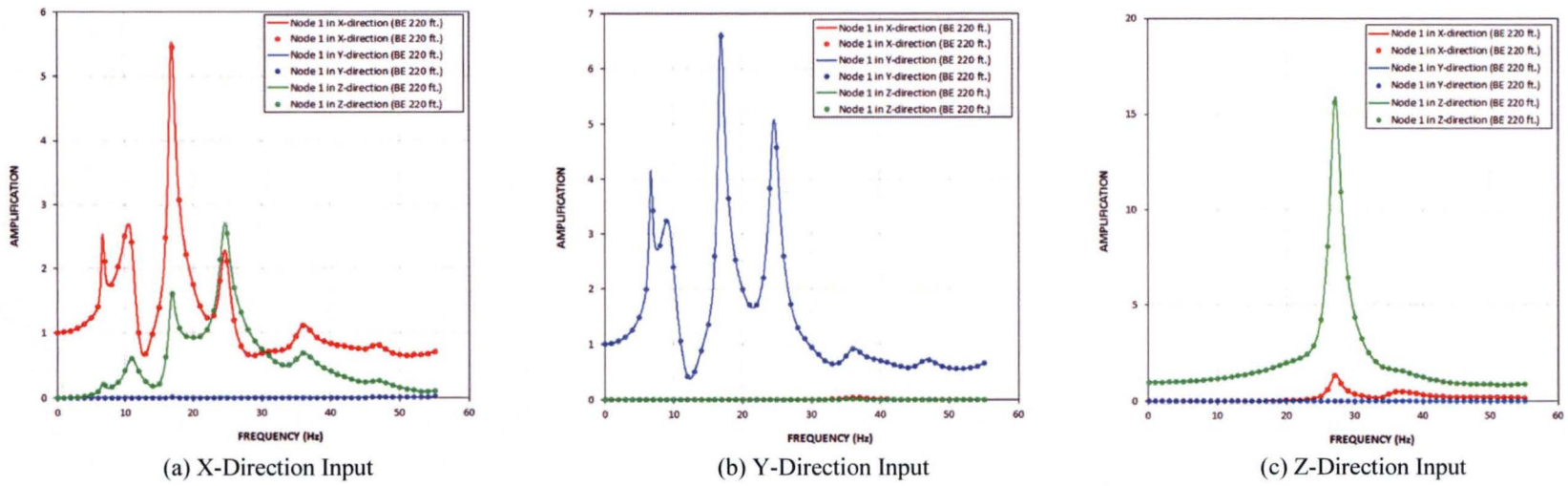

(a) X-Direction Input (b) Y-Direction Input (c) Z-Direction Input

Figure B.3-6b: Transfer Functions for FWS Basemat Response from Analysis of CR_{SSE} Model of BE Profile and Deep Input Motion at El. 220 ft

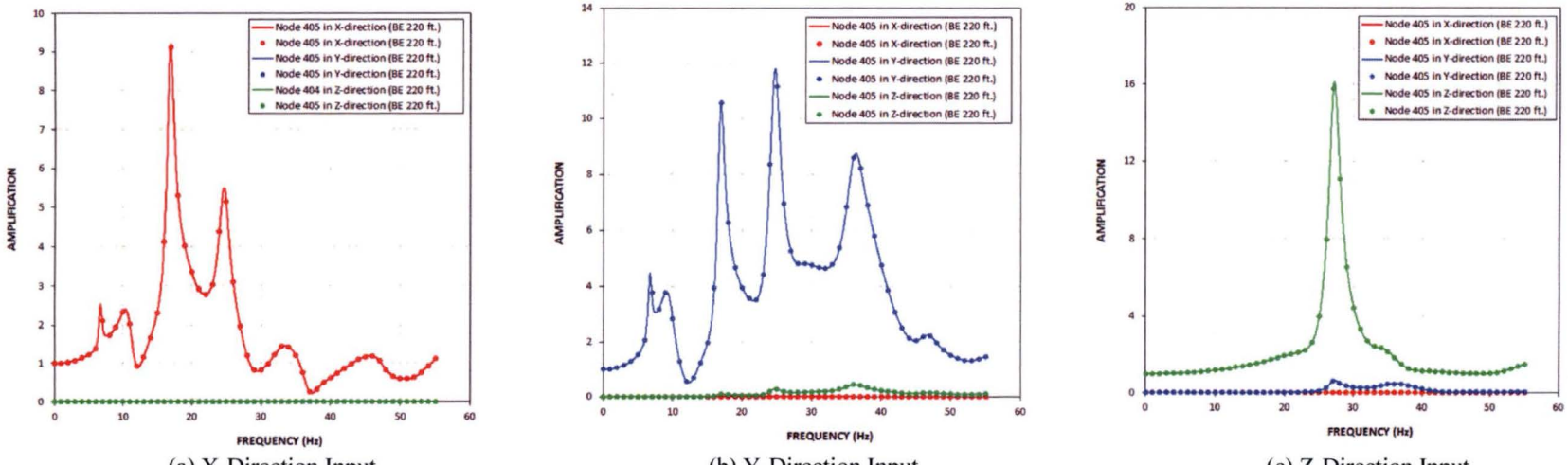

(a) X-Direction Input (b) Y-Direction Input (c) Z-Direction Input

Figure B.3-6c: Transfer Functions for FPE Top Response from Analysis of CR_{SSE} Model of BE Profile and Deep Input Motion at El. 220 ft

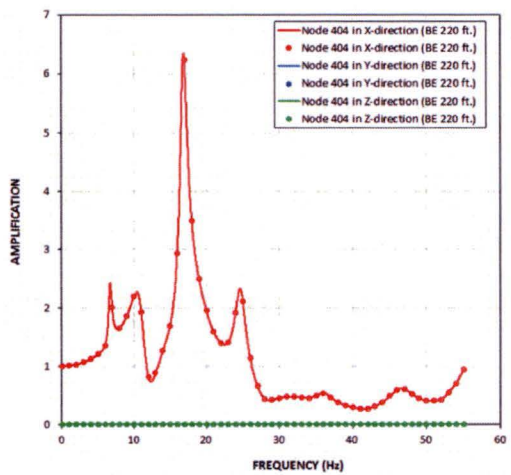

(a) X-Direction Input

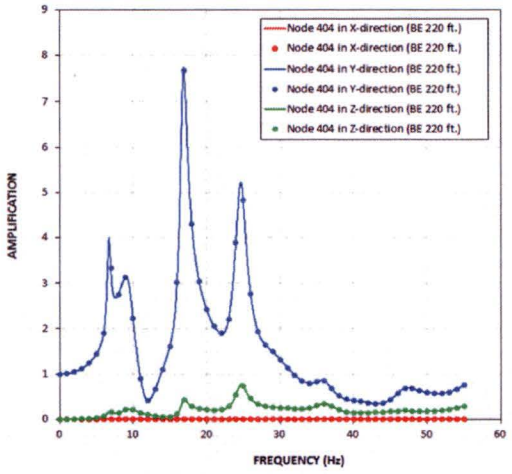

(b) Y-Direction Input

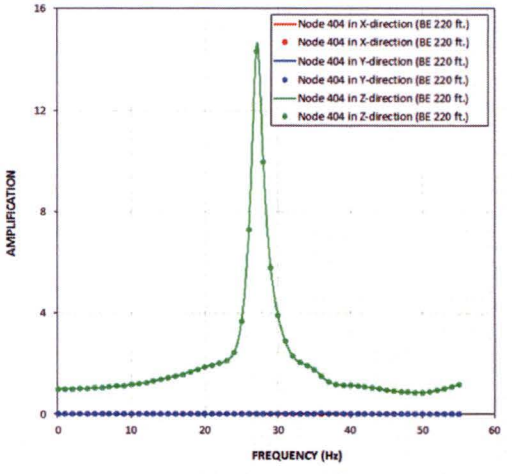

(c) Z-Direction Input

Figure B.3-6d: Transfer Functions for FPE Basemat Response from Analysis of CR_{SSE} Model of BE Profile and Deep Input Motion at El. 220 ft

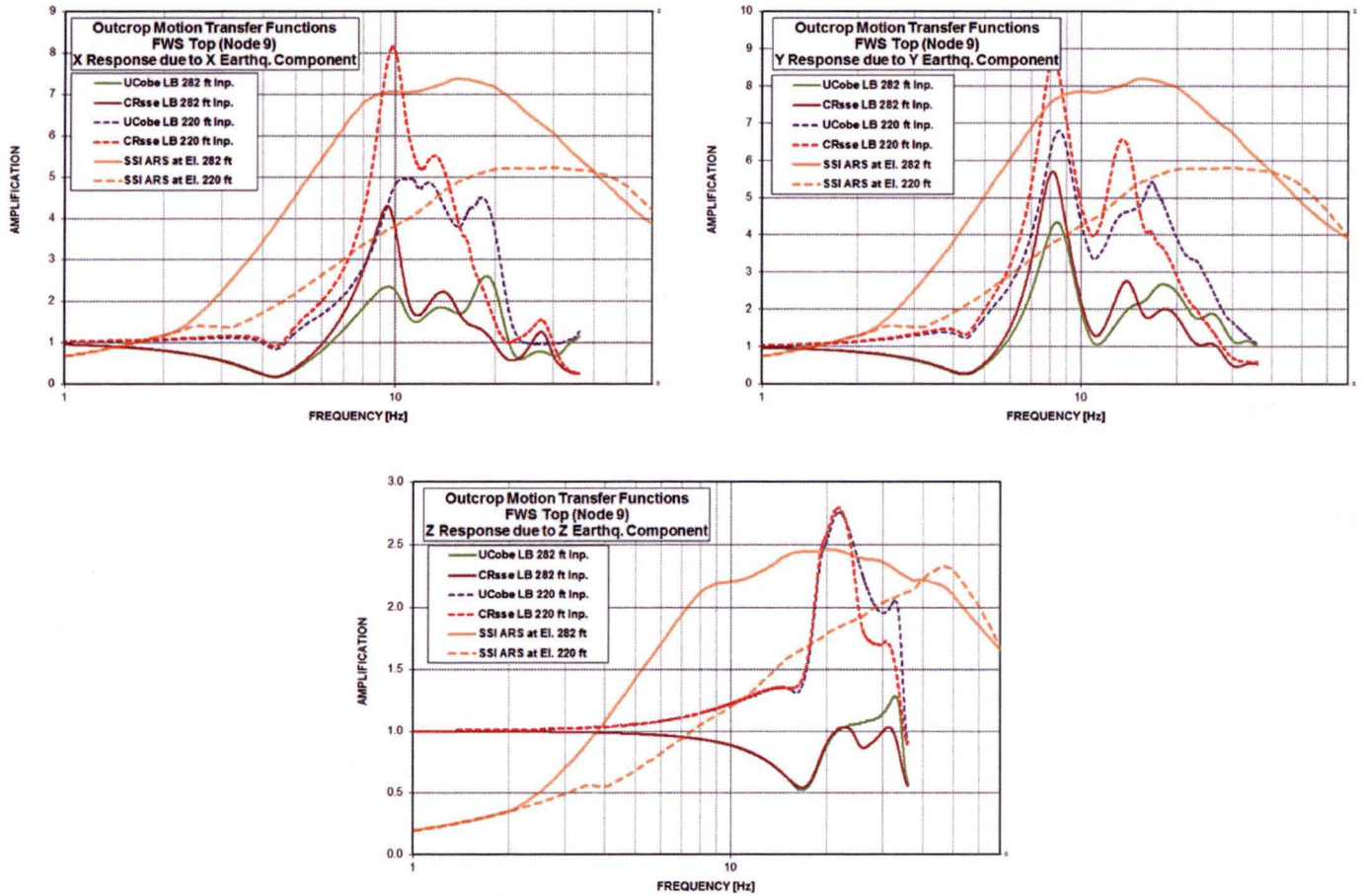

Figure B.3-7a: Outcrop Motion Transfer Functions for FWS Response – LB Subgrade Profile Analyses

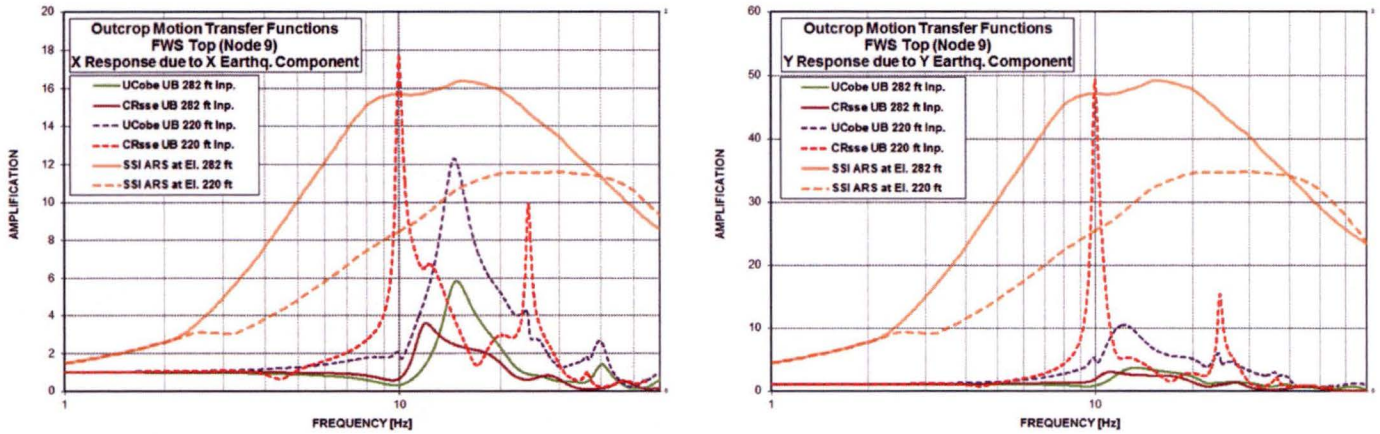

Figure B.3-7b: Outcrop Motion Transfer Functions for FWS Response – UB Subgrade Profile Analyses

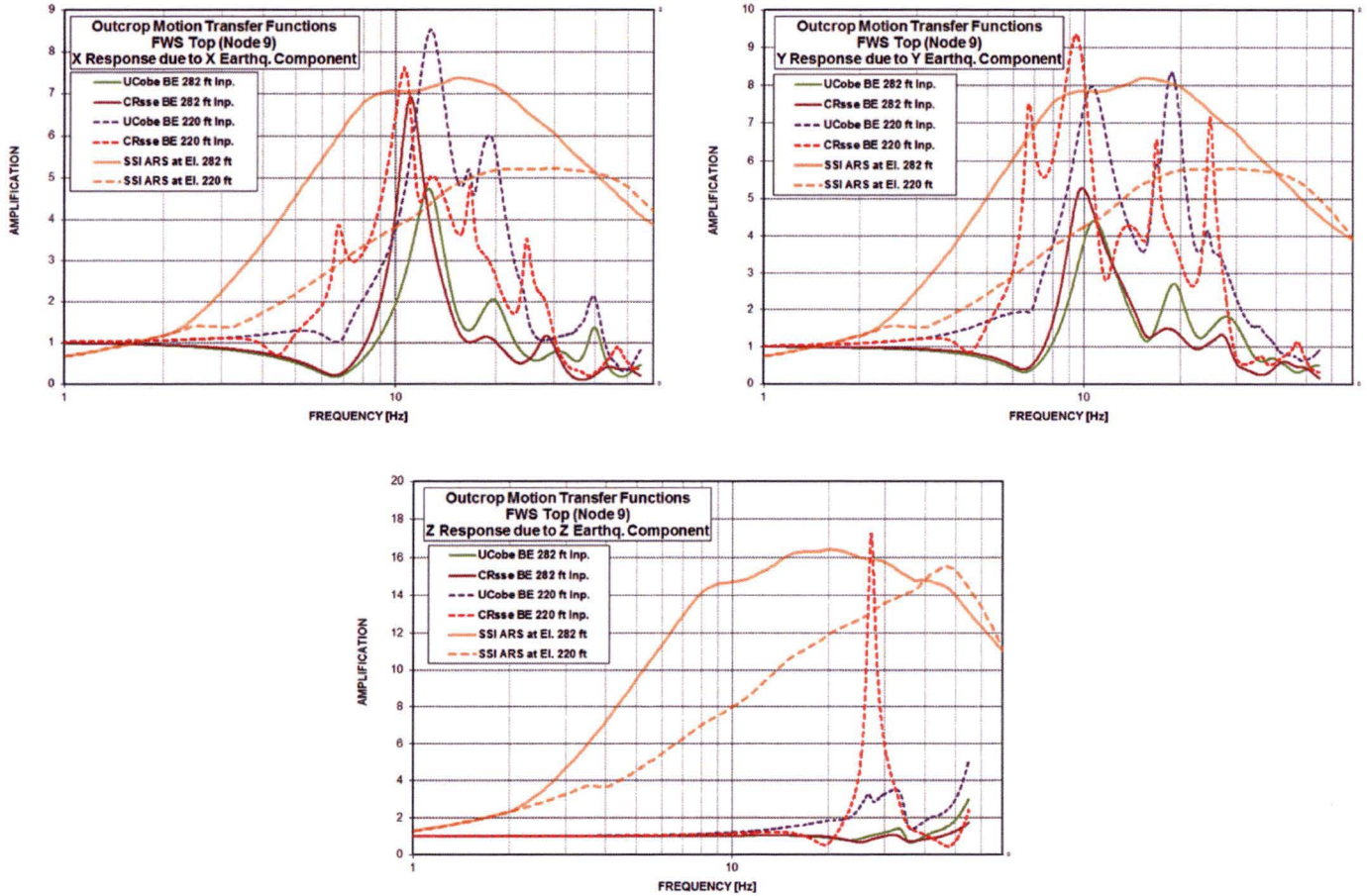

Figure B.3-7c: Outcrop Motion Transfer Functions for FWS Response – BE Subgrade Profile Analyses

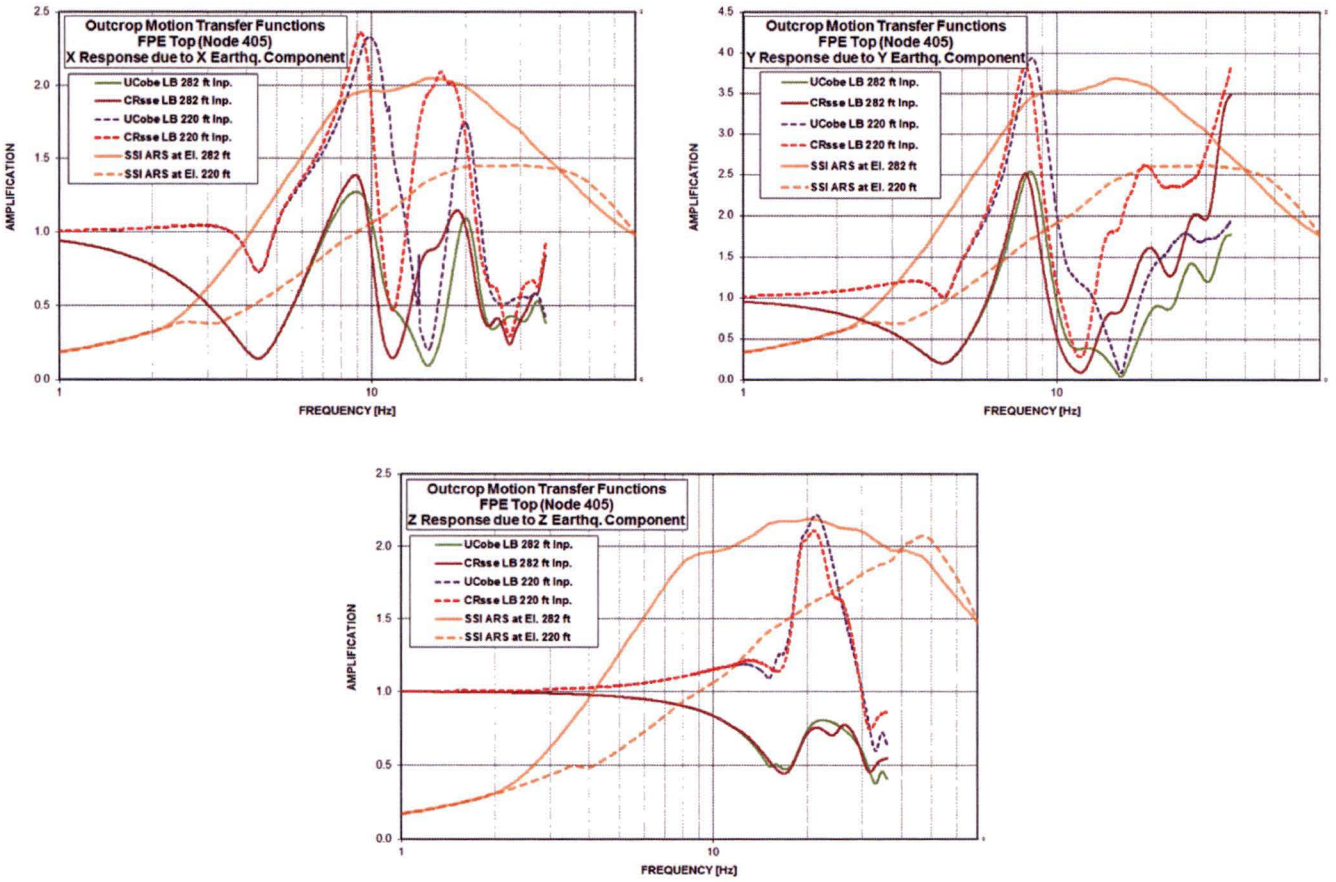

Figure B.3-8a: Outcrop Motion Transfer Functions for FPE Response – LB Subgrade Profile Analyses

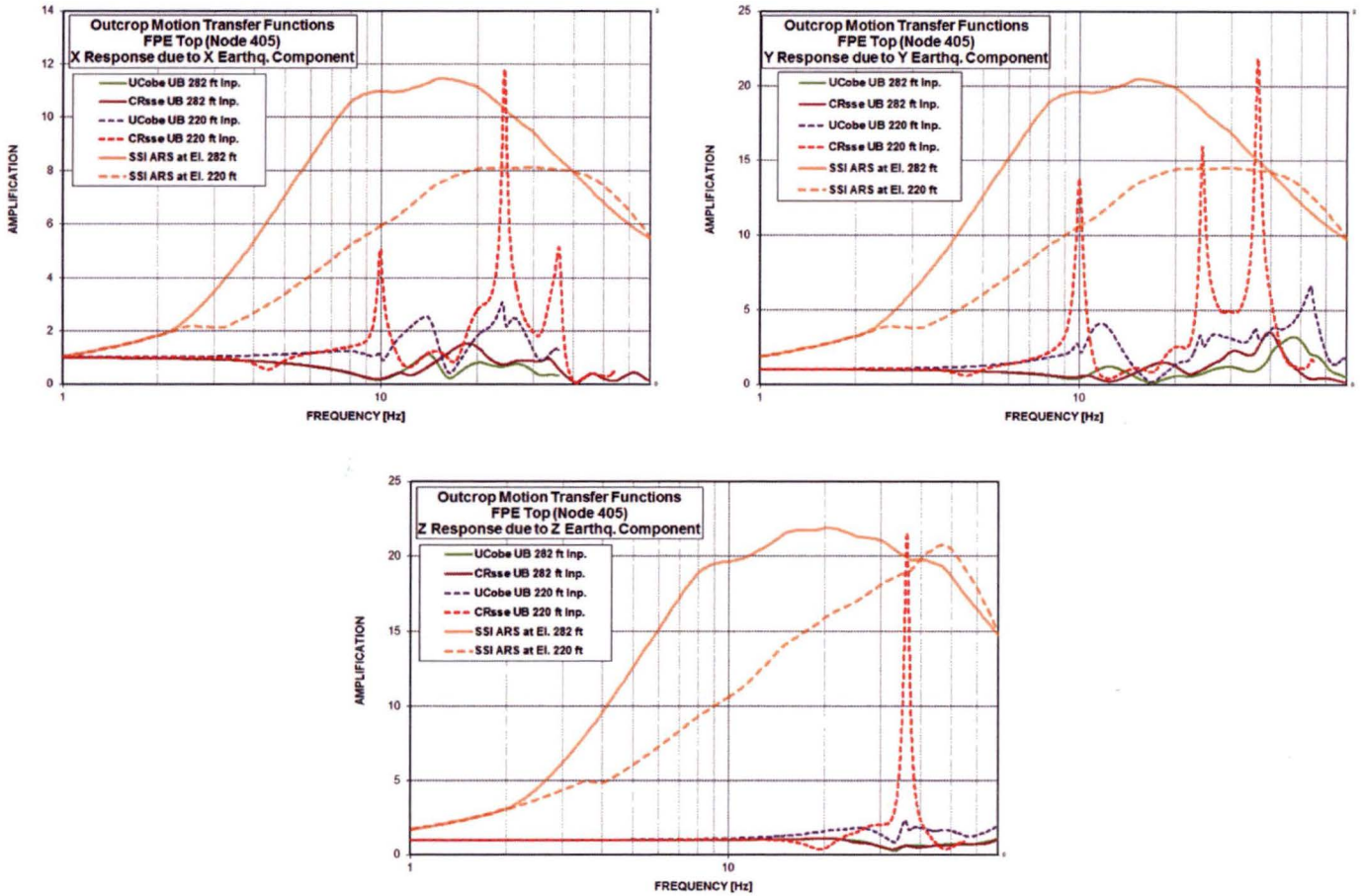

Figure B.3-8b: Outcrop Motion Transfer Functions for FPE Response – UB Subgrade Profile Analyses

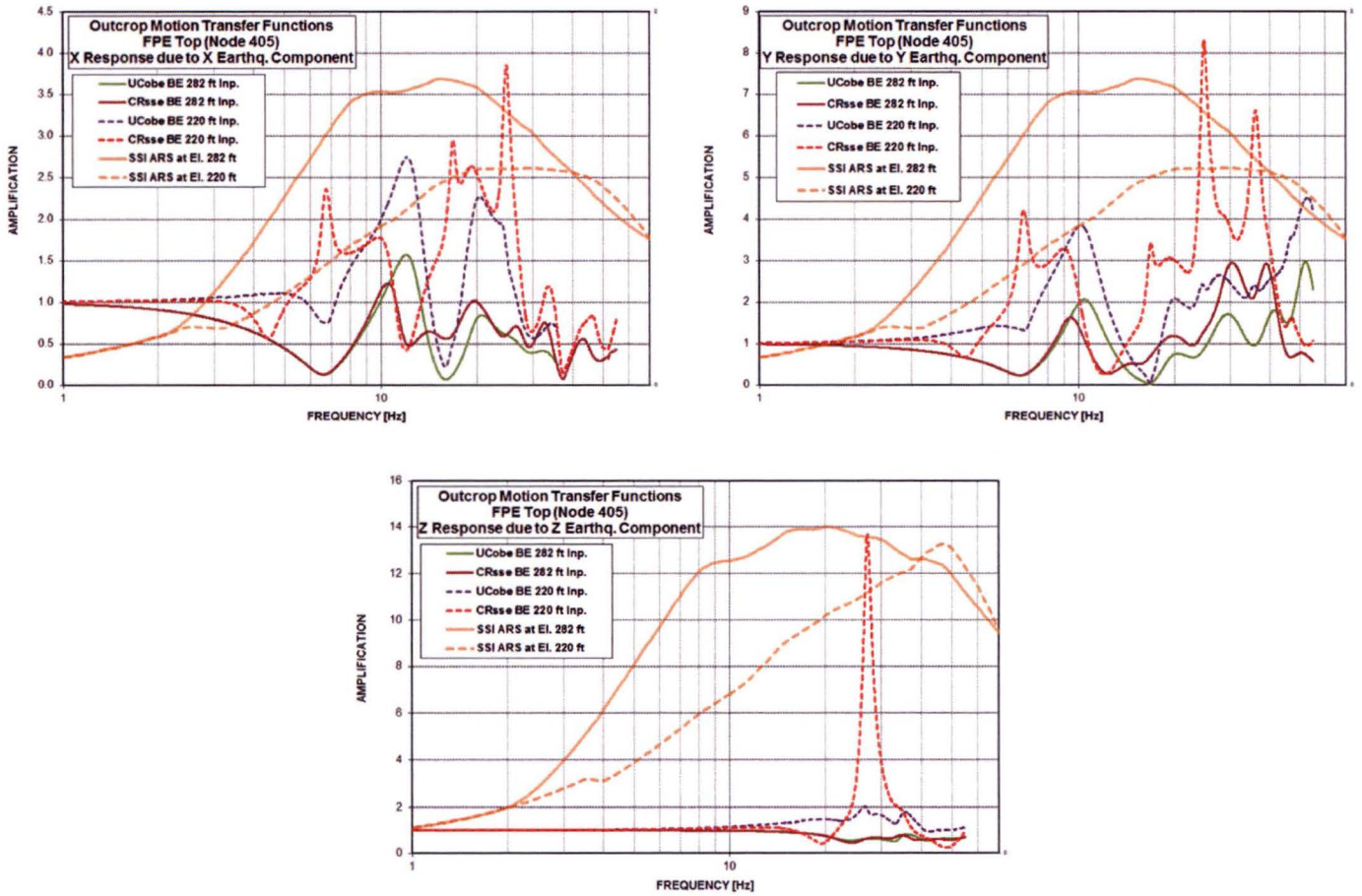

Figure B.3-8c: Outcrop Motion Transfer Functions for FPE Response – BE Subgrade Profile Analyses

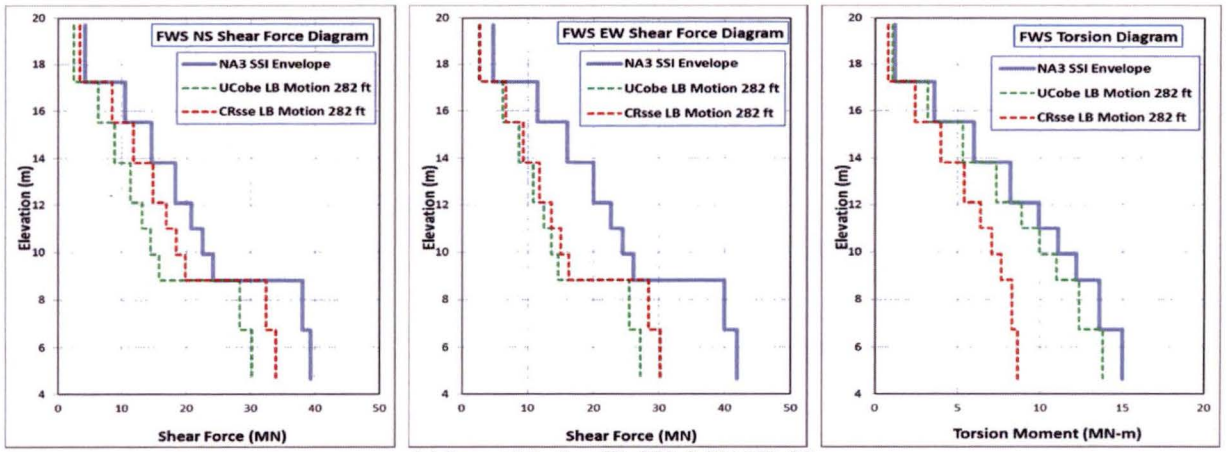

(a) **Input Motion El. 282 ft NAVD 88**

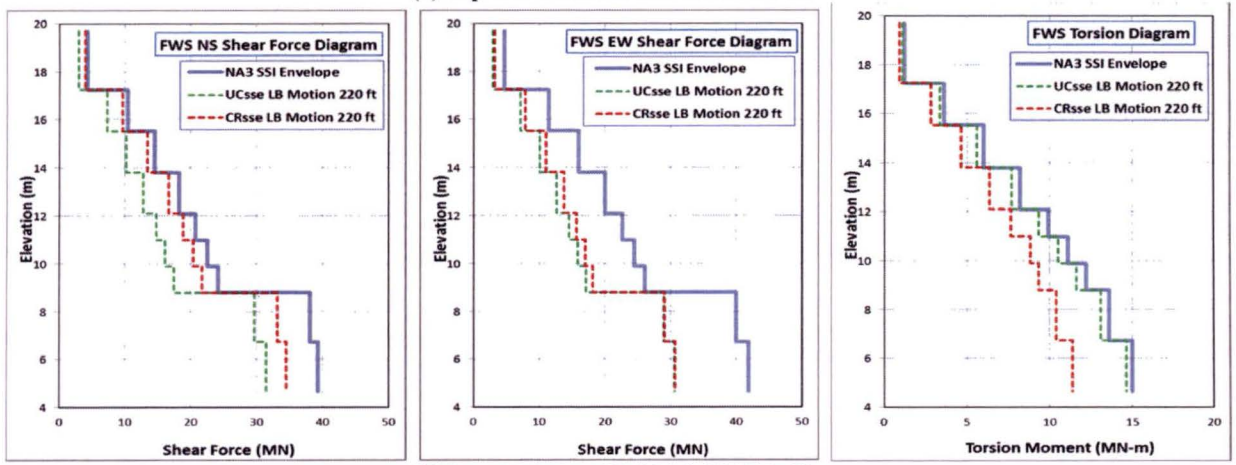

(b) **Input Motion El. 220 ft NAVD 88**

Figure B.4-1: Comparison of Horizontal Seismic Load Demands on FWS from LB Profile Analyses

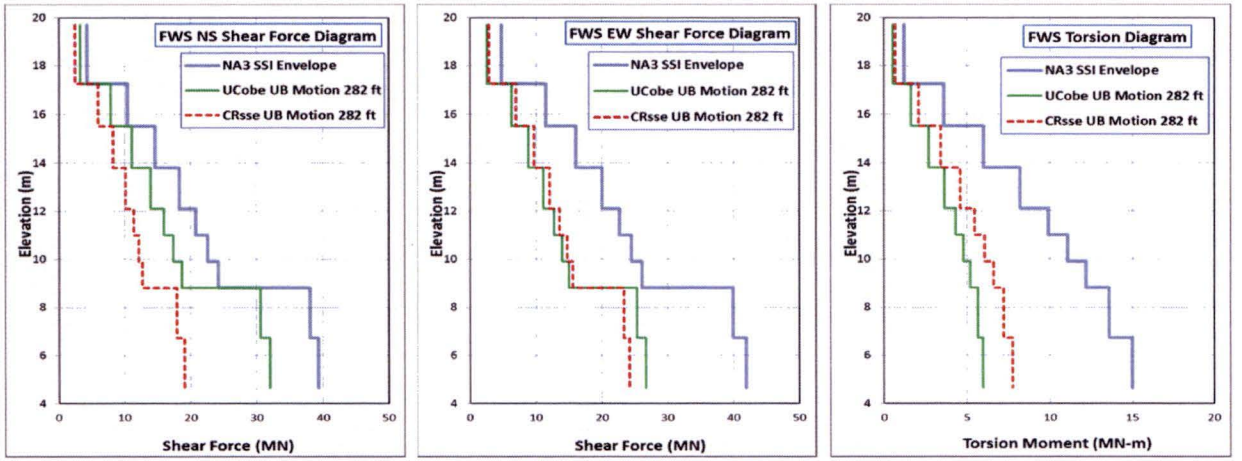

(a) **Input Motion El. 282 ft NAVD 88**

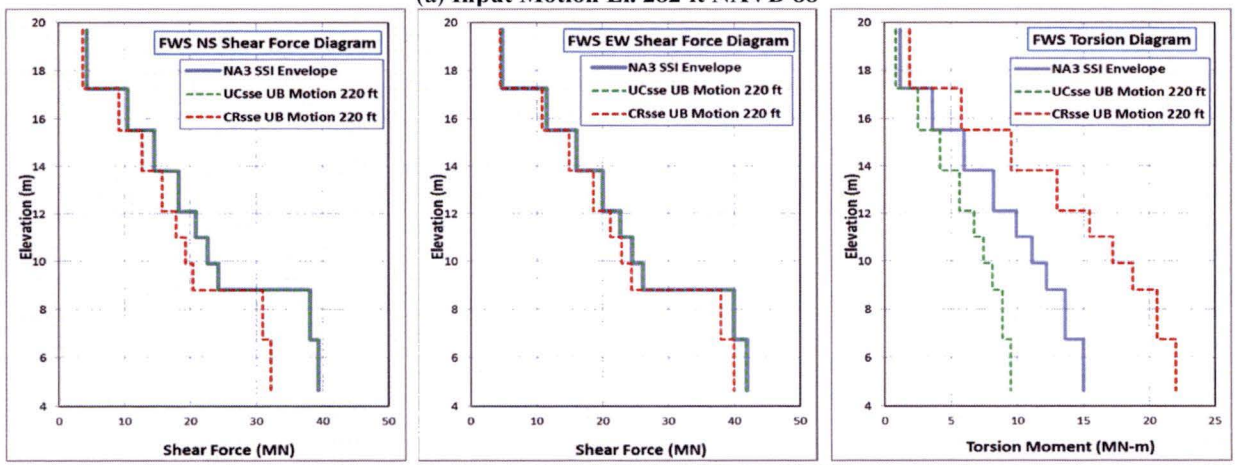

(b) **Input Motion El. 220 ft NAVD 88**

Figure B.4-2: Comparison of Horizontal Seismic Load Demands on FWS from UB Profile Analyses

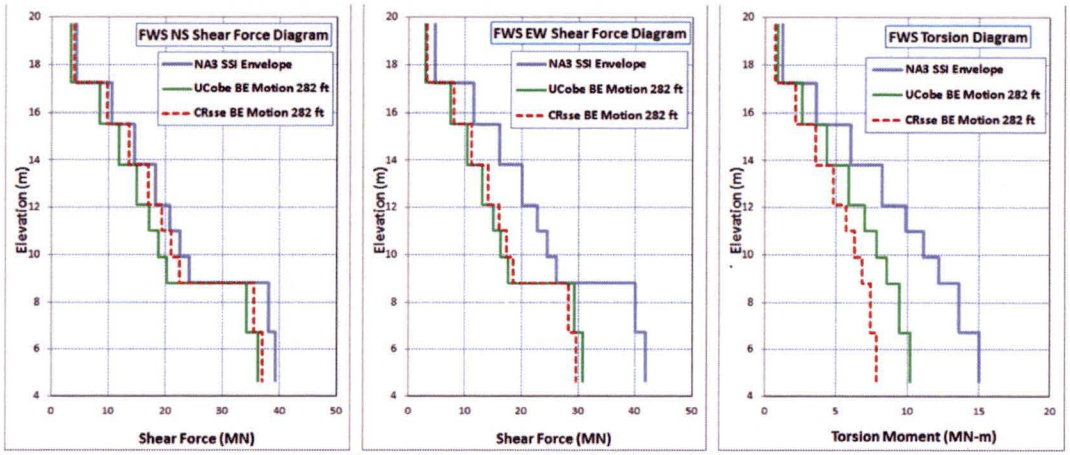

(a) **Input Motion El. 282 ft NAVD 88**

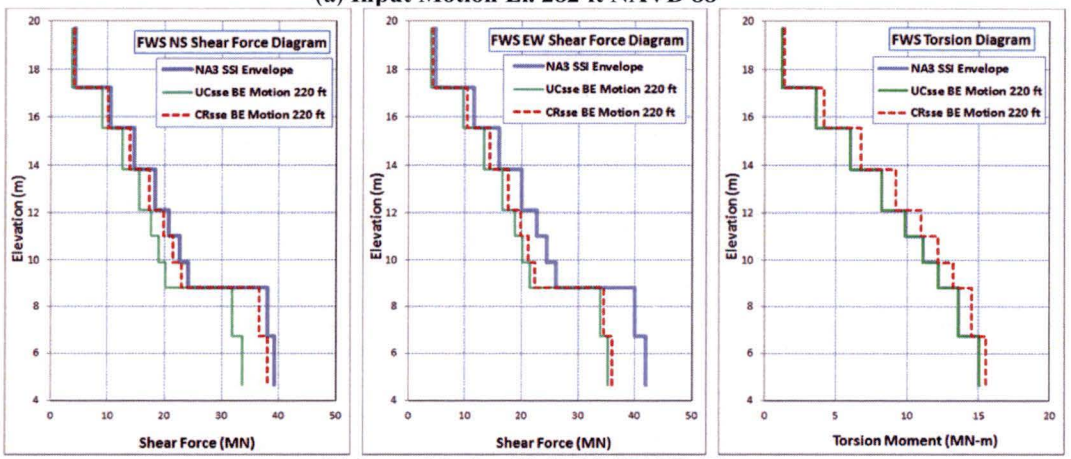

(b) **Input Motion El. 220 ft NAVD 88**

Figure B.4-3: Comparison of Horizontal Seismic Load Demands on FWS from BE Profile Analyses

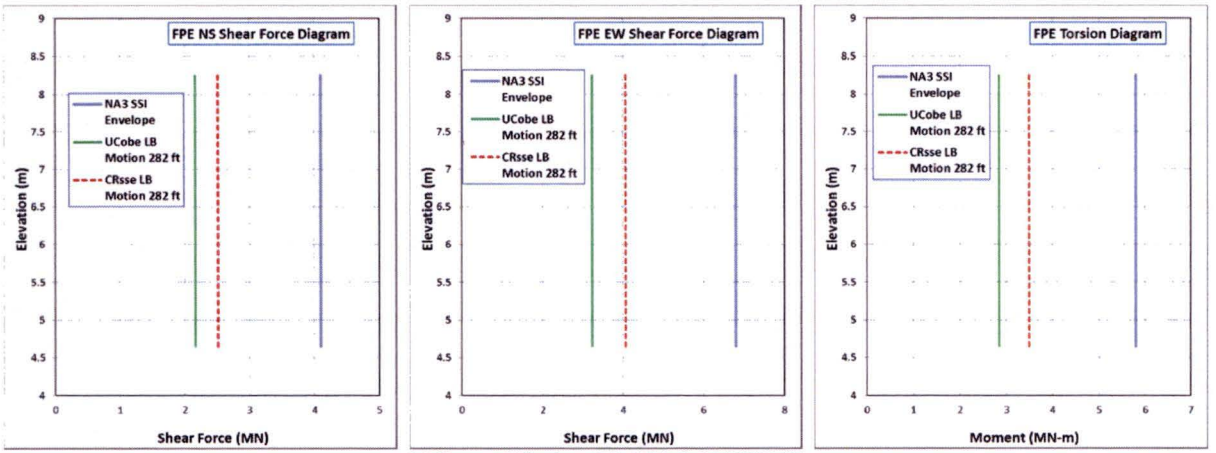

(a) **Input Motion El. 282 ft NAVD 88**

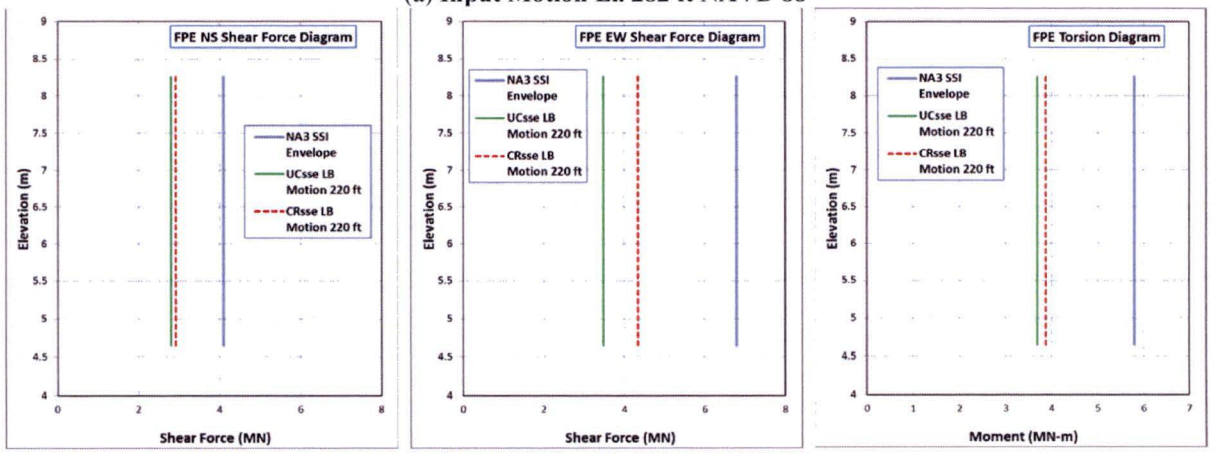

(b) **Input Motion El. 220 ft NAVD 88**

Figure B.4-4: Comparison of Horizontal Seismic Load Demands on FPE from LB Profile Analyses

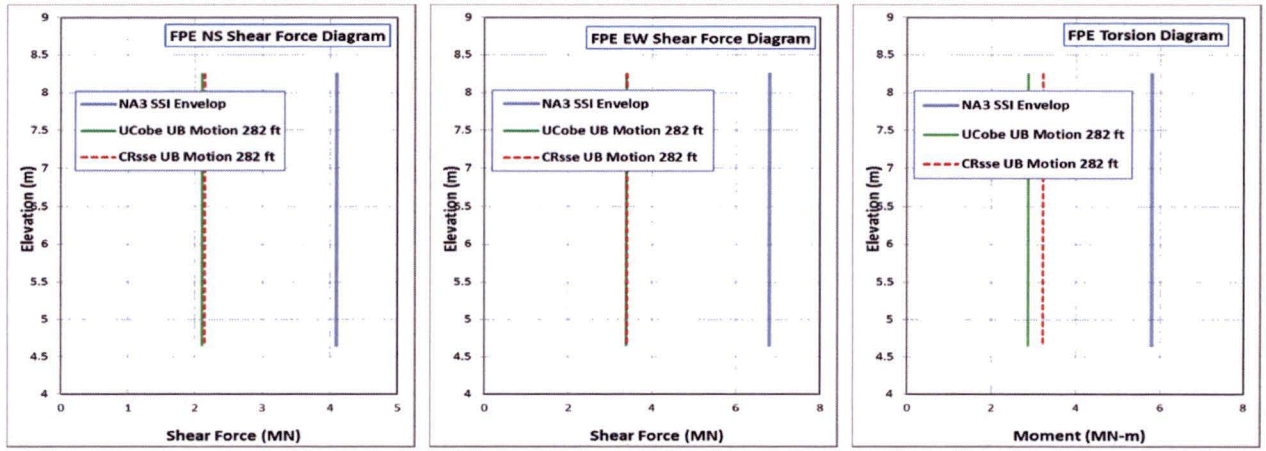

(a) **Input Motion El. 282 ft NAVD 88**

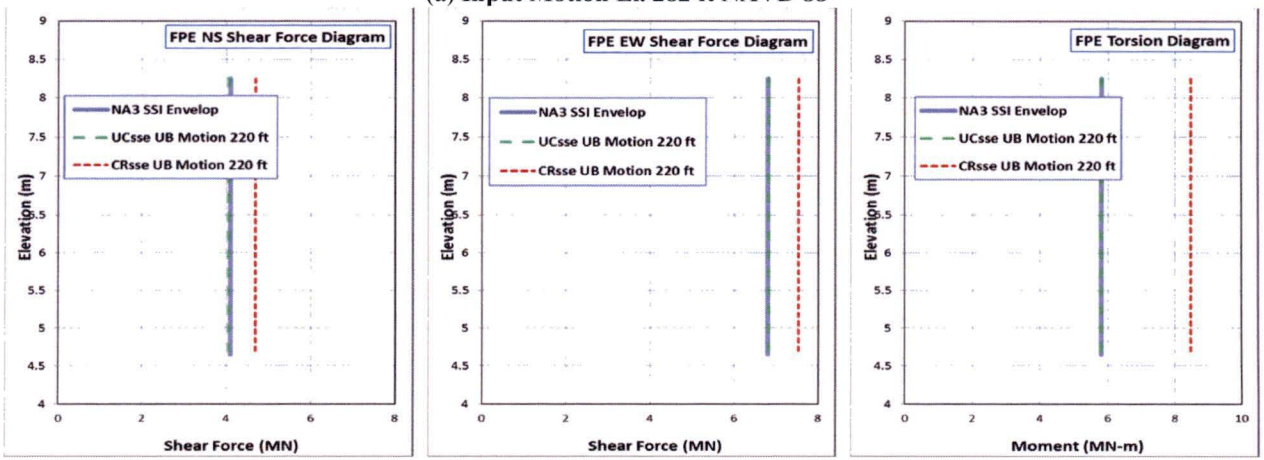

(b) **Input Motion El. 220 ft NAVD 88**

Figure B.4-5: Comparison of Horizontal Seismic Load Demands on FPE from UB Profile Analyses

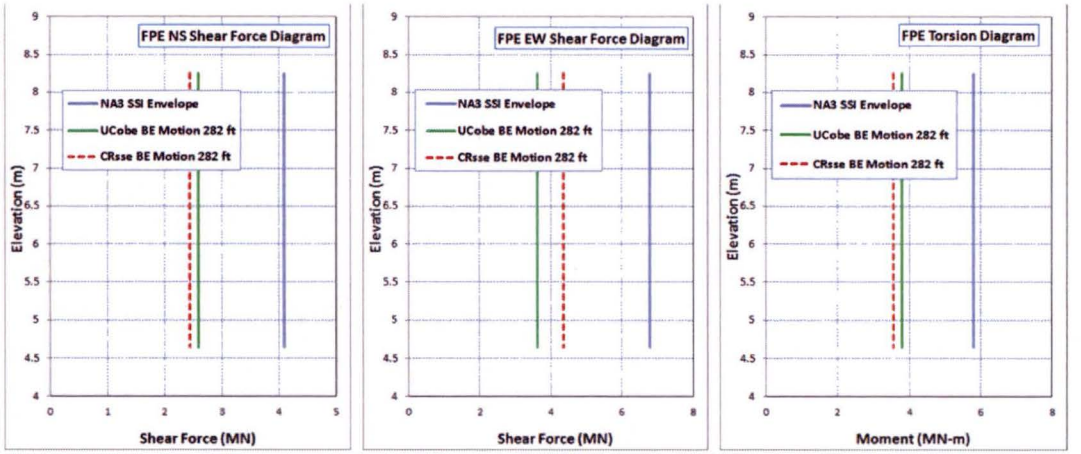

(a) **Input Motion El. 282 ft NAVD 88**

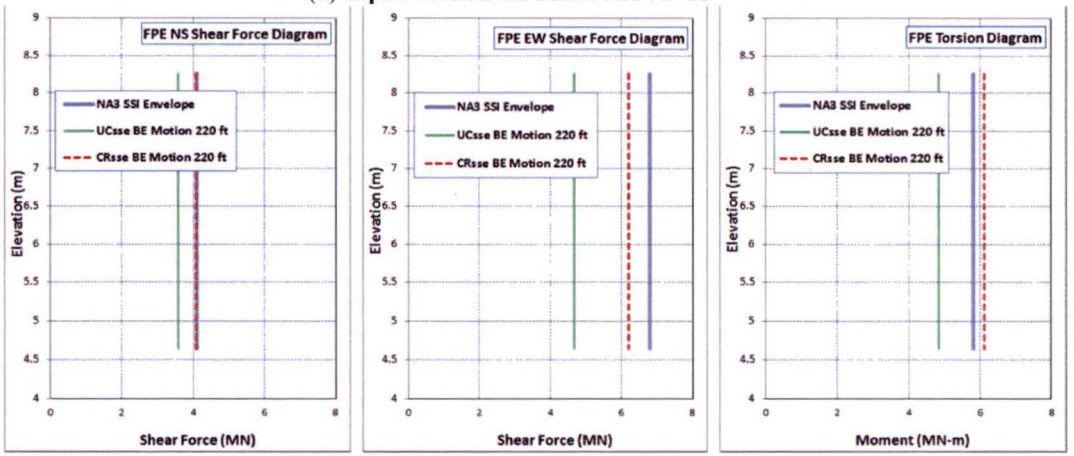

(b) **Input Motion El. 220 ft NAVD 88**

Figure B.4-6: Comparison of Horizontal Seismic Load Demands on FPE from BE Profile Analyses

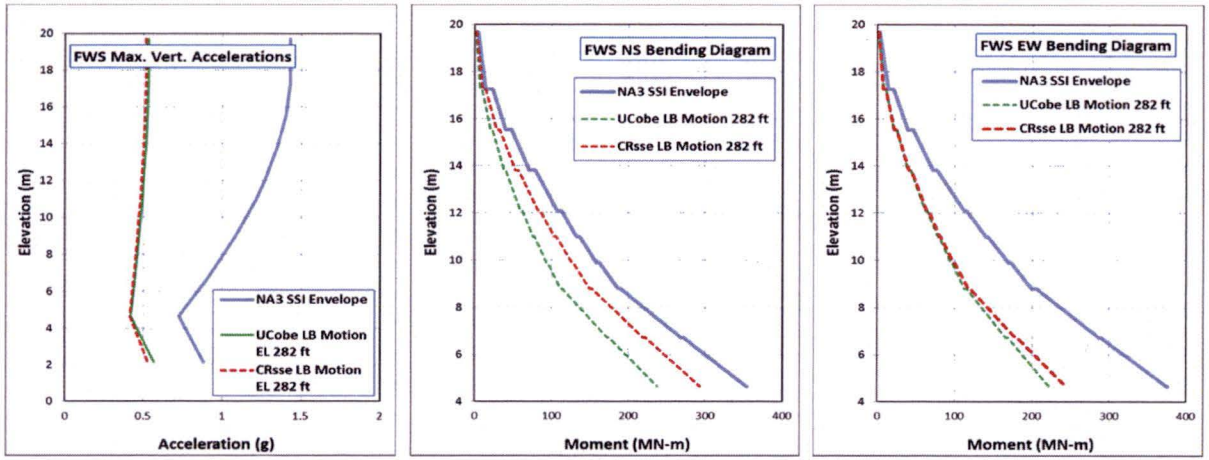

(a) **Input Motion El. 282 ft NAVD 88**

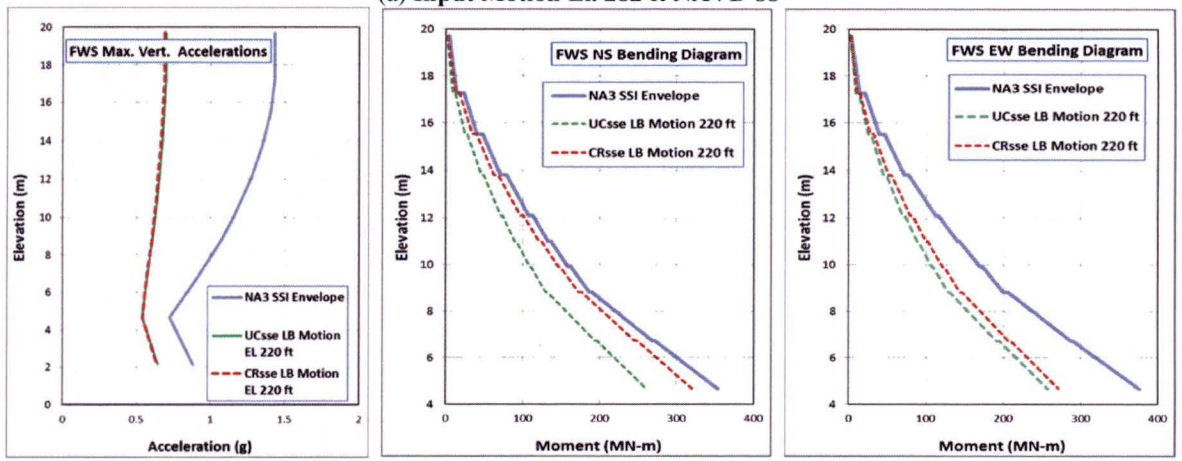

(b) **Input Motion El. 220 ft NAVD 88**

Figure B.4-7: Comparison of Vertical Seismic Load Demands on FWS from LB Analyses

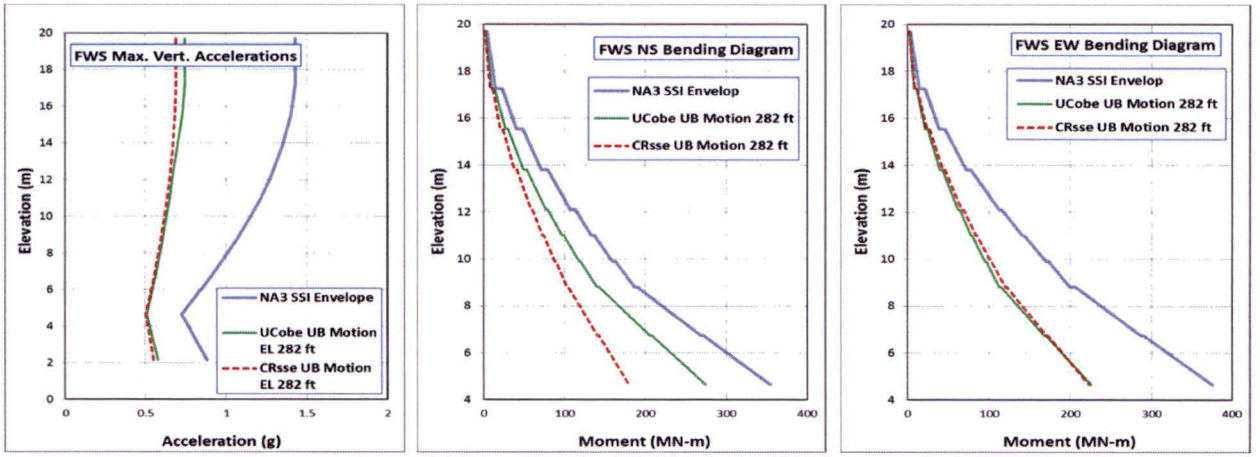

(a) **Input Motion El. 282 ft NAVD 88**

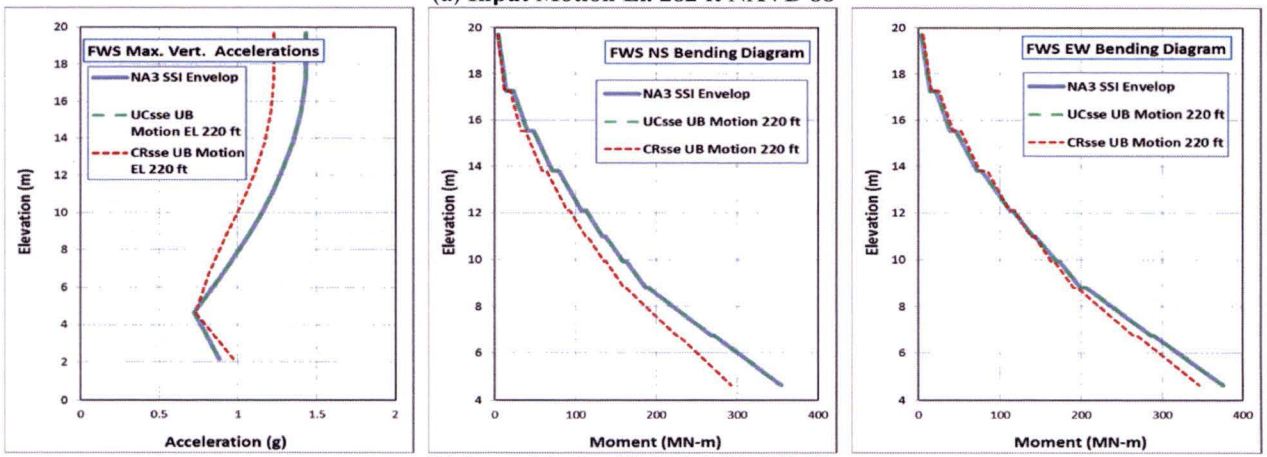

(b) **Input Motion El. 220 ft NAVD 88**

Figure B.4-8: Comparison of Vertical Seismic Load Demands on FWS from UB Analyses

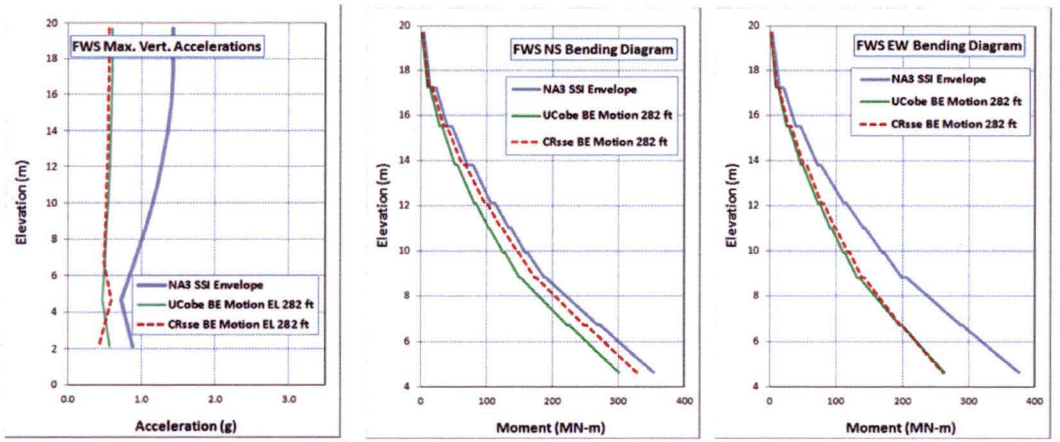

(a) **Input Motion El. 282 ft NAVD 88**

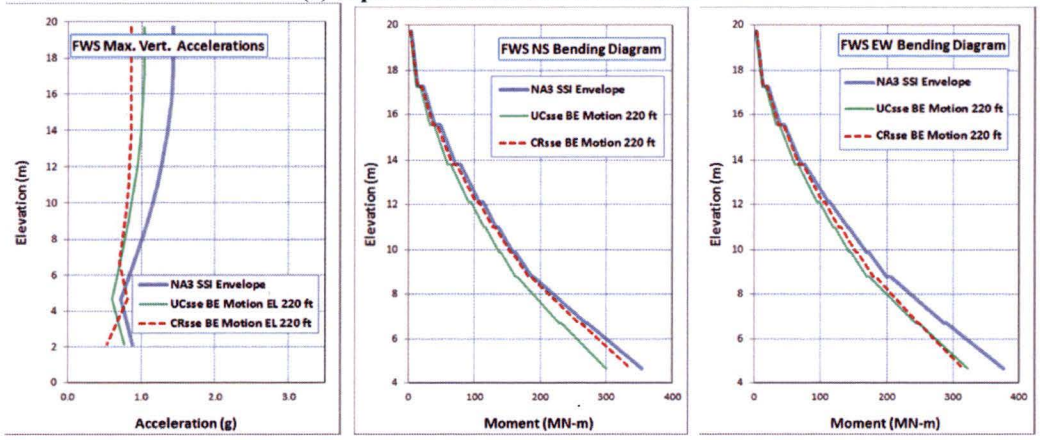

(b) **Input Motion El. 220 ft NAVD 88**

Figure B.4-9: Comparison of Vertical Seismic Load Demands on FWS from BE Analyses

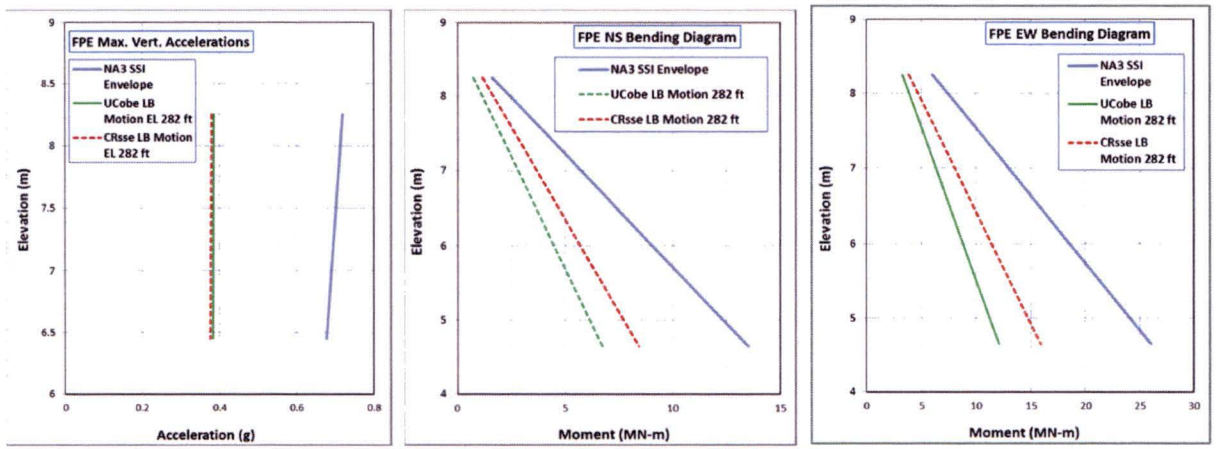

(a) **Input Motion El. 282 ft NAVD 88**

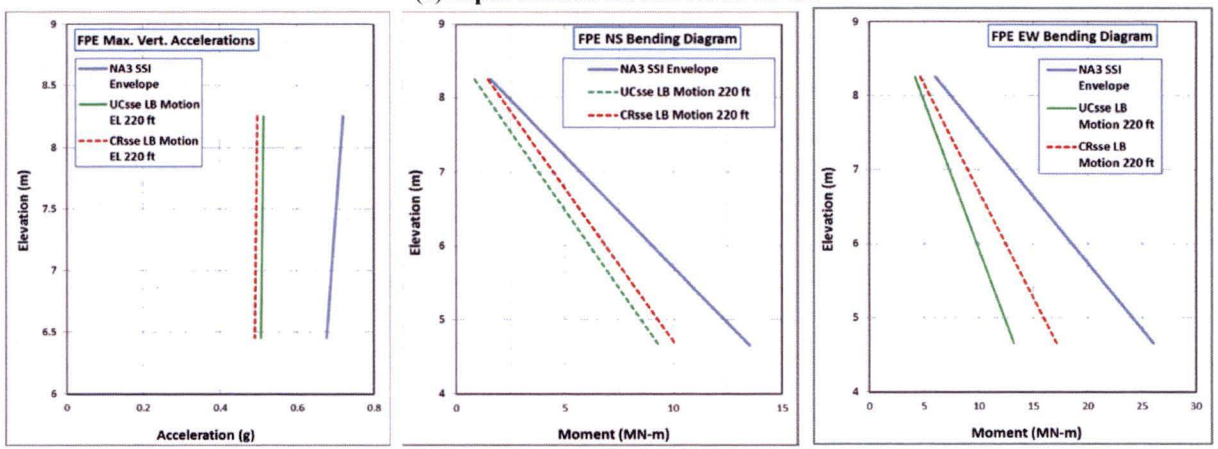

(b) **Input Motion El. 220 ft NAVD 88**

Figure B.4-10: Comparison of Vertical Seismic Load Demands on FPE from LB Analyses

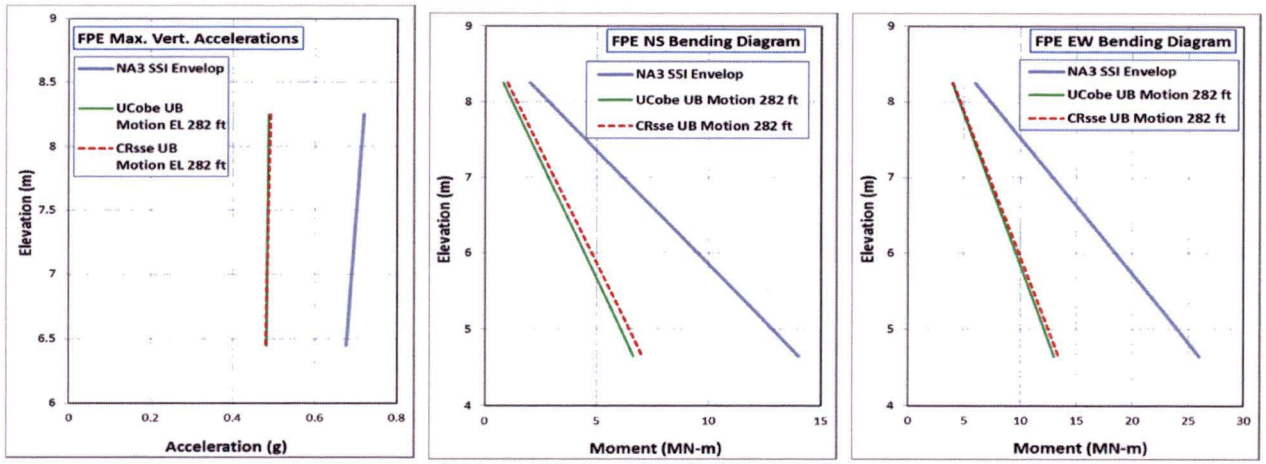

(a) **Input Motion El. 282 ft NAVD 88**

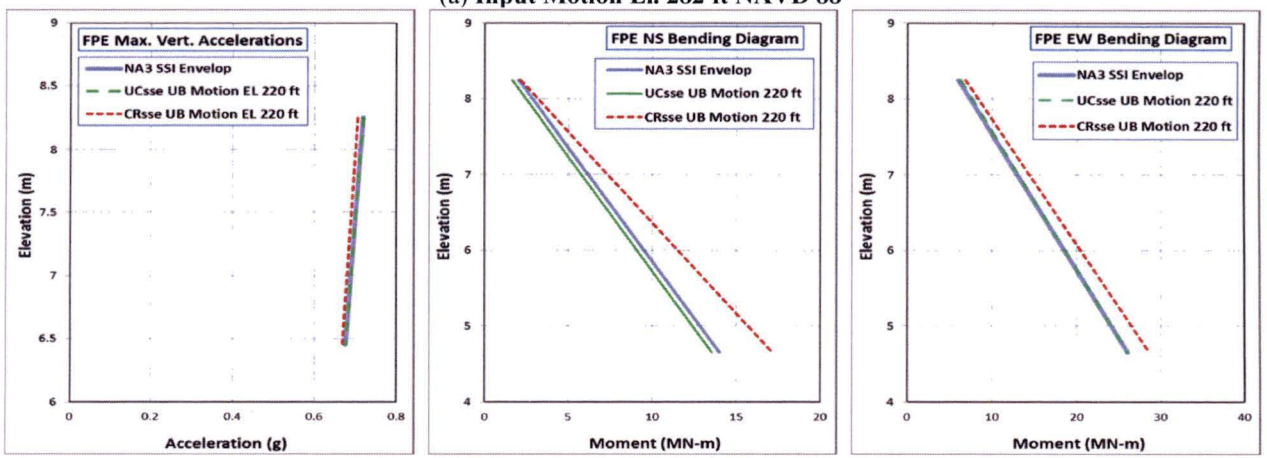

(b) **Input Motion El. 220 ft NAVD 88**

Figure B.4-11: Comparison of Vertical Seismic Load Demands on FPE from UB Analyses

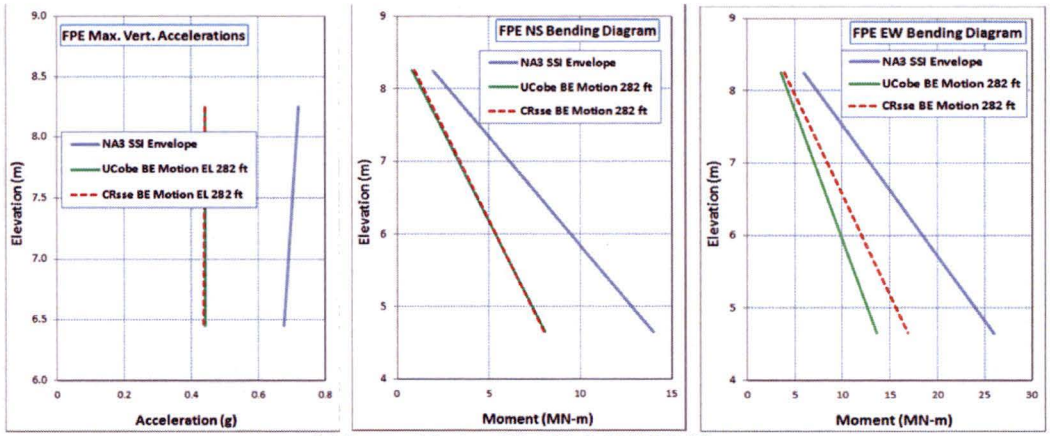

(a) **Input Motion El. 282 ft NAVD 88**

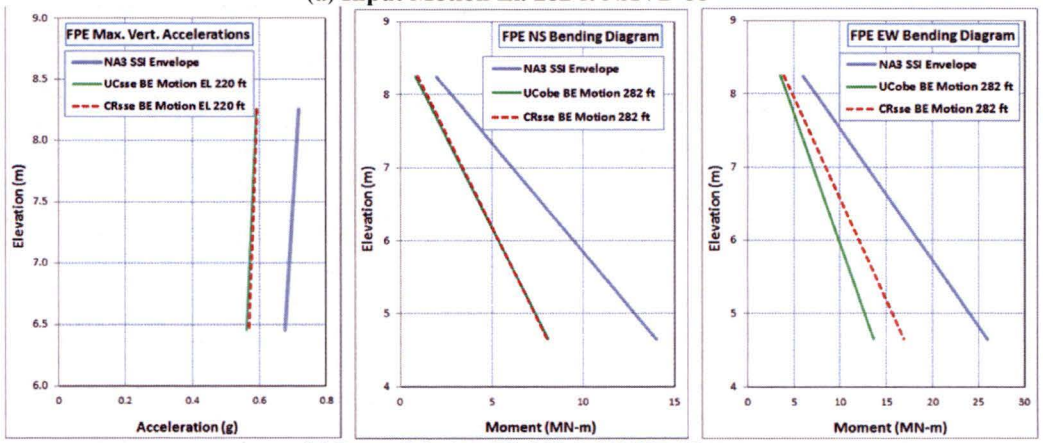

(b) **Input Motion El. 220 ft NAVD 88**

Figure B.4-12: Comparison of Vertical Seismic Load Demands on FPE from BE Analyses

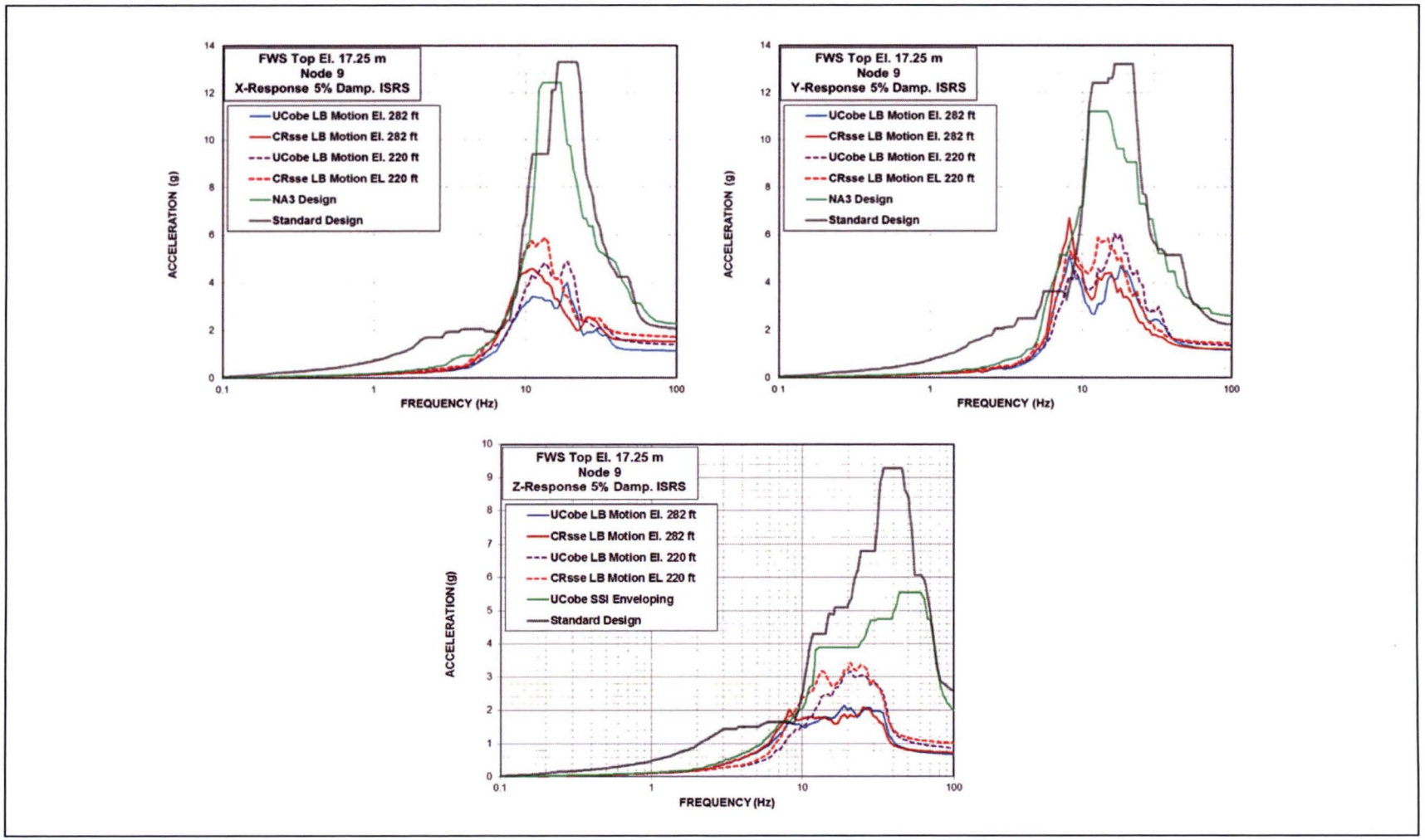

Figure B.4-13: Comparison of ISRS – FWS Wall Top for LB Profile Analyses

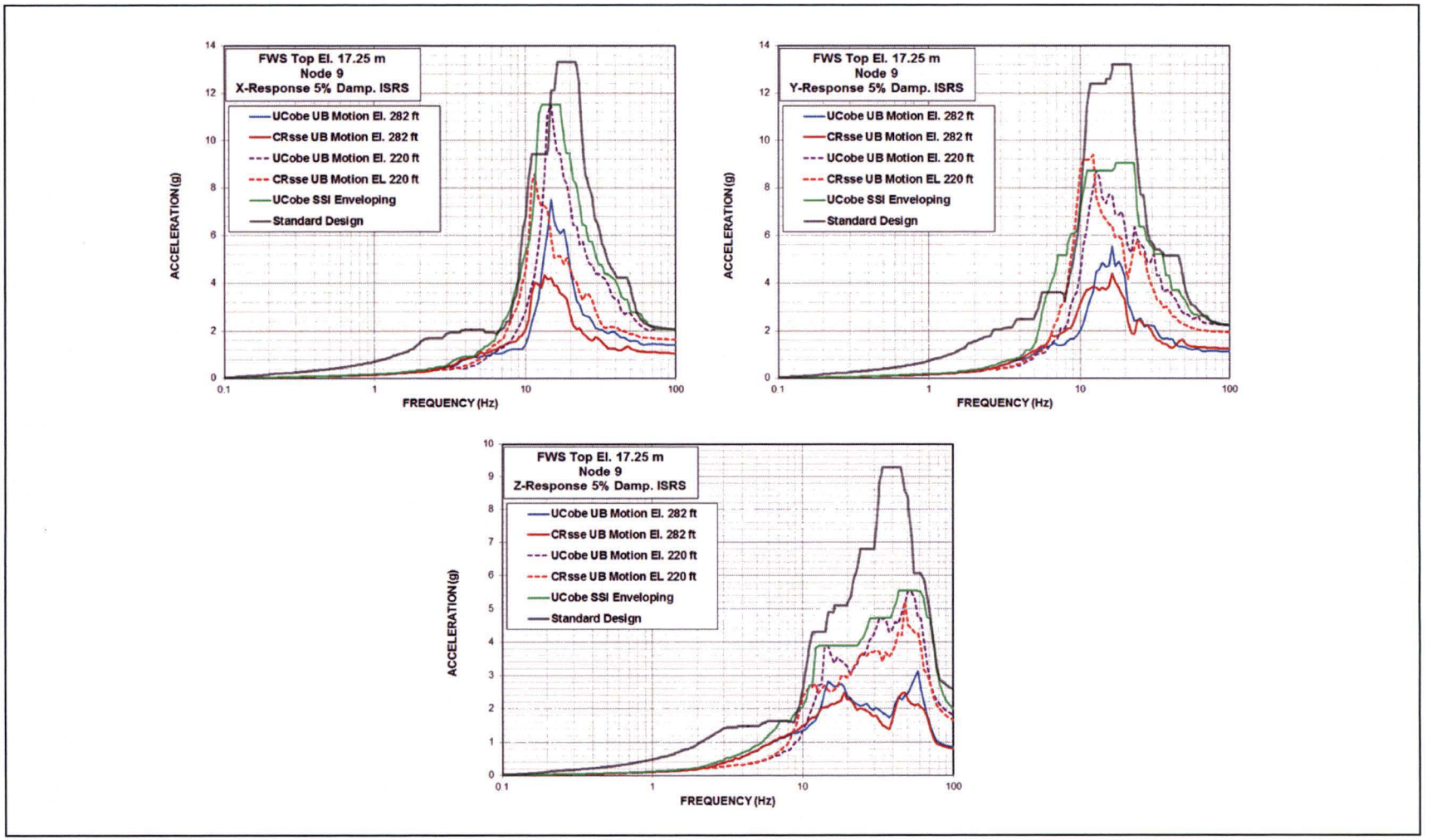

Figure B.4-14: Comparison of ISRS – FWS Wall Top for UB Profile Analyses

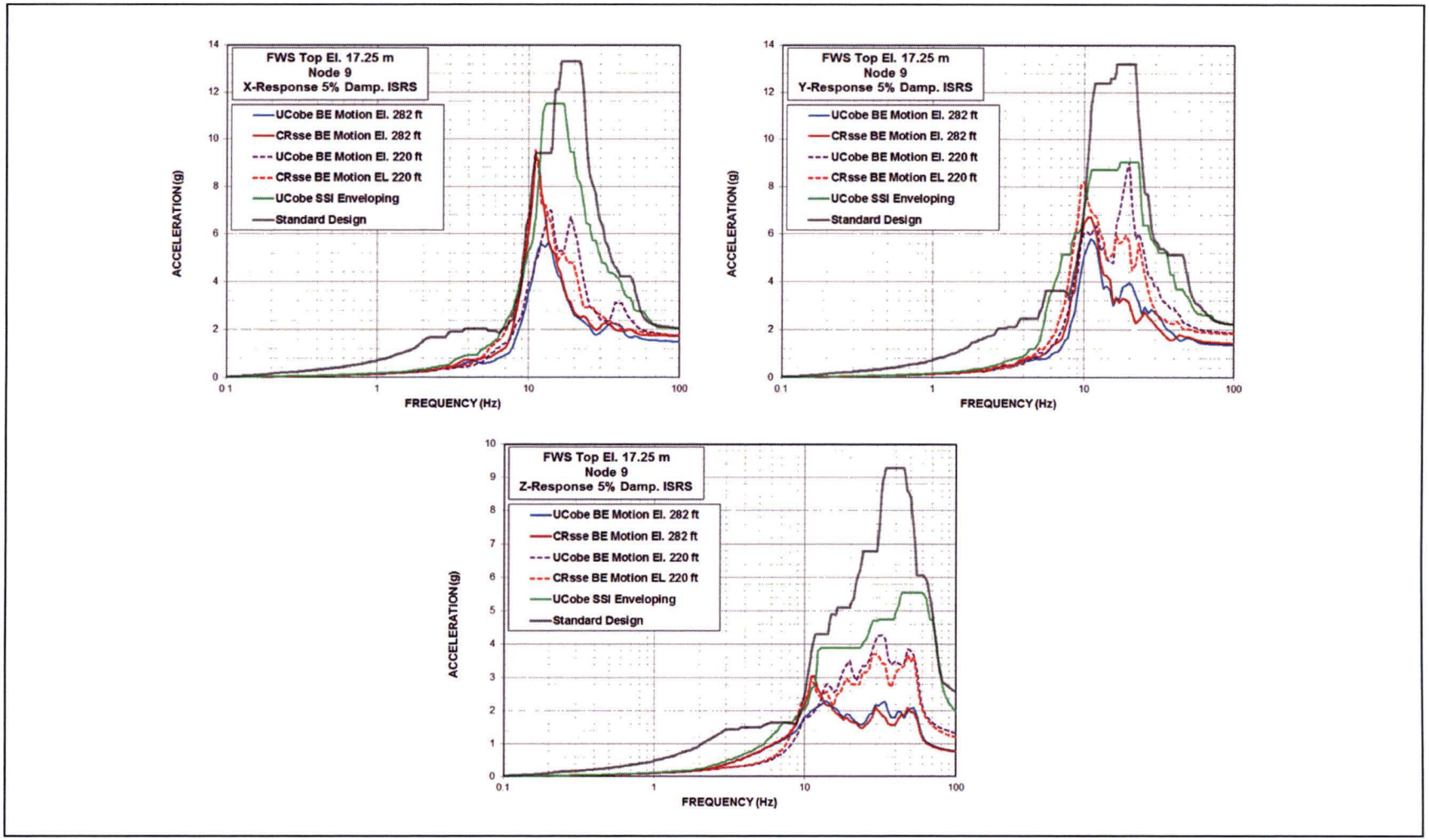

Figure B.4-15: Comparison of ISRS – FWS Wall Top for BE Profile Analyses

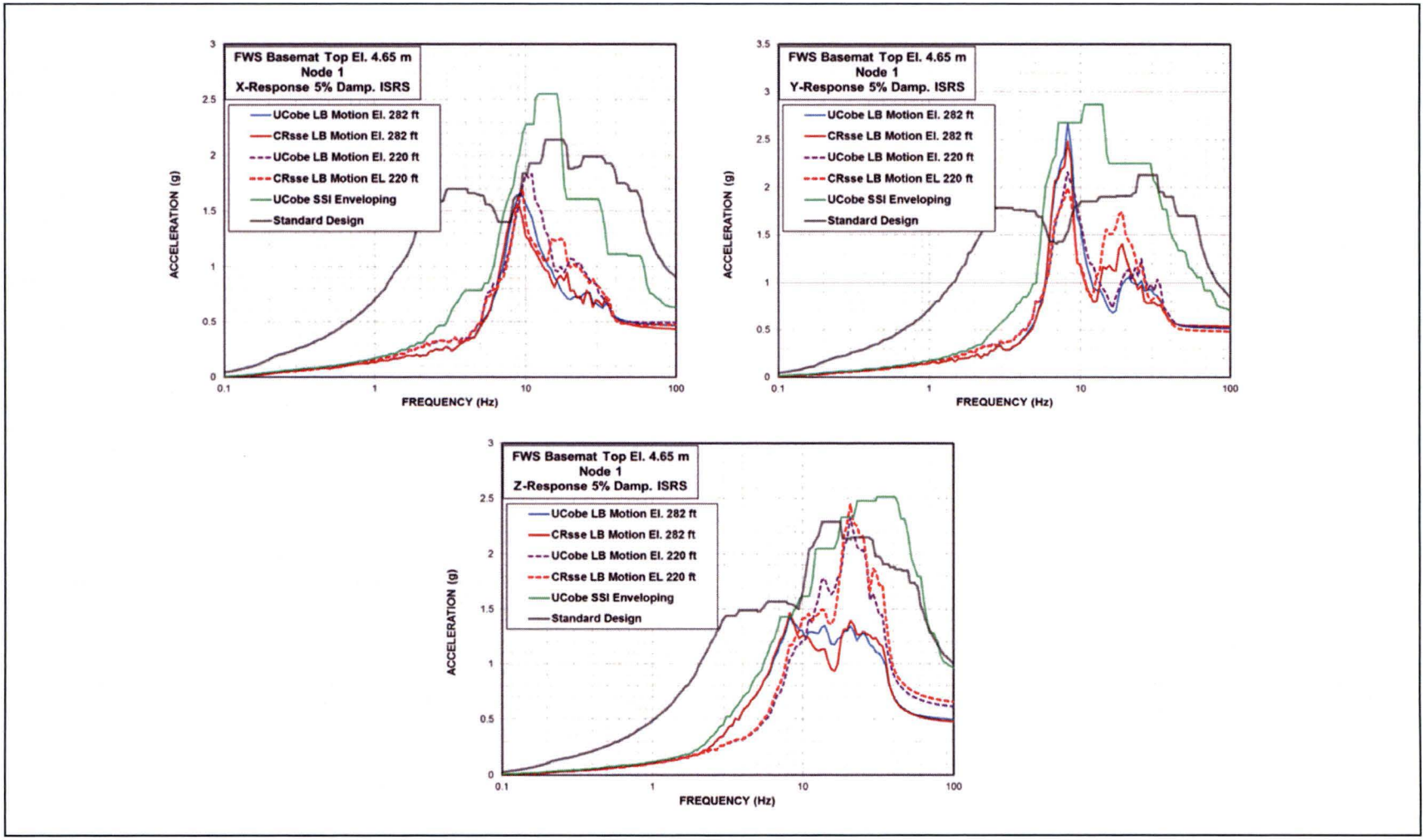

Figure B.4-16: Comparison of ISRS – FWS Basemat Top for LB Profile Analyses

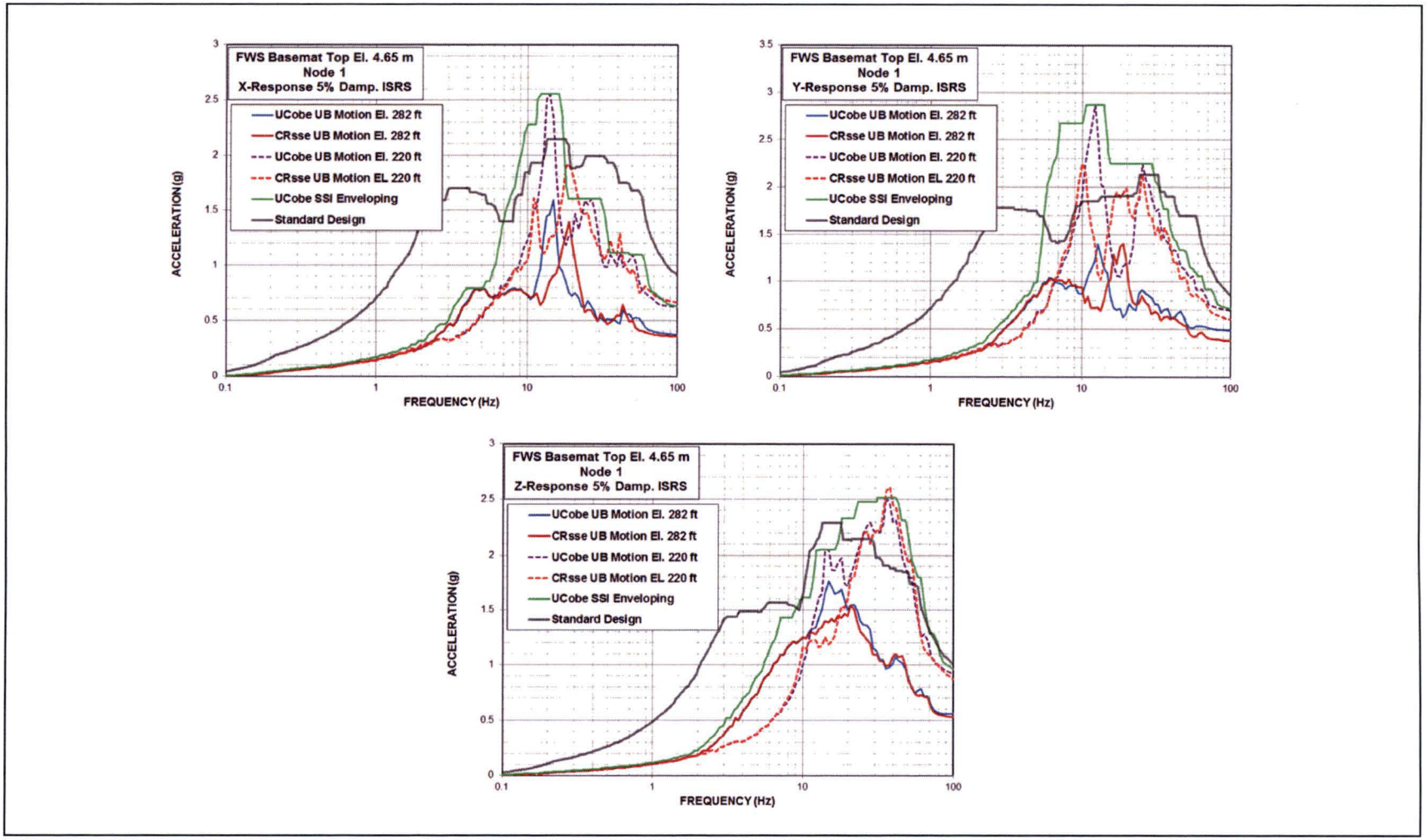

Figure B.4-17: Comparison of ISRS – FWS Basemat Top for UB Profile Analyses

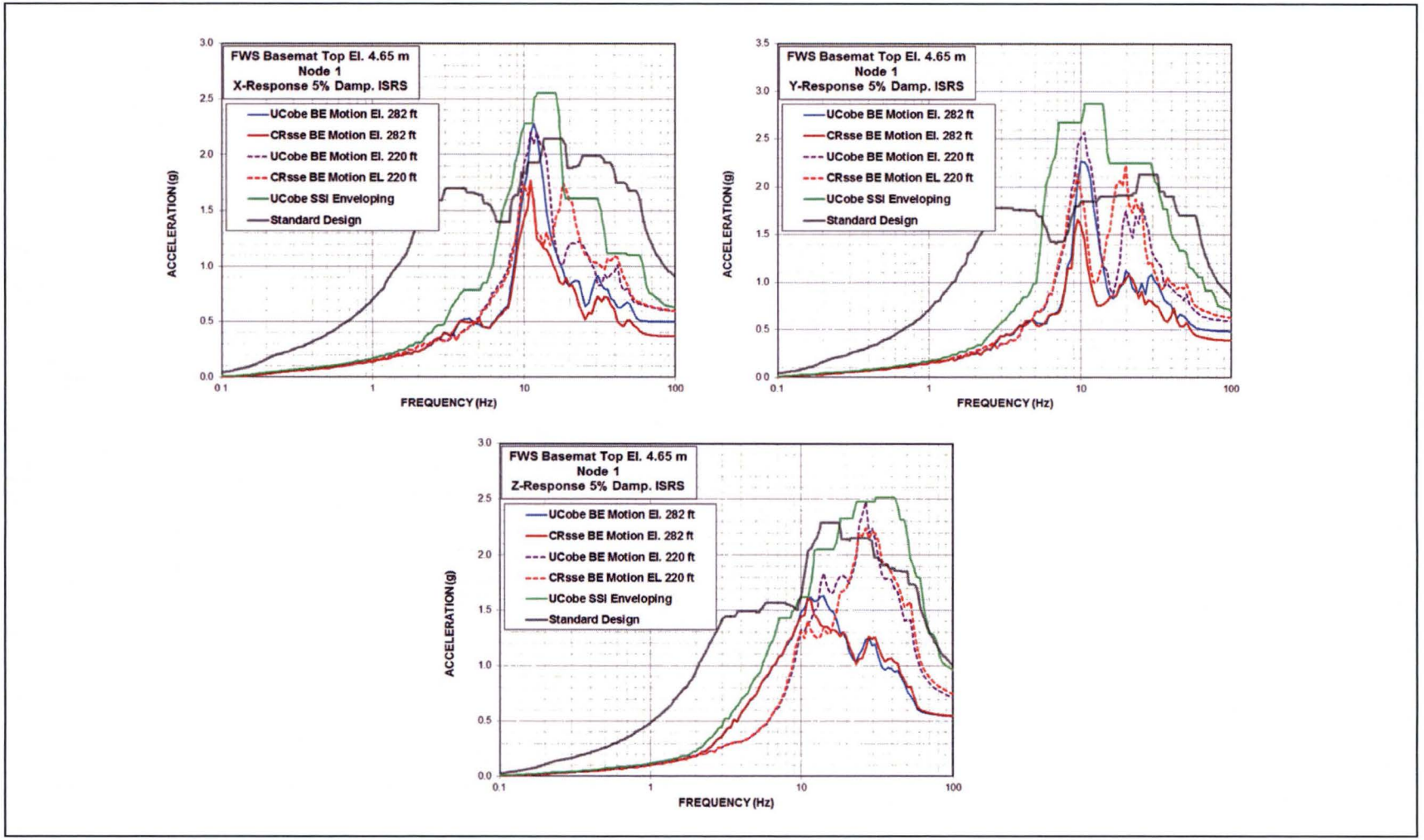

Figure B.4-18: Comparison of ISRS – FWS Basemat Top for BE Profile Analyses

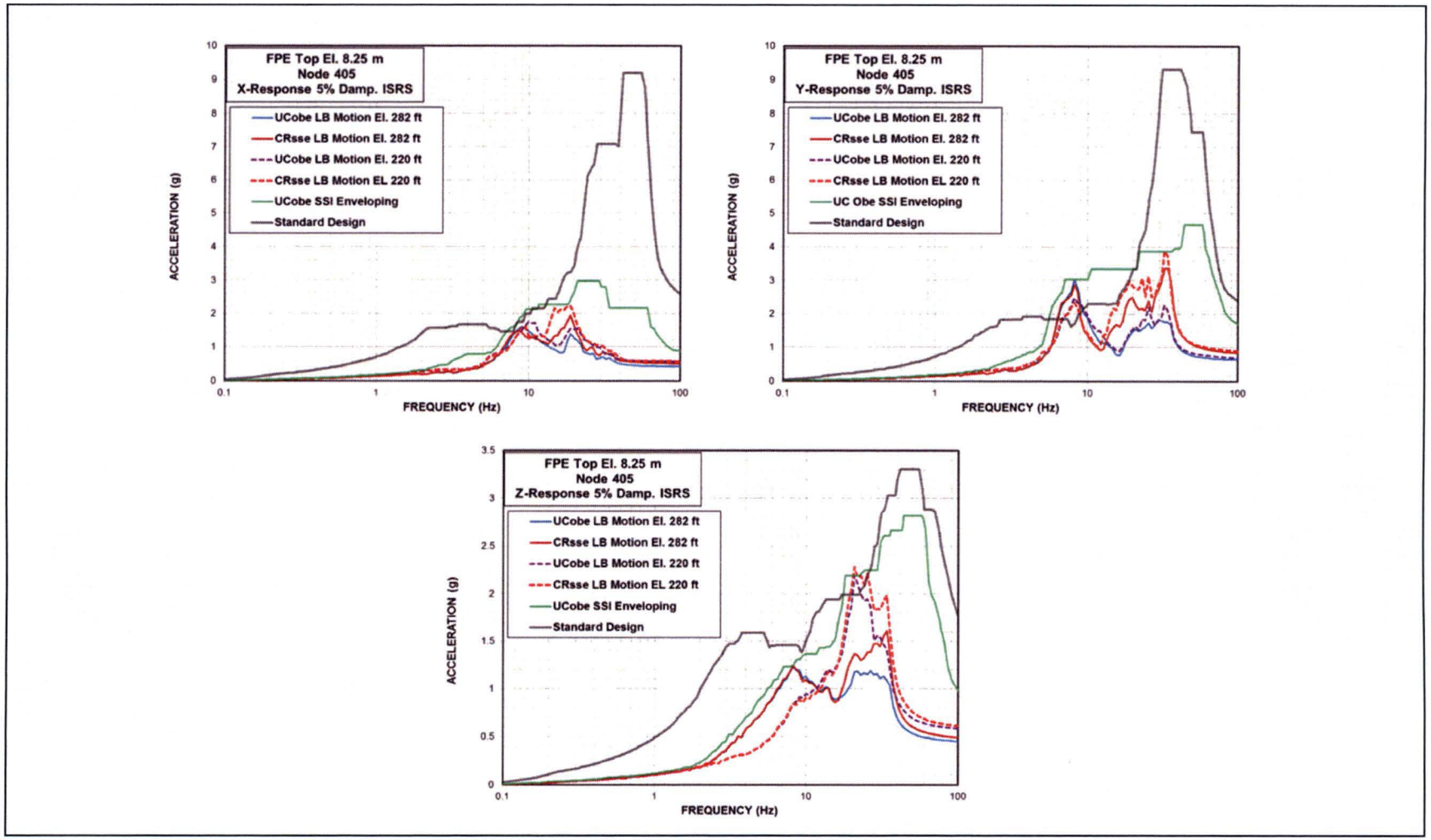

Figure B.4-19: Comparison of ISRS – FPE Top for LB Profile Analyses

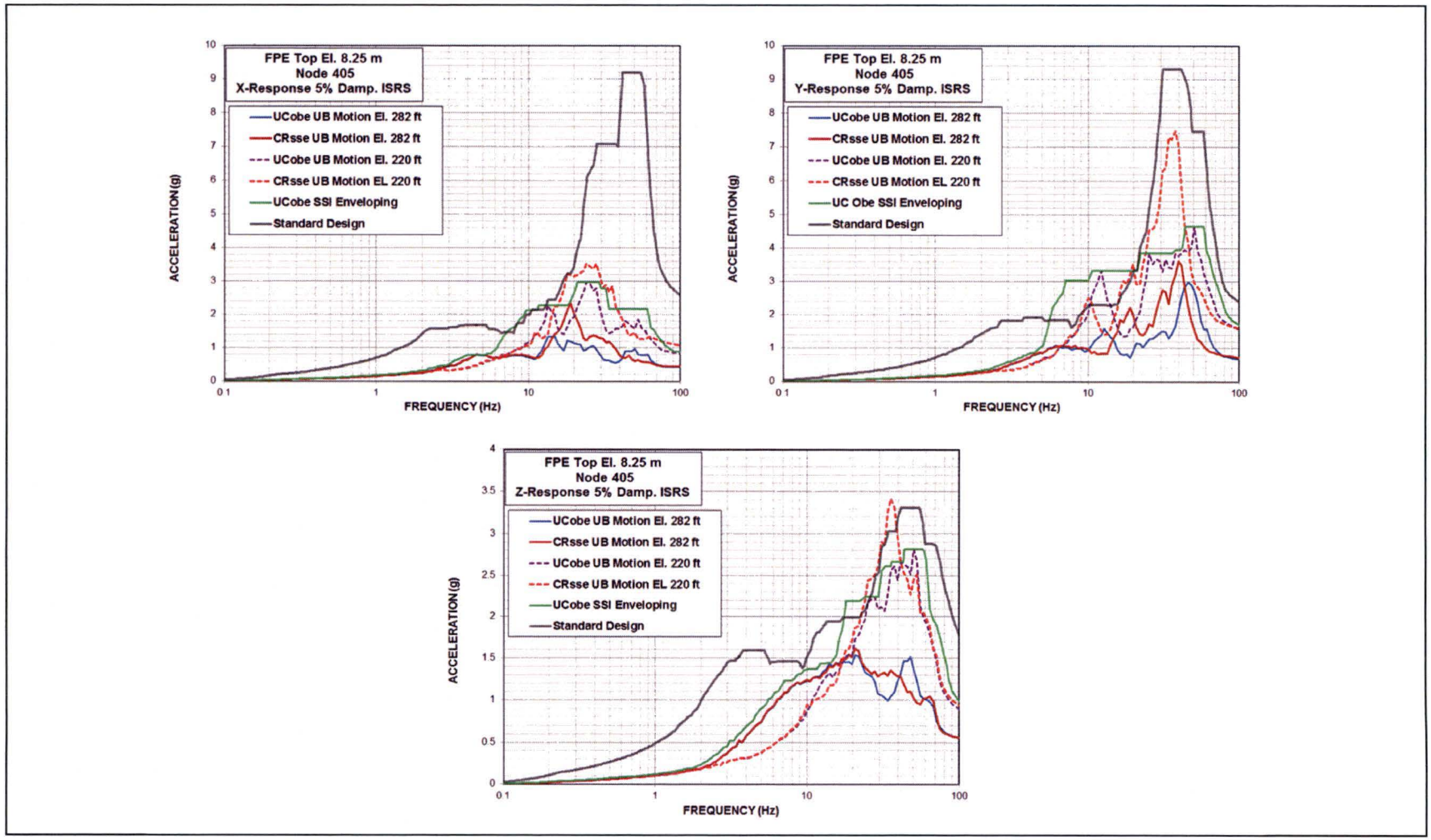

Figure B.4-20: Comparison of ISRS – FPE Top for UB Profile Analyses

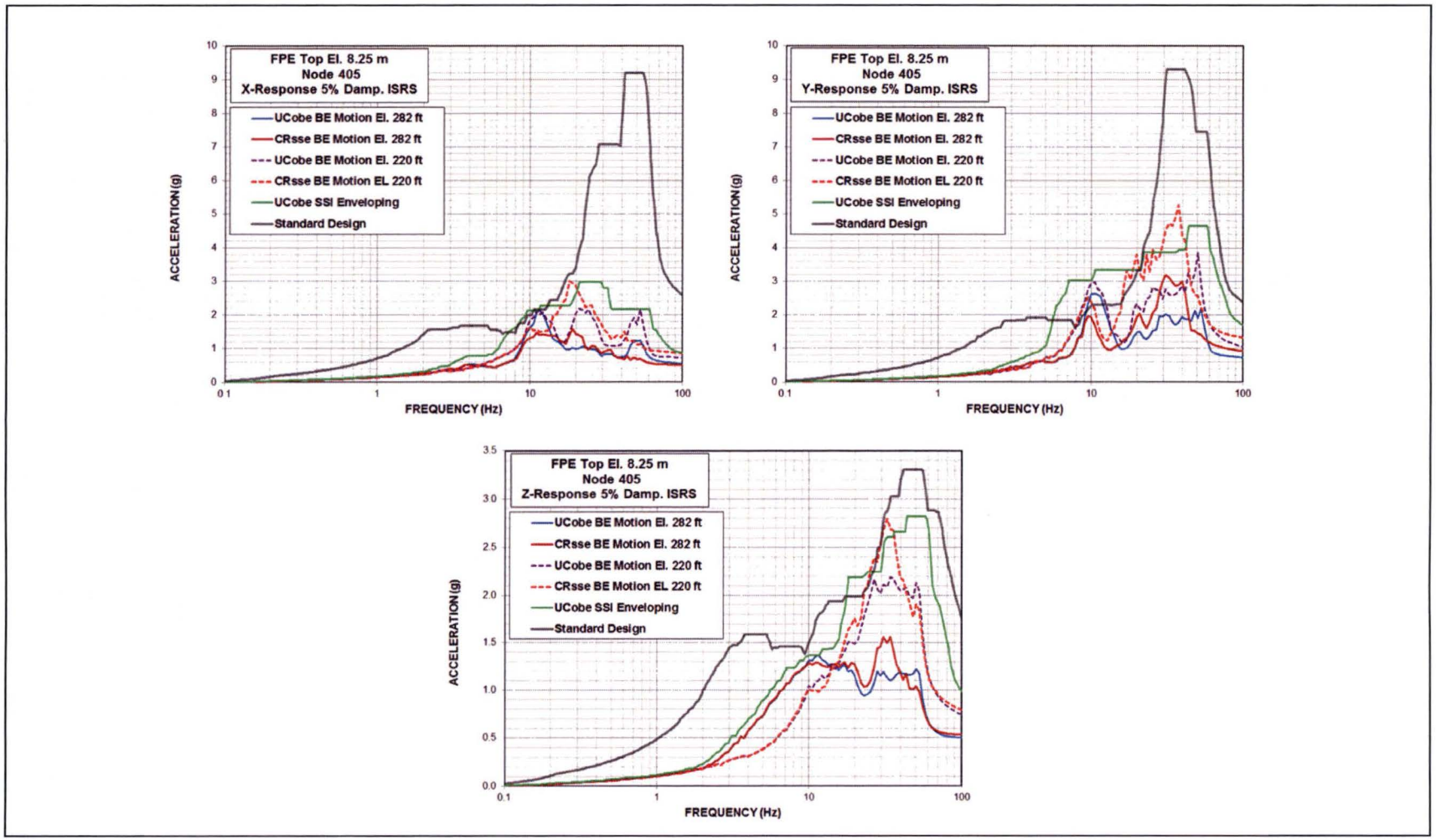

Figure B.4-21: Comparison of ISRS – FPE Top for BE Profile Analyses

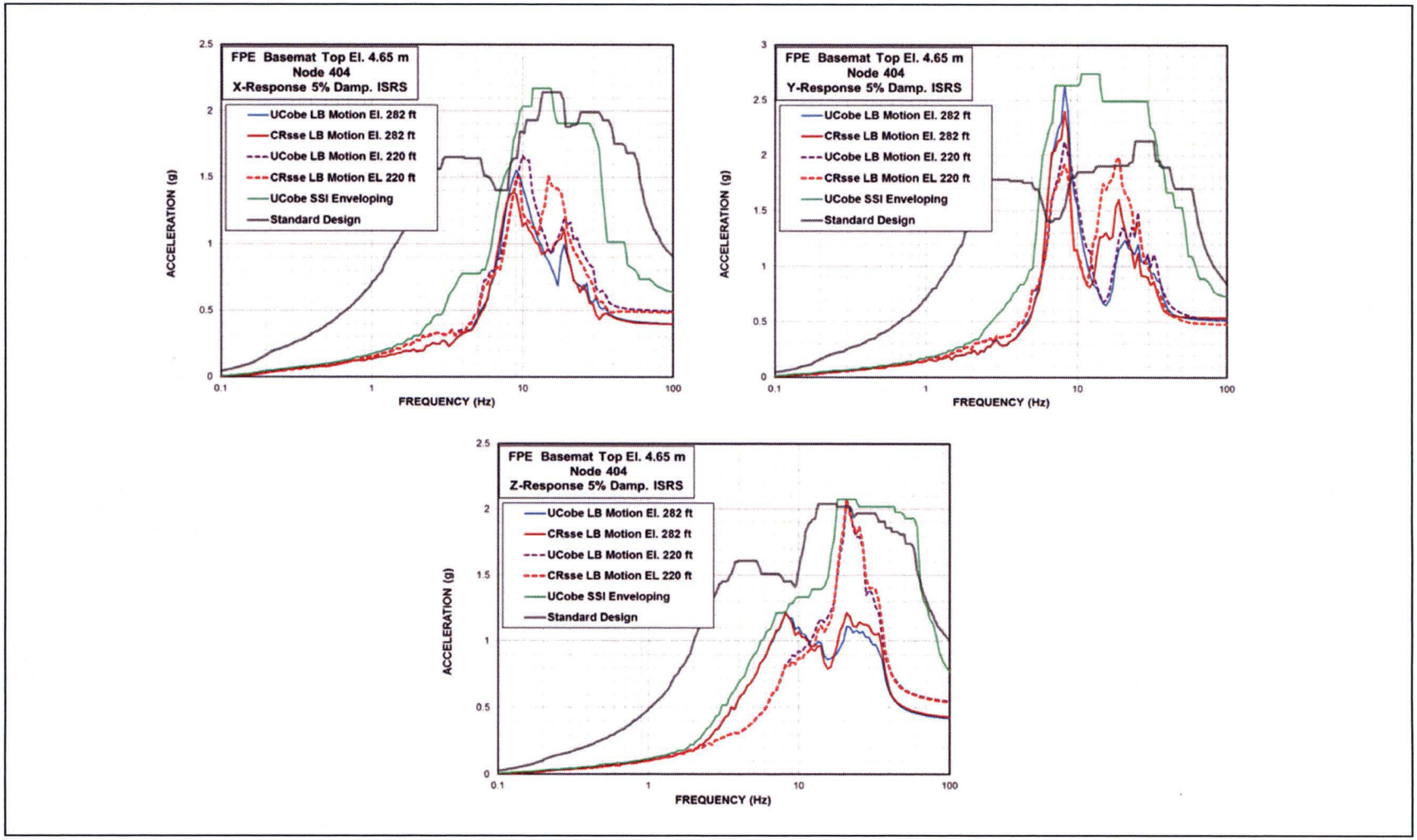

Figure B.4-22: Comparison of ISRS– FPE Basemat Top for LB Profile Analyses

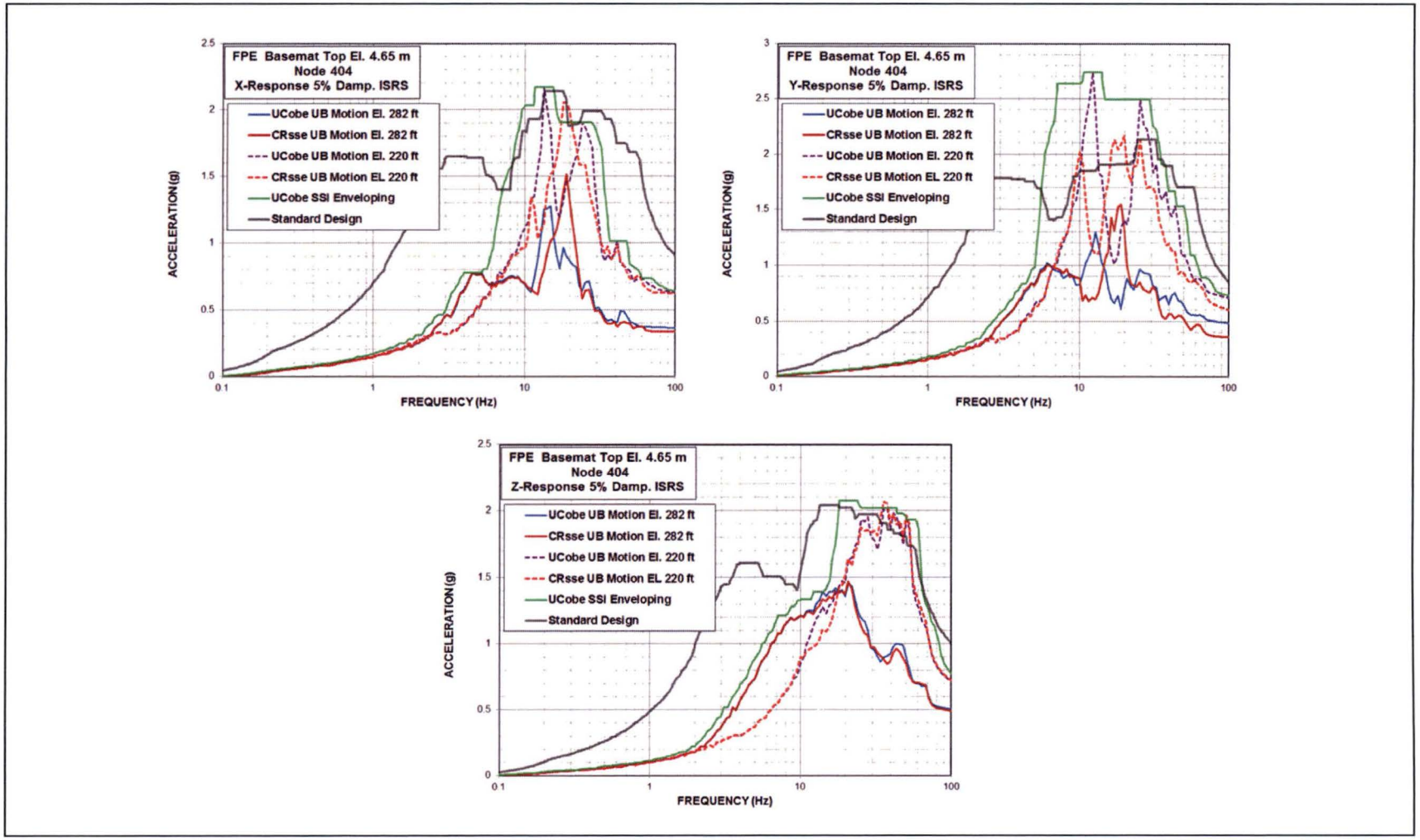

Figure B.4-23: Comparison of ISRS– FPE Basemat Top for UB Profile Analyses

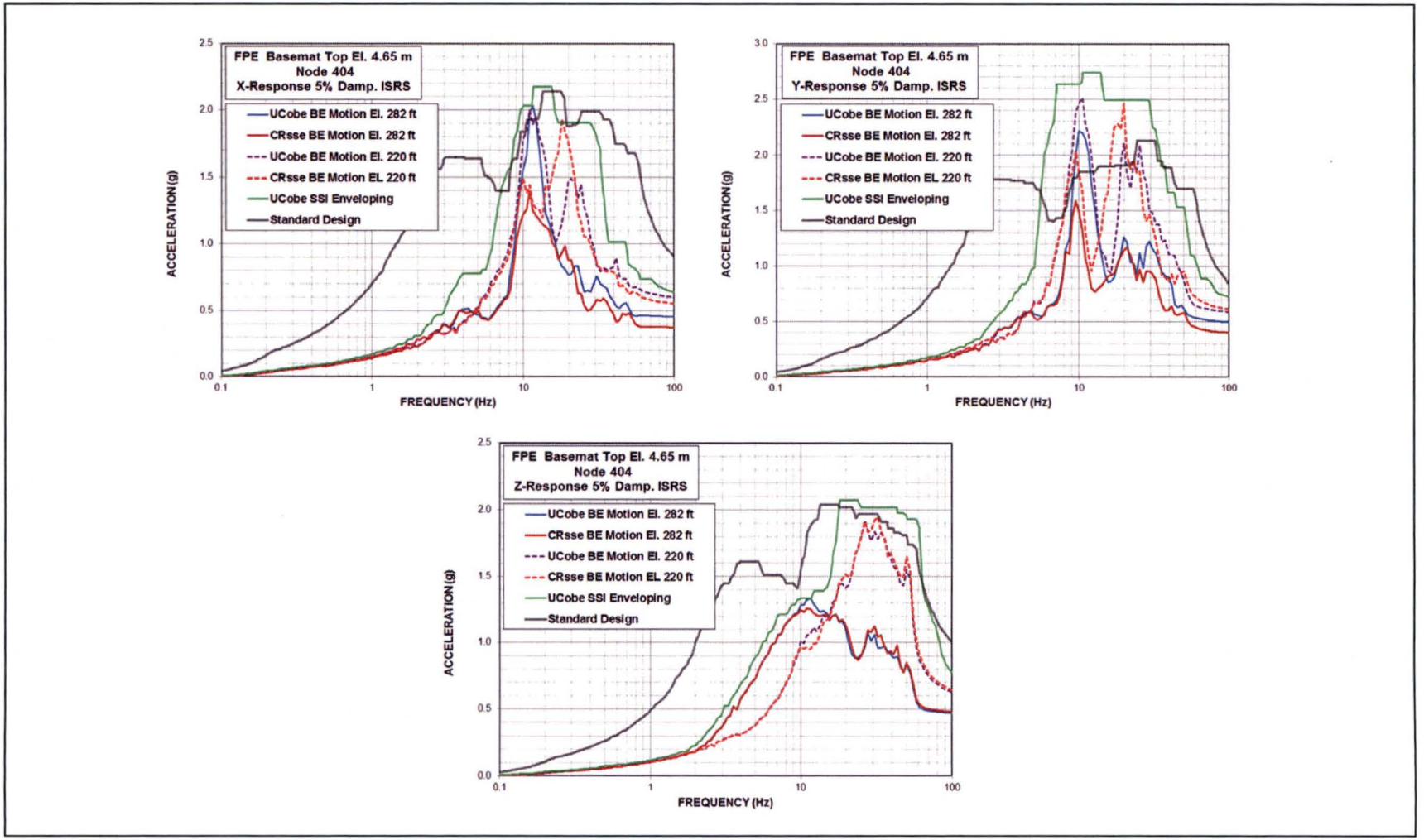

Figure B.4-24: Comparison of ISRS– FPE Basemat Top for BE Profile Analyses

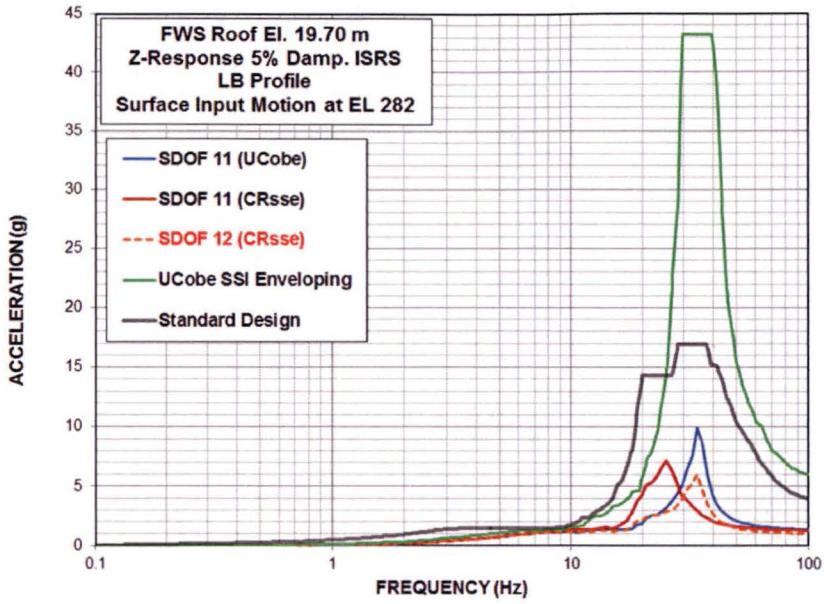

(a) LB Profile with Surface Input Motion at El. 282 ft NAVD 88

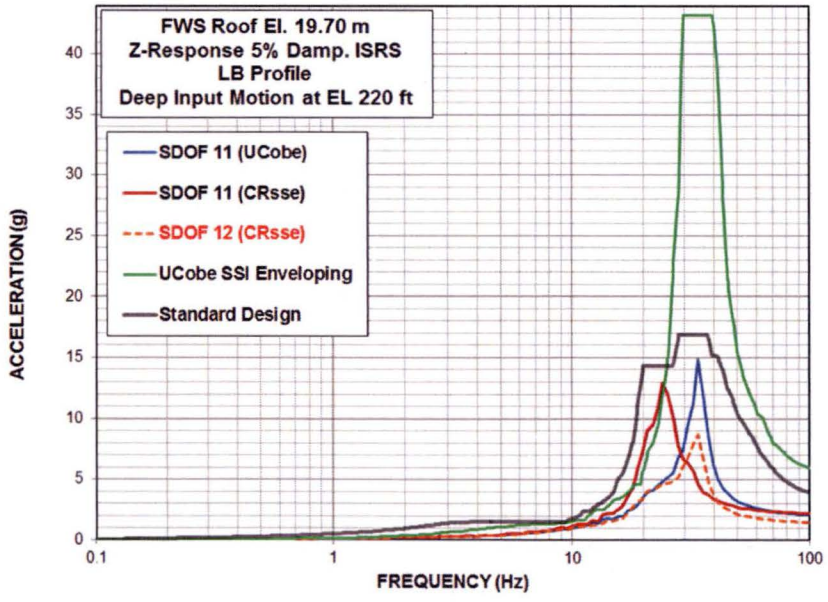

(b) LB Profile with Deep Input Motion at El. 220 ft NAVD 88

Figure B.4-25: Comparison of Out-of-Plane ISRS for LB Profile - FWS Roof

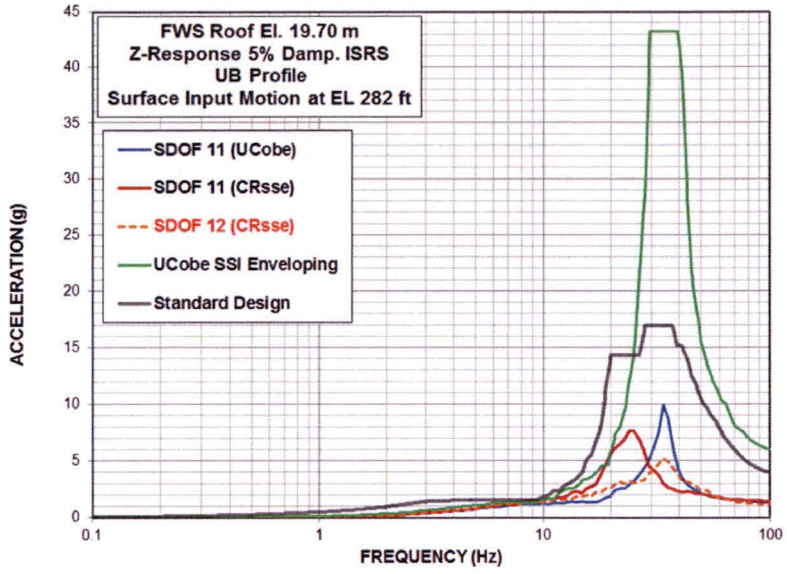

(a) UB Profile with Surface Input Motion at El. 282 ft NAVD 88

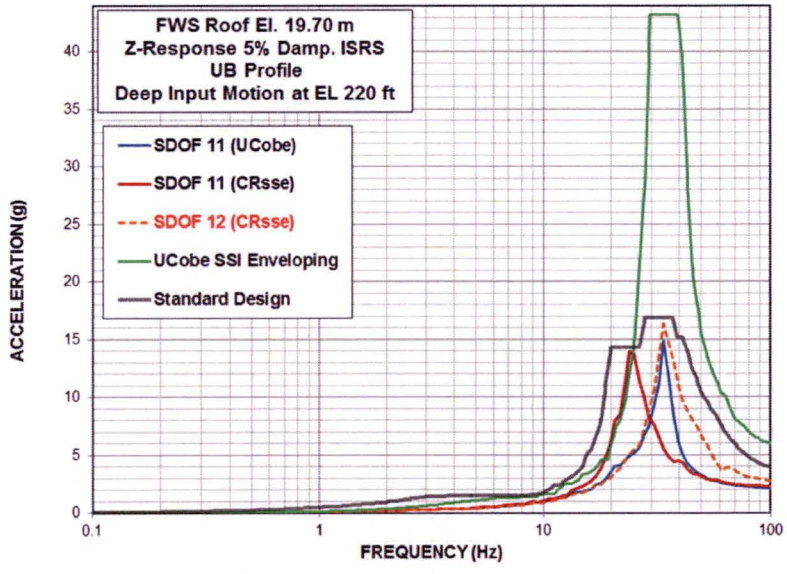

(b) UB Profile with Deep Input Motion at El. 220 ft NAVD 88

Figure B.4-26: Comparison of Out-of-Plane ISRS for UB Profile - FWS Roof

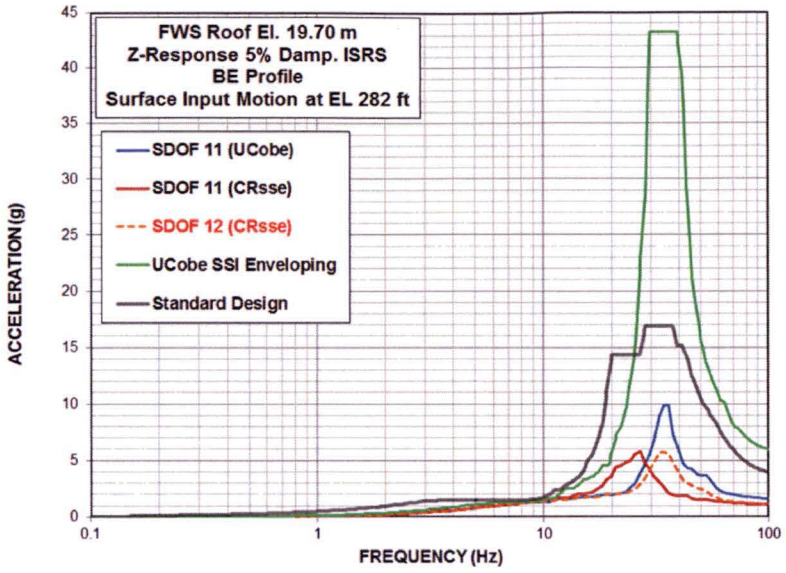

(a) BE Profile with Surface Input Motion at El. 282 ft NAVD 88

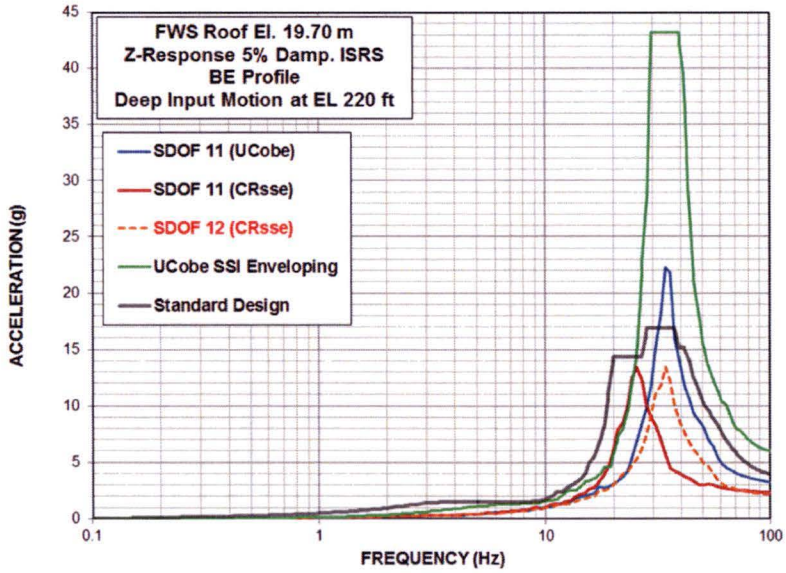

(b) BE Profile with Deep Input Motion at El. 220 ft NAVD 88

Figure B.4-27: Comparison of Out-of-Plane ISRS for BE Profile - FWS Roof

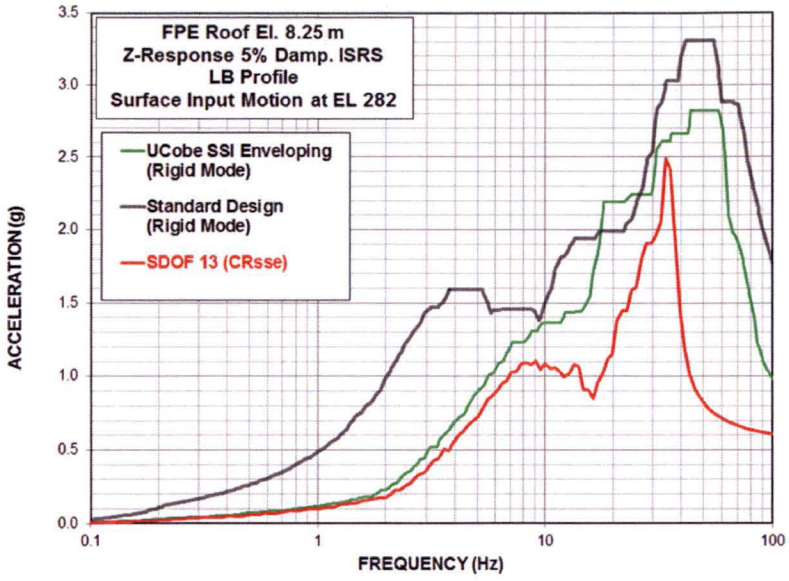

(a) LB Profile with Surface Input Motion at El. 282 ft NAVD 88

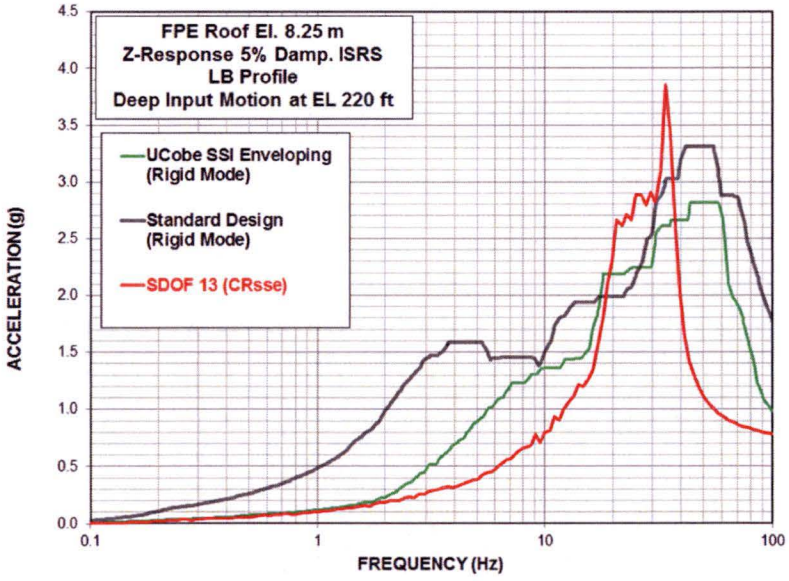

(b) LB Profile with Deep Input Motion at El. 220 ft NAVD 88

Figure B.4-28: Comparison of Out-of-Plane ISRS for LB Profile - FPE Roof

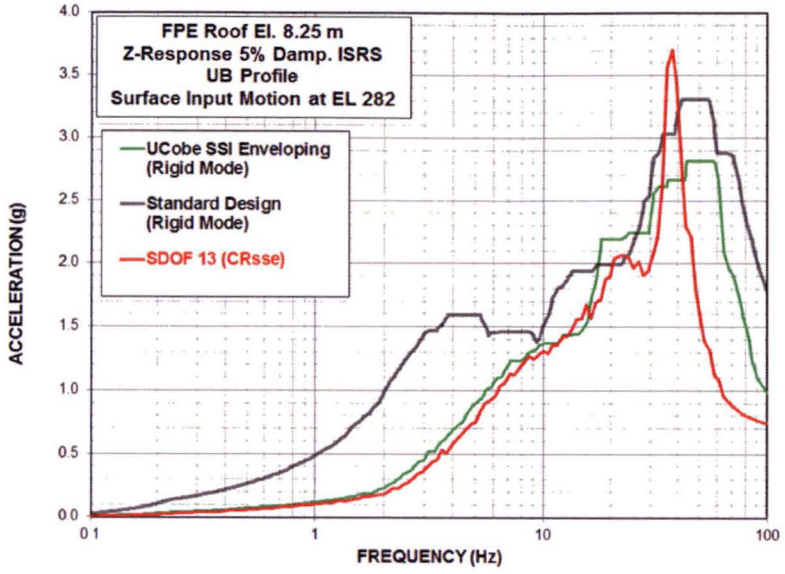

(a) UB Profile with Surface Input Motion at El. 282 ft NAVD 88

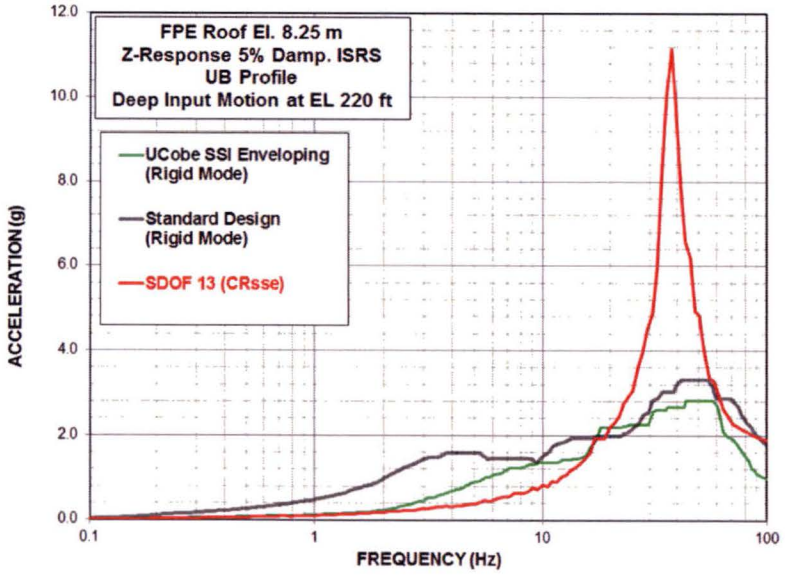

(b) UB Profile with Deep Input Motion at El. 220 ft NAVD 88

Figure B.4-29: Comparison of Out-of-Plane ISRS for UB Profile - FPE Roof

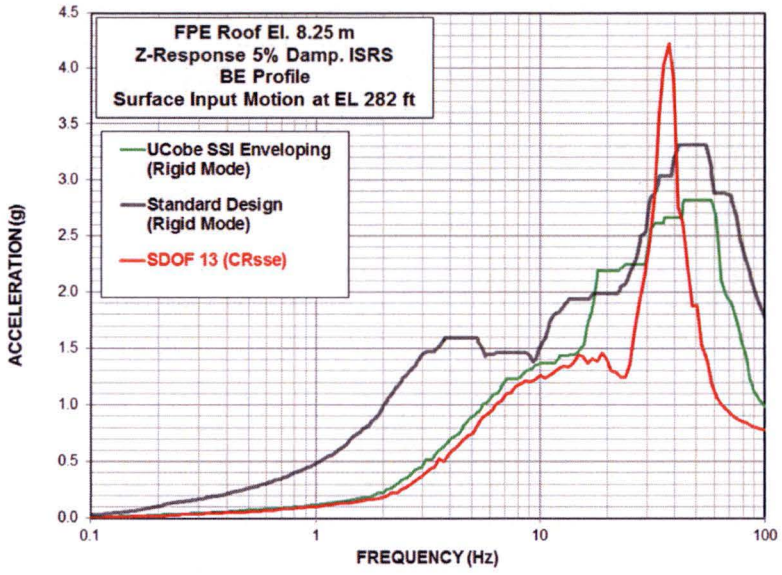

(a) BE Profile with Surface Input Motion at El. 282 ft NAVD 88

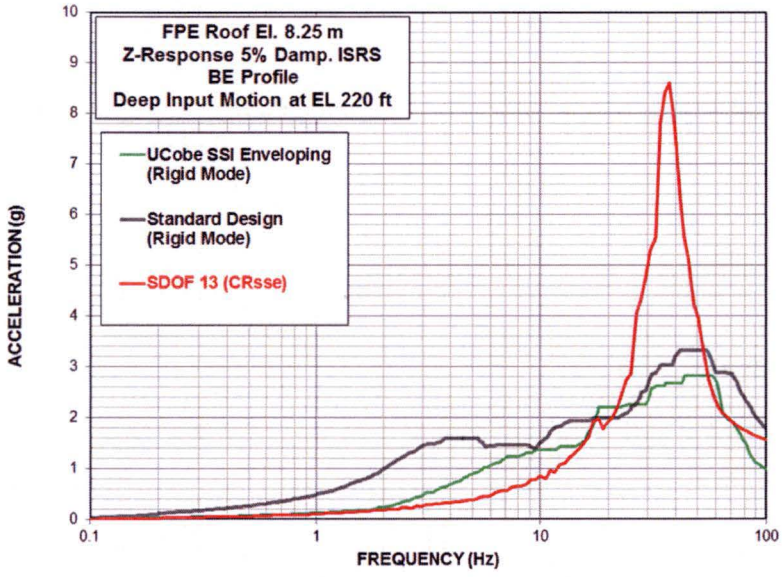

(b) BE Profile with Deep Input Motion at El. 220 ft NAVD 88

Figure B.4-30: Comparison of Out-of-Plane ISRS for BE Profile - FPE Roof

APPENDIX C
Not Used

APPENDIX D
Not Used

APPENDIX E
Site-Specific In-Structure Response Spectra

LIST OF TABLES

LIST OF FIGURES

Table E-1: Figure Numbers for Site-Specific In-Structure Response Spectra

Structure	Elevation (m)	Node Number	Figure Number of Floor Response Spectra		
			X (NS)	Y (EW)	Z (Vrt)
FWS	17.25	9	E-1	E-12	E-23
	15.53	8	E-2	E-13	E-24
	13.81	7	E-3	E-14	E-25
	12.10	6	E-4	E-15	E-26
	11.00	5	E-5	E-16	E-27
	9.90	4	E-6	E-17	E-28
	8.81	3	E-7	E-18	E-29
	6.73	2	E-8	E-19	E-30
	4.65	1	E-9	E-20	E-31
FPE	8.25	405	E-10	E-21	E-32
	4.65	404	E-11	E-22	E-33
FWS Roof Oscillator	19.70	11			E-34

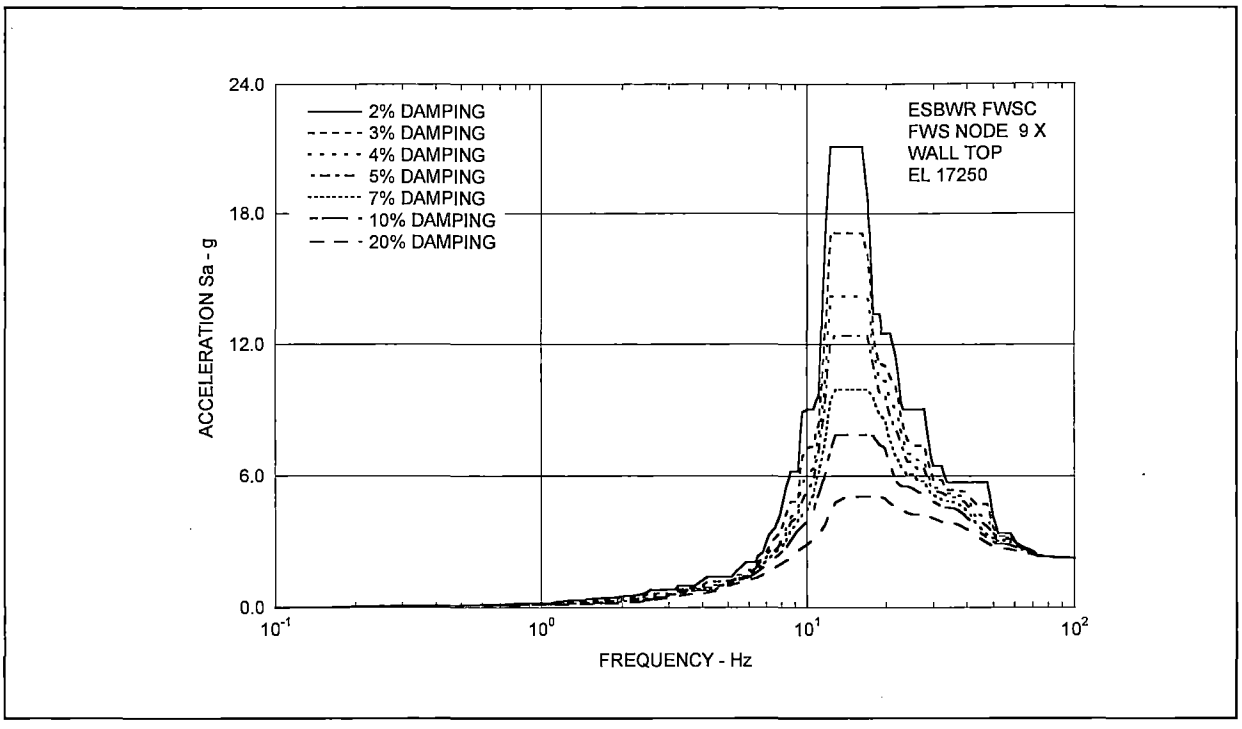

Figure E-1: Site-Specific In-Structure Response Spectra - FWS Node 9 X -

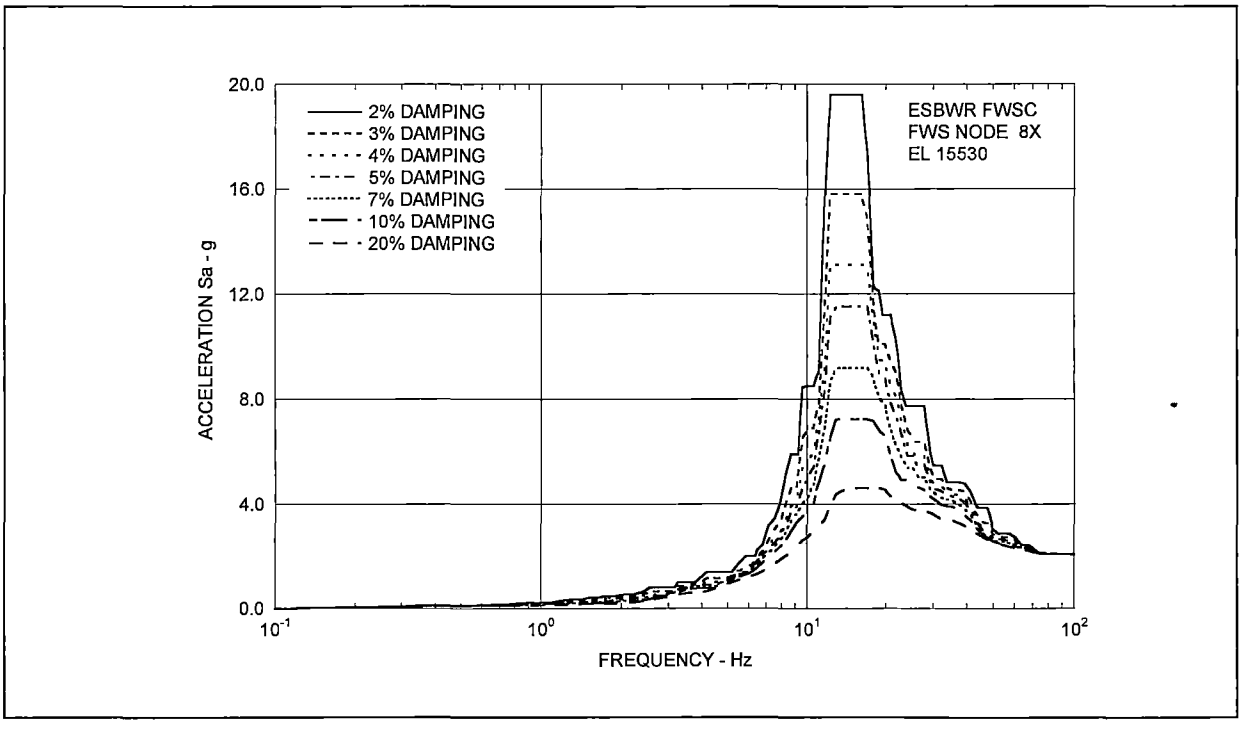

Figure E-2: Site-Specific In-Structure Response Spectra - FWS Node 8 X -

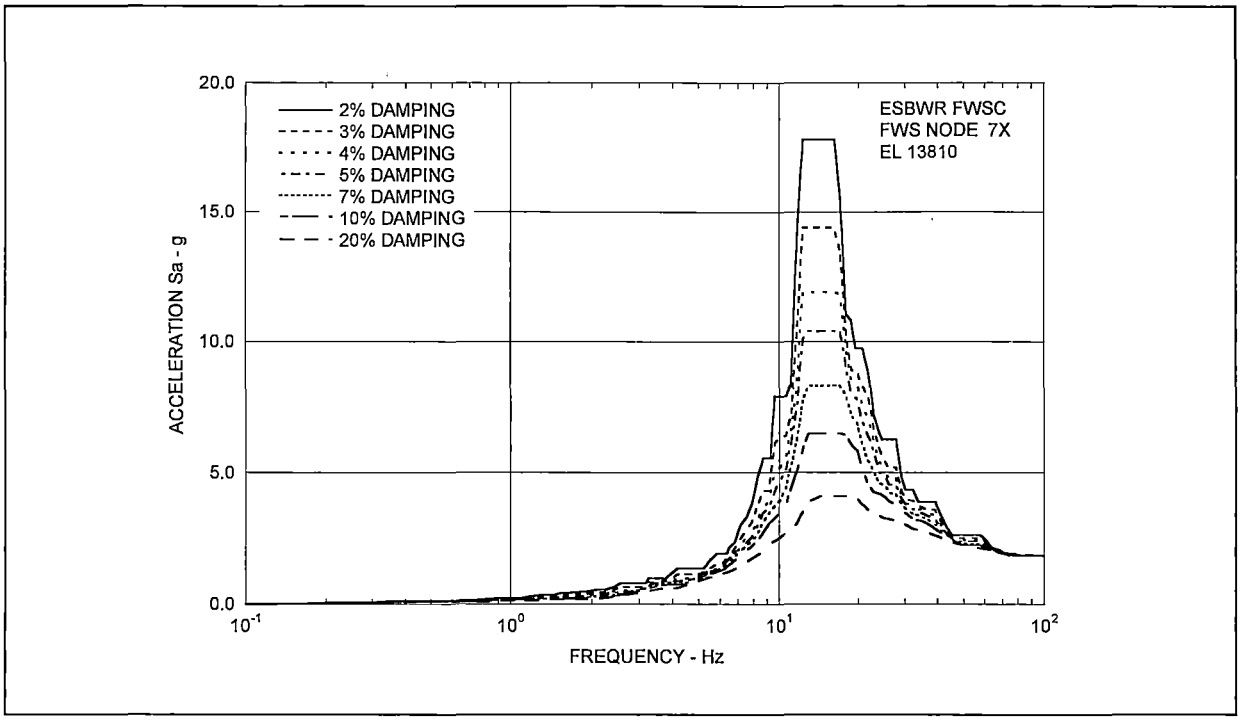

Figure E-3: Site-Specific In-Structure Response Spectra - FWS Node 7 X -

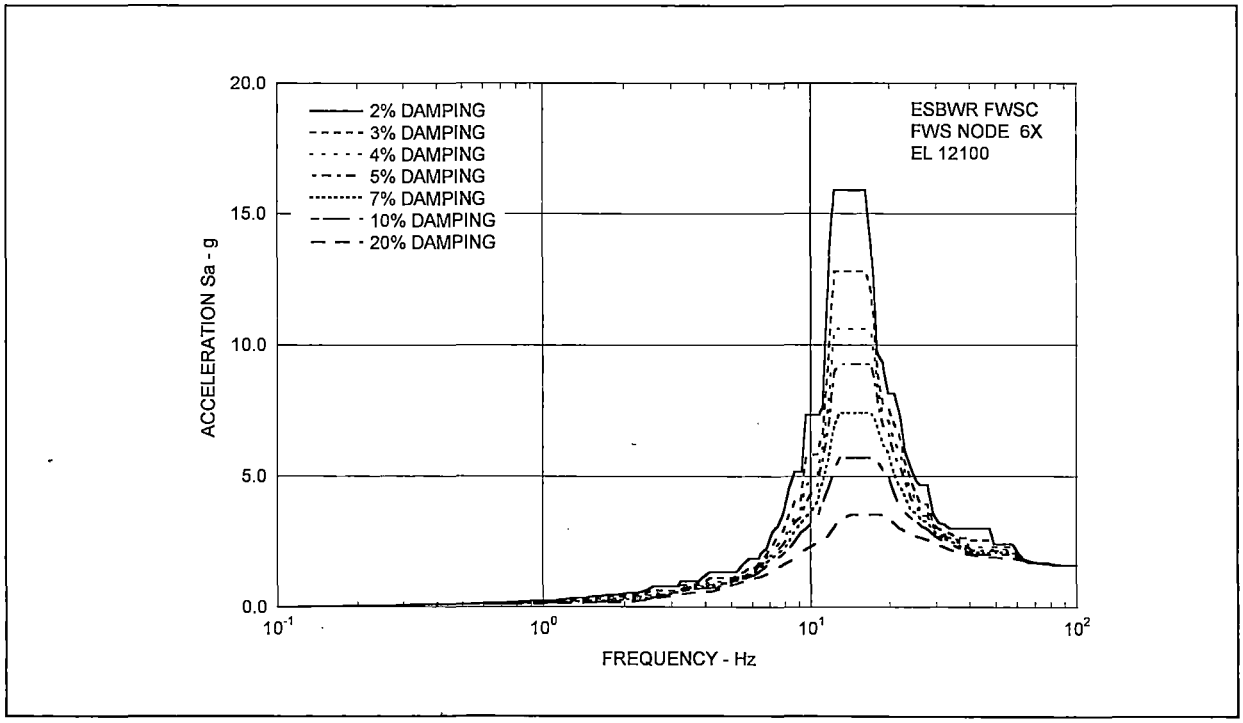

Figure E-4: Site-Specific In-Structure Response Spectra - FWS Node 6 X -

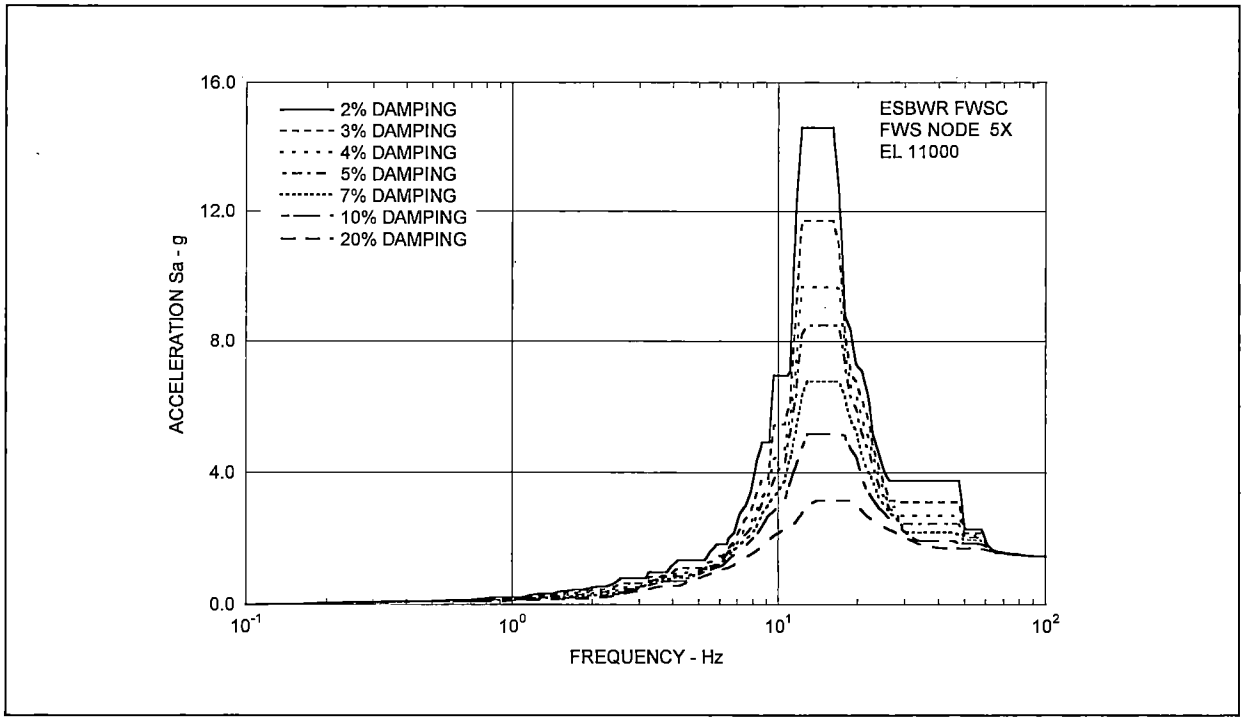

Figure E-5: Site-Specific In-Structure Response Spectra - FWS Node 5 X -

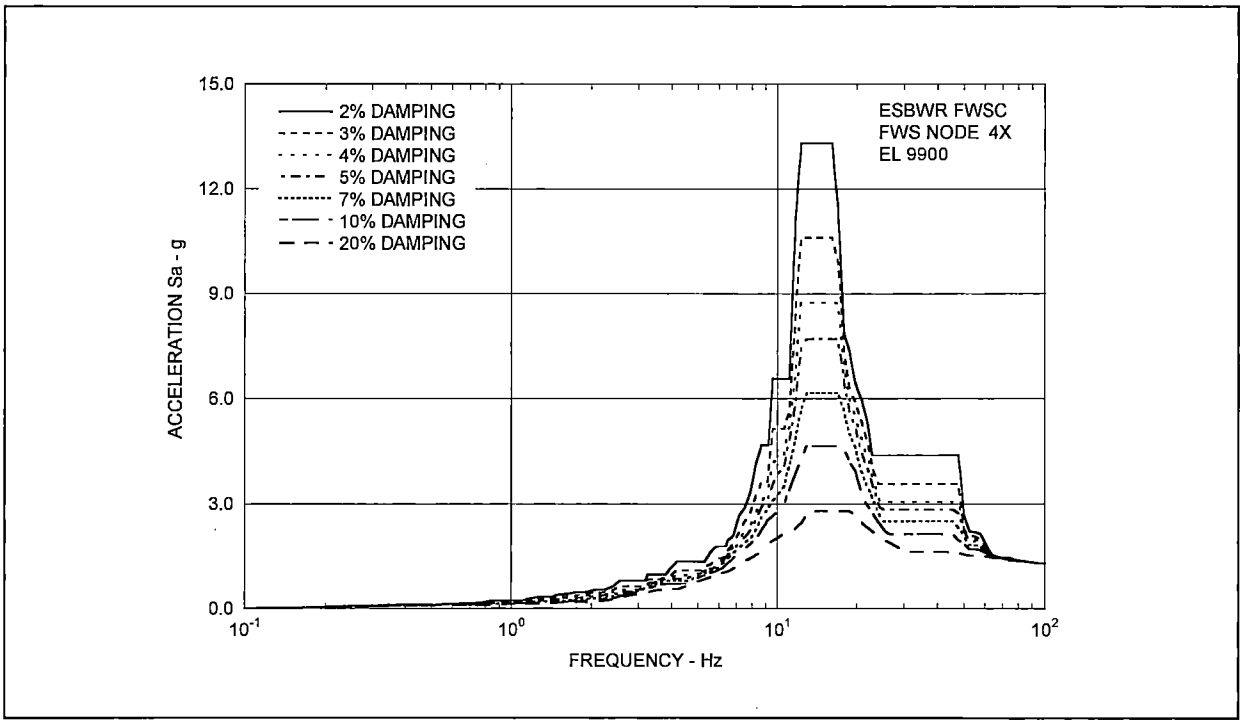

Figure E-6: Site-Specific In-Structure Response Spectra - FWS Node 4 X -

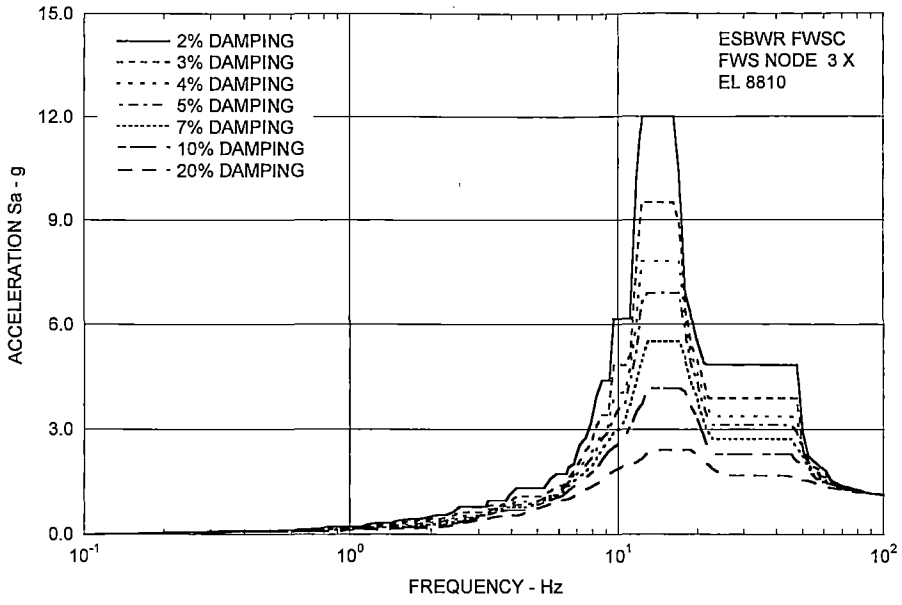

Figure E-7: Site-Specific In-Structure Response Spectra - FWS Node 3 X -

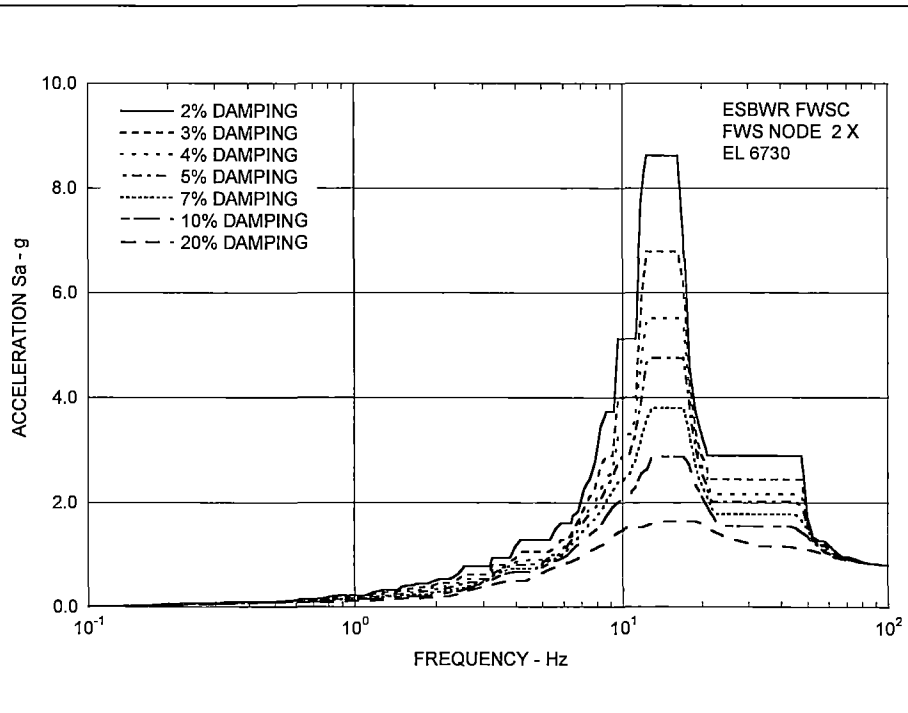

Figure E-8: Site-Specific In-Structure Response Spectra - FWS Node 2 X -

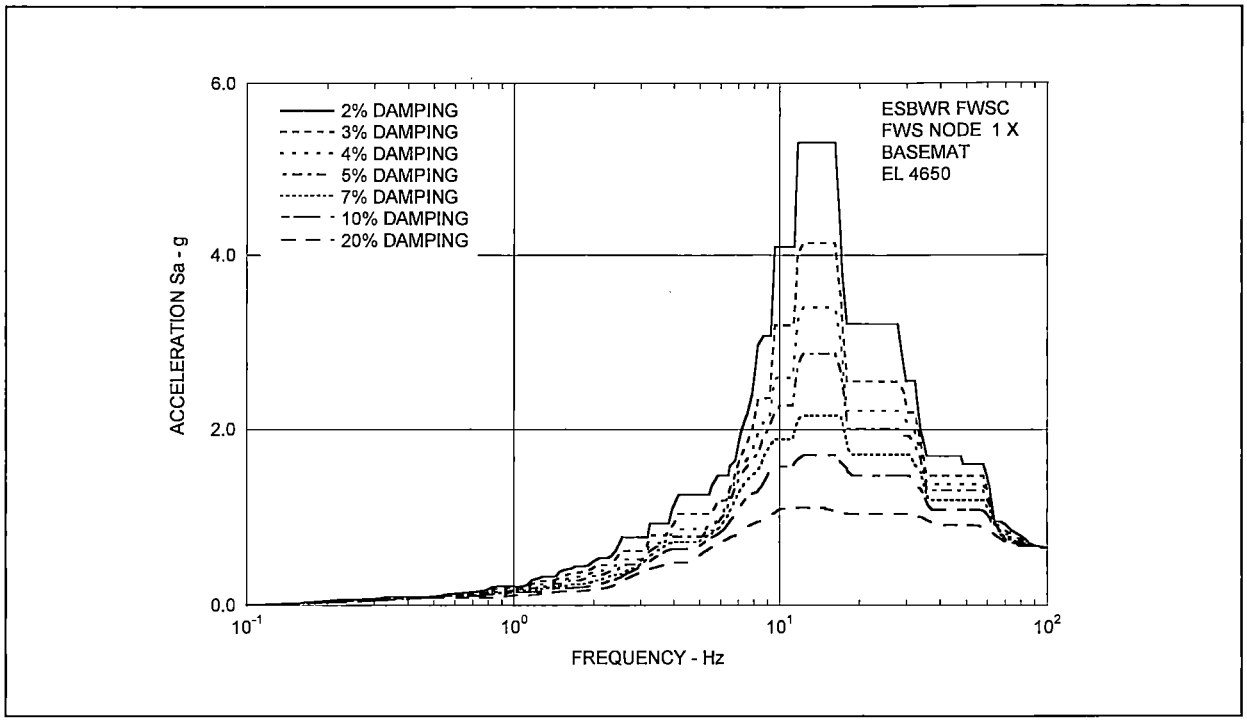

Figure E-9: Site-Specific In-Structure Response Spectra - FWS Node 1 X -

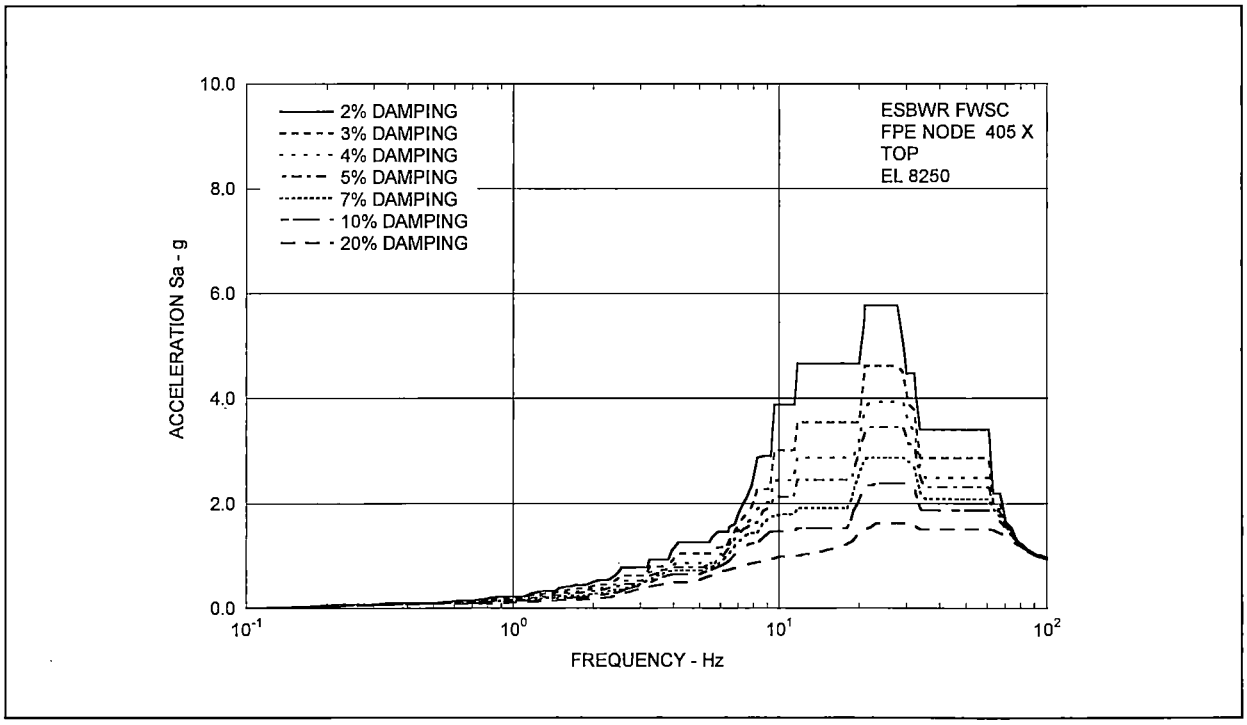

Figure E-10: Site-Specific In-Structure Response Spectra - FPE Node 405 X -

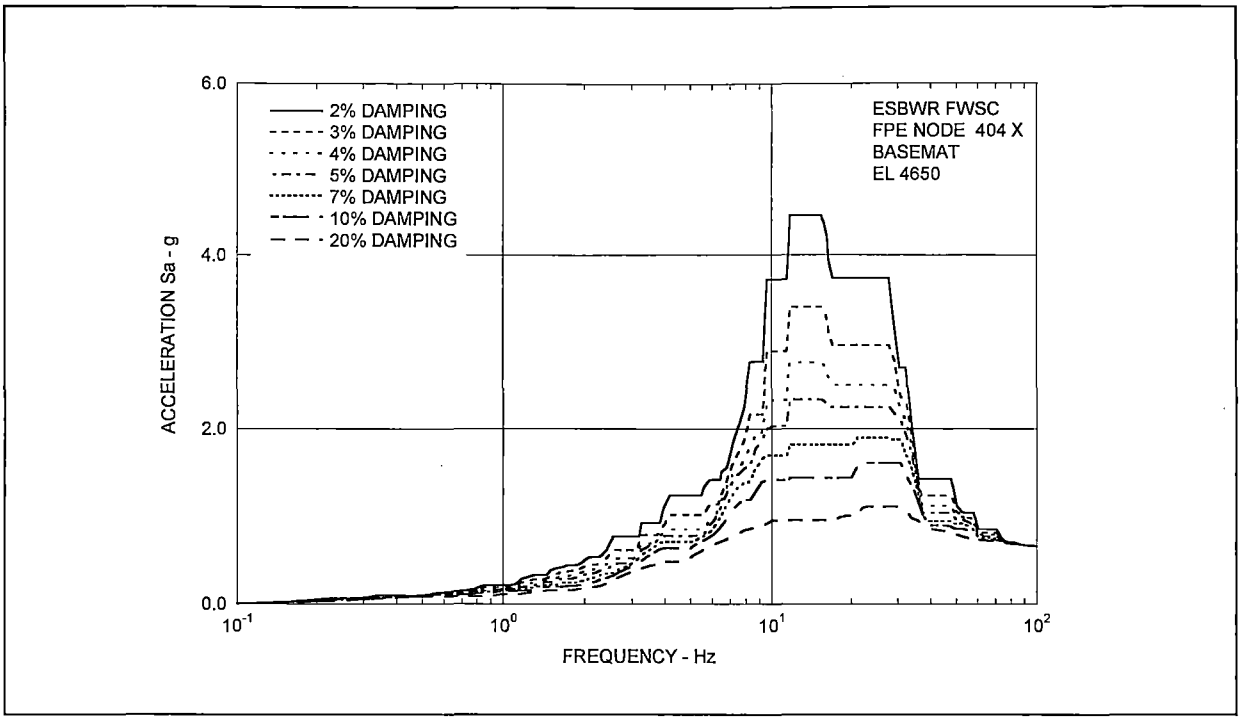

Figure E-11: Site-Specific In-Structure Response Spectra - FPE Node 404 X -

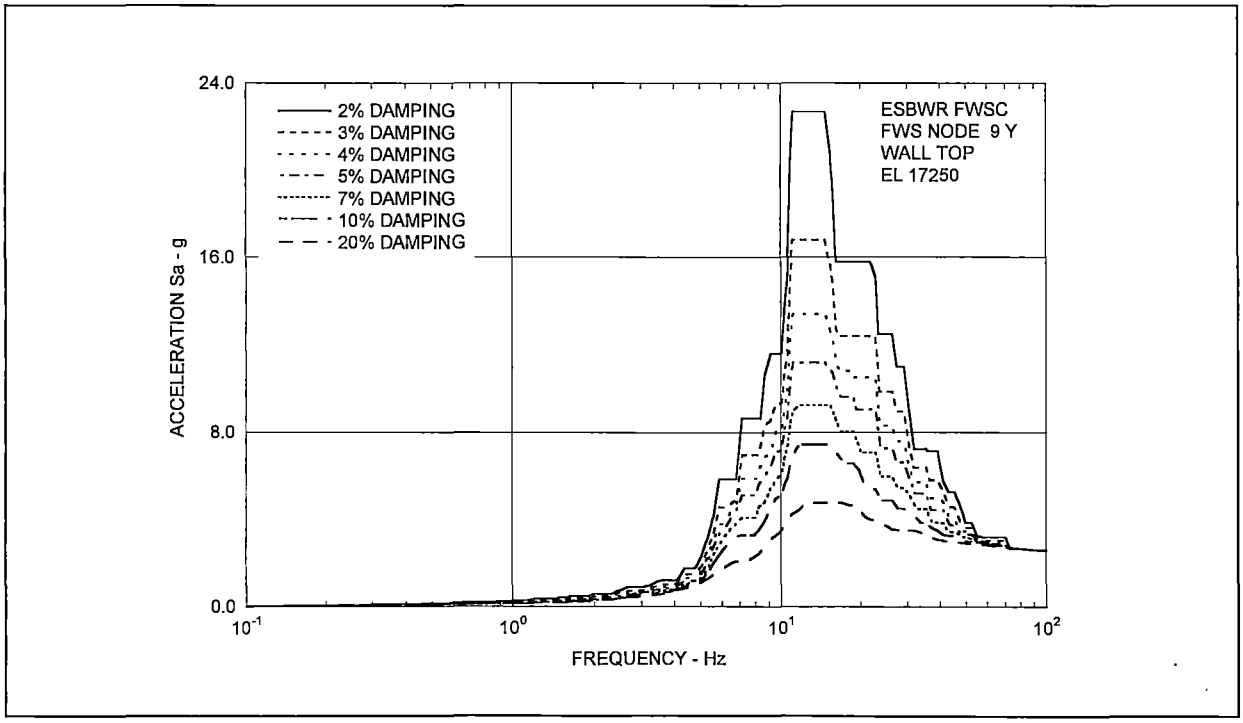

Figure E-12: Site-Specific In-Structure Response Spectra - FWS Node 9 Y -

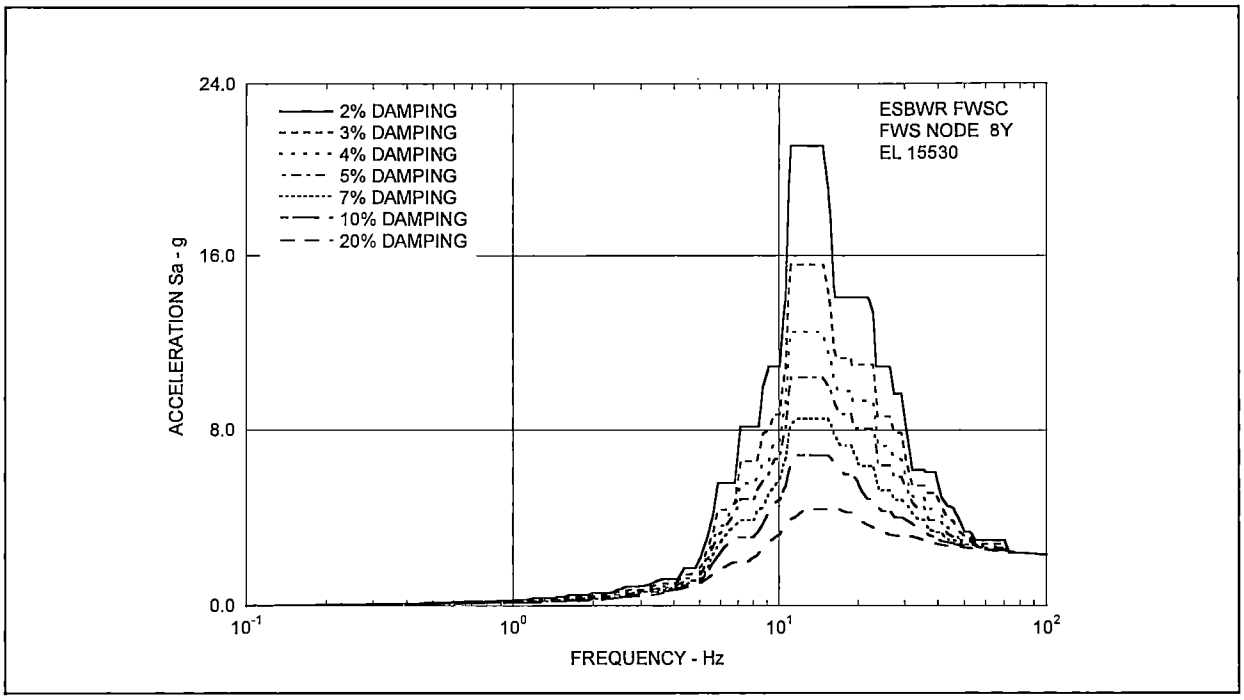

Figure E-13: Site-Specific In-Structure Response Spectra - FWS Node 8 Y -

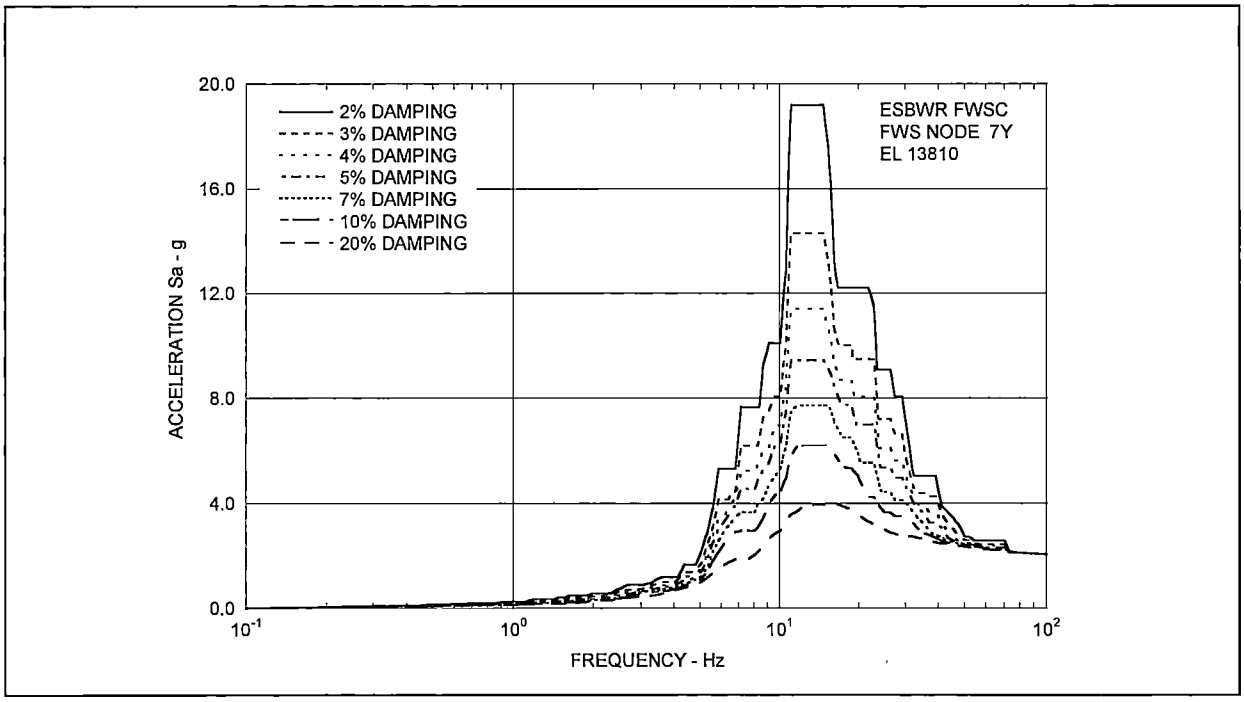

Figure E-14: Site-Specific In-Structure Response Spectra - FWS Node 7 Y -

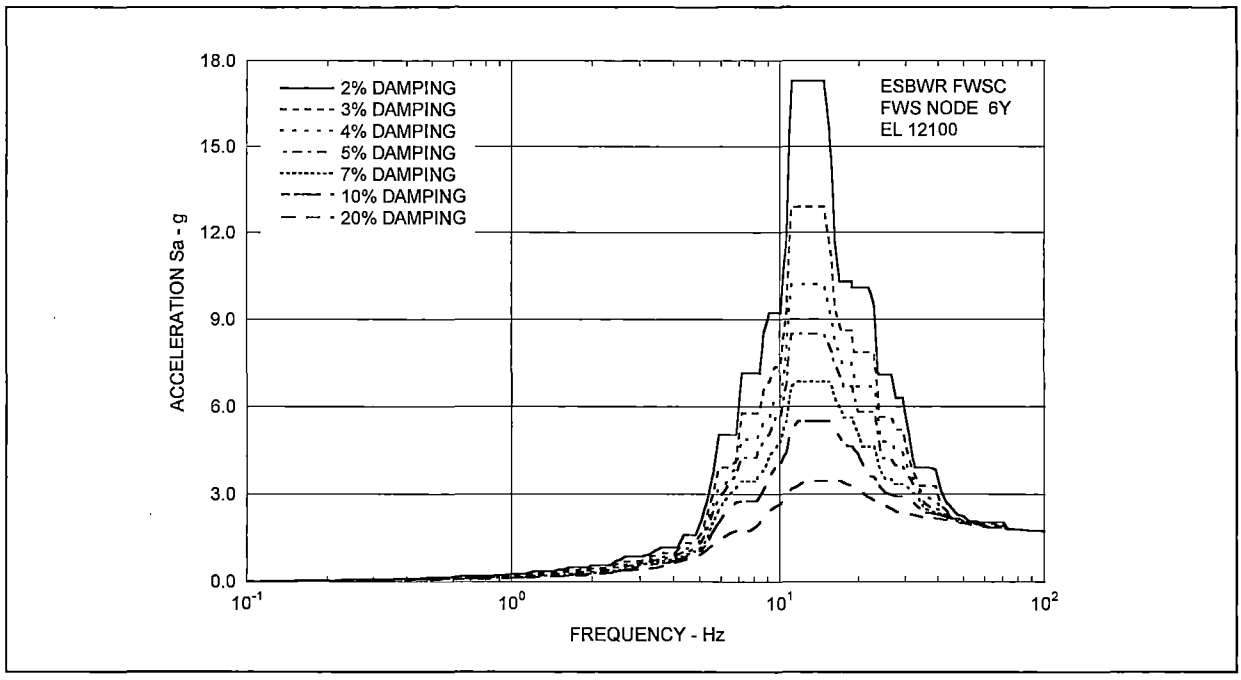

Figure E-15: Site-Specific In-Structure Response Spectra - FWS Node 6 Y -

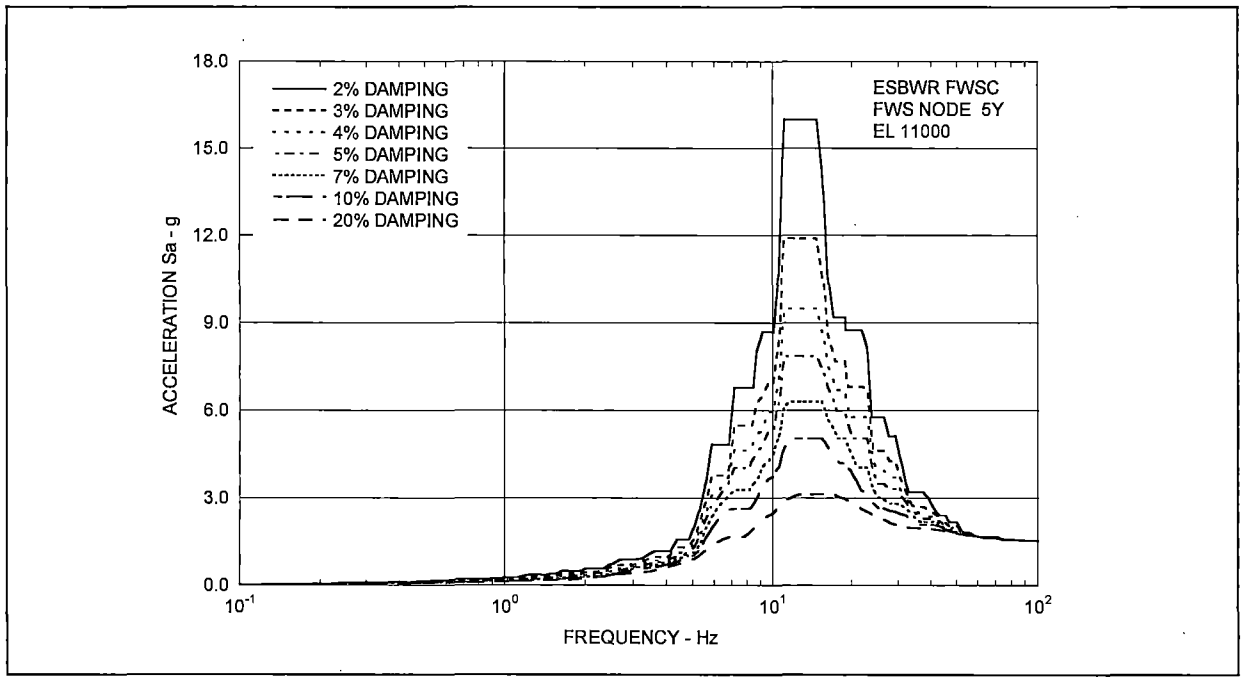

Figure E-16: Site-Specific In-Structure Response Spectra - FWS Node 5 Y -

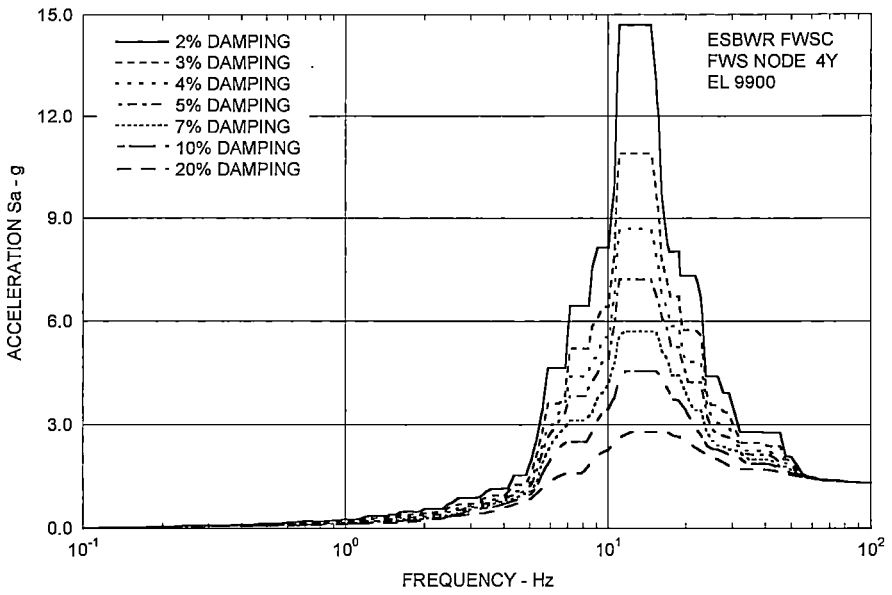

Figure E-17: Site-Specific In-Structure Response Spectra - FWS Node 4 Y -

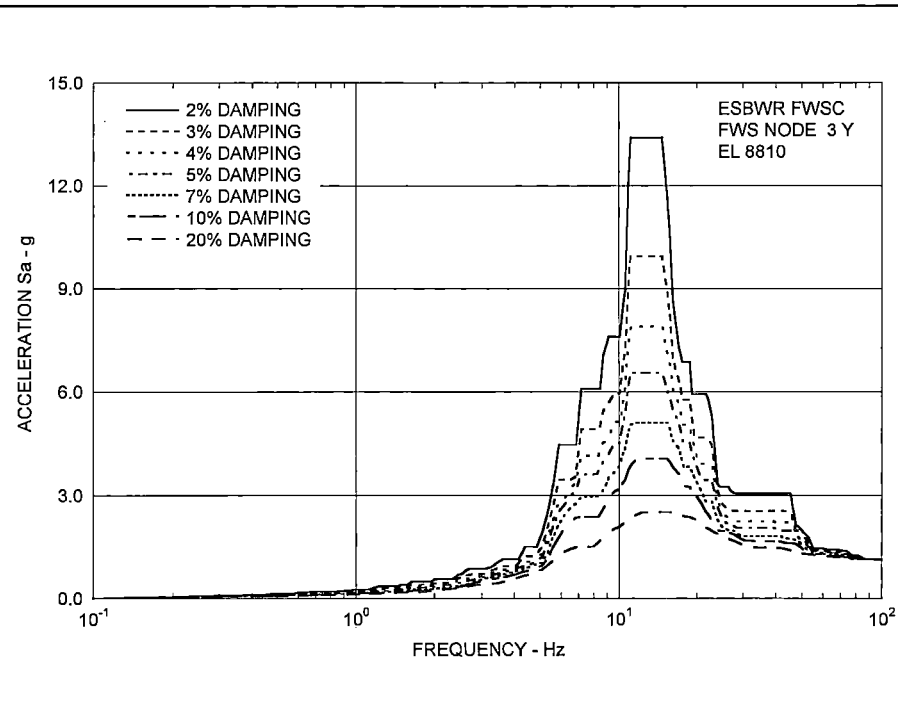

Figure E-18: Site-Specific In-Structure Response Spectra - FWS Node 3 Y -

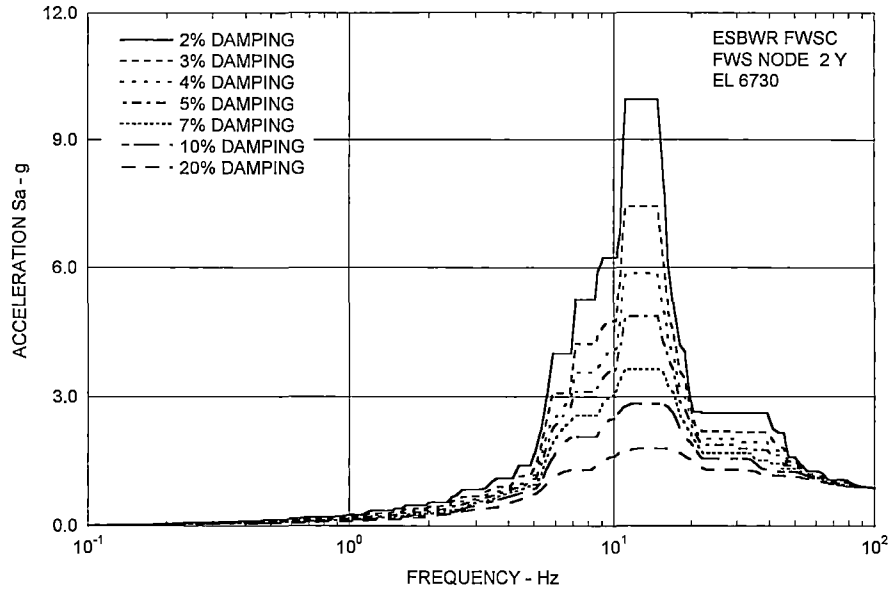

Figure E-19: Site-Specific In-Structure Response Spectra - FWS Node 2 Y -

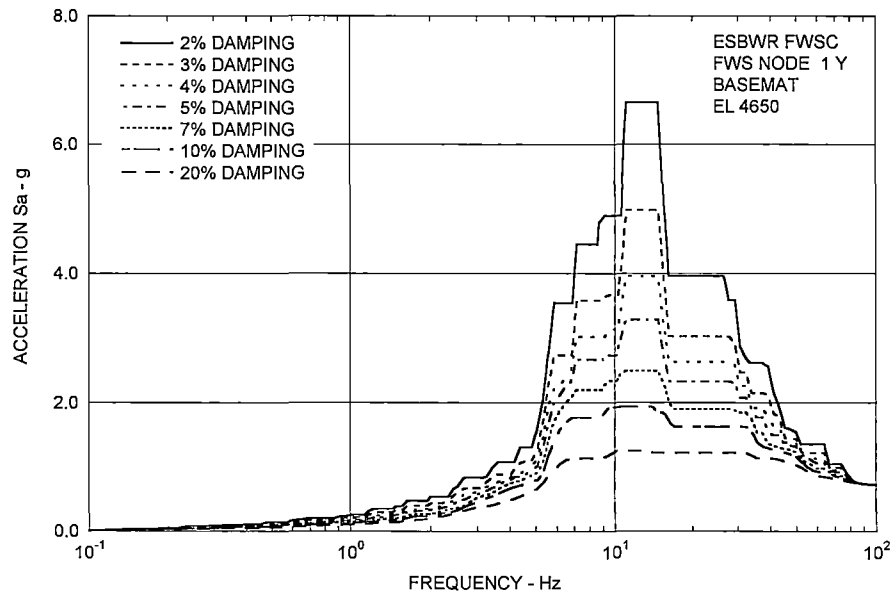

Figure E-20: Site-Specific In-Structure Response Spectra - FWS Node 1 Y -

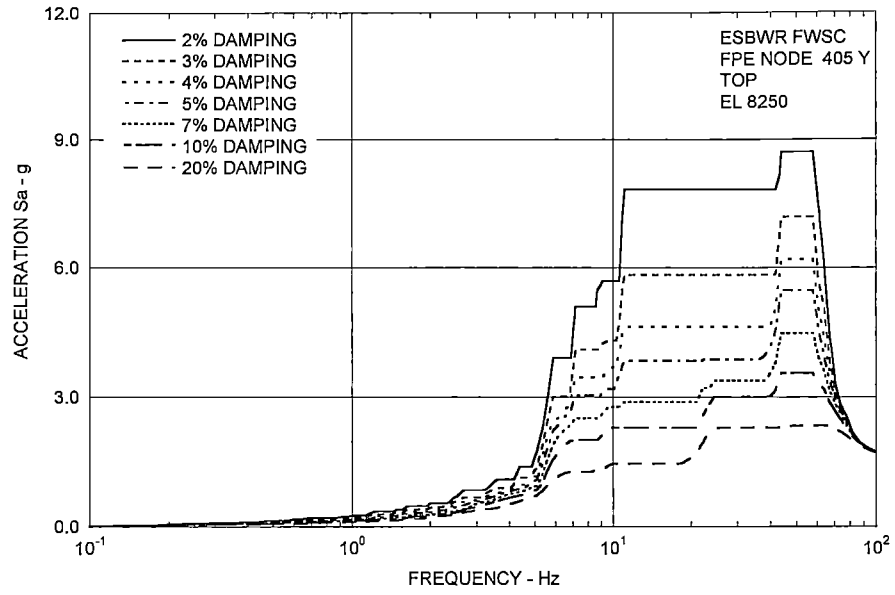

Figure E-21: Site-Specific In-Structure Response Spectra - FPE Node 405 Y -

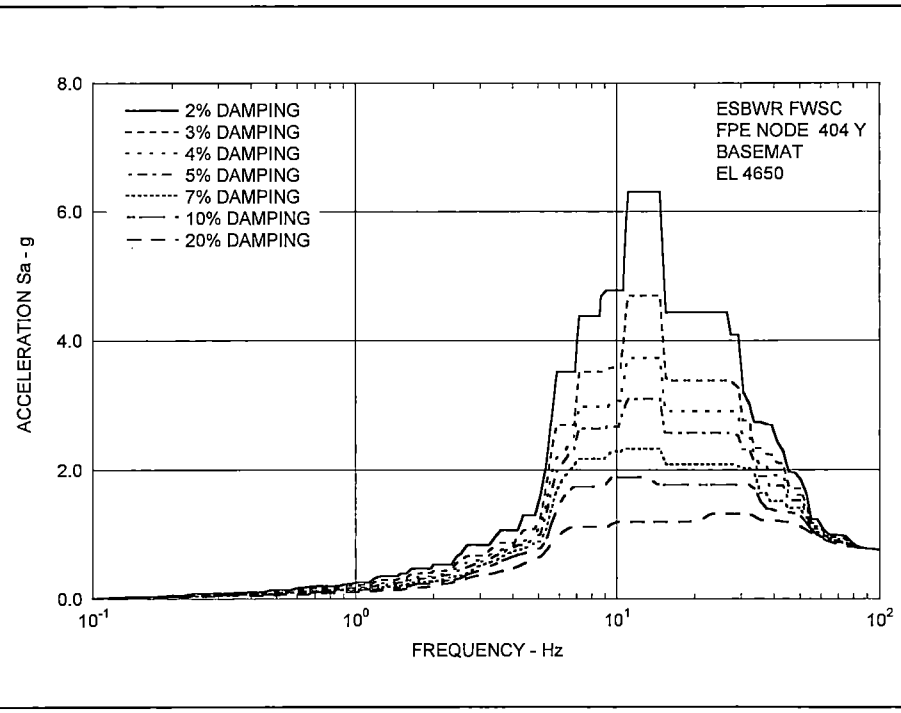

Figure E-22: Site-Specific In-Structure Response Spectra - FPE Node 404 Y -

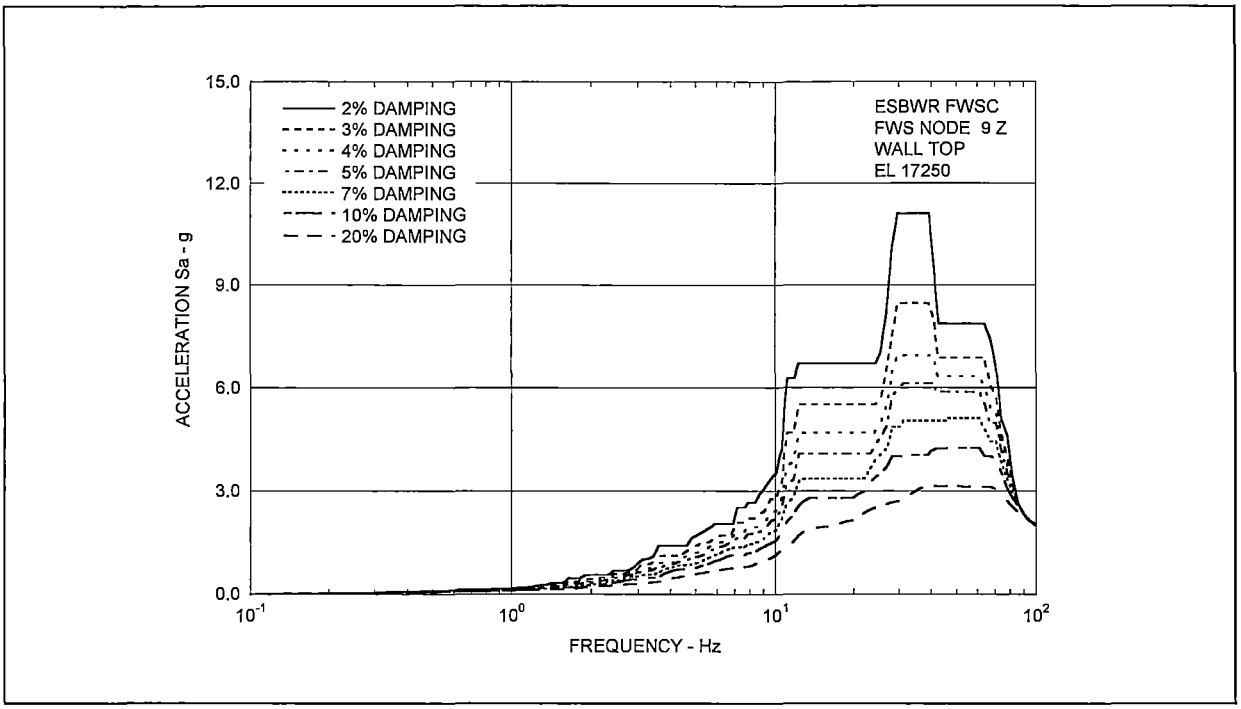

Figure E-23: Site-Specific In-Structure Response Spectra - FWS Node 9 Z -

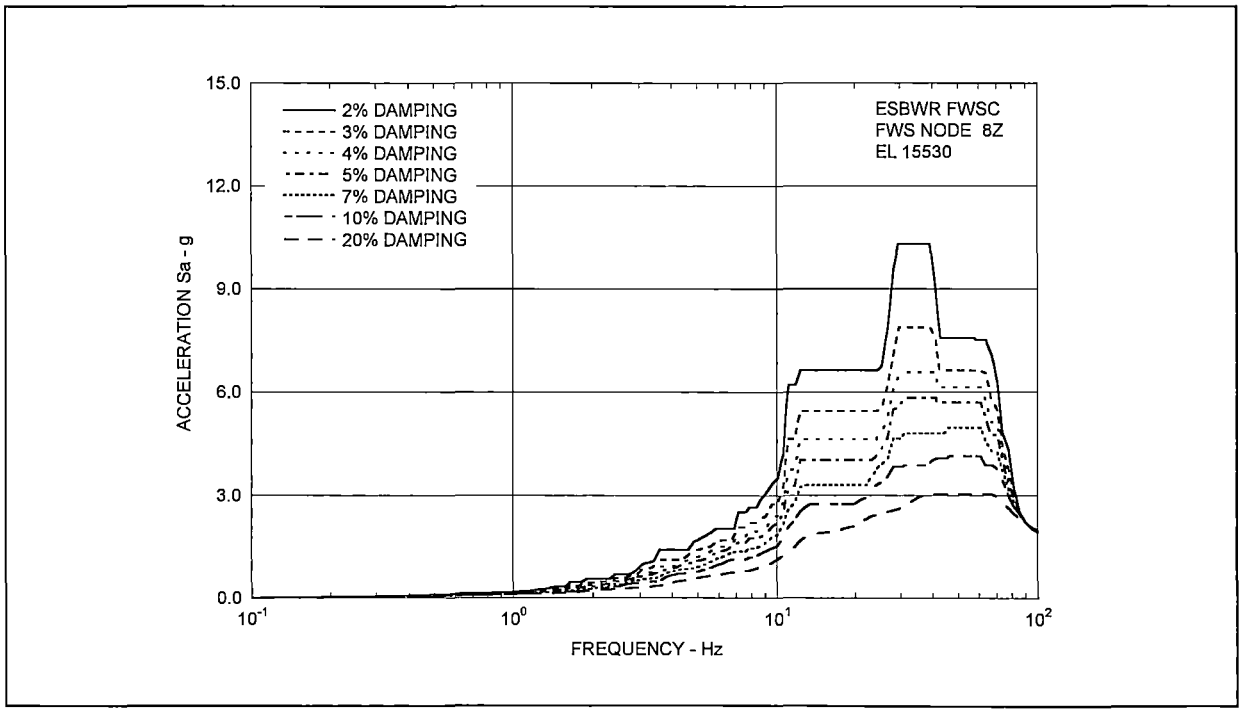

Figure E-24: Site-Specific In-Structure Response Spectra - FWS Node 8 Z -

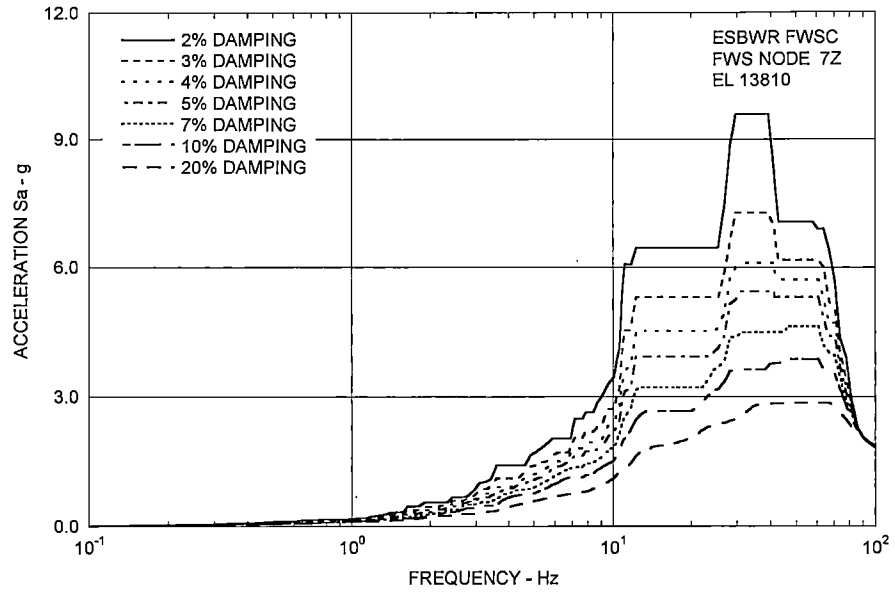

Figure E-25: Site-Specific In-Structure Response Spectra - FWS Node 7 Z -

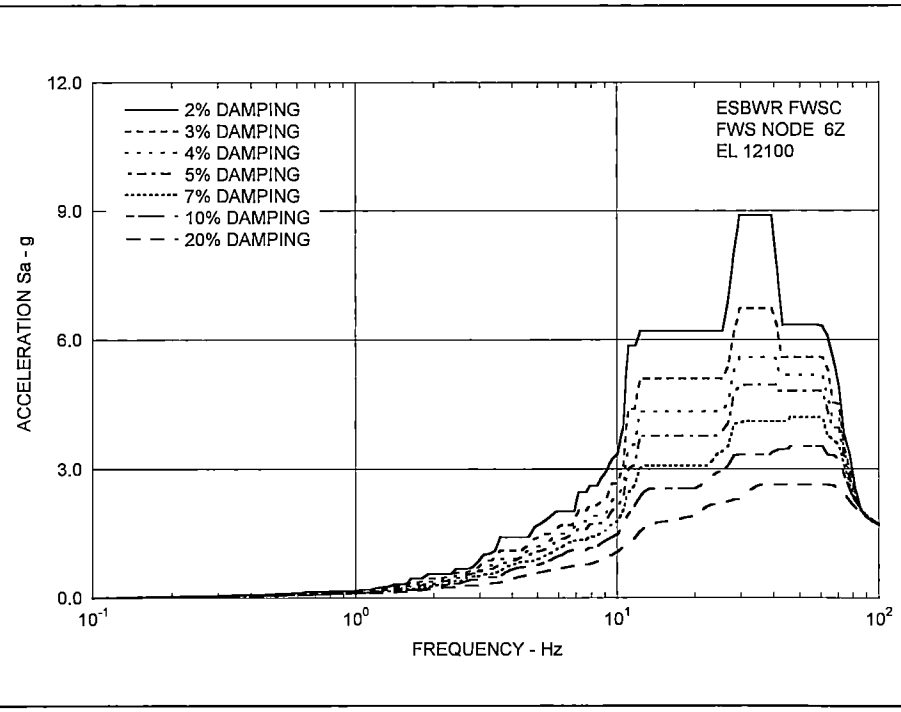

Figure E-26: Site-Specific In-Structure Response Spectra - FWS Node 6 Z -

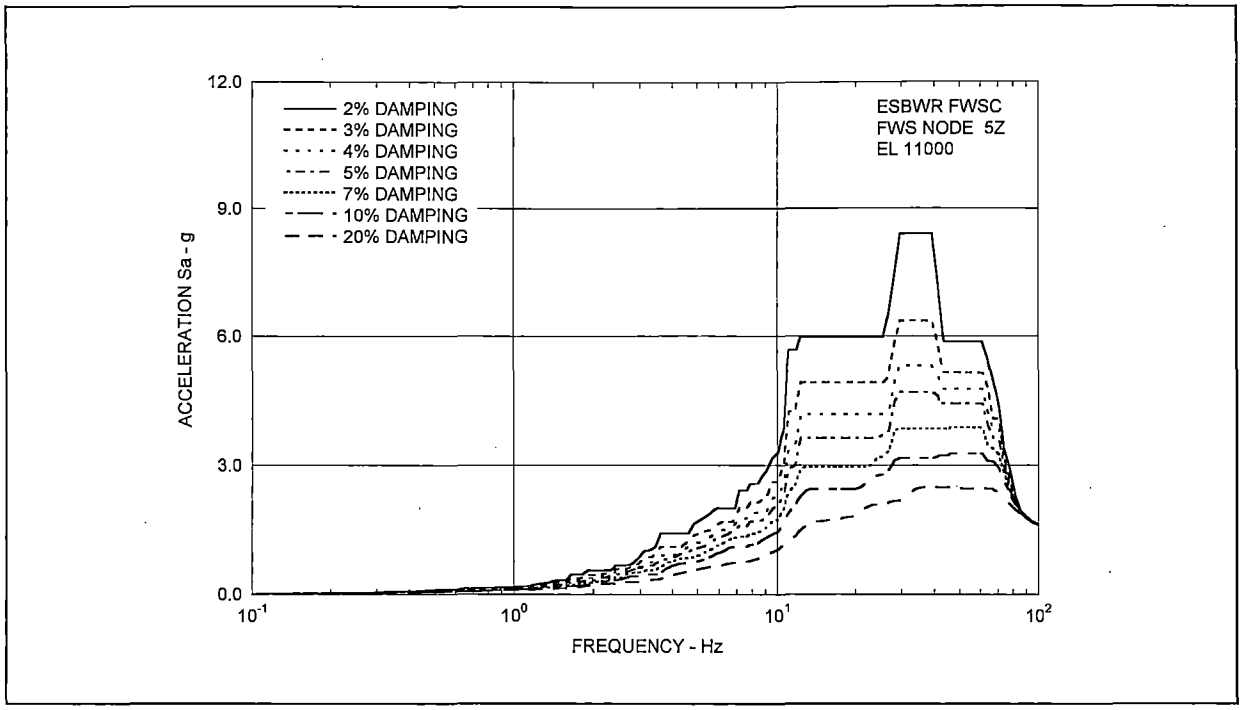

Figure E-27: Site-Specific In-Structure Response Spectra - FWS Node 5 Z -

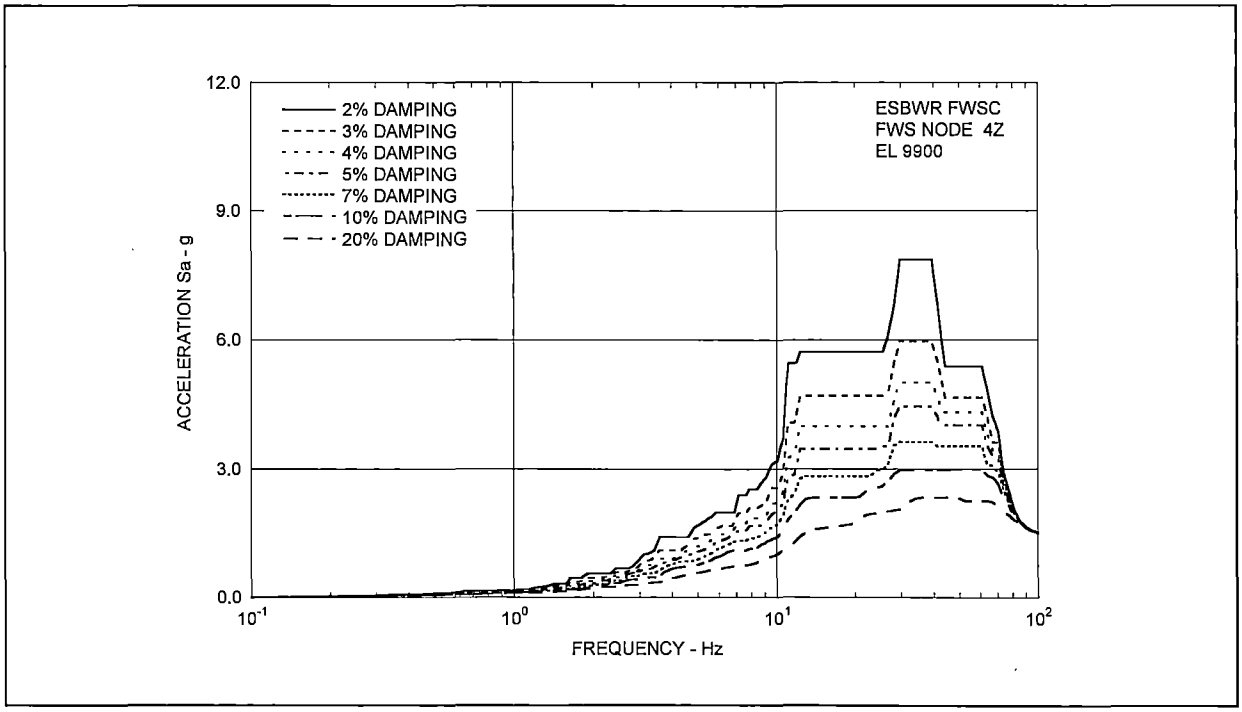

Figure E-28: Site-Specific In-Structure Response Spectra - FWS Node 4 Z -

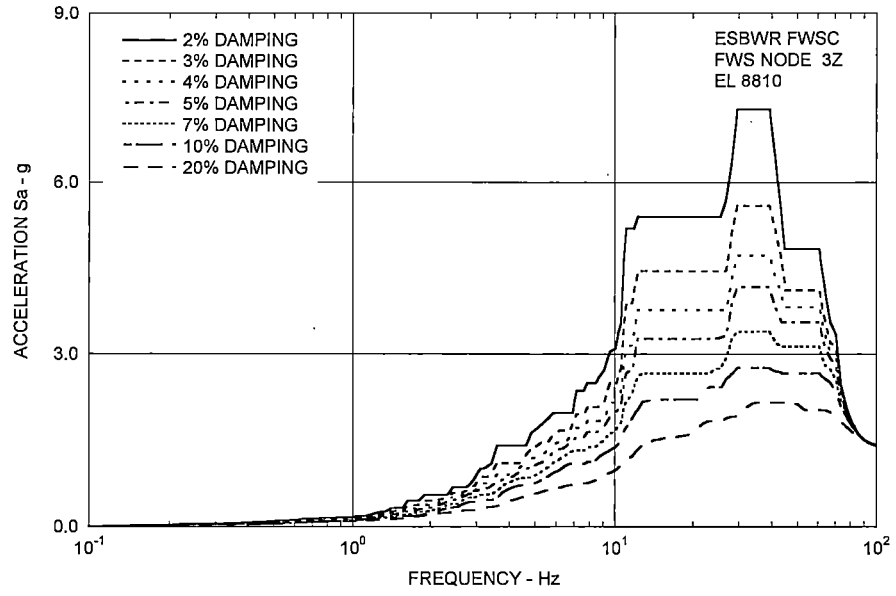

Figure E-29: Site-Specific In-Structure Response Spectra - FWS Node 3 Z -

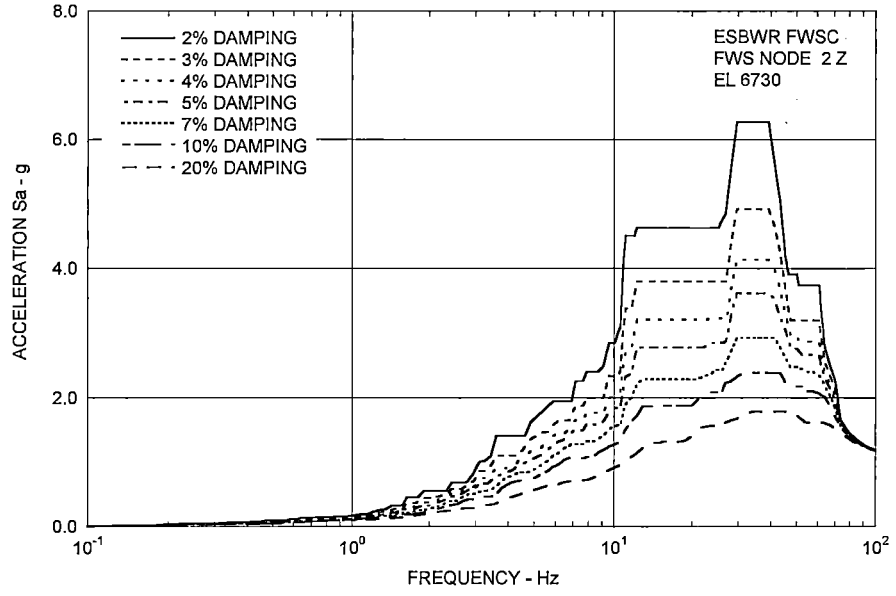

Figure E-30: Site-Specific In-Structure Response Spectra - FWS Node 2 Z -

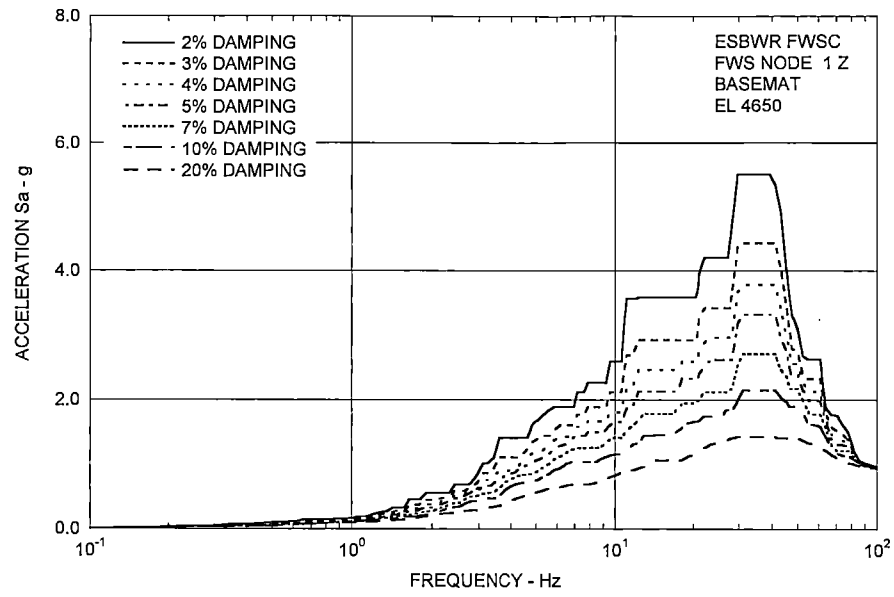

Figure E-31: Site-Specific In-Structure Response Spectra - FWS Node 1 Z -

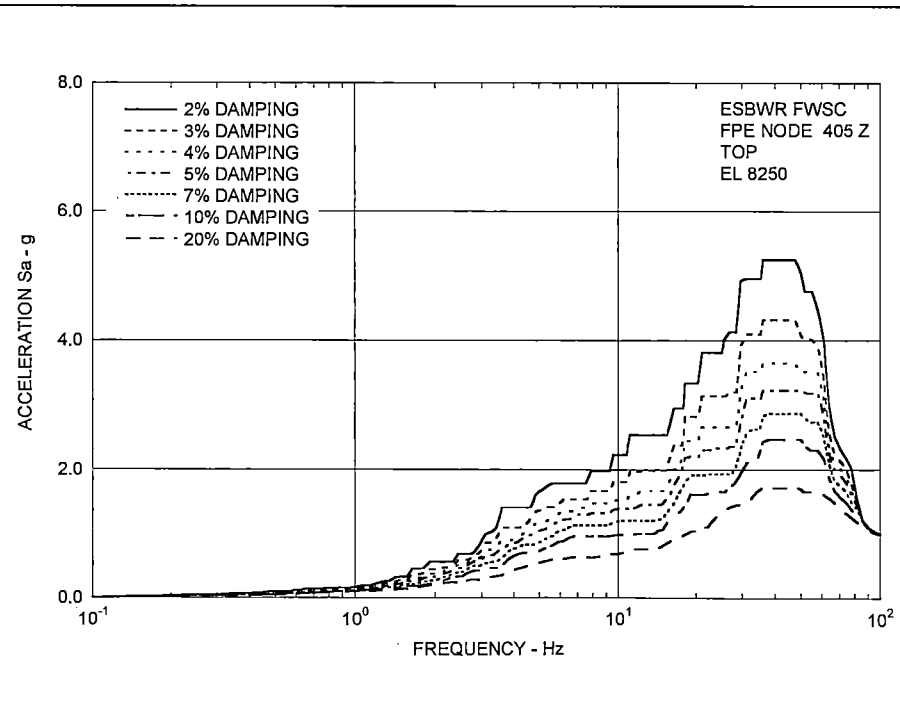

Figure E-32: Site-Specific In-Structure Response Spectra - FPE Node 405 Z -

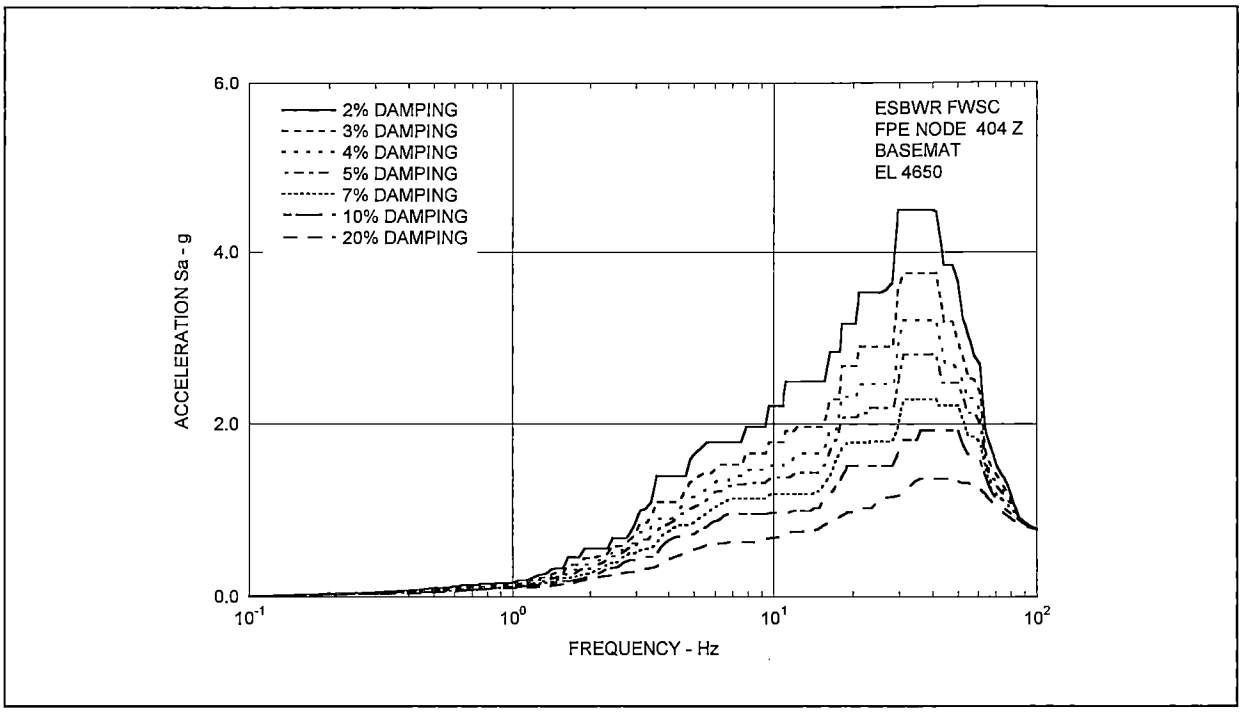

Figure E-33: Site-Specific In-Structure Response Spectra - FPE Node 404 Z -

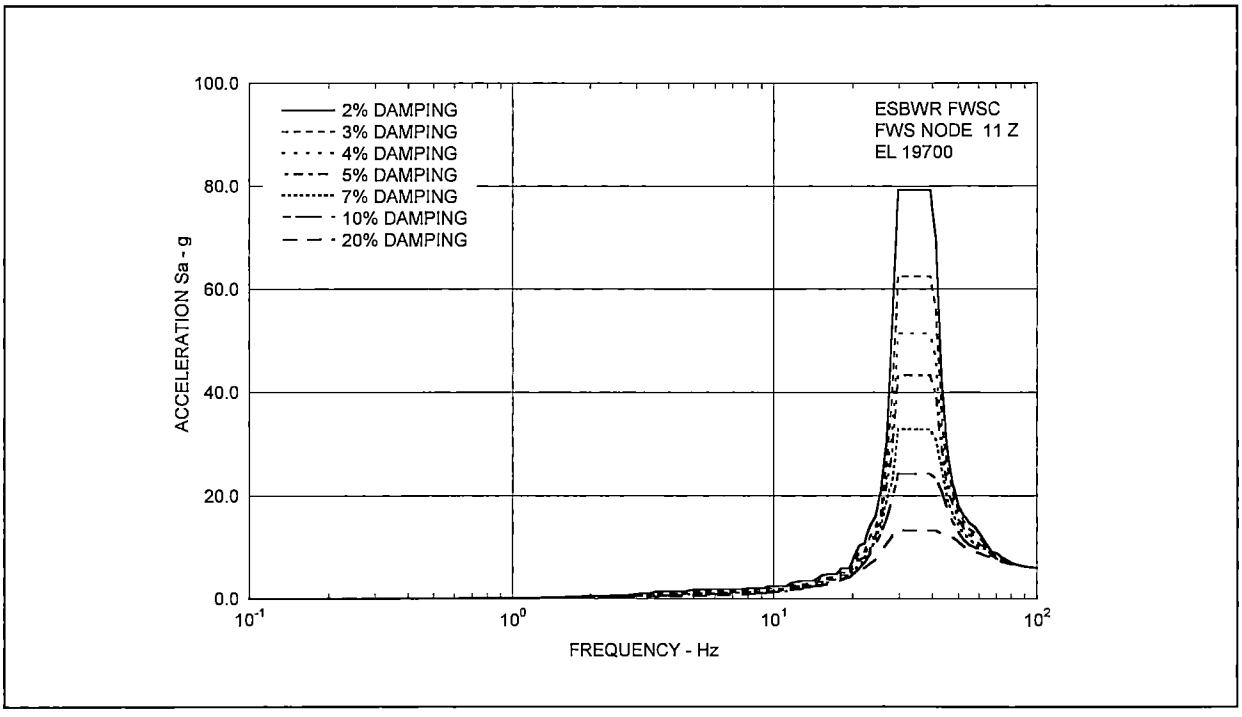

Figure E-34: Site-Specific In-Structure Response Spectra - Oscillator Node 11 Z -

APPENDIX F
SDOF Oscillators 5% Damped Site-Specific ISRS

LIST OF FIGURES

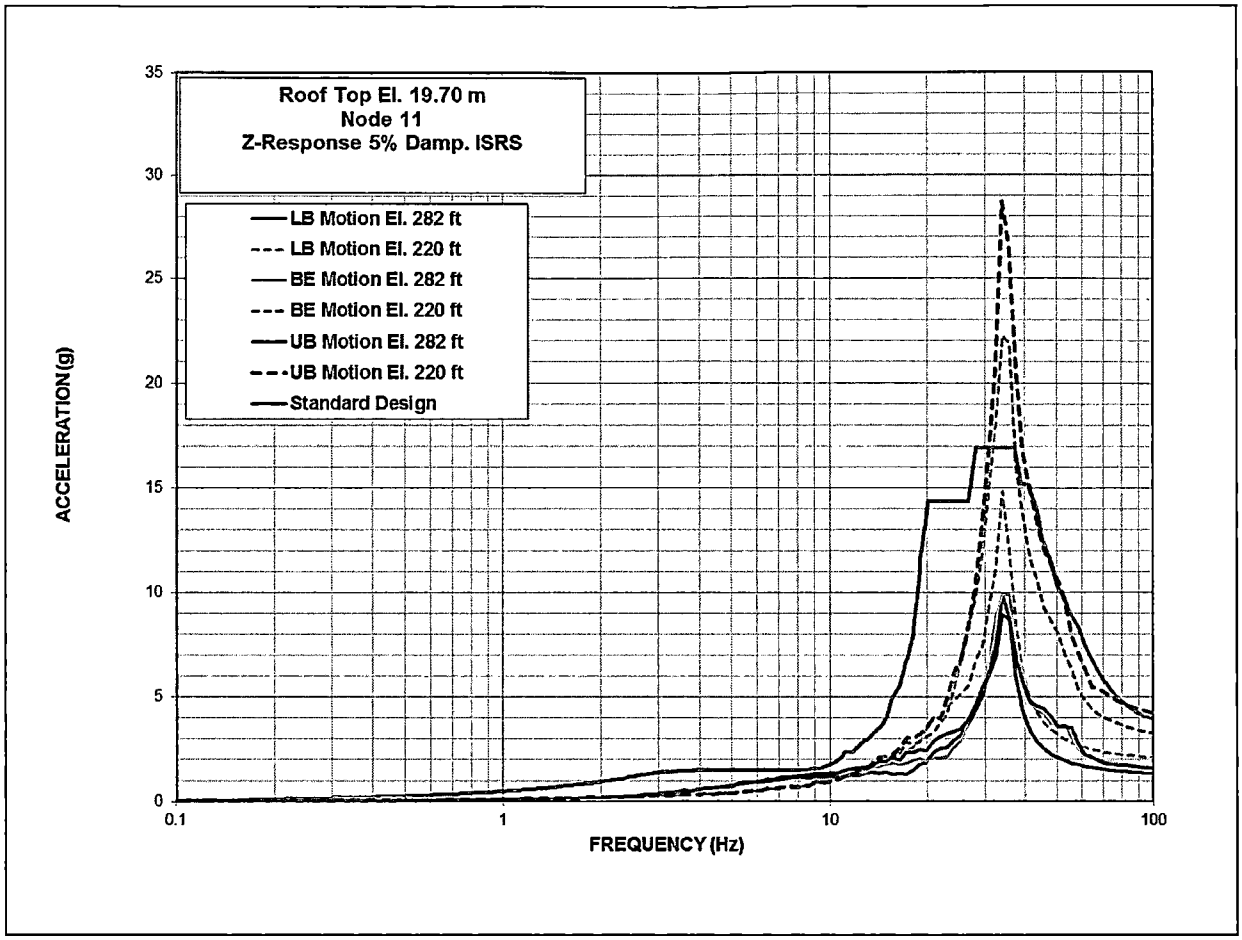

Figure F-1: Comparison of ISRS - Oscillator Node 11

APPENDIX G
Site-Specific SSI Models Node Mapping

TABLE OF CONTENTS

LIST OF TABLES

G.1 SCOPE

This appendix describes the lists of the correlation of node numbers between the DCD stick model shown on Figure 4.3-1 and the actual SASSI model used.

Table G-1: Correlation of Node Numbers between DCD and SASSI Stick Model

	DCD	SASSI
Basemat	8001	5
	8002	400, 6
FWS	1	201
	2	202
	3	203
	4	204
	5	205
	6	206
	7	207
	8	208
	9	209
	10	210
FPE	401	401
	402	402
	403	403
	404	404
	405	405
FWS Roof Oscillator	11	291
FWS Hydrodynamic Masses	30	257
	60	256